Multifunctional hairy nanocrystalline cellulose

By

Han Yang

A thesis submitted to McGill University in partial fulfillment of the requirements of the degree of

Doctor of Philosophy

Department of Chemistry
McGill University
Montreal, Quebec, Canada

April, 2016

Abstract

In this thesis the preparation and investigation of various novel nanocrystalline cellulose and their applications are examined. Nanocrystalline cellulose (NCC) is usually prepared from strong acid hydrolysis, and contains negatively charged sulfate half-ester groups. A novel type of nanocellulose was produced by periodate oxidation. For partial oxidation, three products were generated after the oxidized cellulose fibers were subjected to a hot-water treatment: fibrous cellulose, rod-like dialdehyde cellulose nanofibers which we refer to as sterically stabilized nanocrystalline cellulose (SNCC), and soluble dialdehyde modified cellulose (DAMC). These three products were separated by centrifugation and cosolvent addition. SNCC has similar dimensions as conventional NCC, but carries no charges and is sterically stabilized by protruding DAMC chains. Very few methods have been developed for preparation of positively charged nanocellulose. We prepared a hairy cationic nanocellulose (CNCC) by a two-step reaction. First dialdehyde modified cellulose (DAMC) fibers were prepared by periodate oxidation of cellulose fibers and subsequently DAMC fibers were cationized by a reaction between the aldehyde groups of the fibers and the amine groups of (2-hydrazinyl-2-oxoethyl)-trimethylazanium chloride (Girard's reagent T (GT)) to produce cationic dialdehyde modified cellulose (CDAMC) fibers. Subjecting the suspension of CDAMC fibers to a hot-water treatment at 60 °C, resulted in the formation of cationic rod-like nanocrystalline cellulose (CNCC). This is a simple and environmentally friendly method. Electrosterically stabilized nanocrystalline cellulose (ENCC) is another novel type of nanocrystalline cellulose we prepared. We take advantage of the rod-like structure of ENCC which has the dicarboxylated cellulose (DCC) chains protruding from both ends, providing electrosterical stability for ENCC particles, to chemically end-to-end assemble these particles into long nanocellulose fibers. It is the first chemically end-to-end assembly of nanocellulose fibers by a bottom-up route, and provides the possibility to assemble nanocellulose with desired aspect ratio. Finally, a novel biomaterial-based adsorbent aerogel was prepared by crosslinking bi-functional nanocrystalline cellulose (BNCC) and carboxymethylated chitosan through a Schiff base reaction. The maximum adsorption capacity of this aerogel for methylene blue was found to be 785 mg/g at room temperature. To the best of our knowledge, this is the highest removal capacity for any reusable adsorbent prepared from biomaterials.

Résumé

Dans cette thèse, la préparation et l’investigation des divers nouveaux nanocelluloses cristallines et leurs applications sont examinées. Nanocellulose cristalline (NCC) est souvent préparé à partir de l'hydrolyse acide forte, et contient des groupes de demi-ester de sulfate chargés négativement. Un nouveau type de nanocellulose a été produit par oxydation au periodate. Pour l'oxydation partielle, trois produits ont été générés après que les fibres de cellulose oxydée ont été soumises à un traitement à l'eau chaude : cellulose fibreuse, nano fibres de cellulose dialdéhyde en forme de bâtonnets que nous appelons nanocellulose cristalline stériquement stabilisée (SNCC), et cellulose soluble dialdéhyde modifiée (DAMC). Ces trois produits ont été séparés par la centrifugation et l’addition d'un cosolvant. SNCC a des dimensions similaires à celles de NCC conventionnelle, mais ne porte pas de charges et est stériquement stabilisée par des chaînes DAMC protubérants. Très peu de méthodes ont été développées pour la préparation de nanocellulose chargée positivement. Nous avons préparé une nanocellulose cationique poilue (CNCC) par une réaction en deux étapes. Tout d'abord les fibres de la cellulose modifiée dialdéhyde (DAMC) ont été préparées par l’oxydation au periodate des fibres de cellulose et ensuite les fibres DAMC ont été cationisées par une réaction entre les groupes aldéhydes des fibres et des groupes amine de (2-hydrazinyl-2-oxoéthyl) -triméthyl azanium chlorure (réactif de Girard T (GT)) pour produire les fibres de la cellulose modifiée dialdéhyde cationique(CDAMC). Sousmettre la suspension de fibres CDAMC à un traitement à l'eau chaude de 60 °C a entraîné la formation de nanocellulose cristalline cationique en forme de bâtonnet (CNCC). C’est une méthode simple et respectueuse de l'environnement. La nanocellulose cristalline électrostériquement stabilisée (ENCC) est un autre nouveau type de nanocellulose cristalline que nous avons préparé. Nous profitons de la structure de bâtonnet de l’ENCC qui possède les chaînes de cellulose dicarboxyle (DCC) protubérants des deux bouts, assurant la stabilité électrostérique pour les particules ENCC, pour assembler chimiquement de bout en bout ces particules dans les fibres de nanocellulose longues. Il est le premier assemblage de bout en bout chimique des fibres de nanocellulose par une voie ascendante, et il offre la possibilité d'assembler la nanocellulose avec un ratio d'aspect désiré. Enfin, un nouvel aérogel adsorbant à base de biomatériau a été préparé par la réticulation de la nanocellulose cristalline bi-fonctionnelle (BNCC) et le chitosan carboxyméthylé via une réaction de la base de Schiff. La capacité d'adsorption maximale de cette aérogel pour le bleu de méthylène était de 785 mg/g à la température ambiante. Au meilleur de notre connaissance, c’est la plus grande capacité d'enlèvement pour tout adsorbant réutilisable préparé à partir de biomatériaux.

Acknowledgements

First of all, I would like to express my deep appreciation for my supervisor, Professor Theo van de Ven, for his guidance and constant support through the years. I learned not only from his knowledge of chemistry, but also from his vision and passion for science. I also appreciate the opportunities he provided to me for attending conferences to present my work. It is my great honor to have Professor van de Ven as my mentor, he is my role model in both academic achievements and personality, which will inspire me during my whole life.

I sincerely thank all the group members in Professor Theo van de Ven's group for their encouragement and support. Dr. Nur Alam, Dr. Alvaro Tejado, Dr. Amir Sheikhi and Mr. Louis Godbout for their great help and valuable discussion of my research work. I also thank Georgios, Goeun, Kevin, Salman, Dezhi, Wei, Leila, Zohreh, Paul and Sabrina. It was great fun to work with you all.

I am grateful to my research committee members, Professor Derek Gray and Professor Mark Andrews, I appreciate the constructive feedback and suggestions I received during my review meetings. I also thank Mrs. Chantal Marotte and Mrs. Colleen McNamee for their kind help for the administration assistance.

I would also like to thank the following people for their kind help: Dr. Kelly Sears, Dr. David Liu, Jeannie Mui at the Facility for Electron Microscopy Research for helping me to develop my TEM and SEM skills; Mohini and Petr at the Centre for Self-Assembled Chemical Structures for training on AFM and many other instruments (e.g. FTIR, TGA and UV-vis); Dr. Fred Morin, for his help in NMR; Dr. Shang, for her help in XPS and XRD; Prof. Tufenkji in the Department of Chemical Engineering for kindly letting me use the Zetasizer in her lab; Prof. Mittermaier in Chemistry department for kindly letting me use the centrifuge and freeze-dry instruments.

Last but not least, I am greatly grateful to my parents and other family members in China, for their forever love and support.

Contribution of authors

Dr. Theo van de Ven provided supervision, intellectual advice and raised funding for all the projects described in this thesis.

Chapter 2 describes a sterically stabilized nanocrystalline cellulose. Han Yang initially started this project, then Han Yang and Dezhi Chen performed the experiment work separately and wrote the related sections for the manuscript. The experiments, result interpretation and manuscript writing were performed under the supervision and guidance from Dr. Theo van de Ven. This work has been published: Preparation and characterization of sterically stabilized nanocrystalline cellulose obtained by periodate oxidation of cellulose fibers. Han Yang, Dezhi, Chen, Theo van de Ven. Cellulose, 2015, 22, 1743-1752.

Chapter 3 describes a method for preparation of hairy cationic nanocrystalline cellulose. Han Yang performed all the experiment work and wrote the manuscript. The experiments, result interpretation and manuscript writing were performed by the author with inspiration and guidance from Dr. Theo van de Ven. This work is in press: Preparation of hairy cationic nanocrystalline cellulose. Han Yang, Theo van de Ven. Cellulose, 2016.

Chapter 4 describes a bottom-up route to a chemically end-to-end assembly of nanocellulose fibers. Han Yang performed all the experiment work and wrote the manuscript. The experiments, result interpretation and manuscript writing were performed under the supervision and guidance from Dr. Theo van de Ven. This work has been submitted to Biomacromolecules.

Chapter 5 describes a reusable green adsorbent aerogel prepared from crosslinked cellulose nanofibers and modified chitosan which can be used for cationic dye removal. Han Yang performed all the experiment work and wrote the manuscript. The experiments, result interpretation and manuscript writing were performed by the author with inspiration and guidance from Dr. Theo van de Ven. This work is ready for submission.

Appendix 1 describes various novel hairy nanocellulose. Amir Sheikhi initially started this work. Han Yang wrote about thirty percent of the manuscript, especially the “protocol” part, and equally joined the preparation of the video for visual experiments. The experiments, result interpretation and manuscript writing were performed by the authors with inspiration and guidance from Dr. Theo van de Ven. This work is in press: Highly stable, functional hairy nanoparticles and biopolymers from wood fibers: towards sustainable nanotechnology. Amir Sheikhi, Han Yang, Nur Alam and Theo van de Ven, 2016, Journal of visual experiments.

Appendix 2 describes the removal of copper ions from water by using electrosterically stabilized nanocrystalline cellulose (ENCC). Han Yang prepared the ENCC material, and wrote the sections about preparation and characterization of ENCC in the manuscript. Amir Sheikhi and Salman Safari were the two main authors, and performed all other experiments and wrote the related parts. The experiments, result interpretation and manuscript writing were performed under the supervision and guidance from Dr. Theo van de Ven. This work has been published: Copper removal using electrosterically stabilized nanocrystalline cellulose. Amir Sheikhi, Salman Safari, Han Yang and Theo van de Ven. ACS Applied Materials & Interfaces, 2015, 7, 11301-11308.

Appendix 3 describes controlled crosslinking of nanocelluloses using ammonium zirconium carbonate, authored by Amir Sheikhi, Han Yang, Pierre Carreau, Theo van de Ven. In this work, Han Yang prepared various nanoceluloses, including ENCC, hydrolyzed ENCC, SNCC, and conjugated ENCC and NFC (nanofibrillar cellulose) with ethanolamine on which carboxyl groups were replaced with hydroxyl groups, and also wrote the related preparation sections in the manuscript. Amir Sheikhi performed all the rheology experiments and wrote all other sections. The experiments, result interpretation and manuscript writing were performed under the supervision and guidance from Dr. Theo van de Ven and his colleague Dr. Pierre Carreau (École Polytechnique de Montréal). This manuscript is ready for submission, but being delayed due to potential patent implications.

Table of Contents

Abstract……ii
Résumé……iii
Acknowledgements……..iv
Contribution of authors……v
Table of contents……...vii
List of Tables……xii
List of Schemes……xii
List of Figures……...xiii
List of abbreviation and symbols……..xvi

Chapter 1. Introduction
1.1 Cellulose……..1
1.2 Nanocellulose……..3
1.2.1 Nanocrystalline cellulose……...3
1.2.2 Electrosterically stalilized nanocrystalline cellulose……..…6
1.2.3 Nanofibrillar cellulose……...8
1.3 Principles of various reactions…….……..13
1.3.1 Periodate and chlorite oxidation……....13
1.3.2 Schiff base reaction……...15
1.3.3 Chitosan and carboxymethylation……16
1.3.4 Click chemistry……..17
1.4 Aerogel……18
1.5 Thesis outline and objectives……..19
1.6 References……...21

Chapter 2. Preparation and characterization of sterically stabilized nanocrystalline cellulose obtained by periodate oxidation of cellulose fibers
2.1 Abstract……30
2.2 Introduction……..31
2.3 Experimental section……32

2.3.1 Materials……...33
2.3.2 Periodate oxidation of cellulose pulp……33
2.3.3 Determination of aldehyde content……...33
2.3.4 Preparation and separation of SNCC……34
2.3.5 Fourier transform infrared spectra (FTIR)…….35
2.3.6 Solid carbon-13 NMR measurements……35
2.3.7 Atomic force microscopy (AFM) measurement……35
2.3.8 Particle size distribution…….35
2.3.9 Thermal properties - thermogravimetric analysis (TGA)……..36
2.3.10 Viscosity measurements……36
2.3.11 Gel permeation chromatography…….....……...36
2.4 Results and discussion……....36
2.4.1 Solubility of DAC in various solvents……..36
2.4.2 Separation of periodate oxidized products……37
2.4.3 Particle morphology……..38
2.4.4 Dynamic light scattering of SNCC suspensions in water-propanol mixtures……...39
2.4.5 FTIR spectra……..40
2.4.6 Solid state carbon -13 NMR ……....41
2.4.7 Thermal stability……...42
2.4.8 Viscosity……...43
2.4.9 Gel permeation chromatography (GPC) of DAC…….44
2.5 Conclusions……45
2.6 Acknowledgements……45
2.7 References……..46

Bridging Section between Chapters 2 and 3……49

Chapter 3. Preparation of hairy cationic nanocrystalline cellulose
3.1 Abstract……..50
3.2 Introduction……....51
3.3 Experimental section……..53

3.3.1 Materials…….53
3.3.2 Periodate oxidation of cellulose pulp…….53
3.3.3 Cationization of dialdehyde cellulose……54
3.3.4 Preparation of cationic nanocellulose…….54
3.3.5 Morphological properties……54
3.3.6 The content of cationic groups……...….55
3.3.7 Zeta potential measurement…….55
3.3.8 Surface chemical properties…….55
3.3.9 Solid carbon-13 NMR measurements……..……55
3.3.10 X-ray photoelectron spectroscopy (XPS) analysis…….…....55
3.3.11 X-ray diffraction (XRD) analysis…….……...……....56
3.4 Discussion……...….56
3.4.1 Preparation of CNCC……..….56
3.4.2 Morphology of CNCC……..59
3.4.3 Zeta potential and charge content……..……...59
3.4.4 Chemical properties of CNCC……..60
3.4.5 XPS analysis…….....62
3.4.6 Crystalline properties…….……...64
3.5 Conclusion…….…...66
3.6 Acknowledgements……...……...66
3.7 References…….……...67

Bridging Section between Chapters 3 and 4……...…..71

Chapter 4. A bottom-up route to a chemically end-to-end assembly of nanocellulose fibers
4.1 Abstract…….……..72
4.2 Introduction…….73
4.3 Experimental section……...……75
4.3.1 Materials……...……75
4.3.2 Preparation of ENCC……...……75
4.3.3 Preparation of HENCC……..……...76

4.3.4 Preparation of HENCC with alkyne groups (HENCC-AK)…….76
4.3.5 Preparation of HENCC with azide groups (HENCC-AZ)……..…..77
4.3.6 Preparation of clicked HENCC……...…….77
4.3.7 Preparation of HENCC with -NH2 groups……..78
4.3.8 Preparation of cross-linked HENCC……79
4.3.9 Conductometric titration……...…80
4.3.10 Surface chemical properties……...…….80
4.3.11 Dynamic light scattering (DLS) measurements……..……80
4.3.12 Morphological properties……..…..81
4.4 Results and discussion ……...…….81
4.4.1 Preparation of ENCC and HENCC…….81
4.4.2 FTIR analysis…….….84
4.4.3 Assembly of HENCC by a click reaction……...……86
4.4.4 Assembly of HENCC by a bioconjugation reaction……..…….89
4.5 Conclusion…….…….90
4.6 Acknowledgements……90
4.7 References……..……91

Bridging Section between Chapters 4 and 5…….……...94

Chapter 5. Reusable green adsorbent aerogel from crosslinked cellulose nanofibers and modified chitosan for dye removal
5.1 Abstract…….….95
5.2 Introduction……...…….96
5.3 Experimental section……..…….98
5.3.1 Materials…….……98
5.3.2 Preparation of bifunctional NCC (BNCC)…….98
5.3.3 Preparation of carboxymethylated chitosan……...……99
5.3.4 Preparation of aerogel (BNCC-CMCT)……...……..99
5.3.5 Dye adsorption……..….99
5.3.5.1 Equilibrium experiments……100

5.3.5.2 Kinetic experiments……..……..100
5.3.5.3 Effect of pH on adsorption…….100
5.3.5.4 Reusability of adsorbent…….101
5.3.6 Conductometric titration……...…….101
5.3.7 Solid carbon-13 NMR measurements……...…….101
5.3.8 AFM measurement……...……..101
5.3.9 SEM measurement…….102
5.3.10 Porosity measurement……...……102
5.4 Results and discussion…….……..102
5.4.1 Characterizations of BNCC and aerogel……..……..102
5.4.2 Solid C-13 NMR……...…….104
5.4.3 Adsorption isotherm……..……108
5.4.4 Adsorption kinetics……..……..111
5.4.5 Effects of pH on adsorption process……..……113
5.4.6 Desorption and regeneration……..116
5.5 Conclusion…….117
5.6 Acknowledgements…….……..117
5.7 References…….....117

Chapter 6. Conclusions and future work suggestions
6.1 Conclusions……..…….121
6.2 Suggestions for future work……..……123

Appendix 1.
Highly stable, functional hairy nanoparticles and biopolymers from wood fibers: towards sustainable nanotechnology……...….125

Appendix 2.
Copper removal using electrosterically stabilized nanocrystalline cellulose……..143

Appendix 3.

Controlled crosslinking of nanocelluloses using ammonium zirconium carbonate …….....160

List of Tables

Table 2.1 Solubility of DAC in various solvents at both room and elevated temperatures…….37

Table 2.2 Molecular weights of DAC after different heating conditions……..45

Table 5.1 Isotherm parameters for MB adsorption in 0 M and 0.1 M NaCl at 22 °C…….109

Table 5.2 Comparison of the maximum MB adsorption by various adsorbents…….111

Table 5.3 Langmuir isotherm parameters for MB adsorption for various pHs at 22 °C…….115

Table 6.1 Summarization of physical properties of various nanocellulose material……...122

List of Schemes

Scheme 1.1 Reaction for periodate oxidation of cellulose……..13

Scheme 1.2 Reactions for (a) conversion of dialdehyde cellulose to dicarboxyl cellulose by chlorite, (b) hydrogen peroxide used as HClO scavenger, and (c) reaction without adding H_2O_2……....14

Scheme 1.3 (a) Schematic illustration of Schiff base reaction, (b) Schiff base reaction between primary amino and 2,3-dialdehyde cellulose……..16

Scheme 1.4 Schematic representation of carboxymethylation reaction of chitosan……...17

Scheme 1.5 Schematic representation of Cu(I)-catalyzed Huisgen 1,3-cycloaddition reaction..18

Scheme 3.1 (a) periodate oxidation of cellulose to produce dialdehyde modified cellulose (m < n), (b) cationization of dialdehyde cellulose (Note that it is difficult to attach the second quaternary ammonium group to the same glucose unit due to steric hindrance and electrostatic repulsion)…….53

Scheme 4.1 The reaction between HENCC and 1-amino-3-butyne, for the production of HENCC-AK……76

Scheme 4.2 The reaction between HENCC and 3-azido-1-propanamine, for the production of HENCC-AZ……..77

Scheme 4.3 The cross-linking reaction between HENCC-ZK and HENCC-AZ…….78

Scheme 4.4 The reaction between HENCC and ADH, for the production of HENCC-NH2…..79

Scheme 4.5 The cross-linking reaction between HENCC-NH2 and HENCC…….80

Scheme 6.1. Preparation of various nanocellulose material, including SNCC, DAC, ENCC, HENCC, CNCC and BNCC…….121

List of Figures

Figure 1.1 Molecular structure of cellulose. The numbering of the carbon atoms in a glucose unit is shown, n is the degree of polymerization (DP), based on the glucose repeat unit……1

Figure 1.2 TEM images of dried dispersion of cellulose nanocrystals derived from (a) tunicate (b) bacterial (c) ramie, and (d) sisal (Adapted with permission from ref. [8]. Copyright 2010 American Chemical Society)…….4

Figure 1.3 AFM image for ENCC with charge density of 6.6 mmol/g. (Adapted with permission from ref. [49]. Copyright 2013 Springer)……..7

Figure 1.4. Schematics of TEMPO-mediated oxidation mechanism of primary alcohols in a mildly alkaline environment. (Adapted with permission from ref. [58]. Copyright 2004, Plenum Publishing Corporation)……...10

Figure 1.5 (a) TEM image of NFC from TEMPO/NaClO/NaBr system oxidation (Adapted with permission from ref. [61]. Copyright 2006 American Chemical Society), (b) TEM image of NFC from TEMPO/NaClO/$NaClO_2$ system oxidation, inset shows the corresponding highly viscous and transparent NFC dispersion at 0.3%. (Adapted with permission from ref. [63]. Copyright 2009 American Chemical Society)……11

Figure 1.6 Field-Emission Scanning Electron Microscopy (FESEM) image of the nanofibril with a carboxyl content 0.69 mmol/g prepared from sequential periodate-chlorite oxidation followed by mechanical treatment. (Adapted with permission from ref. [64]. Copyright 2012 American Chemical Society)…….12

Figure 1.7 TEM image of frozen 2% w/w MFC gel after enzymatic hydrolysis and homogenization processes, showing fibers with a diameter of 5-6 nm and some thicker fibers with diameter of 10-20 nm. (Adapted with permission from ref. [67]. Copyright 2007 American Chemical Society)…….13

Figure 2.1 Scheme of separation process of products produced by periodate oxidation of cellulose…….34

Figure 2.2 Separation of SNCC and DAMC using propanol as co-solvent, expressed as weight percent of the original supernatant……38

Figure 2.3 AFM height image for (a) SNCC, and (b) NCC……..39

Figure 2.4 DLS size of SNCC particles as a function of cosolvent addition, expressed as weight percent of original SNCC suspension. Schematic representation of (a) SNCC with protruding DAMC chains which provide steric stability, (b) DAMC chains contracted with addition of propanol, and (c) SNCC aggregation upon further addition of propanol…….40

Figure 2.5 FTIR spectra of original cellulose pulp, NCC, and SNCC. The curve on the right side is an enlarged curve of SNCC in the range 2000 - 500 cm^{-1}……41

Figure 2.6 Solid state carbon-13 NMR spectra of original cellulose pulp, NCC, and SNCC…..42

Figure 2.7 Derivative weight loss (DWL) curves for SNCC, NCC, and original cellulose pulp..43

Figure 2.8 Relative viscosity versus concentration of SNCC and NCC suspensions……...44

Figure 3.1 Optical microscopy images: (a) starting cellulose fibers, (b) DAMC fibers, (c) cationic DAMC fibers and (d) cationic DAMC fibers with negative dye……..57

Figure 3.2 Schematic representation of the liberation of CNCC from positively charged cellulose fibers (CDAMC) under hot water treatment at 60 °C……...57

Figure 3.3 (a) photographs of suspension of DAMC fibers (left) and after treatment by 60 °C hot water for half an hour (right), (b) optical microscopy image of DAMC fibers after hot water treatment, and (c) photographs of suspension of cationic DAMC fibers (left, the translucence is due to the high degree of swelling of cationic DAMC fibers) and the suspension turns clear after treatment by 60 °C hot water for half an hour (right)……...58

Figure 3.4 (a) AFM height image of CNCC, (b) TEM image of CNCC……..59

Figure 3.5 Conductometric titration of CNCC suspension, titrated with 10 mM AgNO3……....60

Figure 3.6 FTIR spectra of DAMC fibers and CNCC……...61

Figure 3.7 Solid state carbon-13 NMR spectra of starting cellulose fibers, DAMC fibers, and CNCC……....61

Figure 3.8 XPS wide survey scan spectra of (a) DAMC fibers and (b) CNCC……..…..63

Figure 3.9 XPS high resolution scan of C 1s spectra of (a) DAMC fibers and (b) CNCC…..….64

Figure 3.10 X-ray diffractograms of (a) starting pulp, (b) DAMC fibers, (c) CDAMC fibers, and (d) CNCC…….….65

Figure 4.1 AFM images for the morphology of (a) ENCC (charge density 6 mmol/g) and (b) HENCC (charge density 1.2 mmol/g)……...83

Figure 4.2 Schematic representation of (a) the alternative arrangement of crystalline and amorphous regions in cellulose fibers, (b) the releasing of ENCC particles by sequential oxidation and chlorite oxidation, and (c) protruding DCC chains on ENCC were cut (shortened) by HCl hydrolysis. The dots on the chains represent carboxyl groups……...…..83

Figure 4.3 Schematic representation of the formation of ENCC aggregation from crosslinking with adipic acid dihydrazide (ADH) through a bio-conjugation reaction……....84

Figure 4.4 FITR spectra for (a) the starting pulp, (b) ENCC, and (c) HENCC…….….85

Figure 4.5 AFM images of (a) HENCC-AK and (b) HENCC-AZ…….….85

Figure 4.6 FITR spectra of (a) HENCC conjugated with 3-azido-1-propanamine (HENCC-AZ), (b) HENCC conjugated with1-amino-3-butyne (HENCC-AK), and (c) crosslinked HENCC-AZ and HENCC-AK by click reaction……..86

Figure 4.7 Assembled cellulose nanofiber from HENCC-AK and HENCC-AZ through click reaction……..…..87

Figure 4.8 Schematic representation of (a) two sets of HENCC derivatives: HENCC-AK and HENCC-AZ, (b) HENCC-AK and HENCC-AZ alternatively assembled into one dimensional nanochains through end-to-end assembly, and (c) the possibility for forming side chains along the assembled cellulose nanofiber chains……..88

Figure 4.9 Assembled cellulose nanofibers from HENCC-AK and HENCC-AZ through click reaction with HENCC from prolonged hydrolysis. The nanofibers are much longer than those of HENCC, as can be concluded by comparison with Figure 4.1(b)……...……89

Figure 4.10 Assembled cellulose nanofiber from HENCC-NH2 and HENCC through a bioconjugation reaction……...….90

Figure 5.1 Molecular structure of MB…….....98

Figure 5.2 AFM image of BNCC nanoparticles……..104

Figure 5.3 (a) Photograph of transparent hydrogel in an upside down vial, (b) photograph of a piece of aerogel standing on the tip of the fine awns of a green foxtail, and (c) SEM image of the aerogel, with the inset showing an enlargement of the “walls” formed in the aerogel……...104

Figure 5.4 Solid carbon -13 NMR spectra for (a) cellulose pulp and BNCC, (b) chitosan and CMCT, and (c) aerogel prepared from BNCC and CMCT…….....107

Figure 5.5 (a) Schematic crosslinking reaction between BNCC and CMCT, (b) cartoon for the formation of hydrogel…….……107

Figure 5.6 Langmuir plot for MB adsorption by BNCC-CMCT in zero salt and 0.1 M NaCl at pH 7.5 and 22 °C…….….109

Figure 5.7 Experimental data and Freundlich isotherm fitting for MB adsorption by BNCC-CMCT in zero salt and 0.1 M NaCl at pH 7.5 and 22 °C……...110

Figure 5.8 Adsorption MB onto BNCC-CMCT aerogel as function of time, and fitting curves to the Langmuir kinetic model, goodness of fit R2 = 0.970. (The initial MB concentration is 240 mg/L, corresponding to n_0 = 1.53, pH 7.5 and T = 22 °C)…….……113

Figure 5.9 Adsorption isotherms of MB adsorption by BNCC-CMCT for various pHs at 22 °C……...114

Figure 5.10 Langmuir plots for MB adsorption by BNCC-CMCT for various pHs at 22 °C…115

Figure 5.11 Adsorption of MB onto BNCC-CMCT aerogel over a few successive adsorption and desorption cycles. (The initial concentration of MB solution is 50 mg/L at 22 °C)……..116

List of abbreviation and symbols

ADH	adipic acid dihydrazide
AFM	atomic force microscopy
AGU	anhydroglucose units
ATR	attenuated total reflectance
BNA	polyoxyethylene(9)-nonylphenyl ether
BNCC	bifunctional nanocrystalline cellulose
CDAMC	cationic dialdehyde modified cellulose
C.I.	crystalline index
CMC	carboxymethylation cellulose
CMCT	carboxymethylated chitosan

CNC	cellulose nanocrystals
CNCC	cationic nanocrystalline cellulose
CNF	cellulose nanofibrils
CNT	carbon nanotube
CTAB	cetyltetramethylammoniumbromide
DAC	dialdehyde cellulose
DAMC	dialdehyde modified cellulose
DCC	dicarboxylated cellulose
DLS	dynamic light scattering
DMA	dimethyl acetamide
DMF	dimethyl formamide
DP	degree of polymerization
DWL	derivative weight loss
EDC	N-(3-dimethylaminopropyl)-N'-ethylcarbodiimide hydrochloride
EDTA	ethylenediaminetetraacetic acid
ENCC	electrosterically stabilized nanocrystalline cellulose
EPTMAC	epoxypropyltrimethylammonium chloride
ESA	electrokinetic-sonic-amplitude
FESEM	field-emission scanning electron microscopy
FI	flocculation index
FTIR	Fourier transform infrared spectra
GPC	gel permeation chromatography
GT	Girard's reagent T (2-hydrazinyl-2-oxoethyl)-trimethylazanium chloride
HENCC	hydrolyzed electrosterically stabilized nanocrystalline cellulose
HENCC-AK	hydrolyzed electrosterically stabilized nanocrystalline cellulose with alkyne group
HENCC-AZ	hydrolyzed electrosterically stabilized nanocrystalline

	cellulose with azide group
MB	methylene blue
MW	molecular weight
MWCO	molecular weight cut-off
NCMC	N-carboxymethyl chitosan
NCC	nanocrystalline cellulose
NFC	nanofibrillar cellulose
NMR	nuclear magnetic resonance spectroscopy
NOCMC	N,O-carboxymethyl chitosan
OCMC	O-carboxymethyl chitosan
PDA	photometric dispersion analysis
SEM	scanning electron microscopy
SNCC	sterically stabilized nanocrystalline cellulose
TEM	transmission electron microscopy
TEMPO	2,2,6,6-tetramethylpiperidiny-1-oxyl
TGA	thermogravimetric analysis
TOSS	total suppression of spinning sidebands
UV-vis	ultraviolet-visible spectroscopy
XPS	x-ray photoelectron spectroscopy
XRD	x-ray diffraction
χ	Flory-Huggins parameter
χ^c	critical Flory-Huggins parameter
$[\eta]$	intrinsic viscosity
η_0	medium viscosity
C_0	initial concentrations
Ce	equilibrium concentrations
C_t	concentration at time t
m	weight

V	volume
K	equilibrium constant
K_F	constant for Freundlich isotherm
Γ_e	amount of dye adsorbed for one gram of adsorbent
Γ_t	amount of dye adsorbed for one gram of adsorbent at time t
Γ_m	maximum adsorption capacity
ε	porosity
ρ	density
θ	fractional coverage
τ_{ads}	characteristic time of adsorption
τ_{des}	characteristic time of desorption
k_{ads}	adsorption rate constant
k_{des}	desorption rate constant
x	mean square displacement
D	diffusion coefficient
k	Boltzmann constant

Chapter 1. Introduction

1.1 Cellulose

Cellulose is the most abundant and almost inexhaustible polymer on earth [1]. Cellulose, the main constituent of the plant cell wall, was first named by the French chemist Anselme Payen in 1838, who also determined that its molecular formula was $(C_6H_{10}O_5)_n$, by using elemental analysis [2]. Cellulose is isolated mainly from higher plants; for example, the mass fraction of cellulose in wood is 40 - 50%, in flax 80%, and in cotton 90% [3]. Cellulose is also isolated from marine plants (such as algae) [4], sea creatures (such as tunicate) [5], and bacteria (such as acetobacter xylnium or cyanobacteria) [6, 7]. Cellulose is naturally reproducible and thus is considered as a renewable resource.

Cellulose is classified as a carbohydrate. The polymeric structure of cellulose was determined by the German chemist Hermann Staudinger in 1920. Cellulose consists of repeating cellobiose, which comprises two anhydroglucose units (AGU) joined through a covalent β-1,4 glycosidic linkage between the C1 anomeric carbon and the C4 oxygen atom [8]. Every second AGU ring is rotated 180˚ in the plane in order to obtain the preferred bond angles of the acetal oxygen bridges, in order to from a sterically stable structure [9]. The cellulose chain is not directionally symmetric, and has a hemiacetal unit on one end (the reducing end) and a pendant hydroxyl group on the other end (the non-reducing end) as shown in Figure 1. 1.

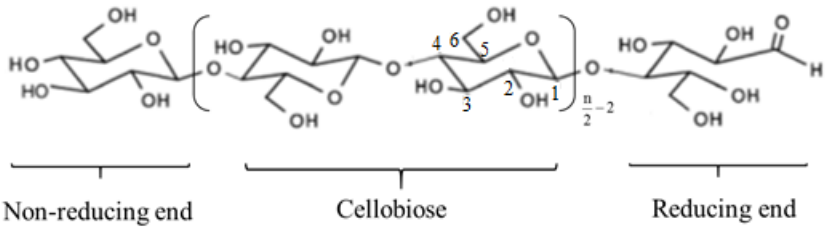

Figure 1.1 Molecular structure of cellulose. The numbering of the carbon atoms in a glucose unit is shown, n is the degree of polymerization (DP), based on the glucose repeat unit.

The length of a cellulose chain is expressed in the number of constituent AGU or degree of polymerization (DP), which is dependent on the origin and treatment of the raw material. For example, the DP values for wood typically vary from 300 to 3300, for raw cotton they are in the range of 10000 -15000, and bacteria cellulose has DP values ranging from 2500 to 6000 [10]. The

biosynthesis of cellulose does not produce isolated individual cellulose molecules, but assembled units which are called elementary fibrils. Subsequently these elementary fibrils are aggregated, resulting in the formation of microfibrils with a diameter varying from 4 to 35 nm, depending on the source of cellulose. Finally these microfibrils are assembled into cellulose fibers [11]. The intra- and intermolecular hydrogen bonds and van der Waals interactions make cellulose a relatively stable polymer, which does not readily dissolve in water and many other common solvents. However, the dislocation of cellulose chains results in the formation of defects or amorphous regions. On the other hand, the tight packing of cellulose chains leads to the formation of crystalline regions which are stabilized by a strong intra- and intermolecular hydrogen-bonded network [12]. The hydrogen-bonded network and molecular orientation in cellulose depends on the original source and treatments, which leads to the formation of cellulose allomorphs. Currently six allomorphs of cellulose have been identified, namely, I, II, III_I, III_{II}, IV_I and IV_{II}. Among them, I, III_I and IV_I have parallel chain packing, while II, III_{II} and IV_{II} have antiparallel chain packing [13]. The term “parallel” means that all the cellulose chains are arranged with the 1-to-4 linkage point in the same direction, and “antiparallel” describes that cellulose chains are alternately stacking between different hydrogen bonded planes. Native cellulose is typically cellulose-I according to its crystal form. This cellulose-I crystal form comprises two types of allomorphs, namely cellulose Iα (a monoclinic unit cell) and Iβ (a triclinic unit cell) [14]. The ratio of these two allomorphs varies depending on the original source. For example bacterial cellulose is rich in the Iα form, while cellulose from cotton and tunicate is mainly in the Iβ form [15]. Cellulose II can be obtained by chemical regeneration or mercerization of cellulose I. Compared to the parallel up chain arrangement in cellulose I, the chains in cellulose II are in an antiparallel arrangement, yielding a thermodynamically more stable structure [16]. III_I and III_{II} are produced by exposing cellulose I or II to ammonia or various amines upon removal of the swelling agent [17]. Cellulose IV_I and IV_{II} can be obtained by heating cellulose III_I or III_{II} up to 260 °C in glycerol [18].

Historically, cellulose has been used by mankind in the form of wood and other plant fibers (such as cotton, flax) as an energy source, and material for buildings, paper making and clothing for thousands of years. Industrially, for the past nearly 150 years, cellulose has been used as a raw chemical material for the preparation of various products. Milestones on this pathway were the discovery of cellulose nitrate by a reaction of cellulose with nitric acid by Schönbein in 1846.

Subsequently an industrial scale process based on this reaction to produce “celluloid”, the very first thermoplastic polymer material form cellulose, was developed by the Hyatt Manufacturing Company in 1870 [19]. A large range of various products based on cellulose from wood are being produced since the chemical modification of cellulose has been realized on an industrial scale. The first example was the preparation of regenerated cellulose filaments by spinning a cellulose solution, in which cellulose is dissolved in a solvent of cuprammonium hydroxide $[Cu(NH_3)_4](OH)_2$ formed by mixing of copper hydroxide and aqueous ammonia. This development was followed by the viscose process, currently the most important large-scale technical process for producing rayon fibers and filaments. The large-scale production of cellulose esters and ethers have opened up many novel applications of cellulose such as coatings, membranes, films, building materials, pharmaceuticals and food products [2]. From today’s perspective, cellulose is a very important source of raw material for the increasing demand for renewable and environmentally friendly materials.

1.2 Nanocellulose

Nanotechnology is defined as the manipulation of matter with at least one dimension in the range of 1 to 100 nm. Recently nanotechnology has attracted huge attention in many research areas due to the unique chemical and physical properties of nanomaterials. The combination of cellulose and nanotechnology has opened up many opportunities in cellulose research and in the forest industry. Nanocellulose is a term referring to nano-structured cellulosic materials with at least one dimension in the nanometer range [20]. Currently, the preparation or isolation of cellulose nanoparticles is generating a lot of activity, since they provide the necessary starting materials for research on cellulose nanomaterials. Based on their dimensions, nanocelluloses may be classified into two major subcategories, namely nanocrystalline cellulose (NCC) also called cellulose nanocrystals (CNC) and nanofibrillar cellulose (NFC) also called cellulose nanofibrils (CNF), respectively.

1.2.1 Nanocrystalline cellulose

The history of discovery of nanocrystalline cellulose goes back to almost seventy years ago. In 1947, Nickerson and Habrle reported that during the hydrolysis of cellulosic fibers with aqueous hydrochloric and sulfuric acids at boiling temperatures, the disordered intercrystalline chain

network appears to be attacked first, while the hydrolysis of the crystallite surface appears to be limited [21]. This observation leads to the first report on the preparation of cellulose micelles by Rånby in the year 1949 in Sweden, who obtained a type of cellulose colloidal suspension from the degradation of cellulose fibers by using sulfuric acid hydrolysis [22]. Dried needle-shaped cellulose nanoparticles were observed for the first time, using transmission electron microscopy (TEM) [23]. These nanoparticles have the same crystalline structure as the original cellulose fibers, as concluded from X-ray diffraction [24]. Later the conditions of the acid hydrolysis procedure were further optimized in Canada by Gray and his colleagues [25, 26].

In an acid hydrolysis treatment, amorphous regions of cellulose are preferentially hydrolyzed and removed while crystalline regions have a higher resistance to acid hydrolysis and remain intact, thus cellulose rod-like nanocrystals are released. The ratio between acid and cellulose, and the reaction temperature and time are important parameters that affect the formation of NCC. NCC has been prepared from several sources of cellulose, such as bleached softwood pulp [27], bleached hardwood pulp [28], cotton [29], tunicates [30, 31], bacterial cellulose [32, 33], ramie [34], sisal [35]. Examples of a few NCC obtained from various sources are shown in Figure 1.2.

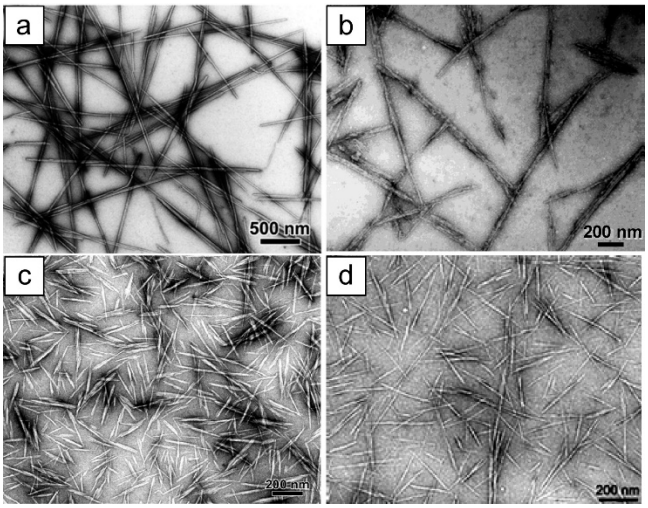

Figure 1.2 TEM images of dried dispersion of cellulose nanocrystals derived from (a) tunicate (b) bacterial (c) ramie, and (d) sisal (Adapted with permission from ref. [8]. Copyright 2010 American Chemical Society)

Sulfuric acid has been extensively used for the preparation of NCC. A typical concentration is about 64% or 65% by weight, the temperature can range from room temperature up to 70 °C and the corresponding hydrolysis time can vary from 30 min to overnight, depending on the

temperature. Prolongation of the hydrolysis time or increasing the temperature results in a decrease in the nanocrystal length and an increase in the surface charge [28, 29]. Sulfuric acid reacts with the surface hydroxyl groups of cellulose to yield negatively charged sulfate esters which electrostatically stabilize NCC and promote the dispersibility of NCC in water. However, the thermostability of NCC decreases with the introduction of charged sulfate half-ester groups [32].

Other types of acid also have been used to prepare NCC. Phosphoric acid hydrolysis of cellulose yields NCC with negatively charged phosphate groups, which disperse well in polar solvents and which have a much higher thermal stability than sulfonated NCC [36]. Ammonium persulfate oxidation can also produce NCC, but with carboxylic acid groups on the surface providing electrostatic stability [37]. NCCs prepared by hydrolysis in hydrochloric acid [38] or hydrobromic acid [39], have a limited dispersion ability, due to the absence of any charged groups.

The morphological properties of NCC are usually investigated by various microscopics techniques, such as atomic force microscopy (AFM) and transmission electron microscopy (TEM) [40]. With AFM one can obtain surface topography of NCC under ambient conditions at length scales down to the ångström level. However, AFM topography may show larger cross-sectional profiles than expected, due to artifacts from tip-broadening. TEM images need be taken under high vacuum conditions, and usually require negative staining of samples. The dimensions of NCC from different cellulose sources and obtained with these two techniques vary widely, depending on the source of the cellulose material and the hydrolysis conditions [8]. For example, NCC from wood are 3 - 5 nm in width and 100 - 200 nm in length, and NCC from cotton are 5 - 10 nm in width and 100 - 300 nm long, while NCC from for tunicate are 10 - 20 nm in width and 500 - 2000 nm long, and NCC from bacterial source are 10 - 50 nm in width and 100 - 1000 nm in length.

Owing to their high aspect ratio, large surface area of several hundred square meters per gram and high strength (theory prediction elastic modulus of about 138 GPa, comparable to that of steel) [41], NCC have potential applications in reinforcing composites. Another interesting observation of NCC is that NCC in aqueous suspensions above a critical concentration align spontaneously in a specific pattern. NCC can self-assemble to give a liquid-crystalline chiral nematic phase, with unique optical properties [42]. This extends the use of NCC to additional applications.

In order to improve the surface chemical properties of NCC, or increase its dispersibility in nonpolar solvents or in composites to improve mechanical properties of the composites, NCC can be modified in two major ways: (i) noncovalent surface modifications via adsorption of surfactants (or polymers) on NCC, such as phosphoric ester of polyoxyethylene(9)-nonylphenyl ether (BNA) [43] or cetyltetramethylammoniumbromide (CTAB) [44]; (ii) due to the many hydroxyl groups at the surface of NCC, various molecules can be covalently attached to NCC via different chemical reactions with hydroxyl groups, such as reacting with carboxylic acid halides create ester linkages, epoxides create ether linkages , while chlorosilanes create an oligomeric silylated layer [45].

1.2.2 Electrosterically stabilized NCC

In addition to the preparation of NCC by acid hydrolysis, a new method was developed by the van de Ven group in 2011[46, 47], by which it is possible to introduce large amount of negatively charged carboxyl groups onto cellulose fibers and easily separate them into nanosized rod-like particles by purely chemical reactions, without any extensive strong acid hydrolysis and/or mechanical treatment. This method contains three steps: (i) periodate oxidation selectively oxidizing a certain fraction of C2 and C3 hydroxyl groups to 2,3-dialdehyde units on the cellulose chain; (ii) conversion of the dialdehyde groups to dicarboxyl groups by chlorite oxidation, typically up to 2.5 mmol/g of charge groups; (iii) converting primary hydroxyl groups on C6 to carboxyl groups by TEMPO-mediated oxidation with a total content of charge groups of up to 3.5 mmol/g. The principle of periodate and chlorite reaction will be described in Section 1.3.1 of this chapter. The NCC produced in this way has similar dimensions to NCC made by acid hydrolysis but has a much larger charge density, exceeding the theoretical maximum for NCC, implying that a large number of di- and tricarboxylated cellulose chains are protruding from their surface. This form of NCC is referred to as electrosterically stabilized NCC (ENCC). Tejado et al. found that the isolation of cellulose nanofibers can be achieved almost in the absence of any mechanical energy if the charge density introduced by oxidation is higher than 3 mmol/g. Surpassing this charge density leads to solubilisation of the amorphous domains and to a spontaneous disintegration of cellulose fibers [48]. The oxidation method has been modified to avoid the TEMPO-mediated oxidation step in 2012 [49], producing ENCC with a charge content between 3.5 and 6.5 mmol/g by sequential periodate-chlorite oxidation. The products from the oxidized

cellulose were separated into three different fractions (including ENCC and soluble dicarboxylated cellulose (DCC)) by ethanol addition and centrifugation. ENCC prepared in this way also has rod-like shape. A typical AFM image of ENCC with a charge density of about 6.5 mmol/g is shown in Figure 1.3, which shows particles with a width of about 13 nm and a length of about 120 - 200 nm. This new type of ENCC opens up a way to produce highly charged NCC and has a potential for further modification or crosslinking.

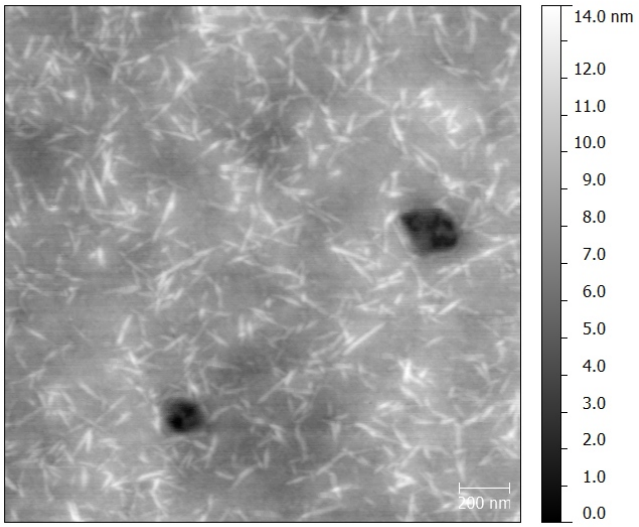

Figure 1.3 AFM image for ENCC with charge density of 6.6 mmol/g. (Adapted with permission from ref. [49]. Copyright 2013 Springer)

The properties of NCC and ENCC were compared by characterization based on measurements of the electrokinetic-sonic-amplitude and acoustic attenuation over a wide range of pH and ionic strength [50], the results show that ENCC exhibits superior colloidal stability via an electrosteric stabilization. ENCC disperse at ionic strengths up to at least 200 mmol /L adjusted by adding KCl, while NCC dispersions become a gel at KCl concentrations greater than about 25 mmol /L. The study of the intrinsic viscosity of aqueous suspensions of ENCC as a function of pH and ionic strength shows that low pH or high ionic strength reduces the ENCC to rigid rod-like particles while a polyelectrolyte-like behavior is observed for ENCC suspension around pH 7 and at low ionic strength; the large values for the relative viscosity and the intrinsic viscosity of ENCC are also observed at pH 7, suggesting that the charges are more likely to be present on the protruding chains of the ENCC than on the crystalline part [51].

Although ENCC is a very recently discovered nanomaterial, it already attracted a lot of attention and showed its advantages in various applications. Flexible transparent films can be fabricated from ENCC suspension by vacuum filtration; these films show high tensile strength and a low water vapor transmission rate, opening up potential applications in biodegradable packaging and other high technology products [47].

Duo to the highly negatively charged DCC chains protruding from ENCC and its biorenewability, ENCC becomes a promising candidate for the removal of heavy metal ions in wastewater treatment [52]. ENCC scavenges copper ions by different mechanisms depending on the ion concentration. At low concentration of Cu^{2+} ions, head-to-head aggregation of ENCC occurs. With increasing the concentration of Cu^{2+} ions, raftlike aggregates form due to the charge neutralization. The copper removal capacity is about 185 mg/g at pH 4, which places ENCC among adsorbents with a very high copper removal capacity.

Compared to the acid hydrolysis method of preparation which offers little flexibility for controlling the surface charge of NCC, the charge on ENCC is tunable either by adjusting the periodate and/or chlorite oxidation levels in the preparation step or by gradually cutting off the protruding DCC chains on ENCC by moderate hydrolysis. ENCC are promising candidates as nanocarriers in nanomedicine and biotechnology [53]. A high surface carboxyl content on ENCC allowed for facile conjugation of fluorophores to the nanocrystals without compromising its colloidal stability, making them being useful nanoparticles to study the mechanism for cellular uptake [53].

1.2.3 Nanofibrillar cellulose (NFC)

NFC, another type of nanocellulose, is produced from the disintegration of cellulose fibers along their long axis which are bound together by strong hydrogen bonds formed due to the high content of hydroxyl groups on the cellulose chains. The disintegration process includes mechanical disintegration or sometimes in combination with chemical or enzymatic pretreatments. The first work on fibrillation of cellulose fibers into nano- or micro- sized structures by pure mechanical treatment was reported by Herrick et al. [54] and Turbak et al. [55] in 1983. A gel-like suspension of highly fibrillated cellulose was obtained from this treatment, called microfibrillated cellulose (MFC). It is hard to completely separate all the fibers and lots of them still consist of bundles of

fibers; in addition, huge amounts of energy are required during this treatment. An improved mechanical treatment was developed by Nakagaito in 2005 [56]. By using a disk refiner, the pulp-water mixture was forced through a gap repeatly between rotor and stator disks at high pressure, and much more homogenous nanosized fibers with width between 20 - 100 nm and length of a few micrometers were obtained in this treatment, though the energy consumption was still high.

In order to reduce the energy consumption during the disintegration of cellulose fibers into nanosized structures, chemical or enzymatic pretreatments are applied on cellulose prior to the mechanical disintegration. One of the major chemical pretreatments is TEMPO (2,2,6,6-tetramethylpiperidine-1-oxyl)-mediated oxidation. TEMPO is a water-soluble and highly stable nitroxyl radical compound. The use of TEMPO for the selective oxidation of primary alcohols was first demonstrated by Semmelhack et al [57]. The proposed mechanism of TEMPO-mediated oxidation is presented in Figure 1.4 [58], which shows that the primary hydroxyl groups are oxidized to aldehyde groups by nitrosonium ions, which are generated from TEMPO by the primary oxidant; at the same time, the nitrosonium ions are reduced to hydroxylamine molecules, which each will react with one nitrosonium ion to regenerate two TEMPO radicals. Several papers have reported the applications of TEMPO-mediated oxidation of carbohydrates. De Nooy et al first applied the TEMPO-mediated oxidation to water soluble polysaccharides [59], such as starch or inulin, at alkaline conditions (pH 9 - 11) with NaClO and NaBr as a primary oxidant and co-oxidant, respectively. NaBr generated the more reactive hydrobromite (-OBr) molecules which could accelerate the reaction.

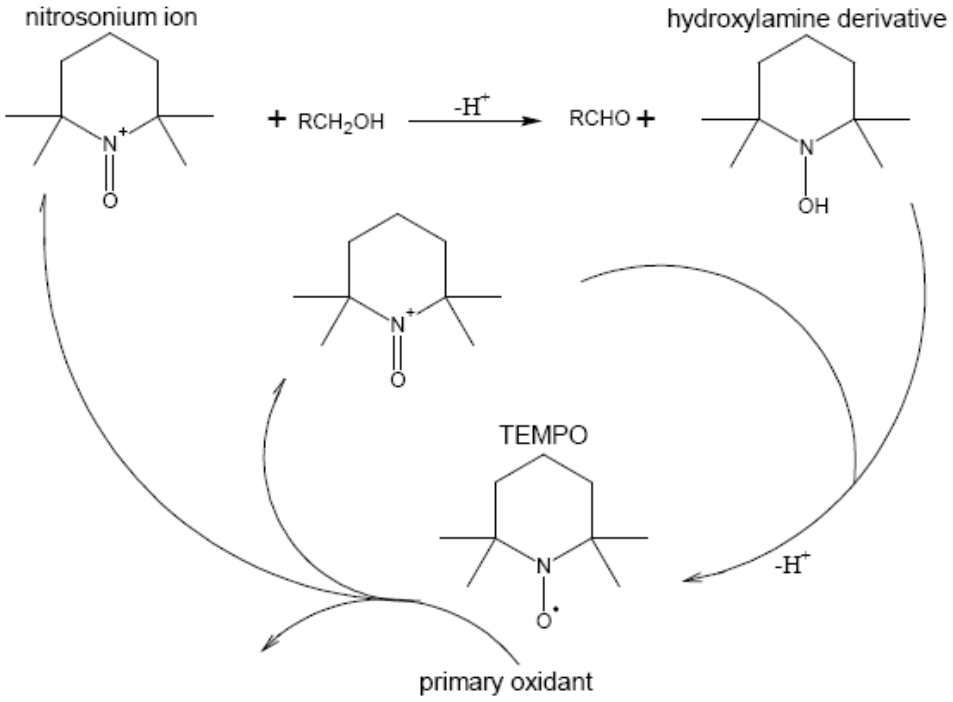

Figure 1.4 Schematics of TEMPO-mediated oxidation mechanism of primary alcohols in a mildly alkaline environment. (Adapted with permission from ref. [58]. Copyright 2004, Plenum Publishing Corporation)

Saito and Isogai investigated the TEMPO/NaClO/NaBr system oxidation of cellulose [60, 61]. Hydroxyl groups on C-6 of cellulose were selectively converted to aldehyde and carboxyl groups on crystal surfaces and in amorphous regions of cellulose. However, a great depolymerization of cellulose by β-elimination occurred in this system. Then the oxidized fibers were homogenized with a Waring Blendor, and NFC with a few nanometers in width were produced (Figure 1.5 (a)). Since the degree of polymerization is an important factor for the strength and flexibility of cellulose fibers [62], in order to maintain the degree of polymerization of cellulose during the TEMPO-mediated oxidation, Saito et al. developed a new oxidation system with TEMPO/NaClO/ $NaClO_2$ which works under neutral or weak acid conditions [63]. The proposed mechanism assumes that NaClO oxidizes TEMPO to nitrosonium ions, which can quickly oxidize the primary hydroxyl groups to aldehyde groups under neutral or weak acid conditions, in the process being reduced to hydroxylamine; the aldehyde is then oxidized to carboxyl by the primary oxidant $NaClO_2$, which is reduced to regenerate NaClO; the hydroxylamine is oxidized to regenerate the nitrosonium ion again by NaClO. Then mechanical disintegration was applied

on the oxidized cellulose fibers by a domestic blender and an ultrasonic homogenizer. Individual nanosized cellulose fibers with 5 nm in width and at least 2 μm in length were obtained (Figure 1.5 (b)).

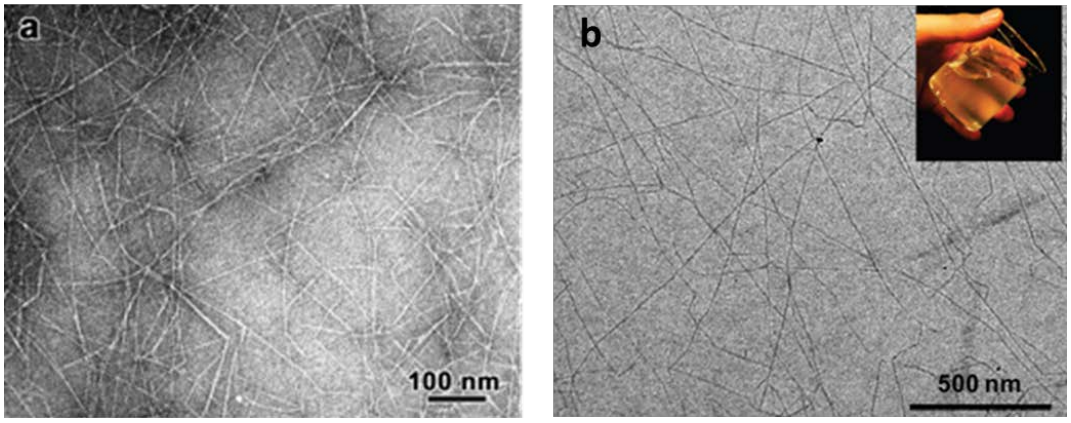

Figure 1.5 (a) TEM image of NFC from TEMPO/NaClO/NaBr system oxidation (Adapted with permission from ref. [61]. Copyright 2006 American Chemical Society), (b) TEM image of NFC from TEMPO/NaClO/$NaClO_2$ system oxidation, inset shows the corresponding highly viscous and transparent NFC dispersion at 0.3%. (Adapted with permission from ref. [63]. Copyright 2009 American Chemical Society)

Introducing carboxyl groups onto cellulose fibers by sequential periodate-chlorite oxidation is another efficient chemical pretreatment, which also increased electrostatic repulsion between the fibrillar constituents and resulted in an easier nanofibrillation [64, 65]. After passing the periodate-chlorite oxidized cellulose fibers through a homogenizer, a transparent gel obtained containing nanofibrils with a width of about 25 nm (Figure 1.6), which is much thicker than the NFC obtained from TEMPO-oxidized cellulose, but the required oxidation level and viscosity and transmittance of these nanofibrils were comparable with NFC made from TEMPO-oxidized cellulose [64].

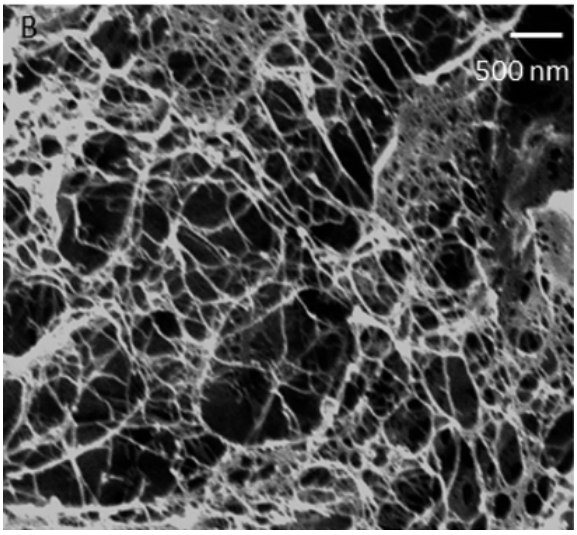

Figure 1.6 Field-Emission Scanning Electron Microscopy (FESEM) image of the nanofibril with a carboxyl content 0.69 mmol/g prepared from sequential periodate-chlorite oxidation followed by mechanical treatment. (Adapted with permission from ref. [64]. Copyright 2012 American Chemical Society)

Enzymatic pretreatment is another option for preparation of NFC. Cellulose enzymes can attack the amorphous regions of cellulose, thus making it possible to nanofibrillate cellulose fibers into nanofiber with reduced energy consumption in the subsequent mechanical disintegration step. Pretreating fibers with a very low enzyme concentration (0.02%) was enough for successful disintegration [66]. Long and well defined cellulose nanofibers with a diameter of about 5 nm (Figure1.7) are obtained by applying the pretreatment of enzymatic hydrolysis on cellulose, followed by a mechanical process, in which the energy consumption was significantly reduced [67]. The combination of enzymatic pretreatment and mechanical shearing on cellulose for preparation of NFC is an environmentally friendly process without any solvents or chemical reactants.

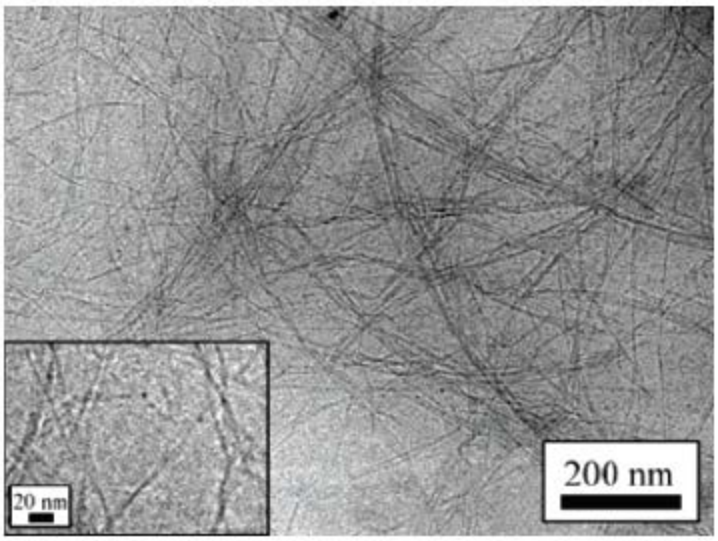

Figure 1.7 TEM image of frozen 2% w/w MFC gel after enzymatic hydrolysis and homogenization processes, showing fibers with a diameter of 5-6 nm and some thicker fibers with diameter of 10-20 nm. (Adapted with permission from ref. [67]. Copyright 2007 American Chemical Society)

1.3 Principles of various reactions

1.3.1 Periodate and chlorite oxidation

Periodate oxidation has been widely used in structural analysis of complex carbohydrates due to it is a highly regiospecific reaction [68], and also been used in the production of oxidized starch in industry [69]. Periodate oxidation of cellulose was first investigated by Jackson and Hudson in 1937 [70]. When applied to cellulose, periodate oxidation cleaves C2-3 bonds of glucose rings and selectively oxidizes C-2 and C-3 vicinal hydroxyl groups to form 2, 3-dialdehyde units along the cellulose chains [71]; the principle of this reaction is shown in Scheme 1.1.

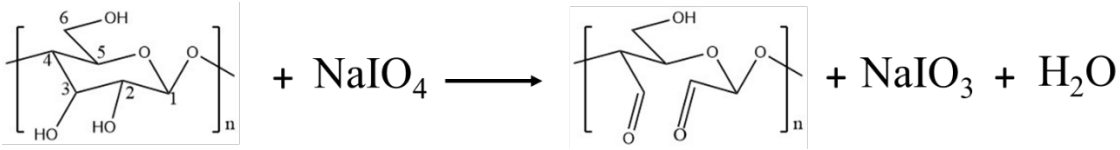

Scheme 1.1. Reaction for periodate oxidation of cellulose.

Application of the periodate reaction with cellulose, however, has been hampered by the complexity arising from the crystalline nature of cellulose. Cellulose from wood fibers usually contains 60 - 70% crystalline regions which have a much lower accessibility than amorphous regions for periodate oxidation. As a result periodate oxidation of cellulose presents problems in

low reactivity and low yield. Periodate oxidation can be improved by adding different types of salt such as LiCl or $ZnCl_2$, which reduce the amount of inter and intra molecular hydrogen bonds between the cellulose and improve the accessibility of cellulose [72]. Another economic method is adding an inert salt (such as NaCl). Due to the presence of nanopores in cellulose fibers, the concentration of periodate ions in the pores can be increased by adding NaCl, which does not participate in the reaction, but shifts the Donnan equilibrium, so the increased concentration of periodate ions in pores results in faster reaction kinetics [73]. Periodate oxidation can also be improved by increasing the reaction temperature, reaction time and NaIO4/cellulose ratio [74].

The dialdehyde modified cellulose (DAMC) can serve as a useful intermediate to produce various products, since dialdehyde groups can be further converted to carboxylic groups [75, 76], primary alcohols [77], or imines [78]. An effective method for oxidation of dialdehyde groups to dicarboxyl groups is by sodium chlorite in an aqueous acid medium [76]. Hydrogen peroxide is added as an inexpensive HClO scavenger, which reduces the cost of sodium chlorite (without H_2O_2, three equivalent chlorite is consumed for the oxidation of one aldehyde group). It also avoids the evolution of toxic chlorine dioxide in a side reaction [79] (Scheme 1.2). The principle of this reaction is shown in Scheme 1.2.

(a) 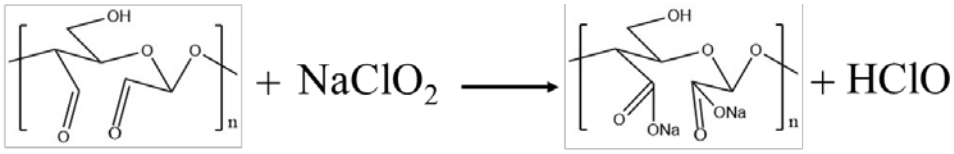

(b) $HClO + H_2O_2 \longrightarrow HCl + H_2O + O_2$

(c) $HClO + 2\,NaClO_2 \longrightarrow 2\,ClO_2 + NaCl + NaOH$

Scheme 1.2. Reactions for (a) conversion of dialdehyde cellulose to dicarboxyl cellulose by chlorite, (b) hydrogen peroxide used as HClO scavenger, and (c) reaction without adding H_2O_2.

1.3.2 Shiff base reaction

The Schiff base reaction was first proposed by the German chemist Hugo Schiff in 1864 [80]. The Schiff base reaction is a nucleophilic addition reaction between a class of compounds containing aldehydes (or ketones) and amino groups, resulting in imine groups which can be represented by the general formula $R_1R_2C=NR_3$, the substituents R_1 and R_2 may be hydrogen, alkyl, aryl, heteroaryl, and the substituent R_3 may be hydrogen, alkyl, aryl, heteroaryl, or metallo (such as Si, Al, B). The reaction is presented in Scheme 1.3 (a). The Schiff base reactions proceed under ambient conditions without requirement of activation and produce only water as a byproduct. They are widely used in many fields, such as biomedicine, organic and analytical chemistry due to their mild reaction conditions and high reaction rates. The Schiff base bond is a dynamic covalent bond [81, 82], which provides extraordinary reversibility for Schiff base with changing pH, as the stability of these bonds decreases as the pH decreases. This feature is preferable especially for the application in biomedicine such as pH-triggered drug release [83]. The Schiff base can be further reduced to form more stable secondary amines by using a weak reductant, such as sodium borohydride ($NaBH_4$) or sodium cyanoborohydride ($NaBH_3CN$) [84].

Schiff base reaction between primary amino and 2,3-dialdehyde cellulose is a facile and useful chemical derivatization procedure to modify cellulose. The reaction is shown in Scheme 1.3 (b). The Schiff base reaction can also be used in the internally crosslinking of dialdehyde cellulose fibers, prior to a hydrophobization treatment with alkylamines, which fiber disintegration [85]. Dialdehyde modified NCC can react with diamine derivative to form amino-functionalized NCC, which can be applied as an adsorbent to remove anionic dyes in solution at acidic conditions, with a very high adsorption capability [86]. Aerogels were also prepared form hydrazide and aldehyde-functionalized NCC via a Schiff base reaction, and these chemically cross-linked NCC aerogels showed enhanced mechanical properties and shape recovery ability compared to previously reported physically cross-linked NCC aerogels [87].

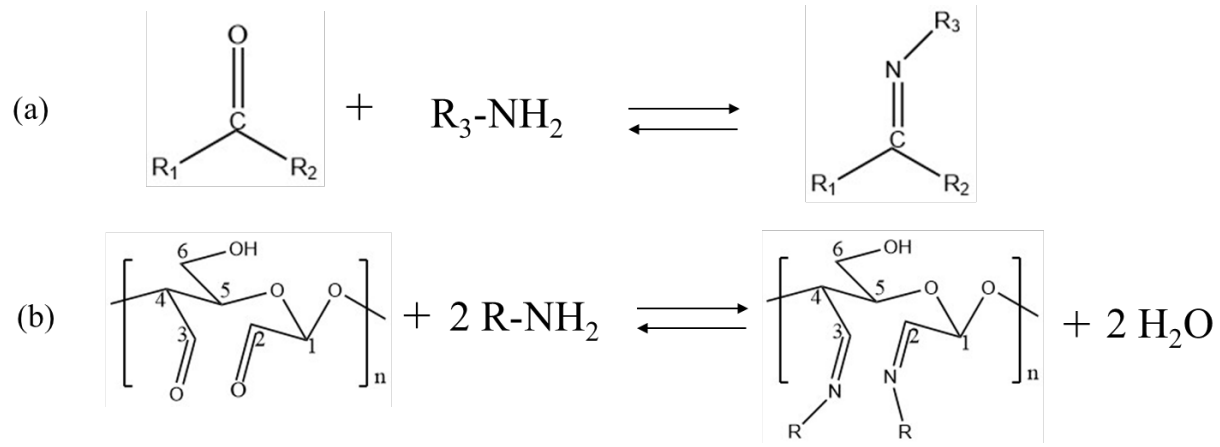

Scheme 1.3 (a) Schematic illustration of Schiff base reaction, (b) Schiff base reaction between primary amino and 2,3-dialdehyde cellulose.

1.3.3 Chitosan and carboxymethylation

Chitosan, a linear cationic copolymer (when pH< 6.5) of 2-amino-2-deoxy-D-glucopyranose and 2-acetamide-2-deoxy-D-glucopyranose linked via β(1→4) bonds, is derived from deacetylation of a natural biopolymer, chitin, which is the third most abundant polysaccharide in the world (after cellulose and hemicellulose) [88] and is mostly obtained from the skeleton of crustaceans such as crabs or shrimps [89]. Chitosan has many distinct properties such as nontoxicity, biodegradability, and biocompatibility, which makes it suitable for various applications, such as in drug delivery [90], tissue engineering [91] and water treatment [92]. However chitosan is soluble only in acidic aqueous solutions below pH 6.5, but not in neutral or alkaline pH due to its very stable crystalline structure arising from strong hydrogen bonds; this poor solubility limits its applications [93]. To improve the solubility of chitosan, several chemical modifications can be applied on the amino, primary hydroxyl and secondary hydroxyl groups of chitosan, such as acylation, etherification, esterification, sulfonation, carboxymethylation and quaternization [94]. Among the water-soluble chitosan derivatives, carboxymethyl chitosan (CMC) form carboxymethylation has been widely studied due to its ease of synthesis and its potential in many applications.

The carboxymethylation of chitosan can be achieved with three types: N-carboxymethyl chitosan (NCMC), N,O-carboxymethyl chitosan (NOCMC), and O-carboxymethyl chitosan (OCMC). The $-NH_2$ group of chitosan unit is reacted with the carbonyl group of glyoxylic acid, followed by the reduction by sodium cyanoborohydride or sodium borohydride to yield N-carboxymethyl chitosan [95]. In our work, we will use chitosan as a green crosslinker by taking advantage of its $-NH_2$

groups participating in the formation of covalent crosslinking bonds, so we prefer to work with OCMC which has free -NH_2 groups. OCMC is prepared in mixed solvents of water and isopropanol in the presence of monochloroacetic acid and sodium hydroxide [96]. Chitosan is swollen in concentrated NaOH, which increases the accessibility of chitosan to chemicals and the reactivity of hydroxyl groups of chitosan. This reaction is usually carried at room temperature or between 0 - 30 ˚C, and the C6-OH group has the highest degree of substitution. The reaction is shown is Scheme 1.4. NOCMC is obtained if this reaction is performed at high temperature such as 60 ˚C [97]. Carboxymethylation has also been applied on cellulose, to produce carboxymethylated cellulose, which is one of the most commonly used cellulose ethers [98], or used in the analysis of the structure of wood cellulose [99].

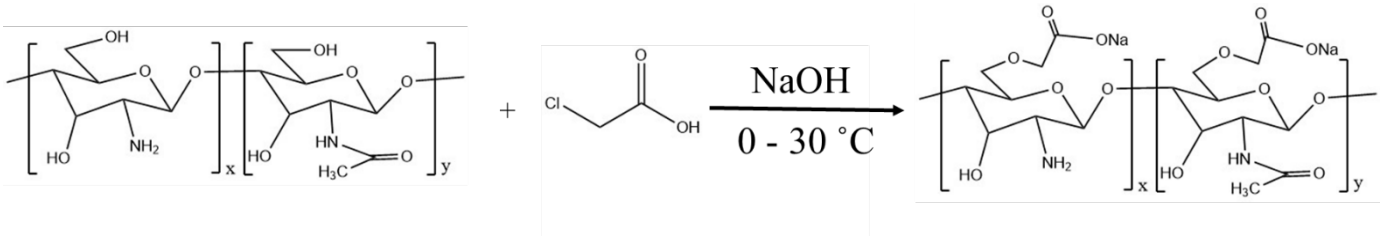

Scheme 1.4 Schematic representation of carboxymethylation reaction of chitosan.

1.3.4 Click Chemistry

Click chemistry is a newly identified class for a set of powerful and selective reactions that form heteroatom linkages, such as cycloaddition reactions, nucleophilic ring-opening reactions, and additions to carbon-carbon multiple bonds [100]. The Huisgen 1,3-dipolar cycloaddition reaction (also called as the azide-alkyne cycloaddition) is one of the most popular click reactions. It was first discovered by Huisgen in 1963, however, the original Huisgen 1,3-cycloaddition reaction proceeds slowly and requires high temperatures and pressures, and produces a mix of 1,4-and 1,5-regioisomers [101]. It was not popular till 2002 when Cu(I) was employed as a catalyst, allowing this reaction to process fast at room temperature [102, 103]. This reaction links together two unsaturated reactants (azides and terminal alkynes) and forms a type of five-membered heterocycle (Scheme 1.5).

The Cu(I) catalyst used in click reactions is not only known to lower the activation barrier, but also promotes the regiospecific formation of 1,4-disubstituted 1,2,3-triazole products [104]. A few of Cu(I) sources, such as CuI or CuOTfC6H6 can be used in this reaction, but the formation of

byproducts usually occurs [103]. To overcome these problems, the Cu(I) catalyst is better to be prepared in situ by reducing copper(II) salts (such as CuSO4) with a reducing agent (such as sodium ascorbate) [102].

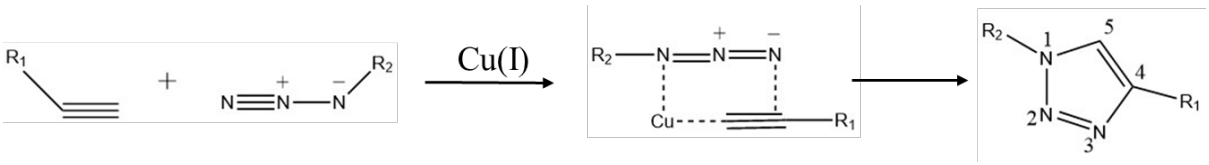

Scheme 1.5 Schematic representation of Cu(I)-catalyzed Huisgen 1,3-cycloaddition reaction.

This azide-alkyne "click" cycloaddition is popular due to its many advantages, such as mild reaction conditions, high yield and selectivity [105]. This reaction not only played an import role in various research fields, such as drug discovery and polymer synthesis [106], but is recently also applied in cellulose research. Cellulose hydrogel can be prepared in aqueous solution though crosslinking by this 1,3-dipolar cycloaddition reaction [107]. A nano-scaled gel, "nanoplatelet gel", was obtained for the first time by the crosslinking of nanocrystalline cellulose (NCC) via the click reaction [108]. This click reaction was also used to modify the surface properties of NCC [109] or nanofibrillar cellulose (NFC) [110] to extend their potential applications.

1.4 Aerogel

Aerogels are highly porous solids made from wet gels in which the liquid phase in the gels has been replaced by a gas (usually is air) [111]. The methods for removing liquid include supercritical drying and freeze-drying. Aerogels exhibit many unique properties, such as low density (can have a density that is only three times that of air), high porosity (usually up to 99%), large surface area, ultralow thermal conductivity, ultralow refractive index and ultralow dielectric constant [112]. Thus aerogels have found wide applications in various fields, such as catalysts, electronics and thermal/acoustic insulations [113]. The most investigated aerogels are traditionally prepared from silica (such as silica dioxide) and several kinds of non-silica inorganic oxides (for example, titanium, tin, or aluminum). However, aerogels based on these material are often brittle and fragile, which limits their applications when mechanical strength is required [112]. Recently, aerogels from synthetic polymers, natural polymers (for example, starch, chitosan and cellulose) [114] and nanoparticles like carbon nanotube (CNT) have been proposed to overcome these problems. Cellulose, especially nanocellulose shows particular promise in the preparation of flexible and

environmentally friendly aerogels due to their high strength, low density, biodegradability and biocompatibility [45]. Nanofibrillar cellulose (NFC) is usually a few micrometers long and possesses crystalline and amorphous regions, making them very flexible and easily to be entangled. Thus such aerogels can be prepared from NFC by simple physical entanglement [115] or chemical cross-linking, which improves their stability in the wet state [116]. The NFC aerogels are flexible, ultralight and highly porous, and have potential applications as green cleaner for oil absorbents [117]. Nanocrystalline cellulose (NCC) is also used to prepare aerogel directly by freeze-drying a NCC suspension [118]. Although NCC is not able to form effective entanglements between rigid nanorods, NCC has enhanced mechanical properties due to their higher crystallinity when compared with NFC, thus NCC can be used as a nanofiller within a polymer matrix to prepare a reinforced aerogel [119]. Recently, an aerogel was also prepared with NCC alone through chemically cross-linking. This "all NCC" aerogel shows good mechanical properties and shape recovery abilities and has the potential use as a superabsorbent and as an oil/water separation material [87].

1.5 Thesis outline and objectives

The aim of the research presented in this thesis was to prepare various multifunctional hairy nanocelluloses and demonstrate their potential applications.

Chapter 2 describes the preparation and characterization of sterically stabilized nanocrystalline cellulose (SNCC) obtained by periodate oxidation of cellulose fibers. Compared with the conventional nanocrystalline cellulose (NCC) prepared from sulfuric acid hydrolysis, SNCC has similar dimensions to NCC but without any charge, it is sterically stabilized by the protruding dialdehyde modified cellulose chains. Several techniques were applied to characterize SNCC and its properties were presented in this chapter.

In Chapter 3, a simple method was developed for the preparation of hairy cationic nanocrystalline cellulose (CNCC). CNCC was produced by periodate oxidation and cationization with (2-hydrazinyl-2-oxoethyl)-trimethylazanium chloride (GT) of cellulose fibers, then followed by a hot

water treatment at 60 °C for half an hour. This is an easy and environmentally friendly method performed under mild aqueous conditions.

Chapter 4 introduced a bottom-up route to a chemically end-to-end assembly of nanocellulose fibers. Electrosterically stabilized nanocrystalline cellulose (ENCC) with shorter dicarboxyl cellulose (DCC) chains can be obtained by a mild hydrolysis of ENCC with HCl, and subsequently the hydrolyzed ENCC (HENCC) was assembled into nanofibers with high aspect ratio by chemically cross-linking HENCC from one end to another by a click reaction or a bioconjugation reaction. End-to-end assembled HENCC nanofibers with a length of more than one μm were obtained. To the best of our knowledge, it is the first chemical assembly of rod-shaped nanocellulose by an end-to-end route in one dimension. It also provides evidence that most of the protruding DCC chains were located on the two ends of ENCC nanorods.

Chapter 5 describes an application of one of those hairy nanocrystalline cellulose. A novel biomaterial-based adsorbent aerogel was prepared by crosslinking bifunctional cellulose nanofibers (BNCC) and carboxymethylated chitosan through a Schiff base reaction. BNCC was obtained from sequential periodate and partially chlorite oxidation on cellulose followed by a hot water treatment. This highly porous and negatively charged aerogel was characterized by various techniques. The adsorption performance of the aerogel was investigated by using a cationic dye, methylene blue, in various conditions.

Chapter 6 summarizes the major contributions of this research work and describes the potential future work and applications for those novel hairy nanocrystalline cellulose.

Appendix 1, 2, and 3 deal with papers in which Han Yang was a co-author.

1.6 References

[1] Kaplan DL. Biopolymers from renewable resources. Berlin: Springer; 1998.

[2] Klemm D, Heublein B, Fink HP, Bohn A. Cellulose: Fascinating biopolymer and sustainable raw material. Angew Chem Int Edit 2005;44:3358-93.

[3] Stephen AM, Philips GO, Williams PA. Polysaccharides and their applications. 2 ed. Boca Raton, FL: Taylor & Francis Group; 2006.

[4] Brown RM. The biosynthesis of cellulose. J Macromol Sci Pure 1996;A33:1345-73.

[5] Belton PS, Tanner SF, Cartier N, Chanzy H. High-resolution solid-state C-13 nuclear magnetic-resonance spectroscopy of tunicin, an animal cellulose. Macromolecules 1989;22:1615-7.

[6] Ross P, Mayer R, Benziman M. Cellulose biosynthesis and function in bacteria. Microbiol Rev 1991;55:35-58.

[7] Nobles DR, Romanovicz DK, Brown RM. Cellulose in cyanobacteria. Origin of vascular plant cellulose synthase? Plant Physiol 2001;127:529-42.

[8] Habibi Y, Lucia LA, Rojas OJ. Cellulose nanocrystals: chemistry, self-assembly, and applications. Chem Rev 2010;110:3479-500.

[9] Hon DNS. Cellulose - a random walk along its historical path. Cellulose 1994;1:1-25.

[10] Wüstenberg T. Cellulose and cellulose derivatives in the food industry : fundamentals and applications. Weinheim : Wiley-VCH 2014:pp 95-8.

[11] Klemm D, Schmauder, H.-P., Heinze, T. Cellulose. Biopolymers Online 2005;6:275-87.

[12] Rowland SP, Roberts EJ. The nature of accessible surfaces in the microstructure of cotton cellulose. Journal of Polymer Science Part A-1: Polymer Chemistry 1972;10:2447-61.

[13] Sarko A. Recent X-ray crystallographic studies of celluloses. Cellulose: Structure, Modification and Hydrolysis 1986.

[14] Atalla RH, Vanderhart DL. Native cellulose: A composite of two distinct crystalline forms. Science 1984;223:283-5.

[15] Atalla RH, VanderHart DL. The role of solid state 13C NMR spectroscopy in studies of the nature of native celluloses. Solid State Nuclear Magnetic Resonance 1999;15:1-19.

[16] Kolpak FJ, Blackwell J. Determination of the structure of cellulose II. Macromolecules 1976;9:273-8.

[17] Marrinan HJ, Mann J. Infrared spectra of the crystalline modifications of cellulose. Journal of Polymer Science 1956;21:301-11.

[18] Gardiner ES, Sarko A. Packing analysis of carbohydrates and polysaccharides. 16. The crystal structures of celluloses IVI and IVII. Canadian Journal of Chemistry 1985;63:173-80.
[19] K. Balser LH, T. Eichler, M. Wendel, A.-J. Astheimer. Ullmann's encyclopedia of industrial chemistry. VCH, Weinheim 1986;Vol. A5 pp 419-59.
[20] Klemm D, Kramer F, Moritz S, Lindstrom T, Ankerfors M, Gray D, et al. Nanocelluloses: A new family of nature-based materials. Angew Chem Int Edit 2011;50:5438-66.
[21] Nickerson RF, Habrle JA. Cellulose intercrystalline structure. Industrial & Engineering Chemistry 1947;39:1507-12.
[22] Rånby BG, Banderet A, Sillén LG. Aqueous colloidal solutions of cellulose micelles. 1949.
[23] Mukherjee SM, Sikorski J, Woods HJ. Electron-microscopy of degraded cellulose fibres. Journal of the Textile Institute Transactions 1952;43:T196-T201.
[24] Mukherjee SM, Woods HJ. X-ray and electron microscope studies of the degradation of cellulose by sulphuric acid. Biochimica et Biophysica Acta 1953;10:499-511.
[25] Hanley SJ, Giasson J, Revol JF, Gray DG. Atomic force microscopy of cellulose microfibrils - comparison with transmission electron-microscopy. Polymer 1992;33:4639-42.
[26] Dong XM, Kimura T, Revol J-F, Gray DG. Effects of ionic strength on the isotropic−chiral nematic phase transition of suspensions of cellulose crystallites. Langmuir 1996;12:2076-82.
[27] Araki J, Wada M, Kuga S, Okano T. Influence of surface charge on viscosity behavior of cellulose microcrystal suspension. J Wood Sci 1999;45:258-61.
[28] Beck-Candanedo S, Roman M, Gray DG. Effect of reaction conditions on the properties and behavior of wood cellulose nanocrystal suspensions. Biomacromolecules 2005;6:1048-54.
[29] Dong X, Revol J-F, Gray D. Effect of microcrystallite preparation conditions on the formation of colloid crystals of cellulose. Cellulose 1998;5:19-32.
[30] Anglès MN, Dufresne A. Plasticized starch/tunicin whiskers nanocomposites. 1. Structural analysis. Macromolecules 2000;33:8344-53.
[31] Elazzouzi-Hafraoui S, Nishiyama Y, Putaux J-L, Heux L, Dubreuil F, Rochas C. The shape and size distribution of crystalline nanoparticles prepared by acid hydrolysis of native cellulose. Biomacromolecules 2008;9:57-65.
[32] Roman M, Winter WT. Effect of sulfate groups from sulfuric acid hydrolysis on the thermal degradation behavior of bacterial cellulose. Biomacromolecules 2004;5:1671-7.

[33] Hirai A, Inui O, Horii F, Tsuji M. Phase separation behavior in aqueous suspensions of bacterial cellulose nanocrystals prepared by sulfuric acid treatment. Langmuir 2009;25:497-502.
[34] Habibi Y, Goffin A-L, Schiltz N, Duquesne E, Dubois P, Dufresne A. Bionanocomposites based on poly(ε-caprolactone)-grafted cellulose nanocrystals by ring-opening polymerization. Journal of Materials Chemistry 2008;18:5002-10.
[35] Garcia de Rodriguez NL, Thielemans W, Dufresne A. Sisal cellulose whiskers reinforced polyvinyl acetate nanocomposites. Cellulose 2006;13:261-70.
[36] Camarero Espinosa S, Kuhnt T, Foster EJ, Weder C. Isolation of thermally stable cellulose nanocrystals by phosphoric acid hydrolysis. Biomacromolecules 2013;14:1223-30.
[37] Leung ACWH, Sabahudin; Lam, Edmond; Liu, Yali;, Male KBM, Khaled A.; Luong, John H. T. Characteristics and properties of carboxylated cellulose nanocrystals prepared from a novel one-step procedure. Small 2011;7:302-5.
[38] Yu H, Qin Z, Liang B, Liu N, Zhou Z, Chen L. Facile extraction of thermally stable cellulose nanocrystals with a high yield of 93% through hydrochloric acid hydrolysis under hydrothermal conditions. J Mater Chem A 2013;1:3938-44.
[39] Feese E, Sadeghifar H, Gracz HS, Argyropoulos DS, Ghiladi RA. Photobactericidal porphyrin-cellulose nanocrystals: synthesis, characterization, and antimicrobial properties. Biomacromolecules 2011;12:3528-39.
[40] Hanley S, Revol J-F, Godbout L, Gray D. Atomic force microscopy and transmission electron microscopy of cellulose from Micrasterias denticulata; evidence for a chiral helical microfibril twist. Cellulose 1997;4:209-20.
[41] Grunert M, Winter W. Nanocomposites of cellulose acetate butyrate reinforced with cellulose nanocrystals. Journal of Polymers and the Environment 2002;10:27-30.
[42] Revol JF, Bradford H, Giasson J, Marchessault RH, Gray DG. Helicoidal self-ordering of cellulose microfibrils in aqueous suspension. International Journal of Biological Macromolecules 1992;14:170-2.
[43] Heux L, Chauve G, Bonini C. Nonflocculating and chiral-nematic self-ordering of cellulose microcrystals suspensions in nonpolar solvents. Langmuir 2000;16:8210-2.
[44] Padalkar S, Capadona JR, Rowan SJ, Weder C, Won Y-H, Stanciu LA, et al. Natural biopolymers: Novel templates for the synthesis of nanostructures. Langmuir 2010;26:8497-502.

[45] Moon RJ, Martini A, Nairn J, Simonsen J, Youngblood J. Cellulose nanomaterials review: structure, properties and nanocomposites. Chemical Society Reviews 2011;40:3941-94.
[46] van de Ven TGM, Tejado A, Alam MN, Antal M. Novel highly charged non-water soluble cellulose products, includes all types of cellulose nanostructures especially cellulose nanofibers, and method of making them. US Provisional Patent Application 3776923-v3 2011.
[47] Yang H, Tejado A, Alam N, Antal M, van de Ven TGM. Films prepared from electrosterically stabilized nanocrystalline cellulose. Langmuir 2012;28:7834-42.
[48] Tejado A, Alam MN, Antal M, Yang H, van de Ven TGM. Energy requirements for the disintegration of cellulose fibers into cellulose nanofibers. Cellulose 2012;19:831-42.
[49] Yang H, Alam MN, van de Ven TGM. Highly charged nanocrystalline cellulose and dicarboxylated cellulose from periodate and chlorite oxidized cellulose fibers. Cellulose 2013;20:1865-75.
[50] Safari S, Sheikhi A, van de Ven TGM. Electroacoustic characterization of conventional and electrosterically stabilized nanocrystalline celluloses. Journal of Colloid and Interface Science 2014;432:151-7.
[51] Lenfant G, Heuzey MC, van de Ven TGM, Carreau PJ. Intrinsic viscosity of suspensions of electrosterically stabilized nanocrystals of cellulose. Cellulose 2015;22:1109-22.
[52] Sheikhi A, Safari S, Yang H, van de Ven TGM. Copper removal using electrosterically stabilized nanocrystalline cellulose. ACS Applied Materials & Interfaces 2015;7:11301-8.
[53] Hosseinidoust Z, Alam MN, Sim G, Tufenkji N, van de Ven TGM. Cellulose nanocrystals with tunable surface charge for nanomedicine. Nanoscale 2015;7:16647-57.
[54] Herrick FW, Casebier RL, Hamilton JK, Sandberg KR. Microfibrillated cellulose: morphology and accessibility. J Appl Polym Sci, Appl Polym Symp 1983;37:797-813.
[55] Turbak AF, Snyder FW, Sandberg KR. Microfibrillated cellulose, a new cellulose product: properties, uses, and commercial potential. J Appl PolymSci: Appl PolymSymp 1983;37:815-27.
[56] Nakagaito AN, Yano H. Novel high-strength biocomposites based on microfibrillated cellulose having nano-order-unit web-like network structure. Appl Phys A 2005;80:155-9.
[57] Semmelhack MF, Chou CS, Cortes DA. Nitroxyl-mediated electrooxidation of alcohols to aldehydes and ketones. Journal of the American Chemical Society 1983;105:4492-4.
[58] Bragd PL, van Bekkum H, Besemer AC. TEMPO-mediated oxidation of polysaccharides: survey of methods and applications. Top Catal 2004;27:49-66.

[59] de Nooy AEJ, Besemer AC, van Bekkum H. Highly selective tempo mediated oxidation of primary alcohol groups in polysaccharides. Recueil des Travaux Chimiques des Pays-Bas 1994;113:165-6.
[60] Saito T, Isogai A. TEMPO-mediated oxidation of native cellulose. The effect of oxidation conditions on chemical and crystal structures of the water-insoluble fractions. Biomacromolecules 2004;5:1983-9.
[61] Saito T, Nishiyama Y, Putaux J-L, Vignon M, Isogai A. Homogeneous suspensions of individualized microfibrils from TEMPO-catalyzed oxidation of native cellulose. Biomacromolecules 2006;7:1687-91.
[62] Iwamoto S, Nakagaito AN, Yano H. Nano-fibrillation of pulp fibers for the processing of transparent nanocomposites. Appl Phys A 2007;89:461-6.
[63] Saito T, Hirota M, Tamura N, Kimura S, Fukuzumi H, Heux L, et al. Individualization of nano-sized plant cellulose fibrils by direct surface carboxylation using TEMPO catalyst under neutral conditions. Biomacromolecules 2009;10:1992-6.
[64] Liimatainen H, Visanko M, Sirviö JA, Hormi OEO, Niinimaki J. Enhancement of the nanofibrillation of wood cellulose through sequential periodate-chlorite oxidation. Biomacromolecules 2012;13:1592-7.
[65] Kekäläinen K, Liimatainen H, Niinimäki J. Disintegration of periodate–chlorite oxidized hardwood pulp fibres to cellulose microfibrils: kinetics and charge threshold. Cellulose 2014;21:3691-700.
[66] Henriksson M, Henriksson G, Berglund LA, Lindström T. An environmentally friendly method for enzyme-assisted preparation of microfibrillated cellulose (MFC) nanofibers. European Polymer Journal 2007;43:3434-41.
[67] Pääkkö M, Ankerfors M, Kosonen H, Nykänen A, Ahola S, Österberg M, et al. Enzymatic hydrolysis combined with mechanical shearing and high-pressure homogenization for nanoscale cellulose fibrils and strong gels. Biomacromolecules 2007;8:1934-41.
[68] Bruneel D, Schacht E. Chemical modification of pullulan: 1. Periodate oxidation. Polymer 1993;34:2628-32.
[69] Michell JH, Purves CB. Probable structure of a crystalline substance derived from starches oxidized with periodate. Journal of the American Chemical Society 1942;64:585-8.

[70] Jackson EL, Hudson CS. Application of the cleavage type of oxidation by periodic acid to starch and cellulose. Journal of the American Chemical Society 1937;59:2049-50.
[71] Hou QX, Liu W, Liu ZH, Bai LL. Characteristics of wood cellulose fibers treated with periodate and bisulfite. Industrial & Engineering Chemistry Research 2007;46:7830-7.
[72] Sirvio J, Hyvakko U, Liimatainen H, Niinimaki J, Hormi O. Periodate oxidation of cellulose at elevated temperatures using metal salts as cellulose activators. Carbohydrate Polymers 2011;83:1293-7.
[73] Alam MN, Antal M, Tejado A, van de Ven TGM. Salt-induced acceleration of chemical reactions in cellulose nanopores. Cellulose 2012;19:517-22.
[74] Coseri S, Biliuta G, Simionescu BC, Stana-Kleinschek K, Ribitsch V, Harabagiu V. Oxidized cellulose—Survey of the most recent achievements. Carbohydrate Polymers 2013;93:207-15.
[75] Maekawa E, Koshijima T. Preparation and characterization of hydroxamic acid derivative and its metal complexes derived from cellulose. Journal of Applied Polymer Science 1990;40:1601-13.
[76] Hofreiter BT, Wolff IA, Mehltretter CL. Chlorous acid oxidation of periodate oxidized cornstarch. Journal of the American Chemical Society 1957;79:6457-60.
[77] Casu B, Naggi A, Torri G, Allegra G, Meille SV, Cosani A, et al. Stereoregular acyclic polyalcohols and polyacetates from cellulose and amylose. Macromolecules 1985;18:2762-7.
[78] Kim U-J, Kuga S. Reactive interaction of aromatic amines with dialdehyde cellulose gel. Cellulose 2000;7:287-97.
[79] Floor M, Hofsteede LPM, Kieboom APG, van Bekkum H, Greenland WPT, Verhaar LAT. Preparation and calcium complexation of oxidized polysaccharides. II: Hydrogen peroxide as co-reactant in the chlorite oxidation of dialdehyde glucans. Recueil des Travaux Chimiques des Pays-Bas 1989;108:384-92.
[80] Schiff H. Mitteilungen aus dem Universitätslaboratorium in Pisa: Eine neue Reihe organischer Basen. Justus Liebigs Annalen der Chemie 1864;131:118-9.
[81] Lehn J-M, Eliseev AV. Dynamic combinatorial chemistry. Science 2001;291:2331-2.
[82] Rowan SJ, Cantrill SJ, Cousins GRL, Sanders JKM, Stoddart JF. Dynamic covalent chemistry. Angewandte Chemie International Edition 2002;41:898-952.

[83] Tauk L, Schröder AP, Decher G, Giuseppone N. Hierarchical functional gradients of pH-responsive self-assembled monolayers using dynamic covalent chemistry on surfaces. Nat Chem 2009;1:649-56.
[84] Borch RF, Bernstein MD, Durst HD. Cyanohydridoborate anion as a selective reducing agent. Journal of the American Chemical Society 1971;93:2897-904.
[85] Sabzalian Z, Alam M, van de Ven TGM. Hydrophobization and characterization of internally crosslink-reinforced cellulose fibers. Cellulose 2014;21:1381-93.
[86] Jin L, Li W, Xu Q, Sun Q. Amino-functionalized nanocrystalline cellulose as an adsorbent for anionic dyes. Cellulose 2015;22:2443-56.
[87] Yang X, Cranston ED. Chemically cross-linked cellulose nanocrystal aerogels with shape recovery and superabsorbent properties. Chemistry of Materials 2014;26:6016-25.
[88] Mary SK, Sasidharan Pillai PK, Amma DB, Pothen LA, Thomas S. Aging and biodegradation of biocomposites. Handbook of biopolymer-based materials: Wiley-VCH Verlag GmbH & Co. KGaA; 2013. p. 777-99.
[89] Ravi Kumar MNV. A review of chitin and chitosan applications. Reactive and Functional Polymers 2000;46:1-27.
[90] Anitha A, Maya S, Deepa N, Chennazhi KP, Nair SV, Tamura H, et al. Efficient water soluble O-carboxymethyl chitosan nanocarrier for the delivery of curcumin to cancer cells. Carbohydrate Polymers 2011;83:452-61.
[91] Peter M, Ganesh N, Selvamurugan N, Nair SV, Furuike T, Tamura H, et al. Preparation and characterization of chitosan–gelatin/nanohydroxyapatite composite scaffolds for tissue engineering applications. Carbohydrate Polymers 2010;80:687-94.
[92] Crini G. Recent developments in polysaccharide-based materials used as adsorbents in wastewater treatment. Progress in Polymer Science 2005;30:38-70.
[93] Zargar V, Asghari M, Dashti A. A review on chitin and chitosan polymers: structure, chemistry, solubility, derivatives, and applications. ChemBioEng Reviews 2015;2:204-26.
[94] Badawy MEI. Chemical modification of chitosan: synthesis and biological activity of new heterocyclic chitosan derivatives. Polymer International 2008;57:254-61.
[95] Song Q, Zhang Z, Gao J, Ding C. Synthesis and property studies of N-carboxymethyl chitosan. Journal of Applied Polymer Science 2011;119:3282-5.

[96] Chen X-G, Park H-J. Chemical characteristics of O-carboxymethyl chitosans related to the preparation conditions. Carbohydrate Polymers 2003;53:355-9.
[97] Li L, Wang N, Jin X, Deng R, Nie S, Sun L, et al. Biodegradable and injectable in situ cross-linking chitosan-hyaluronic acid based hydrogels for postoperative adhesion prevention. Biomaterials 2014;35:3903-17.
[98] Heinze T, Koschella A. Carboxymethyl ethers of cellulose and starch – A review. Macromolecular Symposia 2005;223:13-40.
[99] Sim G, Alam MN, Godbout L, van de Ven T. Structure of swollen carboxylated cellulose fibers. Cellulose 2014;21:4595-606.
[100] Kolb HC, Finn MG, Sharpless KB. Click chemistry: Diverse chemical function from a few good reactions. Angewandte Chemie International Edition 2001;40:2004-21.
[101] Huisgen R. 1,3-Dipolar cycloadditions. Past and future. Angewandte Chemie International Edition in English 1963;2:565-98.
[102] Rostovtsev VV, Green LG, Fokin VV, Sharpless KB. A stepwise Huisgen cycloaddition process: Copper(I)-catalyzed regioselective "Ligation" of azides and terminal alkynes. Angewandte Chemie International Edition 2002;41:2596-9.
[103] Tornøe CW, Christensen C, Meldal M. Peptidotriazoles on solid phase: [1,2,3]-triazoles by regiospecific copper(I)-catalyzed 1,3-dipolar cycloadditions of terminal alkynes to azides. The Journal of Organic Chemistry 2002;67:3057-64.
[104] Bock VD, Hiemstra H, van Maarseveen JH. CuI-catalyzed alkyne–azide "click" cycloadditions from a mechanistic and synthetic perspective. European Journal of Organic Chemistry 2006;2006:51-68.
[105] Nwe K, Brechbiel MW. Growing applications of "click chemistry" for bioconjugation in contemporary biomedical research. Cancer Biotherapy & Radiopharmaceuticals 2009;24:289-302.
[106] Lutz J-F. 1,3-Dipolar cycloadditions of azides and alkynes: A universal ligation tool in polymer and materials science. Angewandte Chemie International Edition 2007;46:1018-25.
[107] Koschella A, Hartlieb M, Heinze T. A "click-chemistry" approach to cellulose-based hydrogels. Carbohydrate Polymers 2011;86:154-61.
[108] Filpponen I, Argyropoulos DS. Regular linking of cellulose nanocrystals via click chemistry: Synthesis and formation of cellulose nanoplatelet gels. Biomacromolecules 2010;11:1060-6.

[109] Chen J, Lin N, Huang J, Dufresne A. Highly alkynyl-functionalization of cellulose nanocrystals and advanced nanocomposites thereof via click chemistry. Polymer Chemistry 2015;6:4385-95.
[110] Pahimanolis N, Hippi U, Johansson LS, Saarinen T, Houbenov N, Ruokolainen J, et al. Surface functionalization of nanofibrillated cellulose using click-chemistry approach in aqueous media. Cellulose 2011;18:1201-12.
[111] Gesser HD, Goswami PC. Aerogels and related porous materials. Chem Rev 1989;89:765-88.
[112] Hüsing N, Schubert U. Aerogels—Airy materials: chemistry, structure, and properties. Angewandte Chemie International Edition 1998;37:22-45.
[113] Pierre AC, Pajonk GM. Chemistry of aerogels and their applications. Chem Rev 2002;102:4243-66.
[114] García-González CA, Alnaief M, Smirnova I. Polysaccharide-based aerogels—Promising biodegradable carriers for drug delivery systems. Carbohydrate Polymers 2011;86:1425-38.
[115] Paakko M, Vapaavuori J, Silvennoinen R, Kosonen H, Ankerfors M, Lindstrom T, et al. Long and entangled native cellulose I nanofibers allow flexible aerogels and hierarchically porous templates for functionalities. Soft Matter 2008;4:2492-9.
[116] Kim C, Youn H, Lee H. Preparation of cross-linked cellulose nanofibril aerogel with water absorbency and shape recovery. Cellulose 2015;22:3715-24.
[117] Jiang F, Hsieh Y-L. Amphiphilic superabsorbent cellulose nanofibril aerogels. J Mater Chem A 2014;2:6337-42.
[118] Heath L, Thielemans W. Cellulose nanowhisker aerogels. Green Chemistry 2010;12:1448-53.
[119] Xu X, Liu F, Jiang L, Zhu JY, Haagenson D, Wiesenborn DP. Cellulose nanocrystals vs. Cellulose nanofibrils: A comparative study on their microstructures and effects as polymer reinforcing agents. ACS Applied Materials & Interfaces 2013;5:2999-3009.

Chapter 2. Preparation and characterization of sterically stabilized nanocrystalline cellulose obtained by periodate oxidation of cellulose fibers

2.1 Abstract

We produced novel nanocellulose particles made from cellulose fibers by periodate oxidation. For partial oxidation (degree of substitution (DS) <2), three products were generated after the periodate oxidized fibers were heat treated: fibrous cellulose, rod-like dialdehyde cellulose nanofibers which we refer to as sterically stabilized nanocrystalline cellulose (SNCC), and dissolved oxidized cellulose chain which is a copolymer of cellulose and dialdehyde cellulose units which we refer to as dialdehyde modified cellulose (DAMC). The products were separated by centrifugation and cosolvent addition. SNCC has similar dimension (100-200 nm in length and 8 nm in width) as conventional nanocrystalline cellulose (NCC) made by sulfuric acid hydrolysis. Several techniques were applied to characterize SNCC and its properties are compared to NCC. DAMC was found to be soluble in hot water or a few solvents (such as dimethyl formamide and dimethyl acetamide) at elevated temperature, but was insoluble in most common solvents at room temperature. The molecular weight of DAC (DS = 2) produced under various conditions (heating time and temperature) was determined by gel permeation chromatography. It was shown that the molecular weight decreased from 85.1 to 4.1 kDa with heating time and residence time when cooled down to room temperature.

*Reproduced with permission from Cellulose, 2015, 22 (3), 1743-1752

2.2 Introduction

Cellulose is a natural carbohydrate polymer consisting of repeating β-D-glucose monomer units and is considered to be an almost inexhaustible raw material, which has the potential to replace oil-based and non-renewable products [1]. Periodate oxidation of cellulose breaks the C2-C3 bond in the glucose repeat units of cellulose, forming 2, 3-dialdehyde groups [2]. This product is commonly referred as dialdehyde cellulose (DAC). DAC is widely used as the intermediate for derivations of cellulose due to the high reactivity of the aldehyde groups [3-6]. However, DAC is hard to dissolve in water, which has hampered its usage in industry. Two approaches were developed to make water-soluble DAC products. Kim et al. found that fully oxidized DAC (DS = 2) can be easily solubilized by heating in water at 80 ^{o}C for 4 hours [7]. Another method is to convert dialdehyde groups into other groups, such as di-alcohols or di-sulfite groups [6, 8]. Recently, Yang et al. employed a chlorite oxidation to convert dialdehyde groups into dicarboxylic groups to produce nanofibers called electrosterically stabilized nanocrystalline cellulose (ENCC) [9]. This research suggests that if the amorphous regions between nanocrystalline regions in cellulose nanofibers can be solubilized we might be able to produce nanofibers this way [10]. To test this hypothesis, we introduced dialdehyde groups in cellulose fibers, which are expected to be preferentially located in the amorphous regions and subsequently we attempted to dissolve these amorphous regions. Here we examine the solubility of DAC not only in water, but also in a number of organic solvents at both room and elevated temperatures, to determine which solvents are a good solvent for DAC and which are poor solvents.

The advances in nanotechnology research in the past decades has opened many new applications in high-tech material fields, and recently also greatly stimulate the interest in preparation, characterization and applications of nanocelluloses, due to their exceptional physical and chemical properties [11]. However, it is not an easy task to break down cellulose fibers into nanosized structures due to the high content of hydroxyl groups on the cellulose chains, which create strong hydrogen bonds [12]. Many proposed methods were developed during the past few years to disintegrate cellulose fibers. Mechanical treatment on cellulose yields nano- or micro-sized cellulose structures [13, 14], but huge amounts of energy are consumed during this treatment [15]. Several enzymatic or chemical pretreatments have been developed to loosen the hydrogen bonds

of cellulose to reduce the energy consumption. The combination of an enzyme hydrolysis pretreatment with a mechanical homogenization process allows one to obtain nanosized fibrils, with significantly reduced energy requirements [16-19]. Individual nanofibrils cellulose (NFC) with 5 nm in width and at least 2 μm in length were produced by a 2,2,6,6 - tetramethylpiperidine-1-oxyl (TEMPO)-mediated oxidation pretreatment on cellulose before mechanical treatment [20,21]. A sequential periodate and chlorite oxidation pretreatment was performed on cellulose to form dicarboxyl groups, resulting in nanofibrils with width of 25 nm after homogenization [22]. Another type of nanocellulose is nanocrystalline cellulose (NCC) [23, 24], which is isolated from cellulose fibers by a strong acid hydrolysis. The treatment consists of disruption and cleavage of amorphous regions of cellulose and liberating the crystalline regions. Electrosterically stabilized nanocrystalline cellulose (ENCC) can be prepared by a two-step periodate and chlorite oxidation, without any mechanical treatment [25]. Generally, the width of NCC and ENCC is a few nanometers, whereas the length ranges from tenths to hundreds of nanometers.

Here we report on a new method to prepare nanocellulose by a periodate oxidation of cellulose fibers, followed by hot-water treatment. Complete oxidation of cellulose by periodate results in the conversion of two of the three hydroxyl groups in the glucose repeat unit to aldehyde groups (and in breaking the bond between the C2 and C3 carbons), resulting in a degree of substitution DS = 2. For partial oxidation (DS < 2), three products were generated: fibrous cellulose, rod-like dialdehyde cellulose nanofibers which we refer to as sterically stabilized nanocrystalline cellulose (SNCC), and dissolved DAC which is a copolymer of cellulose and dialdehyde cellulose units which we refer to as dialdehyde modified cellulose (DAMC). The products were separated by centrifugation and cosolvent addition. SNCC has similar dimensions as conventional nanocrystalline cellulose (NCC) made by sulfuric acid hydrolysis. The properties of SNCC were analyzed and compared to NCC by a variety of techniques: atomic force microscopy (AFM), dynamic light scattering (DLS), Fourier transform infrared spectra (FTIR), solid state carbon-13 NMR, thermogravimetric analysis (TGA) and viscosity measurements.

2.3 Experimental section

2.3.1 Materials

Sheets from Kraft Softwood pulp, produced from black spruce and bleached with elemental free chlorine (Domtar, Canada) were used as starting cellulose material. The fibers of this pulp have an average length of 2.37 mm and contain about 20% hemicellulose. Chemicals for reactions: sodium (meta) periodate, ethylene glycol, propanol, hydroxylamine hydrochloride, sodium hydroxide, and hydrogen chloride standard solutions (0.1 M and 0.5 M) were purchased from Sigma-Aldrich, sodium chloride (ACP chemistry). All chemicals were used as received. Milli-Q water was used in all experiments.

2.3.2 Periodate oxidation of cellulose pulp

Periodate oxidation of cellulose pulp was performed as previously described [9] with minor changes. Typically, 1 g of softwood pulp was soaked in water for 2 days. The wet pulp was dispersed by a disintegrator, and then filtered to remove extra water. Next 0.66 g $NaIO_4$ and 3.87 g NaCl were dissolved in water, and the wet pulp was added to this solution. The total volume of water was 200 mL, including the moisture from the wet pulp. The reaction beaker was wrapped with several layers of aluminum foil to prevent entry of any light. The oxidation reaction was performed at room temperature and stirred at a speed of 105 rpm for 96 hours. Ethylene glycol was added into this mixture to end the reaction by quenching the residual periodate. The oxidized cellulose was thoroughly washed with water by filtration. Another recipe (method 2) was used in order to reduce the reaction time: 1g pulp, 1.32 g $NaIO_4$, 3.87g NaCl and 65 mL water were mixed together for 42 hours. To produce DAC with DS = 2, 1g pulp, 1.85 g $NaIO_4$ (8.65mmol), 3.87 g NaCl (8.64 mmol) and 65 mL water were mixed and stirred for 6 days. Except for the amount of chemicals, all other conditions and treatments were the same.

2.3.3 Determination of aldehyde content

The aldehyde content of oxidized cellulose was determined by the hydroxylamine hydrochloride method [26]. A certain amount of dialdehyde cellulose was suspended in water and the pH was adjusted to 3.5 with HCl, then 10 mL hydroxylamine hydrochloride solution (5%, wt/wt) was added to the suspension. The pH of this suspension was always kept at 3.5 by adding 0.1 mol/L NaOH until no decrease of pH was observed. The cellulose fibers were repeatedly washed with

water and collected by filtration. The weight of each sample was measured after it was completely dry. The aldehyde content was determined by the consumption of the NaOH solution.

2.3.4 Preparation and separation of SNCC

The SNCC was prepared by heating a flask containing the pre-oxidized cellulose in an oil bath. Typically, one gram pre-oxidized cellulose pulp was suspended in 100 g water (including the moisture in the pulp) in a round flask, and the suspension was heated at 80 °C with gentle stirring for 6 hours. After cooling to room temperature, the suspension was centrifuged at 15000 rpm for 10 min (Beckman Coulter J2 centrifuge and JA-25.50 fixed angle rotor) to remove the unfibrilated fibers. Subsequently propanol was added as a cosolvent to the supernatant, which resulted in two precipitates at different propanol additions, one being film-like and one solid-like. These precipitates were further centrifuged at 5000 rpm for 10 minutes to enhance the separation. The separation process is schematically shown in Figure 2.1. These precipitates were either air-dried or re-dispersed in water for future measurements. Nanocrystalline cellulose (NCC) was prepared by sulfuric acid hydrolysis according to Cranston et al. [27]. This allowed us to compare properties of SNCC with those of NCC.

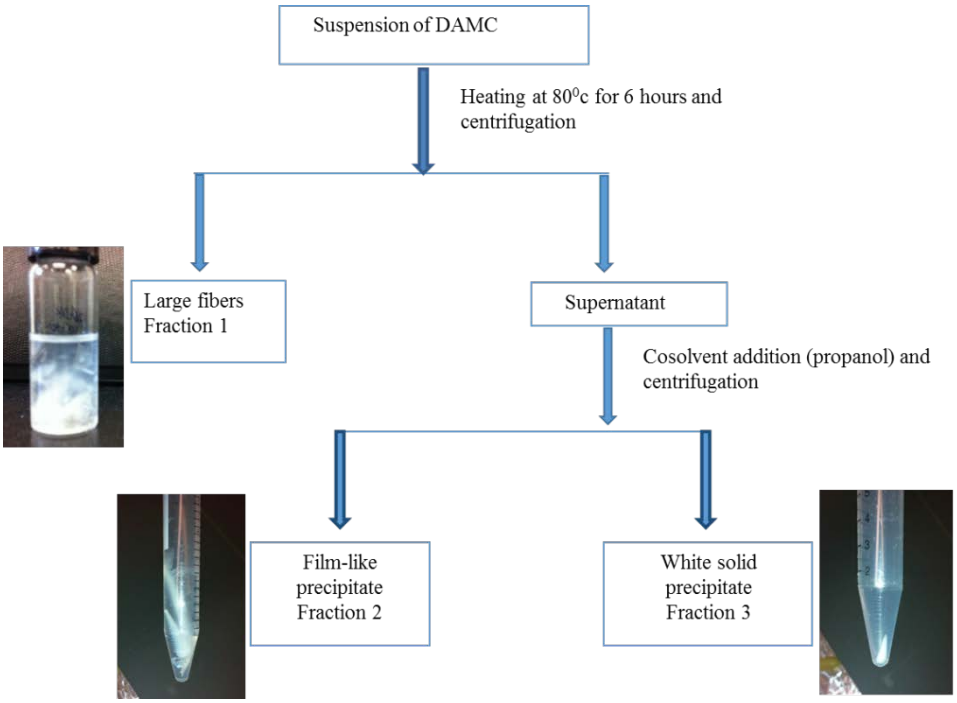

Figure 2.1 Scheme of separation process of products produced by periodate oxidation of cellulose.

2.3.5 Fourier transform infrared spectra (FTIR)

FTIR spectra of samples were collected with a transmission FTIR spectrometer (Perkin Elmer) with single bounce diamond ATR (Attenuated Total Reflectance) accessory. Solid samples were placed directly on the ATR crystal, and all the spectra of measured samples were averaged from 16 scans from 550 to 4000 cm^{-1} with a resolution of 4 cm^{-1}.

2.3.6 Solid carbon-13 NMR measurements

Solid carbon-13 NMR spectra were obtained on a Varian/Agilent VNMRS-400 instrument operating at 100.5 MHz. Samples were packed in 7.5 mm zirconia rotors and spun at 5500 Hz. Spinning sidebands were suppressed using the TOSS sequence. Spectra were acquired using a contact time of 2 ms and a recycle delay of 2 s. Typically 6000 transients were acquired.

2.3.7 Atomic force microscopy (AFM) measurement

The morphological property of particles was investigated by AFM (Nanoscope IIIa MultiMode with Extender (Veeco Metrology Group, Santa Barbara, CA)). Typically, a freshly cleaved mica which was pre-coated with poly-L-Lysine, then a drop of sample was placed on the treated mica surface and the excess sample was rinsed off by milli-Q water after 10 min. All the samples were air-dried before measurements. The experiments were done in tapping mode using silicon cantilevers (ACTA model, AppNano) with a nominal spring constant of 37 N/m, nominal resonant frequency of 300 kHz and nominal tip radius of 6 nm. Nanoscope Analysis 1.4 was used to process the AFM images.

2.3.8 Particle size distribution

The size (equivalent spherical mean diameter) distribution of each sample was determined by dynamic light scattering (DLS). The suspensions were first filtered through a 0.45 μm syringe filter (Acrodisc, PALL) to remove dust and then placed into carefully cleaned glass vials. All the measurements were performed on a Brookhaven light scattering instrument with a BI9000 AT digital correlator, and the data were collected by monitoring the scattered light intensity at 90° scattering angle at 22 °C.

2.3.9 Thermal properties – thermogravimetric analysis (TGA)

TGA analysis was performed on a TA Instruments Q500 TG analyzer. Samples were heated in a pure nitrogen atmosphere (flow rate 60 mL/min) from room temperature to 500 °C at a heating rate of 10 °C /min.

2.3.10 Viscosity measurements

The viscosity of SNCC and NCC suspensions was measured using an Ubbelohde capillary viscometer [28]. Five suspensions with different concentration were prepared from SNCC and NCC. Water was used to determine the calibration constant. All the viscosity measurements were done at 20 °C.

2.3.11 Gel permeation chromatography

Gel permeation chromatography (GPC) was carried out using an aqueous size exclusion column (Polysep-GFC-P 3000, 300 x 7.8 mm I.D., Phenomenex Inc, USA) at a flow rate of 0.8 mL/min. The sample was injected from a sample loop after filtration through a 0.45 µm membrane filter. Elution of solute was monitored by an optical rotation detector and a refractive index detector (Waters 2410 refractive index (DRI)) at 35 °C. A pullulan standard (a water soluble polysaccharide) was used to determine weight- and number-average molecular weights.

2.4 Results and discussion

2.4.1 Solubility of DAC (DS = 2) in various solvents

In order to be able to select a good cosolvent in which DAC and DAMC precipitates out, we determined the solubility of DAC in various solvents. When DS = 2, all cellulose is converted to DAC and after dissolving the fibers, no separation is required. The solubility of DAC was determined by the weight of dissolved DAC divided by the initial weight of DAC. The weight of dissolved DAC was measured as the difference of the initial weight of DAC and the weight of non-dissolved DAC which was obtained after centrifugation and drying. We were unable to find a solvent in which DAC dissolves at room temperature, which would have allowed us to perform the separation at room temperature. DAC (aldehyde content 11.7 mmol/g, DS = 2) dissolves in water, dimethyl formamide (DMF), and dimethyl acetamide (DMA) when heated at elevated

temperatures (80 ^{o}C and above) for 6 hours. The solubilities of all the solvents investigated both at room and elevated temperatures are shown in Table 2.1.

Table 2.1 Solubility of DAC in various solvents at both room and elevated temperatures.

Solvents	Solubility of DAC at room temperature (%)	Solubility of DAC after heating at 80 ^{o}C for 6 hours (%)
Water	< 1	91
Dimethyl formamide	< 1	87
Dimethyl acetamide	< 1	86
Dimethyl sulfoxide	< 1	6

Note: Solubilities of DAC in toluene, chloroform, propanol, acetone, xylene, tetrahydrofuran and acetic acid were all below 1%, both at room temperature and at elevated temperatures.

2.4.2 Separation of periodate oxidized products

After 42 hour periodate oxidation (method 2), the aldehyde content of the oxidized cellulose was 8.2 mmol/g corresponding to a degree of substitution of 1.4. Three products, fibrous cellulose, SNCC, and DAMC, were collected and separated by the method described in section 2.3.4. As shown in the note below Table 1, propanol is a bad solvent for DAC (as well as for cellulose) and, being miscible with water, is an excellent cosolvent of water to precipitate out DAMC. As shown in Figure 2.2, when propanol was added to the supernatant as cosolvent after the initial centrifugation, DAMC nanofibers (SNCC) precipitated out first when the dosage of propanol was about 2.2 g to 3.4 g (weight of the original DAC suspension is 2 g) and formed a transparent film-like precipitate. Subsequently, DAMC polymer was separated out in the form of a white precipitate when propanol addition was between 5.4 g and 10.4 g. No precipitate was formed between 3.4 g and 5.4 g and after 10.4 g, thus SNCC and DAMC are well-separated. Each precipitate was collected and dried to obtain its weight. The weight percentages of three fractions are 30.2, 38.8 and 31 for the fibrous fibers, SNCC, and DAMC. No more precipitation occurred at propanol additions above 11 g.

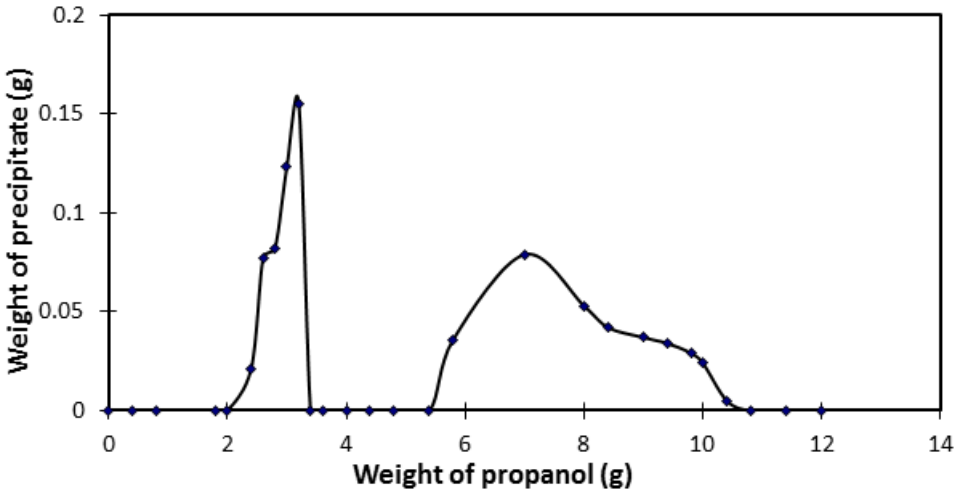

Figure 2.2 Separation of SNCC and DAMC using propanol as co-solvent, expressed as weight percent of the original supernatant

The observation that SNCC precipitates out first is in agreement with theory. The steric force is proportional to ½ - χ [29], whereas the critical Flory-Huggins parameter for polymer phase separation is $\chi^c = \frac{1}{2} + \frac{1}{2n} + \frac{1}{\sqrt{n}}$, n being the number of monomer repeat units in the polymer chain [30]. Thus sterically stabilized particles aggregate when the Flory-Huggins parameter becomes χ = 0.5, whereas DAMC precipitates out at χ^c which is larger than 0.5.

2.4.3 Particle morphology

The AFM image in Figure 2.3 (a) shows that SNCC contains rod-like particles with a length in the range of 100 - 200 nm and a diameter around 8 nm. The length and width of NCC (Figure 2.3 (b)) is 110 - 200 nm and 8 nm, respectively. Thus the dimensions of SNCC and NCC are very similar. Similar as DAC dissolution by heating, amorphous regions between SNCCs were dissolved by thermal treatment and subsequently produced SNCCs.

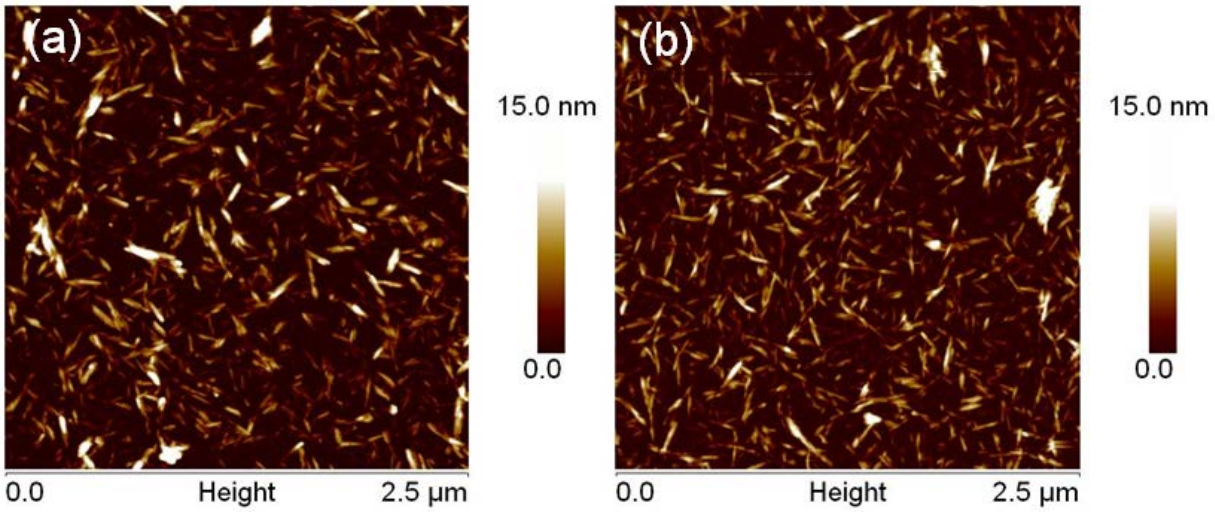

Figure 2.3 AFM height image for (a) SNCC, and (b) NCC.

2.4.4 Dynamic light scattering of SNCC suspensions in water-propanol mixtures

An experiment was conducted to prove that SNCC suspensions are sterically stabilized. DAMC does not dissolve in propanol and thus by adding propanol to the suspension, the Flory-Huggins polymer-solvent interaction parameter χ is increased. When it reaches the value χ^c, DAMC will precipitate out, resulting in particle aggregation. Before reaching this value, the solvent becomes progressively poorer, resulting in a contraction of DAMC chains. Hence one expects the particle size to first decrease due to chain contraction, followed by an increase due to particle flocculation. The changes in size of SNCC after adding propanol to the suspension were examined by dynamic light scattering. As shown in Figure 2.4, the size of SNCC first decreased with cosolvent (propanol) addition and subsequently increased, as expected for sterically stabilized particles. The results show that the amorphous chains protruding from the crystalline regions contracted when the solvent became a poorer solvent for the DAMC chains. With further addition, SNCCs began to aggregate and the size increased. This is strong proof that SNCCs are sterically stabilized in water and justifies calling them sterically stabilized nanocrystalline cellulose (SNCC).

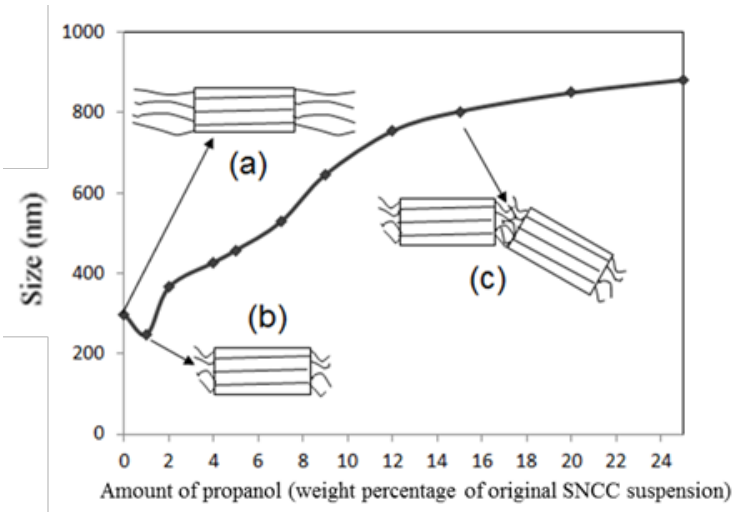

Figure 2.4 DLS size of SNCC particles as a function of cosolvent addition, expressed as weight percent of original SNCC suspension. Schematic representation of (a) SNCC with protruding DAMC chains which provide steric stability, (b) DAMC chains contracted with addition of propanol, and (c) SNCC aggregation upon further addition of propanol.

2.4.5 FTIR

The FTIR spectra are shown in Figure 2.5, the spectra of original cellulose pulp and NCC are very similar to each other, the peak at 3340 cm^{-1} is due to the stretching of -OH groups, the peaks at 2900 cm^{-1} , 1430 cm^{-1} , 1030 cm^{-1} are due to C-H stretching vibration, -CH2 scissoring and CH2-O-CH2 stretching, respectively; and the peak at 899 cm^{-1} is for the β-glycosilic linkages between the sugar units [31]. The spectra for SNCC has two characteristic peaks compared to the previous two spectra, the small peaks at 1730 cm^{-1} and 880 cm^{-1} of SNCC (see vertical dashed lines in Figure 2.5) are due to carbonyl groups stretching and the hemiacetal linkages formed from the dialdehyde groups, respectively [7].

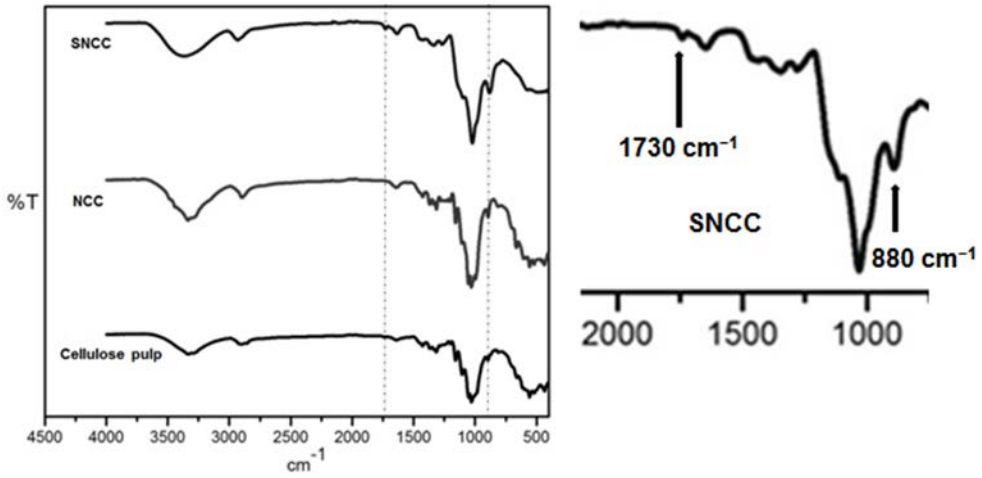

Figure 2.5 FTIR spectra of original cellulose pulp, NCC, and SNCC. The curve on the right side is an enlarged curve of SNCC in the range 2000 - 500 cm^{-1}.

2.4.6 Solid state carbon-13 NMR

The peaks in solid state carbon-13 NMR spectra of the original cellulose pulp are assigned as shown in Figure 2.6, 105 ppm for C1, 90 ppm for C4, 85 ppm for C4', 80-70 ppm region for C2,3,5, and 70-60 ppm for C6, respectively. The shoulder peak for C4' is due to the amorphous regions of cellulose, while the sharp peak for C4 is due to the crystalline regions [32]. The higher intensity ratio of C4/C4' in spectra (b) than (a) indicated that NCC has higher crystallinity. For spectra (c) of SNCC, which has two broad peaks located in 105-85 ppm and 85-60 ppm, the lack of carbonyl signal expected at 175-180 ppm indicates that the aldehyde groups of solid SNCC formed hemiacetal linkages [26].

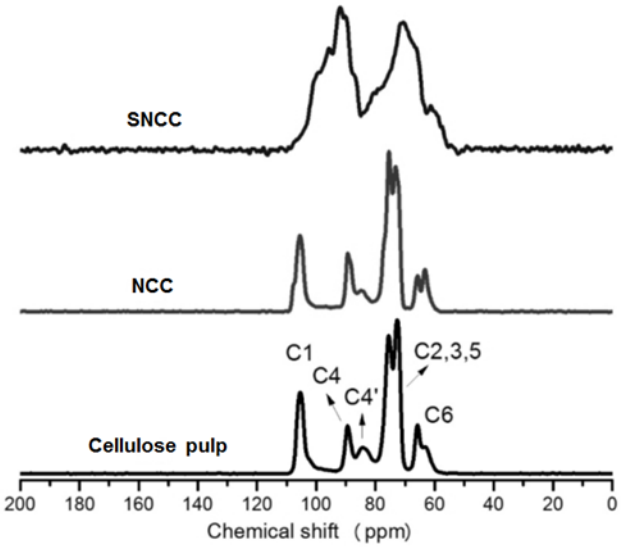

Figure 2.6 Solid state carbon-13 NMR spectra of original cellulose pulp, NCC, and SNCC.

2.4.7 Thermal stability

Derivative weight loss (DWL) curves for all measured samples are shown in Figure 2.7. The DWL curve of the cellulose pulp has the highest temperature (350 °C) for its transition peak, this temperature decreased to 290 °C for NCC. The SNCC has a major wide peak from 200 to 450 °C, and a small peak from 150 to 200 °C. Although the dominant transition peak temperature for SNCC (230 °C) is lower than NCC (290 °C), this wide peak of SNCC shows it has the highest final decomposition temperature (450 °C) when compared with NCC (305 °C) and cellulose pulp (375 °C), indicating that SNCC has a better heat resistance. This is due to the hemiacetal linkage formed between the aldehyde groups of SNCC, thus increasing the thermal stability of SNCC, similar to the improvement of thermal stability of ENCC film by cross-linking of ENCC [9]. The small peak of SNCC with lower decomposition temperature may be due to DAMC chains, which did not form the hemiacetal linkage. It is of interest to note that the SNCC sample becomes lightly yellow if dried in the oven above 100 ^{o}C.

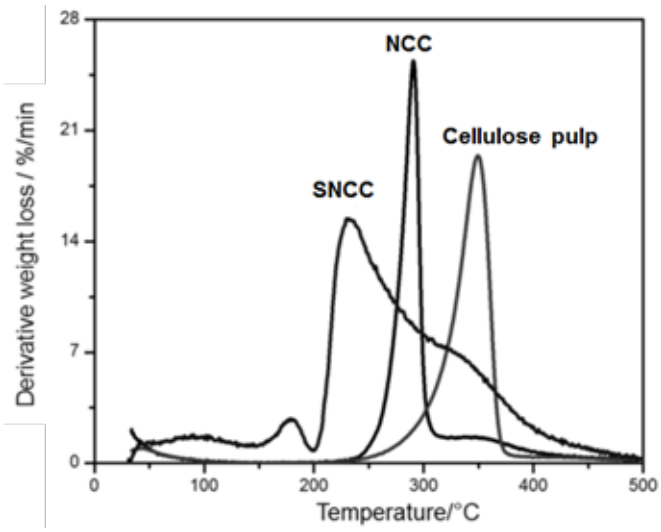

Figure 2.7 Derivative weight loss (DWL) curves for SNCC, NCC, and original cellulose pulp.

2.4.8 Viscosity

The relative viscosity of SNCC and NCC is shown in Figure 2.8. The viscosity of both SNCC and NCC increases with increasing concentration. The intrinsic viscosity was obtained by fitting data using function $\eta/\eta_0=1+ [\eta]c$ (c is the concentration) [33], thus the intrinsic viscosity [η] is equal to the slope of the straight line. The intrinsic viscosity of NCC and SNCC is 96 mL/g and 25 mL/g, respectively. The intrinsic viscosity of SNCC is only one fourth of NCC, this is due to the fact that SNCC is uncharged, while NCC particles are negatively charged, resulting in an increase of the intrinsic viscosity due to the primary electroviscous effect [28]. Also both the effective length and width of SNCC are longer than NCC, because the soluble DAMC chains are likely to occupy an extended volume. Hence the effective axis ratio of SNCC is unknown and might be lower than that of NCC.

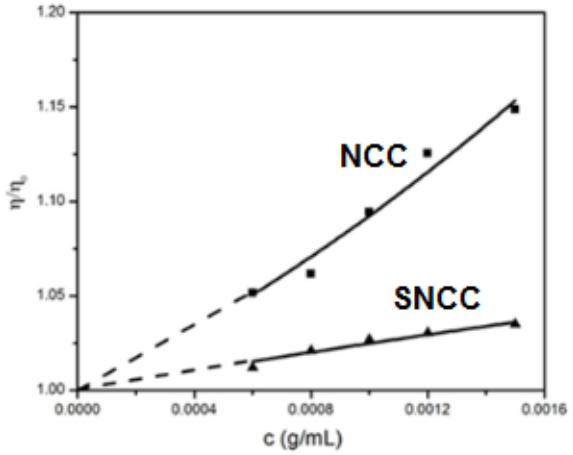

Figure 2.8 Relative viscosity versus concentration of SNCC and NCC suspensions.

2.4.9 Gel permeation chromatography (GPC) of DAC

The molecular weight of DAC dramatically decreases with its residence time in an aqueous solution. As shown in Table 2.2, after leaving DAC in an aqueous solution at room temperature for 1 day, the weight average molecular weight (MW) of DAC is 85.1 kDa, whereas it is only 4.1 kDa when its residence time in the aqueous solution is 2 months. The MW of DAC decreased to 41.3 kDa, when the polymer is in the solution for 15 days, which is about half of the MW for a residence time of 1 day. The degradation may be caused by break-up of DAC chains by heating. However, they must still stay associated together, since high molecular weights are measured in GPC. Subsequently, they gradually dissociate in water to give lower molecular weights with longer residence time [34].

Longer heating times or higher heating temperatures (with the same residence time) also results in a molecular weight decrease of DAC. The MW of DAC after heating at 80 ^{o}C for 10 hours decreases by about 18% compared to 6 hours of heating, while the decrease is about 50% between 17 hours and 6 hours heating at 90 ^{o}C. Meanwhile, the molecular weight of DAC decreases 20% when the heating temperature increases by 10 ^{o}C for a 6 hours heating time.

The reduction of the molecular weight of DAC with heating and residence time is also seen in DAMC chains attached to SNCC. The SNCC particles lose their stability on the time scale of months and sediment out of solutions, likely because of the loss of steric stability.

Table 2.2 Molecular weights of DAC after different heating conditions

Heating temperature (°C)	Heating time (hours)	Residence time in water (days) at room temperature	Average molecular weight (kDa)	Degree of polymerization
80	6	1	85.1	532
80	6	15	41.3	258
80	6	61	4.1	26
80	10	61	3.4	21
90	6	61	3.3	21
90	17	61	1.6	10

2.5 Conclusions

A novel sterically stabilized nanocrystalline cellulose (SNCC) was prepared and separated in a hot water treatment of periodate oxidized cellulose fibers by addition of cosolvent followed by centrifugation. That SNCC is sterically stabilized was proved by cosolvent addition and DLS size measurements. SNCC has similar dimensions as conventional NCC produced by sulfuric acid treatment, but has a better heat resistance due to the hemiacetal linkages. It also has a lower intrinsic viscosity than NCC. DAC (DS = 2) was found to be soluble in water and also in a few solvents at elevated temperatures. GPC measurements showed that the molecular weight of DAC decreased with heating time and also residence time. The decrease in molecular weight of DAMC is likely responsible for the loss of steric stability of SNCC on a time scale of months.

2.6 Acknowledgements

The authors would like to thank the Natural Science and Engineering Research Council of Canada (NSERC) for the funding of an industrial research chair cosponsored by FPInnovations and funding of the NSERC Strategic Research Network on Green Wood Fiber Products. Contributions from the FQRNT Centre for Self-Assembled Chemical Structures (CSACS) are also acknowledged.

2.7 References

[1] Klemn D, Heublein B, Fink HP, Bohn A. Cellulose: Fascinating biopolymer and sustainable raw material. Angew Chem Int Ed, 2005, 44:3358 - 3393

[2] Gal'braikh LS, Rogovin ZA (1971) Cellulose and cellulose derivatives. N. M. Bikales & L. Segal (Eds.), New York

[3] Sabzalian Z (2012) Cross-linking and hydrophobization of chemically modified cellulose fibers. Dissertation, McGill University

[4] Bhattacharyya D, Hestekin JA, Brushaber P, Cullen L, Bachas LG, Sikdar SK. Novel poly-glutamic acid functionalized microfiltration membranes for sorption of heavy metals at high capacity. Journal of Membrane Science, 1998, 141:21–135

[5] Maekawa E, Koshijima T. Properties of 2,3-dicarboxyl cellulose combined with various metalic ions. Journal of Applied Polymer Science, 1984, 29:2289–2297

[6] Casu B, Naggi A, Torri G, Allegra G, Meille SV, Cosani A, Terbojevich M. Stereoregular acyclic polyalcohols and polyacetates from cellulose and amylase. Macromolecules, 1985, 18:2762-2767

[7] Kim UJ, Wada M, Kuga S. Solubilization of dialdehyde cellulose by hot water. Carbohydrate Polymers, 2004, 56: 7-10

[8] Rajalaxmi D, Jiang N, Leslie G, Ragauskas AJ. Synthesis of novel water-soluble sulfonated cellulose. Carbohydrate Research, 2010, 345:284-290

[9] Yang H, Tejado A, Alam MN, Antal M. van de Ven TGM. Films prepared from electrosterically stabilized nanocrystalline cellulose. Langmuir, 2012, 28:7834-7842

[10] Visanko M, Liimatainen H, Sirviö J, Heiskanen J, Hormi O, Niinimäki J. Amphiphilic cellulose nanocrystals from acid-free oxidative treatment: physico-chemical characteristics and use as an oil-water stabilizer. Biomacromolecules, 2014, 15:2769-2775

[11] Isogai A. Wood nanocelluloses: fundamentals and applications as new bio-based nanomaterials. Journal of wood science, 2013, 59(6):449 - 459.

[12] Somerville C, Bauer S, Brininstool G, Facette M, Hamann T, Milne J, Osborne E, Paredez A, Persson S, Raab T, Vorwerk S, Youngs H. Toward a systems approach to understanding plant cell walls. Science, 2004, 306:2206 - 2211

[13] Herrick FW, Casebier RL, Hamilton JK, Sandberg KR. Microfibrillated cellulose: Morphology and accessibility. J Appl Polym Sci Appl Polym Symp, 1983, 37:797 - 813

[14] Nakagaito AN, Yano H. Novel high-strength biocomposites based on microfibrillated cellulose having nano-order-unit web-like network structure. Appl Phys A: Mater Sci Process, 2005, 80:155 – 159

[15] Tejado A, Alam MN, Antal M, Yang H, van de Ven TGM. Energy requirements for the disintegration of cellulose fibers into cellulose nanofibers. Cellulose, 2012, 19:831-842

[16] Henriksson M, Henriksson G, Berglund LA, Lindström T. An environmentally friendly method for enzyme-assisted preparation of microfibrillated cellulose (MFC) nanofibers. Eur Polym J, 2007, 43:3434 - 3441

[17] Pääkkö M, Ankerfors M, Kosonen H, Nykanen A, Ahola S, Osterberg M, Ruokolainen J, Laine J, Larsson PT, Ikkala O, Lindström T. Enzymatic hydrolysis combined with mechanical shearing and high-pressure homogenization for nanoscale cellulose fibrils and strong gels. Biomacromolecules, 2007, 8(6):1934 - 1941

[18] López-Rubio A, Lagaron JM, Ankerfors M, Lindström T, Nordqvist D, Mattozzi A, Hedenqvist MS. Enhanced film forming and film properties of amylopectin using micro-fibrillated cellulose. Carbohydrate Polymers, 2007, 68(4):718 -727

[19] Svagan AJ, Samir MASA, Berglund LA. Biomimetic polysaccharide nanocomposites of high cellulose content and high toughness. Biomacromolecules, 2007, 8(8):2556 - 2563

[20] Saito T, Nishiyama Y, Putaux JL, Vignon M, Isogai A. Homogeneous suspensions of individualized microfibrils from TEMPO-catalyzed oxidation of native cellulose. Biomacromolecules, 2006, 7(6):1687 - 1691

[21] Fukuzumi H, Saito T, Iwata T, Kumamoto Y, Isogai A. Transparent and high gas barrier films of cellulose nanofibers prepared by TEMPO-mediated oxidation. Biomacromolecules, 2009, 10(1) :162–165

[22] Liimatainen H, Visanko M, Sirvio JA, Osmo EO, Hormi OEO, Niinimaki J. Enhancement of the nanofibrillation of wood cellulose through sequential periodate−chlorite oxidation. Biomacromolecules, 2012, 13(5):1592 -1597

[23] Dong XM, Kimura T, Revol JF, Gray DG. Effects of ionic strength on the isotropic−chiral nematic phase transition of suspensions of cellulose crystallites. Langmuir, 1996, 12:2076 - 2082

[24] Beck-Candanedo S, Roman M, Gray DG. Effect of reaction conditions on the properties and behavior of wood cellulose nanocrystal suspensions. Biomacromolecules, 2005, 6(2):1048 - 1054

[25] Yang H, Alam MN, van de Ven TGM. Highly charged nanocrystalline cellulose and dicarboxylated cellulose from periodate and chlorite oxidized cellulose fibers. Cellulose, 2013, 20(4):1865-1875

[26] Kim UJ, Kuga S, Wada M, Okano T, Kondo T. Periodate oxidation of crystalline cellulose. Biomacromolecules, 2000, 1(3):488 - 492

[27] Cranston ED, Gray DG. Morphological and optical characterization of polyelectrolyte multilayers incorporating nanocrystalline cellulose. Biomacromolecules, 2006, 7(9):2522-2530

[28] Jowkarderis L, van de Ven TGM. Intrinsic viscosity of aqueous suspensions of cellulose nanofibrils. Cellulose, 2014, 21(4):2511 – 2517

[29] Napper DH (1984) Polymeric stabilization of colloidal dispersions. Academic Press, London, chapter 5.

[30] Fleer GJ, Cohen Stuart MA, Scheutjens JMHM, Cosgrove T, Vincent B (1993) Polymers at interfaces. Chapman & Hall, London, p 10.

[31] Keshk, SMAS. Homogenous reactions of cellulose from different natural sources. Carbohydrate Polymers, 2008, 74:942 - 945

[32] Atalla RH, VanderHart DL. The role of solid state C-13 NMR spectroscopy in studies of the nature of native celluloses. Solid-State Nucl Magn Reson, 1999, 15:1-19

[33] van de Ven TGM (1989) Colloidal hydrodynamics. Academic Press, London, pp 222-227

[34] VaVeelart S, Wit D, Gotlieb KF, Verhe R. Chemical and physical transition of periodate oxidized potato starch in water. Carbohydrate Polymers, 1997, 33:153-162

Bridging Section between Chapters 2 and 3

In Chapter 2, it was shown that a novel type of nanocrystalline cellulose – sterically stabilized NCC can be obtained from periodate oxidized cellulose fibers followed by a hot-water treatment. SNCC consists of non-charged nanorod particles and is sterically stabilized by protruding dialdehyde modified cellulose chains.

Inspired by the previous chapter, in the next chapter, a hairy cationic nanocrystallne cellulose (CNCC) was prepared by a two-step reaction followed by a hot-water treatment. Cationic dialdehyde modified cellulose (CDAMC) fibers were first prepared by a reaction between the aldehyde groups of periodate oxidized cellulose fibers and (2-hydrazinyl-2-oxoethyl)-trimethylazanium chloride (Girard's reagent T (GT)). Then subjecting the suspension of CDAMC fibers to a hot-water treatment, resulted in the formation of CNCC. This is an easy and environmentally friendly method comparing with existed methods in the literatures. Various characterizations have been performed on the CNCC. The results of this research have been published in the following paper:

Preparation of hairy cationic nanocrystalline cellulose. Han Yang, Theo van de Ven. Cellulose, 2016, 23 (3), 1791-1801.

Chapter 3. Preparation of hairy cationic nanocrystalline cellulose

3.1 Abstract

A hairy cationic nanocellulose (CNCC) was prepared by a two-step reaction. First dialdehyde modified cellulose (DAMC) were prepared by periodate oxidation of cellulose fibers and subsequently DAMC fibers were cationized by a reaction between the aldehyde groups of cellulose and (2-hydrazinyl-2-oxoethyl)-trimethylazanium chloride (Girard's reagent T (GT)) to produce cationic dialdehyde cellulose (CDAMC) fibers. Subjecting the suspension of CDAMC fibers to a hot-water treatment at 60 °C, resulted in the formation of cationic rod-like nanocellulose (CNCC). Atomic force microscopy (AFM) and transmission electron microscopy (TEM) showed the CNCC has a width of 5 nm and a length about 120 nm. Zeta potential measurement, Fourier transform infrared spectroscopy (FTIR), solid carbon-13 NMR and X-ray photoelectron spectroscopy (XPS) confirmed the presence of cationic groups on CNCC. The positive charge content of CNCC is about 1.68 mmol/g measured by conductometric titration. CNCC has a crystalline index of 67% and possesses cellulose I crystalline structure.

*Reproduced with permission from Cellulose, 2016, 23(3), 1791-1801.

3.2 Introduction

Cellulose consists of repeating β-D-glucose monomer units and is one of the most abundant natural polymers. It could become a primary resource in the future due to its renewability, biodegradability, biocompatibility and derivatization ability [1]. Nanocrystalline cellulose (NCC) (also referred to as CNC, cellulose nanocrystals), a cellulose based nanomaterial, has attracted substantial attention due to its superior mechanical properties and the potential of application in industry as reinforcing fillers [2]. NCC obtained from sulfuric acid hydrolysis contains negatively charged sulfate ester groups, but the content of negative charges is low, about 0.2 mmol/g [3]. We recently produced a highly charged nanocrystalline cellulose, electrosterically stabilized nanocrystalline cellulose (ENCC), prepared by a sequential periodate-chlorite oxidation, which was stabilized not only by a high content of negatively charged carboxyl groups (around 6 mmol/g) but also by steric stabilization provided by the protruding hair-like dicarboxylated cellulose chains [4]. ENCC belongs to a class of nanocellulose we call hairy nanocellulose [5]. NCC can also be sterically stabilized by adsorbed or grafted polymers such as poly(ethylene glycol) or poly(styrene) [6-8], or by sequential periodate oxidation-hot water treatment to directly yield dialdehyde chains on NCC, providing steric stabilization [9].

Many studies have focused on the modification of NCC to obtain anionic electrostatic repulsion or steric stabilization, but very little research has been done on the cationic stabilization of NCC. The study reported by Hasani et al. is the first study on cationic modification of NCC [10]. In this method, epoxypropyltrimethylammonium chloride (EPTMAC) was used to introduce quaternary ammonium groups onto NCC, but NCC needs to be alkali-activated prior to EPTMAC treatment, while maintaining the NCC morphology and avoiding the conversion to cellulose II. It was also reported in this study that surface cationization led to a decrease in surface charge density compared to the unmodified starting material (NCC).

A second method used click chemistry through copper (I) catalysed azide–alkyne cycloaddition to introduce imidazolium groups on the surface of NCC [11]. This method yields higher cationic charges (surface DS = 0.36) on NCC than the first method, and enabled the selective modification of only the primary hydroxyl groups. However the experimental steps in click chemistry are

complex and laborious. The third method used 4-(1-bromoethyl/bromomethyl) benzoic acid and pyridine to prepare pyridinium grafted cationic NCC; the surface DS was determined to be 0.38 and 1.10 for benzyl and methylbenzyl pyridinium NCC respectively [12]. However, all these three reported methods need the preparation of NCC by sulfuric acid hydrolysis prior to any cationization treatments. The preparation of NCC involves a time consuming purification dialysis process after the hydrolysis and sonication treatment of almost one week.

Periodate oxidation of cellulose breaks the C2-C3 bond in the glucose repeat units of cellulose, forming 2,3-dialdehyde groups, resulting in dialdehyde modified cellulose (DAMC) fibers [13] (Scheme 3.1 (a)). DAMC fibers are widely used as an intermediate for the derivation of cellulose due to the high reactivity of the aldehyde groups [14-17]. A Schiff base reactions between DAMC fibers and (2-hydrazinyl-2-oxoethyl)-trimethylazanium chloride (Girard's reagent T (GT)) forms imine bond and introduces quaternary ammonium groups onto DAMC fibers [18] (Scheme 3.1(b)). This reaction has been used to prepare highly water-soluble cationic cellulose derivatives [19], cationic cellulosic nanofibrils [20] and industrially to produce cationic starch from dialdehyde starch [21]. Dialdehyde modified cellulose fibers react with an amine via a Schiff base reaction, then followed by mechanical homogenization, produce amino-modified NCC [22, 23]. Periodate oxidation has also been applied on NCC directly, followed by grafting a primary amine [24] or a diamine compound [25] onto NCC through a Schiff base reaction. It is worth noticing that besides the cationic NCC with permanently positive charges described above [10-12], amino groups carry positive charges in acidic conditions due to protonation of the amino groups, thus these amino-modified NCC in acidic conditions also can be treated as one type of cationic NCC. Based on our pervious study [9], sterically stabilized NCC (SNCC) can be obtained from a hot water treatment of DAMC fibers. In this work, we prepared a cationic NCC form periodate oxidation of cellulose followed a Shiff base reaction with GT, and sequentially by a hot water treatment. In this paper, the cationic DAMC fibers were treated in 60 °C hot water for half an hour and yielded cationic NCC (CNCC) with a high positive charge. Similar to ENCC, CNCC is also expected to have protruding hair-like cationic cellulose chains because of its high charge content which exceeds the theoretical maximum surface charge content of traditional NCC particles [4, 5], we refer to this type of CNCC as hairy cationic nanocrystalline cellulose. The positive charges and morphology of CNCC were investigated by various methods.

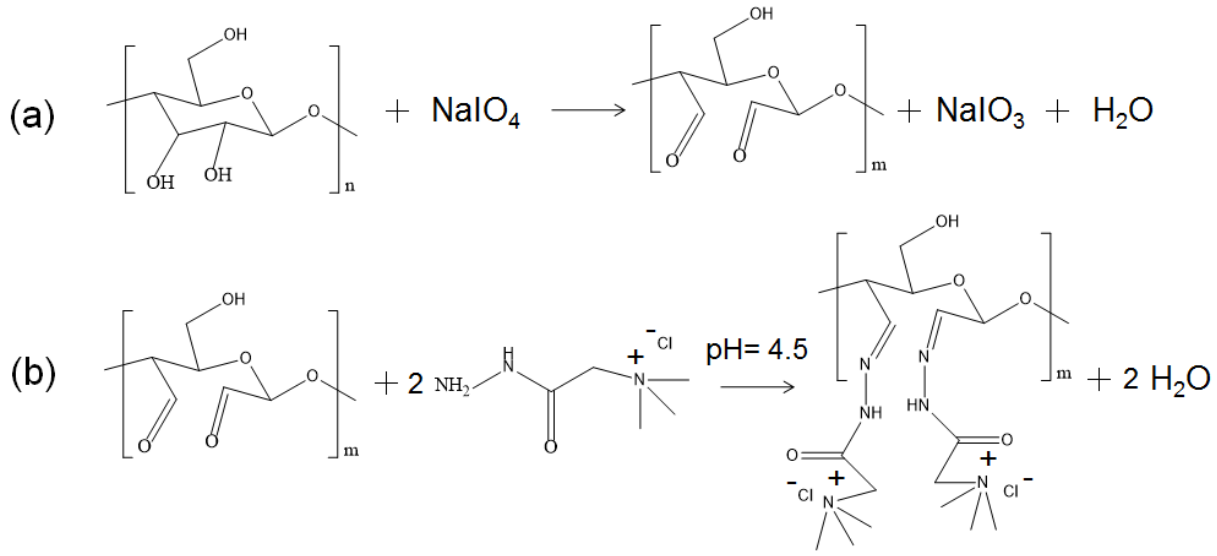

Scheme 3.1 (a) periodate oxidation of cellulose to produce dialdehyde modified cellulose (m < n), (b) cationization of dialdehyde cellulose (Note that it is difficult to attach the second quaternary ammonium group to the same glucose unit due to steric hindrance and electrostatic repulsion).

3.3 Experimental section

3.3.1 Materials

Softwood kraft pulp sheets (Domtar, Canada) were used as starting cellulose material. Chemicals for reactions: sodium (meta) periodate, Girard's reagent T ((2-hydrazinyl-2-oxoethyl)-trimethylazanium chloride, GT), ethylene glycol, hydroxylamine hydrochloride, tartrazine, hydrogen chloride (0.1 M), sodium hydroxide (0.1 M) and $AgNO_3$ standard solutions (10 mM) were purchased form Sigma-Aldrich, and propanol, sodium chloride from ACP chemicals Inc. All chemicals were used as received. Milli-Q water (18.2 MΩ cm, Millipore Milli-Q Purification System) was used in all experiments.

3.3.2 Periodate oxidation of cellulose pulp

One gram of dried softwood kraft pulp (about 6.2 mmol glucose units) was soaked in water and thoroughly dispersed by a disintegrator, and then filtered to remove extra water from the pulp. Next 0.98 g $NaIO_4$ (4.6 mmol) and 0.78 g NaCl (13.3 mmol) were dissolved in water, and the wet pulp was added to this solution. The total volume of water was 67 mL, including the moisture from the wet pulp. The reaction beaker was wrapped with several layers of aluminum foil to prevent entry of any light. The pulp was stirred at room temperature for 24 hours, then 1 mL ethylene

glycol was added into this mixture to end the reaction by quenching the residual periodate. The dialdehyde modified cellulose (DAMC) fibers were washed thoroughly with water by filtration. The aldehyde content of DAMC fibers was determined by the hydroxylamine hydrochloride method previously reported [4].

3.3.3 Cationization of dialdehyde cellulose

Never-dried DAMC fibers (containing 0.5 g dry DAMC fibres), 0.5 g GT (3 mmol), 1.2 g NaCl (20 mmol) and 40 g water were added into a 100 mL beaker. The pH of this suspension was adjusted to 4.5 with HCl and stirred for 24 hours at room temperature. Then the cationic DAMC (CDAMC) fibers were thoroughly washed with water by filtration.

3.3.4 Preparation of cationic nanocellulose

Never-dried CDAMC fibers (containing 0.2 g dry CDAMC fibers) and 20 g water were added into a 50 mL flask, and the suspension was stirred at 60 °C. The suspension became clear after 30 minutes and then was centrifuged at 5250 g for 10 minutes to remove the unfibrilated CDAMC fibers (a negligible amount). Then 30 mL propanol was added to the supernatant, and a gel like precipitate (CNCC) was collected by centrifugation at 2050 g. The CNCC was either freeze-dried (Thermo ModulyoD freeze dryer) or redispersed in water for further characterization.

3.3.5 Morphological properties

The morphology of cellulose, DAMC and CDAMC fibers were imaged by optical microscopy (Nikon ECLIPSE TE2000U inverted research microscope). The morphology of CNCC particles was investigated by AFM (Nanoscope IIIa MultiMode with Extender (Veeco Metrology Group, Santa Barbara, CA)). Typically, a drop of CNCC suspension was placed on a freshly cleaved mica surface and the excess suspension was rinsed off by water after 10 min. The experiments were done in tapping mode using silicon cantilevers (ACTA model, AppNano) with a nominal spring constant of 37 N/m, nominal resonant frequency of 300 kHz and nominal tip radius of 6 nm. Nanoscope Analysis 1.4 was used to obtain the AFM images. Transmission electron microscopy was also used to investigate CNCC. A drop of CNCC suspension was added onto a carbon-coated grid. The excess liquid was removed from the edges of the grid by filter paper. Then 1% of uranyl

acetate aqueous solution was applied as negatively stain. The grid was observed by a FEI Tecnai 12, Philips transmission electron microscopy operated at 120 kV.

3.3.6 The content of cationic groups

The content of cationic groups (trimethylazanium chloride) was determined by conductometric titration with AgNO3 solution (10 mmol/L) on a Metrohm 836 Titrando instrument. Typically, 120 mL of CNCC suspension was titrated with AgNO3 by adding approximately 0.1 mL in 50 seconds intervals.

3.3.7 Zeta potential measurement

Zeta potential measurements were carried out on 0.1% suspensions of CNCC in Milli-Q water at 25 °C, using a Malvern Zetasizer Nano instrument. The recorded zeta potentials were an average of ten measurements.

3.3.8 Surface chemical properties

FTIR spectra were collected with a transmission FTIR spectrometer (Perkin Elmer) with single bounce diamond ATR (Attenuated Total Reflectance) accessory. All the spectra of measured samples were averaged from 32 scans from 550 to 4000 cm^{-1} with a resolution of 4 cm^{-1}.

3.3.9 Solid carbon-13 NMR measurements

Solid carbon-13 NMR spectra were obtained on a Varian/Agilent VNMRS-400 instrument operating at 100.5 MHz. Samples were packed in 7.5 mm zirconia rotors and spun at 5500 Hz. Spinning sidebands were suppressed using the TOSS sequence. Spectra were acquired using a contact time of 2 ms and a recycle delay of 2 s. Typically 6000 transients were acquired.

3.3.10 X-ray photoelectron spectroscopy (XPS) analysis

X-ray photoelectron spectra were recorded on a Thermo Scientific K-Alpha X -ray Photoelectron Spectrometer. The survey spectra were taken with a pass energy of 200 eV and high resolution scans for chemical analysis were collected with a pass energy of 50 eV. All scans were acquired under charge neutralization conditions using a flood gun. The resulting spectra were processed

using Avantage data processing software. The binding energy was referenced to adventitious carbon at 285 eV.

3.3.11 X-ray diffraction (XRD) analysis

X-ray Diffraction measurements were performed on a Bruker Discover D8 Discover two-dimensional diffractometer with VANTEC 2D detector and CuKα radiation (λ=1.54 Å). The X-ray diffractograms were acquired at 40 kV and 40 mA with a 2θ (Bragg angle) range of 5-40°.

3.4 Discussion

3.4.1 Preparation of CNCC

The aldehyde content of DAMC fibers was determined to be 2.8 mmol/g by a hydroxylamine hydrochloride titration after periodate oxidation on cellulose. Cationization of DAMC fibers with GT process was through a Schiff base reaction to produce imine bonds between aldehyde groups of DAMC fibers and amide groups of the cationic reagent GT. The cationization reaction is shown in Scheme 3.1(b). CNCC was formed by heating the cationic DAMC fibers suspension at 60 °C. The white fibrous suspension turned clear after 30 minutes. The morphology of the cellulose fibers at each treatment step was observed by optical microscopy, and the images are shown in Figure 3.1. After periodate oxidation, the DAMC fibers show no significate differences when compared with the original cellulose fibers; the diameter of both fibers was around 30 μm (Figure 3.1(a) and 3.1(b)). However, after reaction with GT, the DAMC fibers were swollen more than twice, with a diameter of around 75 μm (Figure 3.1(c)). In order to see these swollen fibers clearly, a negative dye (tartrazine) was applied (see Figure 3.1(d)), but due to the addition of negative dye, the diameter decreased. After the hot water treatment of cationic DAMC fibers, it is no long possible to observe any features by optical microscopy.

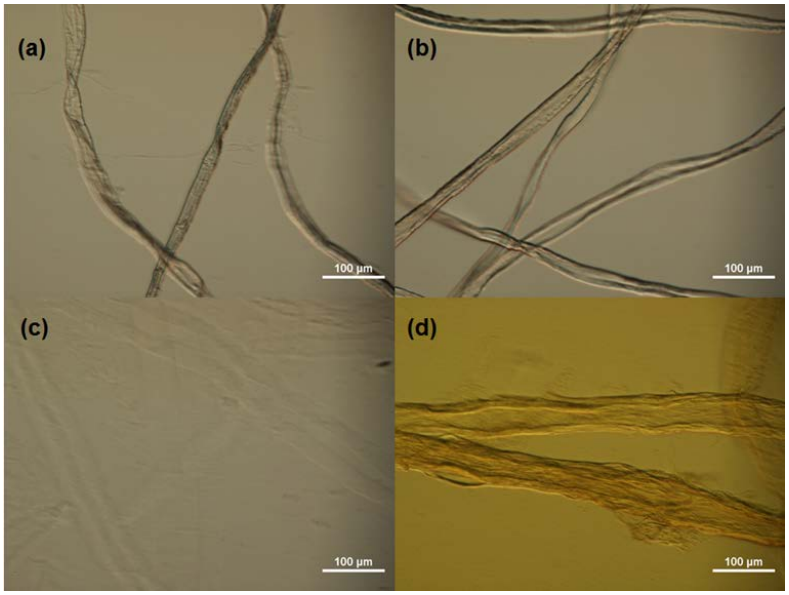

Figure 3.1 Optical microscopy images: (a) starting cellulose fibers, (b) DAMC fibers, (c) cationic DAMC fibers and (d) cationic DAMC fibers with negative dye.

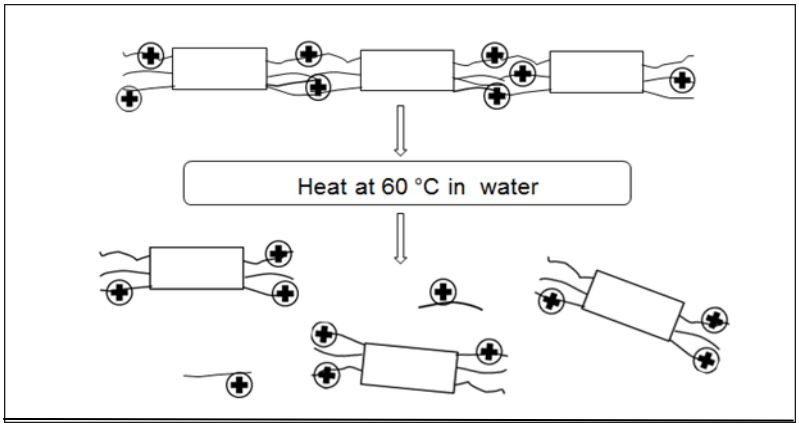

Figure 3.2 Schematic representation of the liberation of CNCC from positively charged cellulose fibers (CDAMC) under hot water treatment at 60 °C.

Cationic DAMC fibers were broken up into nanosize structures by the force of electrostatic repulsion between the nanocellulose structures arising from their positive charges, and moreover, the solubility of the cationically modified amorphous regions increased at elevated temperature. This way the crystalline parts can be released and separated from each other, as shown in Figure 3.2. By treating DAMC fibers in hot water at 60 °C for half an hour, the appearance of DAMC fibers did not change appreciably (Figure 3.3(a), and by comparison of Figure 3.3(b) and Figure 3.1(b)). The weight of unfibrillated DAMC fiber was obtained by filtering the DAMC fibers

though a 4 µm pore size nylon cloth and drying in the oven, and it was found that about 99 % of DAMC fibers were still in the fibrous state. From our previous work [9], DAMC fibers with an aldehyde content of about 8.2 mmol/g can form nanosize cellulose structures (SNCC) by a hot water treatment at 80 °C for six hours, and 30% DAMC fibers are still in a fibrous state. Cellulose fibers can form nanosize structures spontaneously by introducing negatively charged groups onto fibers, at carboxyl group content of least 3.0 - 3.5 mmol/g [4], or by first introducing less charge groups (such as TEMPO (2,2,6,6-tetramethylpiperidinyl-1-oxyl) mediated oxidation [26], carboxylmethylation [27] and periodate-chlorite oxidation [28]), followed by extensive mechanical treatment (such as high pressure homogenization or sonication), which process also yields nanofibril cellulose or nanocrystalline cellulose. The mechanical energy can be reduced by increasing the charge content [28]. Both negative and positive charges can provide electrostatic repulsion between fibers, thus decreasing the energy required to fibrillate fibers into nanosize structures. Here we combined hot water treatment and the introduction of charge groups, by introducing positively charged groups onto cellulose and replacing the subsequent mechanical treatment by a hot water treatment, which does not require any specially designed homogenizers or sonication devices. This method uses no hazardous organic solvents and is environmentally friendly. Sodium periodate is expensive, but can be recycled and recovered with a 94% efficiency [29]. The cost would be high if sodium periodate is not recycled for reuse after the reaction. Almost 99% cellulose fibers were fibrillated (Figure 3.3(c)) and the yield of positively charged NCC was around 45% at the end of the reaction, the remaining being dissolved cationic cellulose.

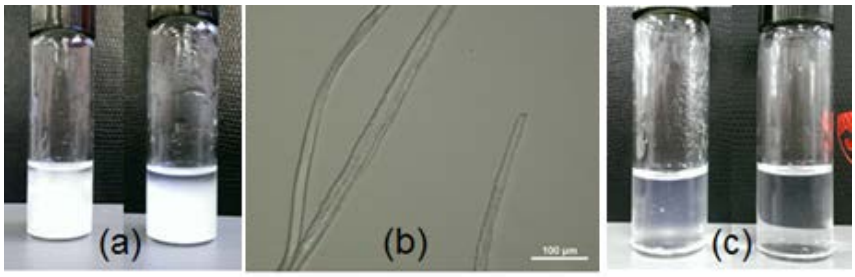

Figure 3.3 (a) photographs of suspension of DAMC fibers (left) and after treatment by 60 °C hot water for half an hour (right), (b) optical microscopy image of DAMC fibers after hot water treatment, and (c) photographs of suspension of cationic DAMC fibers (left, the translucence is due to the high degree of swelling of cationic DAMC fibers) and the suspension turns clear after treatment by 60 °C hot water for half an hour (right).

3.4.2 Morphology of CNCC

AFM image shows rod-like nanosize cellulose formed after hot water treatment of cationic DAMC fibers, we refer to these rod-like nanofibers as cationic nanocrystalline cellulose (CNCC). As shown in Figure 3.4(a), the length of CNCC is around 120 nm, and the width is around 5 nm. Compared to the previously reported methods [10-12], this process does not require the preparation of NCC by a strong acid hydrolysis before the surface cationization. Nanosized cationic NCC formed directly after hot water treatment. TEM image confirmed that the length of these CNCC is around 120 nm (Figure 3.4(b)).

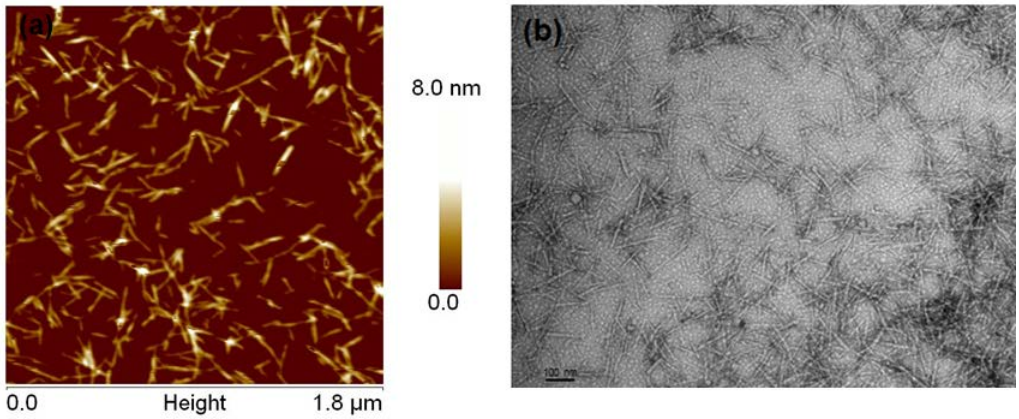

Figure 3.4 (a) AFM height image of CNCC, (b) TEM image of CNCC.

3.4.3 Zeta potential and charge content

The zeta potential of CNCC was found to be + 27 ± 0.7 mV at pH 6.3, which proofs that positive charges were grafted on CNCC. The content of the positive charges of CNCC was determined by conductometric titration of chloride ions with AgNO3 (Figure 3.5). The charge content was determined to be 1.68 mmol/g. For comparison the aldehyde content of DAMC fibers was 2.8 mmol/g, implying that on average more than one cationic group was attached to each dialdehyde group. The aldehyde and cationic charge content of CNCC both exceed the theoretical maximum surface aldehyde or charge content of a rod-like NCC particles. Similar to previously reported ENCC particles which have hair-like protruding dicarboxyl cellulose chains [4, 5]. CNCC particles have also protruding cellulose chains but with cationic groups. We refer to this type of CNCC as hairy cationic nanocrystalline cellulose.

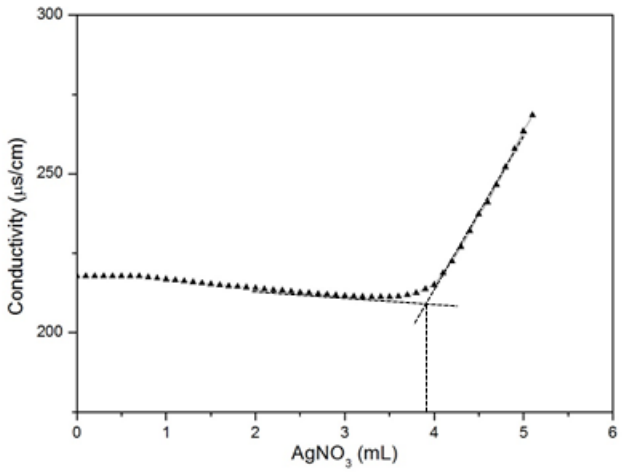

Figure 3.5 Conductometric titration of CNCC suspension, titrated with 10 mM $AgNO_3$.

3.4.4 Chemical properties of CNCC

The DAMC fibers and CNCC were characterized by FTIR, and the spectra are shown in Figure 3.6. The spectrum of DAMC fibers has two characteristics peaks, a small peak at 1730 cm^{-1} and another one at 880 cm^{-1}. These are due to carbonyl groups stretching and the hemiacetal linkages formed from the dialdehyde groups, respectively [30]. The peak at 1700 cm^{-1} of CNCC is due to the carbonyl group in cationic reagent GT, and the peak at 924 cm^{-1} is due to the nitrogen – nitrogen bond in GT, the small peaks at 1480 cm^{-1} and 1415 cm^{-1} are assigned to the methyl groups and carbon-nitrogen bond in the quaternary ammonium groups in GT, respectively. An important evidence of successfully grafting GT with DAMC fibers is the formation of imine bonds with a peak at 1570 cm^{-1}. This peak is assigned to carbon-nitrogen double bonds in imines [31], however, this peak is also assigned to the nitrogen-hydrogen bending vibration in GT [24]. Solid carbon NMR spectra were acquired to further investigate the formation of imine bonds (Figure 3.7). The peaks in the spectrum of the starting cellulose fibers are assigned as follows: 105 ppm for C1, 90 ppm for C4, 85 ppm for C4', 80-70 ppm region for C2,3,5, and 70-60 ppm for C6, respectively [32]. The spectrum of DAMC fibers shows a broad peak located at 105-85 ppm, and the absence of a carbonyl signal expected at 175-172 ppm indicates that the aldehyde groups of solid DAMC fibers formed hemiacetal linkages [33]. Contrary to DAMC fibers, the spectrum of CNCC between 60 and 110 ppm is very similar to the starting cellulose, but CNCC has a very sharp peak at 56 ppm which is due to the carbon signal of methyl groups on the quaternary ammonium group and

the small peak at 172-158 ppm confirms the formation of imine bonds. The broad range of this peak is due to the combination of carbonyl carbon of GT, which usually appears at 172 ppm.

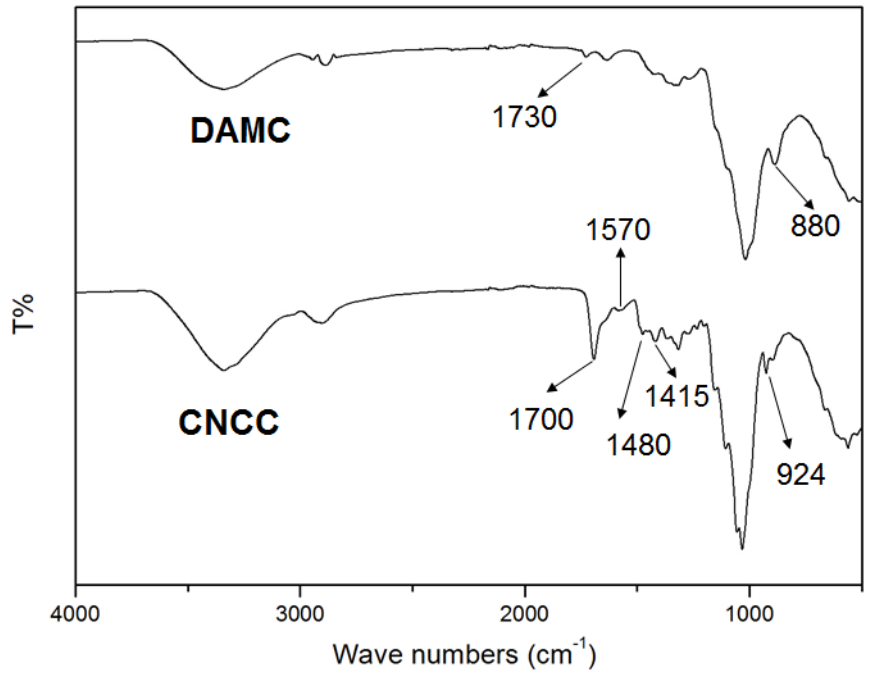

Figure 3.6 FTIR spectra of DAMC fibers and CNCC.

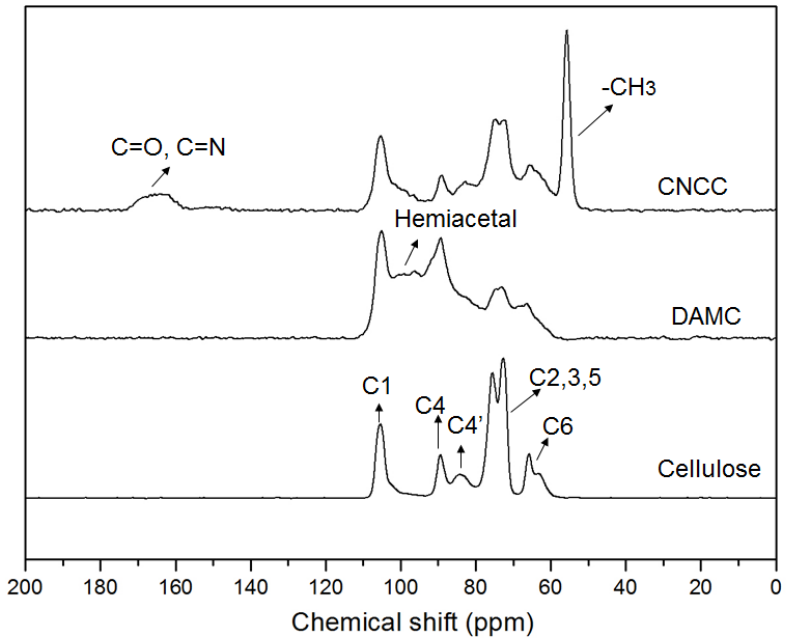

Figure 3.7 Solid state carbon-13 NMR spectra of starting cellulose fibers, DAMC fibers, and CNCC.

3.4.5 XPS analysis

XPS was applied on DAMC fibers and CNCC to further provide more information of grafting positive charges onto nanofibers. The XPS wide survey scan of both DAMC fibers and CNCC show the expected signals of oxygen and carbon at 532 eV and 286 eV (Figure 3.8), but CNCC has two extra peaks at 401 eV and 198 eV for nitrogen and chlorine respectively, which are from the grafted GT molecules. The high resolution C 1s spectra of DAMC fibers and CNCC with their deconvolutions were also obtained (Figure 3.9). The deconvolution of DAMC fibers and CNCC on C 1s gives three similar peaks: peak 1 with binding energy 285 eV corresponds to a carbon atom bound only to other carbon atoms (C-C) or hydrogen atoms (C-H), peak 2 at 286.6 eV represents to a carbon atom bound to a single noncarbonyl oxygen atom C-O, and peak 3 at 287.8 eV corresponds to a carbon atom bound to one carbonyl oxygen atom (C=O) or two noncarbonyl oxygen atoms (O-C-O). For CNCC, a fourth peak shows at 288.5 eV which corresponds to peaks for O=C-N and C-N from GT molecules. A C=N peak should have appeared as well, but no such peaks in the C 1s spectrum were observed, because it is located in the same binding energy region as C-O in peak 2 (286.6 eV) (Figure 3.9(b)). The decreased ratio between peak 3 and peaks 2 of CNCC compared to that of DAMC fibers also indicates that aldehyde groups were consumed, forming new C=N bonds with amine groups. XPS analysis thus further confirms that the cationic grafts did occur.

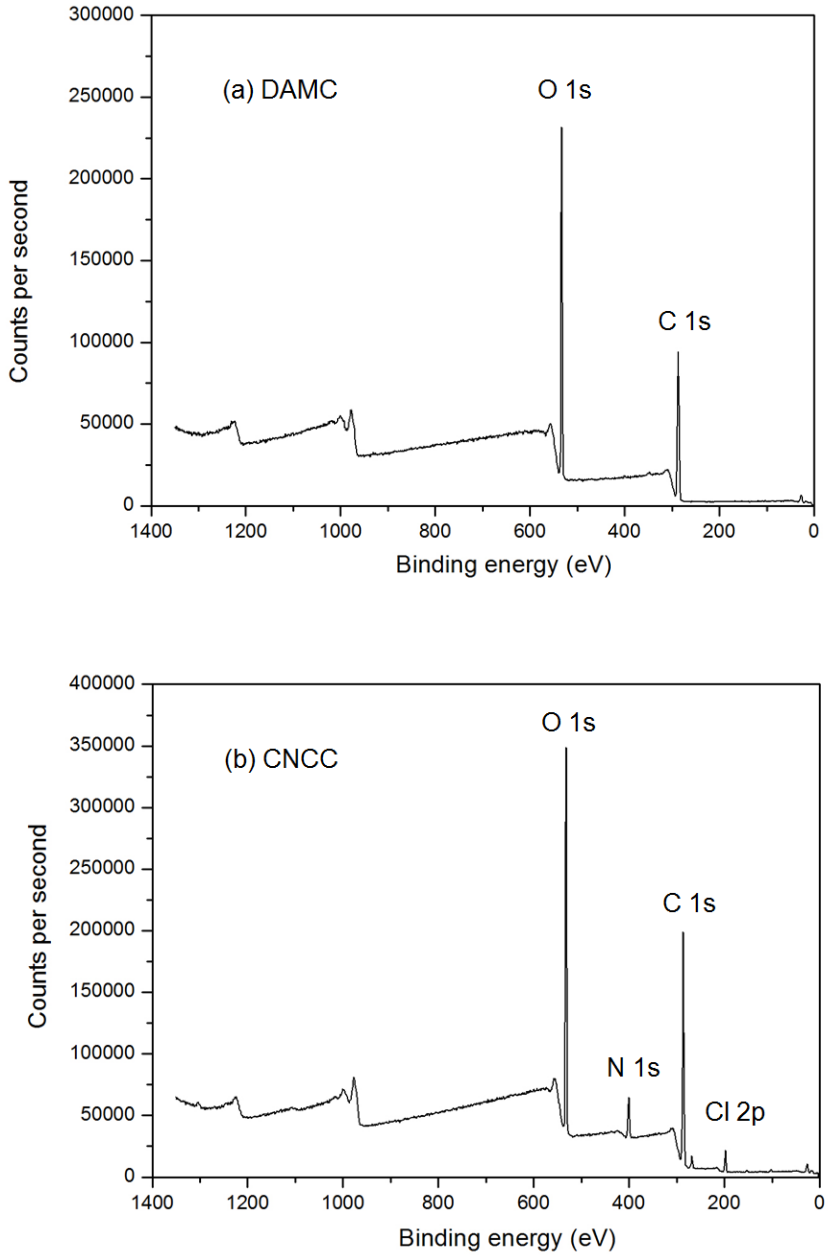

Figure 3.8 XPS wide survey scan spectra of (a) DAMC fibers and (b) CNCC.

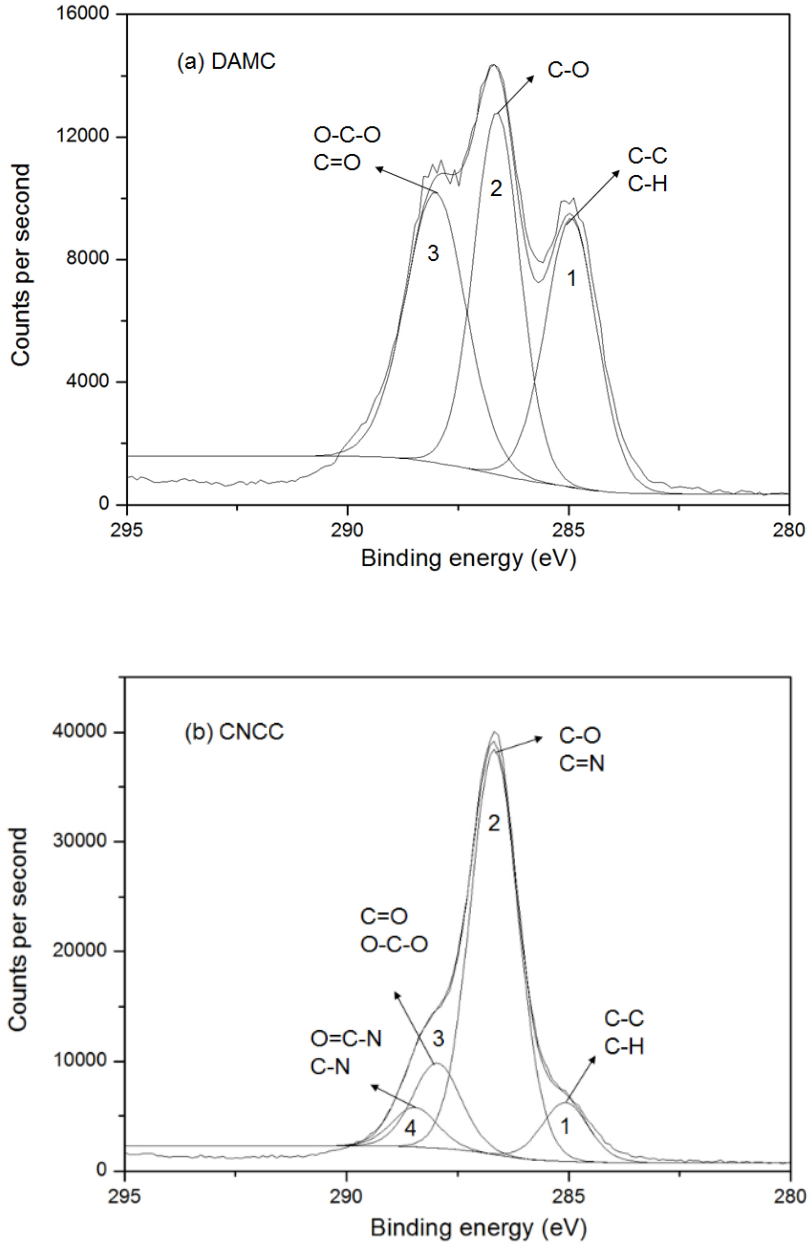

Figure 3.9 XPS high resolution scan of C 1s spectra of (a) DAMC fibers and (b) CNCC.

3.4.6 Crystalline properties

The XRD profiles of starting pulp, DAMC fibers, CDAMC fibers and CNCC are presented in Figure 3.10. The typical peaks of cellulose were assigned according to Nishiyama et al. [34], 2θ angles at 15.3° and 16. 5° correspond to the $(1\ \bar{1}\ 0)$ and $(1\ 1\ 0)$ peaks, which are not clearly

resolved; the (2 0 0) peak is located at a 2θ angle of 22.6°, and corresponds to the main crystalline region of cellulose.

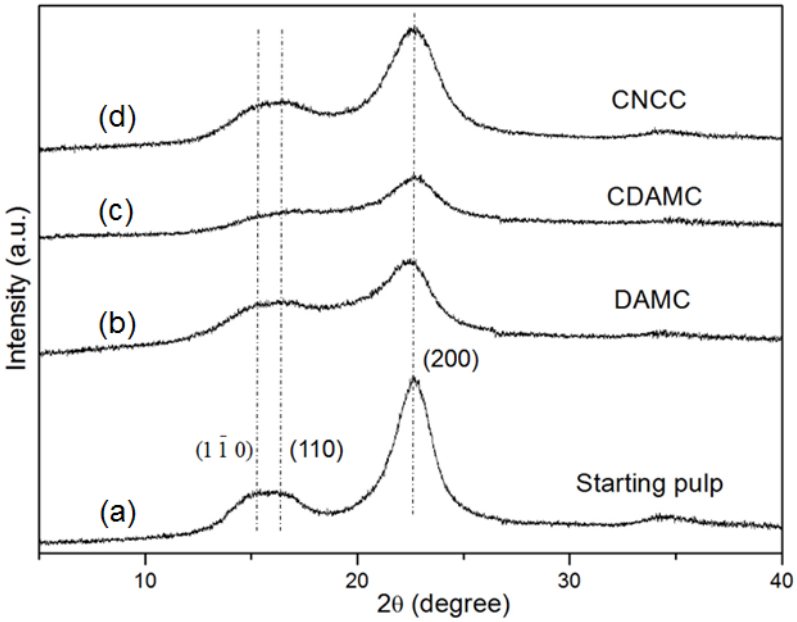

Figure 3.10 X-ray diffractograms of (a) starting pulp, (b) DAMC fibers, (c) CDAMC fibers, and (d) CNCC.

The crystallinity index (C.I.) of cellulose was defined according to Segal et al. [35]:

$$C.I. = \frac{I_{200} - I_{AM}}{I_{200}} \times 100\% \qquad (1)$$

where I_{200} is the intensity of the (2 0 0) plane reflection, I_{AM} is the intensity at 2θ = 18°, corresponding to the minimum between the planes (2 0 0) and (1 1 0) in a diffractogram [36].

Using equation (1), the C.I. of starting cellulose was 75%, it decreased to 49% for DAMC fibers after the periodate oxidation. The amorphous regions and the surface of crystalline regions in cellulose are more accessible to periodate oxidation, the deceasing of crystallinity is due to opening of the glucose rings and partially destructing of the ordered structure of crystalline regions of cellulose [37]. The result is also consistent with previous experiments [33, 38], which found that the crystalline index of cellulose was decreased according to the oxidation level by periodate oxidation. The C.I. of CDAMC fibers decreased to 43%, this is due to the further modification of DAMC fibers with GT reagent. The C.I. of CNCC was 67%, although it is lower than the starting

cellulose, the original crystalline structure of CNCC (cellulose type I) was well preserved from the XRD pattern (Figure 3.10(d)), which is consistent with a previous report on modifying NCC with a cationic surfactant (hexadecyltrimethylammonium (HDTMA) bromide) under various conditions, which also did not considerably change the X-ray patterns of NCC [39]. Comparing to CDAMC fibers, the C.I. of CNCC is much higher. This result also supports our hypothesis of the formation of CNCC (Figure 3.2). The increased C.I. of CNCC is due to part of the cationic dialdehyde cellulose chains which were separated from the CNCC, thus reducing the content of amorphous regions of CNCC. Due to the modification, both the protruding cationic dialdehyde cellulose chains and the surface cationization on crystalline regions of CNCC contribute to the decreasing C.I. of CNCC.

3.5 Conclusion

Hairy cationic nanocrystalline cellulose (CNCC) was produced by periodate oxidation and cationization with (2-hydrazinyl-2-oxoethyl)-trimethylazanium chloride (GT) of cellulose, followed by hot water treatment at 60 °C for half an hour. This is an easy and environmentally friendly method performed under mild aqueous conditions. Introducing positively charged groups onto DAMC fibers, greatly improves the efficiency of fibrillation of DAMC fibers into nanosize structures under aqueous thermo-treatment. CNCC typically has a width of 5 nm and a length about 120 nm, 67% crystalline index and a positive charge content of 1.68 mmol/g. The successful grafting of positive charges onto nanocellulose was confirmed by FTIR, solid carbon-13 NMR and XPS analysis. CNCC has the potential application in anionic dye or heave metal removal, or colloid particle flocculation in water treatment, or used as coagulation aids for anionic fillers.

3.6 Acknowledgements

The authors would like to thank the Natural Science and Engineering Research Council of Canada (NSERC) for the funding of an industrial research chair cosponsored by FPInnovations, funding of the NSERC Strategic Research Network on Green Wood Fiber Products and the FQRNT Centre for Self-Assembled Chemical Structures (CSACS).

3.7 References

[1] Schurz, J. A bright future for cellulose, Prog. Polym. Sci. 1999, 24, 481 - 483.

[2] Roman, M., Winter, W.T. Cellulose nanocrystals: From discovery to application, 2006 International Conference on Nanotechnology.

[3] Abitbol, T., Elisabeth, K., Gray, D. Estimation of the surface sulfur content of cellulose nanocrystals prepared by sulfuric acid hydrolysis. Cellulose, 2013, 20, 785-794.

[4] Yang, H., Alam, Md. N., van de Ven, T.G.M. Highly charged nanocrystalline cellulose and dicarboxylated cellulose from periodate and chlorite oxidized cellulose fibers. Cellulose, 2013, 20 (4):1865-1875.

[5] Sheikhi, A., Yang, H., Alam, Md. N., van de Ven, T.G.M. Highly stable, functional hairy nanoparticles and biopolymers from wood fibers: Towards sustainable nanotechnology. Journal of Visualized Experiments, 2016, accepted.

[6] Elisabeth, K., Derek, G. Surface PEG-grafting of cellulose nanocrystals in aqueous media. Langmuir, 2010, 26 (16), 13450-13456.

[7] Araki, J., Wada, M., Kuga, S. Steric stabilization of a cellulose microcrystal suspension by poly(ethylene glycol) grafting. Langmuir, 2001, 17, 21-27.

[8] Morandi, G., Heath, L., Thielemans, W. Cellulose nanocrystals grafted with polystyrene chains through surface-initiated atom transfer radical polymerization (SI-ATRP). Langmuir 2009, 25, 8280-8286.

[9] Yang, H., Chen, D., van de Ven, T.G.M. Preparation and characterization of sterically stabilized nanocrystalline cellulose obtained by periodate oxidation of cellulose fibers. Cellulose, 2015, 22, 1743-1752.

[10] Hasani, M., Cranston, E. D., Westman, G., Gray, D. Cationic surface functionalization of cellulose nanocrystals. Soft Matter, 2008, 4, 2238-2244.

[11] Eyley, S., Thielemans, W. Imidazolium grafted cellulose nanocrystals for ion exchange applications. Chem. Commun., 2011, 47, 4177-4179.

[12] Jasmani, L., Eyley, S., Wallbridge, R., and Thielemans, W. A facile one-pot route to cationic cellulose nanocrystals. Nanoscale, 2013, 5, 10207-10211.

[13] Hou, Q. X.; Liu, W.; Liu, Z. H.; Bai, L. L. Characteristics of wood cellulose fibers treated with periodate and bisulfite. Ind. Eng. Chem. Res., 2007, 46, 7830-7837.

[14] Sabzalia, Z., Alam, Md. N., and van de Ven, T.G.M. Internally crosslinked and hydrophobically modified cellulose fibers. Cellulose, 2014, 21, 1381-1393.
[15] Bhattacharyya, D., Hestekin, J.A., Brushaber, P., Cullen, L., Bachas, L.G., Sikdar, S.K. Novel poly-glutamic acid functionalized microfiltration membranes for sorption of heavy metals at high capacity. Journal of Membrane Science, 1998, 141, 121-135.
[16] Maekawa, E., Koshijima, T. Properties of 2, 3-dicarboxyl cellulose combined with various metalic ions. Journal of Applied Polymer Science, 1984, 29, 2289-2297.
[17] Casu, B., Naggi, A., Torri, G., Allegra, G., Meille, S.V., Cosani, A., Terbojevich, M. Stereoregular acyclic polyalcohols and polyacetates from cellulose and amylase. Macromolecules, 1985, 18, 2762-2767.
[18] Van Brussel-Verraest, D. L., Besemer, A. C., Thiewes, H. J., Verwillingen, A. M. Y. Cationic cellulosic fibres, 2003, Patent no. WO03006739.
[19] Sirviö, J., Honka, A., Liimatainen, H., Niinimäki, J., Hormi, O. Synthesis of highly cationic water-soluble cellulose derivative and its potential as novel biopolymeric flocculation agent. Carbohydrate Polymers 2011, 86(1), 266-270.
[20] Liimatainen, H., Suopajärvi,T., Sirviöa, J.A., Hormi, O., Niinimäki, J. Fabrication of cationic cellulosic nanofibrils through aqueous quaternization pretreatment and their use in colloid aggregation. Carbohydrate Polymers, 2014, 103, 187-192.
[21] Mehltretter, C.L., Yeates, T.E., Hamerstrand, G.E., Hofreitter, B.T. and Rist, C.E. Preparation of cationic aldehyde starches for wet-strength paper. Tappi, 1962, 45(9), 750-752.
[22] Visankob, M., Liimatainen, H., Sirviöa, J.A., Heiskanen, J.P., Niinimäki, J., Hormi, O. Amphiphilic cellulose nanocrystals from acid-free oxidative treatment: physicochemical characteristics and use as an oil-water stabilizer. Biomacromolecules, 2014, 15 (7), 2769-2775.
[23] Sirviöa, J.A., Visankob, M., Laitinena, O., Ämmäläa, A., Liimatainen, H. Amino-modified cellulose nanocrystals with adjustable hydrophobicity from combined regioselective oxidation and reductive amination. Carbohydrate Polymers, 2016, 136, 581-587.
[24] Dash, R., Elder, T., Ragauskas, A.J. Grafting of model primary amine compounds to cellulose nanowhiskers through periodate oxidation. Cellulose, 2012, 19, 2069-2079.
[25] Jin, L.Q., Li, W.G., Xu, Q.H., Sun, Q.C. Amino-functionalized nanocrystalline cellulose as an adsorbent for anionic dyes. Cellulose, 2015, 22, 2243-2256.

[26] Saito, T., Hirota, M., Tamura, N., Kimura, S., Fukuzumi, H., Heux, L. and Isogai, A. Individualization of nano-sized plant cellulose fibrils by direct surface carboxylation using TEMPO catalyst under neutral conditions. Biomacromolecules, 2009, 10, 1992-1996.

[27] Wågberg, L., Decher, G., Norgren, M., Lindström, T., Ankerfors, M., Axnäs, K. The build-up of polyelectrolyte multilayers of microfibrillated cellulose and cationic polyelectrolytes. 2008, Langmuir, 24, 3, 784-795.

[28] Tejado, A., Alam, Md. N., Antal, M., Yang, H., van de Ven, T.G.M. Energy requirements for the disintegration of cellulose fibers into cellulose nanofibers. Cellulose, 2012, 19, 831-842.

[29] Liimatainen, H., Sirviö, J., Pajari, H., Hormi, O., Niinimäki, J. Regeneration and recycling of aqueous periodate solution in dialdehyde cellulose production. Journal of Wood Chemistry and Technology, 2013, 33 (4), 258-266.

[30] Kim, U.J., Wada, M., Kuga, S. Solubilization of dialdehyde cellulose by hot water. Carbohydrate Polymers, 2004, 56, 7-10.

[31] Lin, H., Yao, L.R., Chen, Y., Wang, H. Structure and properties of silk fibroin modified cotton. Fibers and polymers, 2008, 9 (2), 113-120.

[32] Horri, F., Yamamoto, H., Kitamaru, R., Tanahashi, M., Higuchi, T. Transformation of native cellulose crystals induced by saturated steam at high temperatures. Macromolecules, 1987, 20, 2946– 2949.

[33] Kim, U.J., Kuga, S., Wada, M., Okano, T., and Kondo, T. Periodate oxidation of crystalline cellulose. Biomacromolecules, 2000, 1(3), 488-492.

[34] Nishiyama, Y., Langan, P., Chanzy, H. Crystal structure and hydrogen-bonding system in cellulose I from synchrotron x-ray and neutron fiber diffraction. J. Am. Chem. Soc., 2002, 124, 9074–9082.

[35] Segal, L., Creely, J.J., Martin, A.E., Conrad, C.M. An empirical method for estimating the degree of crystallinity of native cellulose using the X-Ray diffractometer. Textile Res. J., 1959, 29, 786-794.

[36] Duchemin, B., Newman, R., Staiger, M. Phase transformations in microcrystalline cellulose due to partial dissolution. Cellulose, 2007, 14, 311-320.

[37] Sun, B., Hou, Q.X., Liu, Z.H., Ni, Y.H. Sodium periodate oxidation of cellulose nanocrystal and its application as a paper wet strength additive. Cellulose, 2015, 22, 1135-1146.

[38] Varma, A.J., Chavan, V.B. A study of crystallinity changes in oxidised celluloses. Polymer Degradation and Stability, 1995, 49, 245-250.
[39] Kaboorani, A., Riedl, B. Surface modification of cellulose nanocrystals (CNC) by a cationic surfactant. Industrial Crops and Products, 2015, 65, 45-55.

Bridging Section between Chapters 3 and 4

In the previous two chapters, two types of NCC (SNCC and CNCC) have been introduced, both SNCC and CNCC are obtained from a top-down technique, with certain dimensions according to their preparation methods.

In the next chapter, end-to-end assembly of nanocellulose fibers from a bottom-up route will be performed with electrosterically stabilized nanocrystalline cellulose by two different methods, namely a bioconjugation reaction between amine and carboxyl groups, and a 1,3-dipolar cycloaddition click reaction between azide and terminal alkyne groups. To the best of our knowledge, this is the first end-to-end assembly of nanocellulose from a bottom-up route to obtain nanofibers with a high aspect ratio. The methods of the assembly process will be described in detail in the next chapter. The results of this research have been reported in the following paper:

A bottom-up route to a chemically end-to-end assembly of nanocellulose fibers. Han Yang, Theo van de Ven. 2016, Biomacromolecules, in press.

Chapter 4. A bottom-up route to a chemically end-to-end assembly of nanocellulose fibers

4.1 Abstract

In this work, we take advantage of the rod-like structure of electrosterically stabilized nanocrystalline cellulose (ENCC), which has dicarboxylated cellulose (DCC) chains protruding from both ends, providing electrosterical stability for ENCC particles, to chemically end-to-end assemble these particles into nanocellulose fibers. ENCC with shorter DCC chains can be obtained by a mild hydrolysis of ENCC with HCl, and subsequently the hydrolyzed ENCC (HENCC) is suitable to be assembled into high aspect ratio nanofibers by chemically cross-linking HENCC from one end to another. Two sets of HENCC were prepared by carbodiimide-mediated formation of an alkyne and an azide derivative, respectively. Cross-linking these two sets of HENCC was performed by a click reaction. HENCC were also end-to-end crosslinked by a bioconjugation reaction, with a diamine. From atomic force microscopy (AFM) images, about ten HENCC nanoparticles were cross-linked and formed high aspect ratio nanofibers with a width of about 6 nm and a length of more than one micrometer.

4.2 Introduction

Cellulose is a natural carbohydrate polymer, and is the most abundant and sustainable biomaterial on earth [1]. Historically cellulose has been used as a building, combustion, clothing and papermaking material in its various forms such as wood, cotton or ramie for thousands of years [2]. For the past one or two centuries, cellulose has been used as a raw chemical material in industry to produce large scale commercial products such as cellulose esters, which are widely applied in membranes, films, pharmaceuticals, etc. [3]. Recently, nanotechnology has attracted a lot of attention due to the large surface area of the nanosized particles and their unique chemical and physical properties [4]. The combination of cellulose and nanotechnology has opened many opportunities in cellulose research, especially the preparation or isolation of cellulose nanoparticles, which provide the necessary starting materials for research on cellulose nanomaterials.

Two major types of nanocellulose exist, namely nanocrystalline cellulose (NCC) and nanofibrillar cellulose (NFC). NCC (also called CNC, cellulose nanocrystals) is usually prepared from sulfuric acid hydrolysis on cellulose pulp (NCC obtained with this method contains sulfate ester groups) [5], or by ammonium persulfate treatment (NCC containing carboxyl groups) [6]. A different class of nanocellulose can be made in which the particles consist of a central crystalline region from which part of the amorphous regions are protruding from both ends; we refer to these nanoparticles as hairy nanocellulose. An example is electrosterically stabilized NCC (ENCC) which contains a high carboxyl content [7], and which can be produced by a sequential periodate-chlorite oxidation treatment, or by periodate oxidation followed by a hot-water treatment which yields sterically stabilized NCC (SNCC) without any charged groups [8]. NCC prepared from wood fibers by the various methods mentioned above usually has a width of 5 to 10 nm and is 100-250 nm in length. NFC is another type of nanocellulose, which is obtained by mechanical treatment (homogenization or sonication) on chemically or enzymatically [9] pre-treated cellulose fibers. The chemical treatments include 2,2,6,6-tetramethylpiperidine-1-oxyl (TEMPO) radical mediated oxidation reaction [10], or periodate-chlorite sequential oxidation [11] to introduce negative charges onto the cellulose fibers prior to the mechanical treatment; in this way the energy consumption from

the mechanical treatment is reduced [12]. NFC usually has a length of about a few micrometers and a width of 3-25 nm depending on the preparation method.

Although the methods for preparation of nanocellulose from wood fibers involve chemical, physical, or enzymatic methodologies, all of these methods are top-down techniques, which yield nanocellulose with certain dimensions and aspect ratios. A lot of research has been done on the modification or assembly of nanocellulose by taking advantage of its numerous hydroxyl or carboxyl groups. The Huisgen cycloaddition click reaction is a 1,3-dipolar cycloaddition between an azide and a terminal alkyne to yield a 1,2,3-triazole, catalyzed by Cu(I) salts or Cu(II) salts with a reducing agent such as sodium ascorbate [13]. Due to its mild reaction conditions, rapid reaction rates, high selectivity and high yield [14], the click reaction was recently also applied to modify or assemble nanocellulose, thus extending the applications of nanocellulose. A highly fluorescent NFC was prepared by introducing fluorescent groups onto NFC through a click reaction in aqueous media [15]. This decorated NFC could be an interesting material for catalyst carriers or making nanocomposites. Mushroom-like nanoparticles were prepared by conjugating NCC and β-casein protein via a click reaction, which demonstrated the possibility to directly assemble nanobiomaterials and nanovesicles [16]. NCC was also assembled into large-scale forms such as composite films [17], in which NCC shows a promising nanoreinforcing effect for the polymeric matrix by chemical linkages formed though click chemistry.

An attempt to assemble NCC in large nano-scale structure was tried by Filpponen et al [18]. NCC nanorods modified with 11-azido-3, 6, 9-trioxaundecan-1-amine and propargylamine were crosslinked by a click reaction to yield a nanoplatelet gel. This is the first research on the chemically assembly of NCC with a bottom-up route in order to make different nano-scale structures, although the nanoplatelet gel in this work was significantly larger (more than 500 nm in width and 1.5 μm in length) than the initial NCC particles and had a much low aspect ratio (about three). Till now, no research has been done to “grow” nanofibers from by a bottom-up method by end-to-end crosslinking in one dimension through a click reaction or any other method. The major difficulty is that it is hard to control modifications occurring only on the two ends of NCC nano-rods, since all the surface of NCC is exposed to modifications, and hence the ends and sides of NCC will both be modified, although not necessarily with the same rate.

In this work, electrosterically stabilized nanocrystalline cellulose (ENCC) has been mildly hydrolyzed to cut the dicarboxylated cellulose chains protruding from the two ends of the nanorods. Subsequently the hydrolyzed ENCC (HENCC) was modified with an alkyne and an azide, respectively. These two sets of modified HENCC were used as building blocks and cross-linked by click chemistry, hence the HENCC was assembled into long nanofibers end-to-end in one dimension, which resulted in fibers with the same width (about 6 nm) as HENCC, but about 1.2 µm in length, which is equal to about ten HENCC nanorods. The nanocellulose particles at each process were characterized by Fourier transform infrared spectroscopy (FTIR) and atomic force microscopy (AFM). To the best of our knowledge, this is the first end-to-end assembly of nanocellulose to obtain nanofibers with a high aspect ratio.

4.3 Experimental section

4.3.1 Materials

Softwood kraft pulp (Domtar, Canada) was used as a starting cellulose material. Chemicals for the reactions: sodium (meta) periodate, sodium chlorite (80% purity), ethylene glycol, sodium hydroxide, sodium bicarbonate, hydrogen chloride, copper(II) sulfate pentahydrate, ascorbic acid, adipic dihydrazide (ADH), N-(3-dimethylaminopropyl)-N'-ethylcarbodiimide hydrochloride (EDC), 1-amino-3-butyne, 3-azido-1-propanamine, disodium ethylenediaminetetraacetic acid (EDTA) were purchased form Sigma-Aldrich, hydrogen peroxide (30%) (Fisher), sodium chloride (ACP chemistry). All chemicals were used as received. Milli-Q water was used in all experiments.

4.3.2 Preparation of ENCC

ENCC was produced according to a previous procedure [7]. Briefly, softwood pulp was first oxidized by sodium periodate for 96 hours (1 g pulp and 1.33 g $NaIO_4$ were mixed with 66 mL water in a beaker, which was wrapped with aluminum foil to prevent entry of any light). Then the thoroughly washed oxidized pulp was oxidized by chlorite oxidation for 24 hours at pH = 5 (1.41 g $NaClO_2$, 1.41 g H_2O_2, 2.93 g NaCl and 50 mL water were used for 1 g of periodate oxidized pulp). ENCC was separated from the two-step oxidized pulp suspension by the addition of ethanol followed by centrifugation.

4.3.3 Preparation of HENCC

The hydrolysis of ENCC was performed with 3 N HCl (with 0.5 g ENCC) at 45 °C for 5 hours. The excess HCl was neutralized by adding $NaHCO_3$ at the end of hydrolysis. Then the product was purified by dialysis (MWCO = 12000 - 14000). The HENCC was kept as aqueous suspension or recovered by freeze-drying (Thermo ModulyoD freeze dryer).

4.3.4 Preparation of HENCC with alkyne groups (HENCC-AK)

A HENCC suspension (10 mL, 0.2 %) was mixed with a 100 µL EDC stock solution (the stock solution was prepared by dissolving 50 mg EDC in 1 mL water) for 20 min, and then 6 µL 1-amino-3-butyne was added into the suspension, the pH of the suspension was kept at 5 by adding HCl. The reaction was performed at room temperature under stirring for 24 hours (see scheme 4.1). Then the suspension was dialyzed (MWCO = 12000 - 14000) against distilled water for 2 days. The HENCC-AK was kept as an aqueous suspension or recovered by freeze-drying.

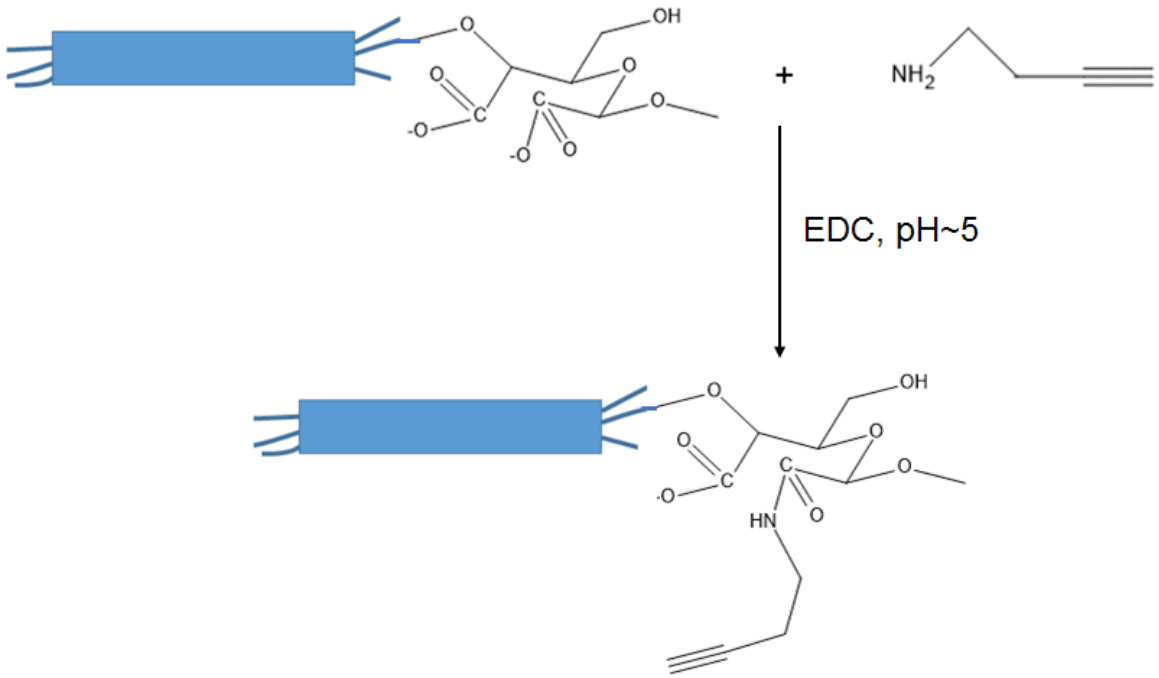

Scheme 4.1 The reaction between HENCC and 1-amino-3-butyne, for the production of HENCC-AK.

4.3.5 Preparation of HENCC with azide groups (HENCC-AZ)

A HENCC suspension (10 mL, 0.2 %) was mixed with a 100 µL EDC stock solution for 20 min, and then 8 µL 3-azido-1-propanamine was added into the suspension, the pH of the suspension was kept at 5 by adding HCl. The reaction was performed at room temperature under stirring for 24 hours (see scheme 4.2). Then the suspension was dialyzed (MWCO = 12000 - 14000) against distilled water for 2 days. The HENCC-AK was kept as an aqueous suspension or recovered by freeze-drying.

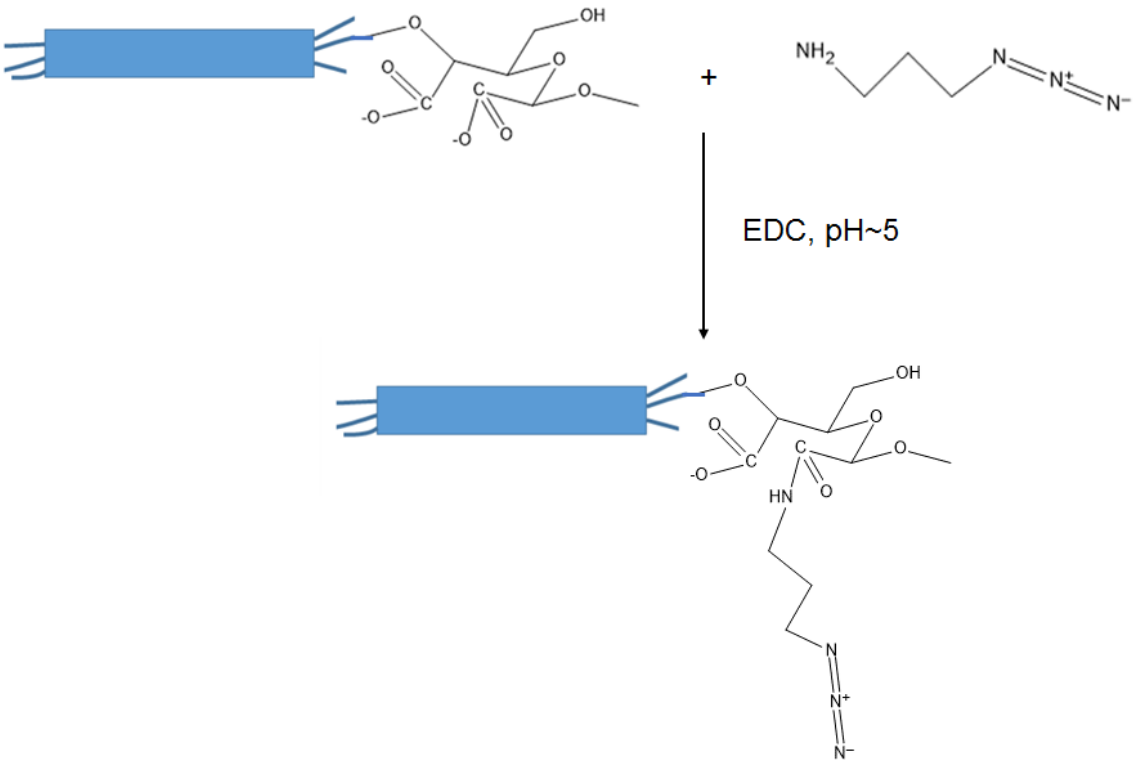

Scheme 4.2 The reaction between HENCC and 3-azido-1-propanamine, for the production of HENCC-AZ.

4.3.6 Preparation of clicked HENCC

Ten mL HENCC-AK suspension (0.1 %) and 10 mL HENCC-AZ suspension (0.1 %) were mixed by stirring for half an hour. Then, 20 µL of an aqueous $CuSO_4$ solution (0.2 mol/L) and 16 µL of ascorbic acid (0.5 mol/L) were added, and the mixture was vigorously stirred under nitrogen overnight (see scheme 4.3). The product was dialyzed (MWCO = 12000 - 14000) against a disodium EDTA solution (5 mM) for 12 h and finally against distilled water for two days.

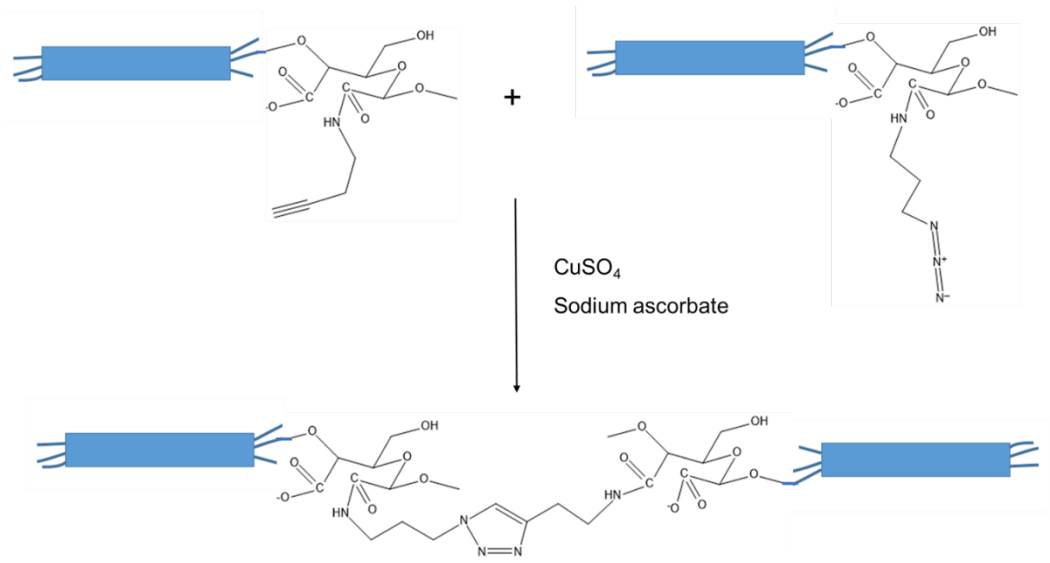

Scheme 4.3 The cross-linking reaction between HENCC-AK and HENCC-AZ.

4.3.7 Preparation of HENCC with –NH_2 groups

ADH (35 mg) was added to 10 mL of a 0.5% w/w HENCC suspension, and the pH was adjusted to 5 by adding 0.1 M HCl. Then 200 µL EDC stock solution (the stock solution was prepared by dissolving 50 mg EDC in 1 mL water) was added to this suspension. The suspension was stirred at room temperature for 8 h, and the pH was maintained at 5 by adding 0.1 M HCl during the reaction (see Scheme 4.4). The reaction was stopped by raising the pH to 6.8. Then the modified NH_2-HENCC suspension was purified by dialysis (MWCO 12000 - 14000). In this reaction, a large excess of ADH was used to prevent crosslinking at this stage.

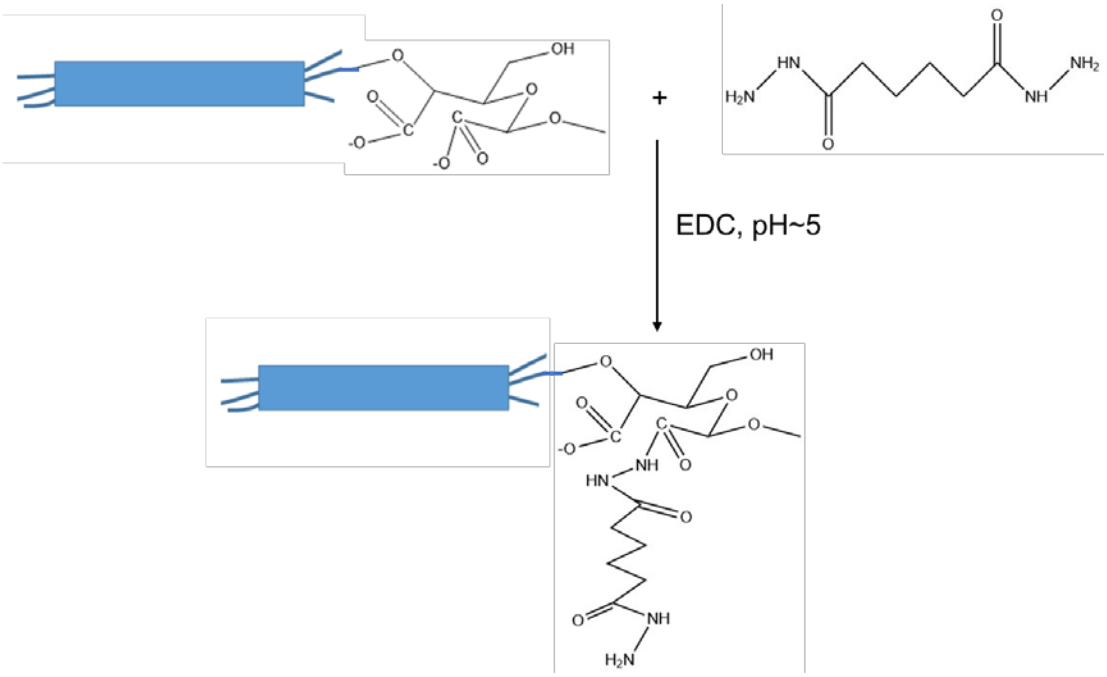

Scheme 4.4 The reaction between HENCC and ADH, for the production of HENCC-NH_2.

4.3.8 Preparation of cross-linked HENCC

Two mL 0.1 % NH_2-HENCC suspension and 2 mL 0.1% HENCC suspension were mixed by stirring for 1 hour, then 10 µL EDC stock solution (the stock solution was prepared by dissolving 50 mg EDC in 1 mL water) was added to this mixed suspension, the pH was maintained at 5 by adding 0.1 M HCl during the reaction (see Scheme 4.5). The reaction was stopped by raising the pH to 6.8. Then the cross-linked HENCC suspension was purified by dialysis (MWCO = 12000 - 14000).

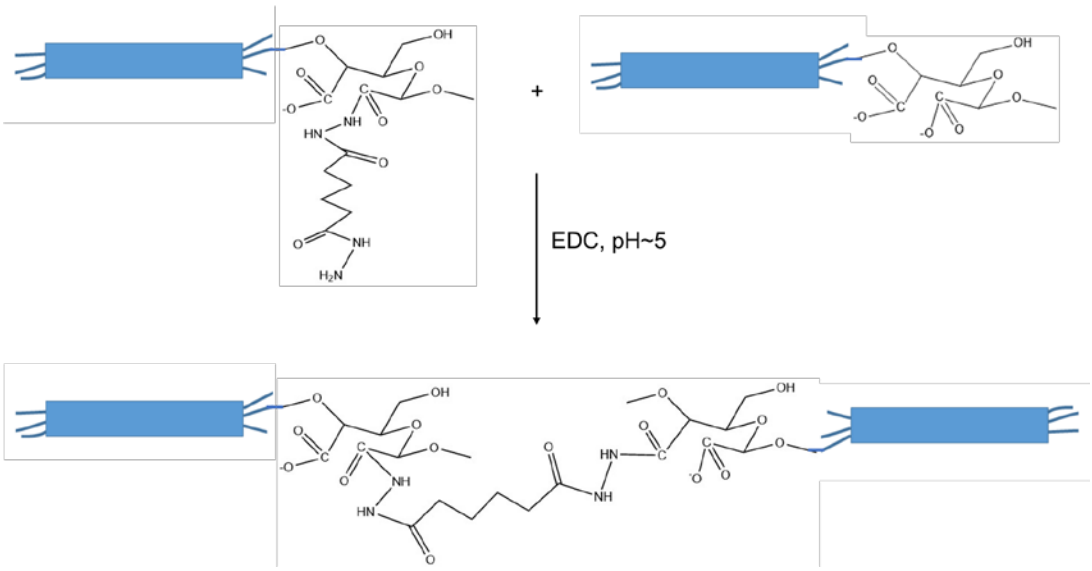

Scheme 4.5 The cross-linking reaction between HENCC-NH_2 and HENCC.

4.3.9 Conductometric titration

Conductometric titration was performed to obtain the charge density of ENCC and HENCC by using a Metrohm 836 Titrando titrator according to a pervious method [19]. A certain amount of sample and 2 mL (20 mmol/L) NaCl solution were mixed with 140 mL milli-Q water, the pH of this mixture was adjusted to around 3.2 by adding 0.1 M HCl. Then a 10 mM NaOH solution was added at a rate of 0.1 mL/min into the mixture up to a pH around 11. The part of the curve which represents weak acid on the titration graph gives the carboxyl content.

4.3.10 Surface chemical properties

The surface chemical properties of each samples were characterized with a FTIR spectrometer (Perkin Elmer UATR Two). Solid samples were placed directly on the ATR crystal and measured. All the spectra were averaged from 16 scans from 500 to 4000 cm^{-1} with a resolution of 4 cm^{-1}.

4.3.11 Dynamic light scattering (DLS) measurements

Hydrodynamic diameters of ENCC and HENCC were measured by Zetasizer (Malvern instruments, Nano-ZS). Sample suspensions were filtered through a 0.45 μm syringe filter (Pall Corporation) into a cuvette, and then the hydrodynamic diameter was obtained from six repeated measurements at room temperature.

4.3.12 Morphological properties

The morphology of ENCC, HENCC, HENCC-AK and HENCC-AZ was investigated by atomic force microscopy (AFM) (Nanoscope IIIa MultiMode with Extender (Veeco Metrology Group, Santa Barbara, CA)). Samples were dropped onto a freshly cleaved mica which was pre-coated with poly-L-Lysine, then the excess liquid was rinsed off by milli-Q water after 10 min. Air-dried samples were measured in tapping mode using silicon cantilevers (ACTA model, AppNano) with a nominal spring constant of 37 N/m, nominal resonant frequency of 300 kHz and nominal tip radius of 6 nm. Nanoscope Analysis 1.4 was used to process the AFM images.

4.4 Results and discussion

4.4.1 Preparation of ENCC and HENCC

ENCC was prepared from sequential periodate oxidation and chlorite oxidation treatment. The periodate oxidation selectively cleaves the C2 and C3 bonds of cellulose glucose units and oxidizes the C2 and C3 hydroxyl groups to 2,3-dialdehyde groups [20], then these 2,3-dialdehyde groups are further converted to 2,3-dicarboxyl groups by using sodium chlorite [21]. The morphology of ENCC was investigated by AFM and shown in Figure 4.1(a). ENCC are rod-like nanoparticles with a width about 7 nm and length about 130 nm. ENCC has a content of carboxyl groups of about 6 mmol/g, which is much higher than conventional NCC prepared from sulfuric acid hydrolysis (which contains charge groups of about 0.2 mmol/g) [22]. The theoretical maximum charge content of NCC calculated form the ratio of surface to total cellulose chains is about 0.8 mmol/g [19], which is much lower than ENCC. The amorphous regions of cellulose are much more accessible to chemical reactions than the crystalline regions, thus most of the dicarboxyl groups are present in the amorphous regions (i.e. in the protruding chains). The critical charge content above which cellulose fibers fall apart into nano-sized particles only by stirring is about 3 mmol/g [12]. The high content of negatively charged carboxyl groups after the modification increased the repulsion between each nanosized building block in the cellulose fibers and also increased the solubility of the amorphous regions, thus solubilizing the amorphous regions, and as a result releasing the crystalline regions, which leads to the formation of ENCC particles (shown in Figure 4.2, (a)-(b)). Most of the carboxyl groups are located on the two ends of ENCC particle, with dicarboxylated cellulose (DCC) chains protruding from the crystalline regions, as shown

previously [7] (Figure 4.2(b)).The protruding DCC chains on ENCC provide sufficient crosslinking sites, and thus by directly cross-linking ENCC particles by cationic metal ions, star-shaped or large raft shaped aggregates are formed [23]. Crosslinking ENCC with adipic acid dihydrazide (ADH) through a bio-conjugation reaction also leads to the formation of aggregates (Figure 4.3), instead of a regular ordered structures [19]. In order to have a better control on the assembly process, and to obtain a high aspect ratio of end-to-end cross-linked cellulose nanofiber chains, we need to reduce the available crosslinking sites on ENCC particles. Thus, as shown in Figure 4.2(b)-(c), hydrolysis was applied on ENCC particles to shorten these protruding DCC chains and eliminate any carboxyl groups on the surface of the crystalline region.

The hydrolysis was performed by using 3 mol/L HCl at elevated temperature, which is not expected to introduce any other charged groups [7, 24]. After hydrolysis, the content of carboxyl groups on ENCC was reduced to 1.2 mmol/g measured by conductometric titration. We refer to these hydrolyzed ENCC particles as HENCC. The morphology of HENCC is shown in Figure 4.1 (b). HENCC are also rod-like nanoparticles, and have a width about 6 nm and a length about 120 nm, which is similar to the dimension of ENCC. But HNECC particles have more sharp and clear edges than ENCC in an AFM image, which may due to the absence of most of the protruding DCC chains on HENCC. From DLS measurements, the hydrodynamic diameter of ENCC is about 188 nm, which is decreased to 86 nm for HENCC. This is due to the cutting of the protruding DCC chains by hydrolysis (Figure 4.2 (c)). The decreasing number of carboxyl groups on HENCC and the reduction in hydrodynamic diameter of HENCC, both show the successfully shortening of the length of protruding DCC chains at the ends of ENCC nanoparticles.

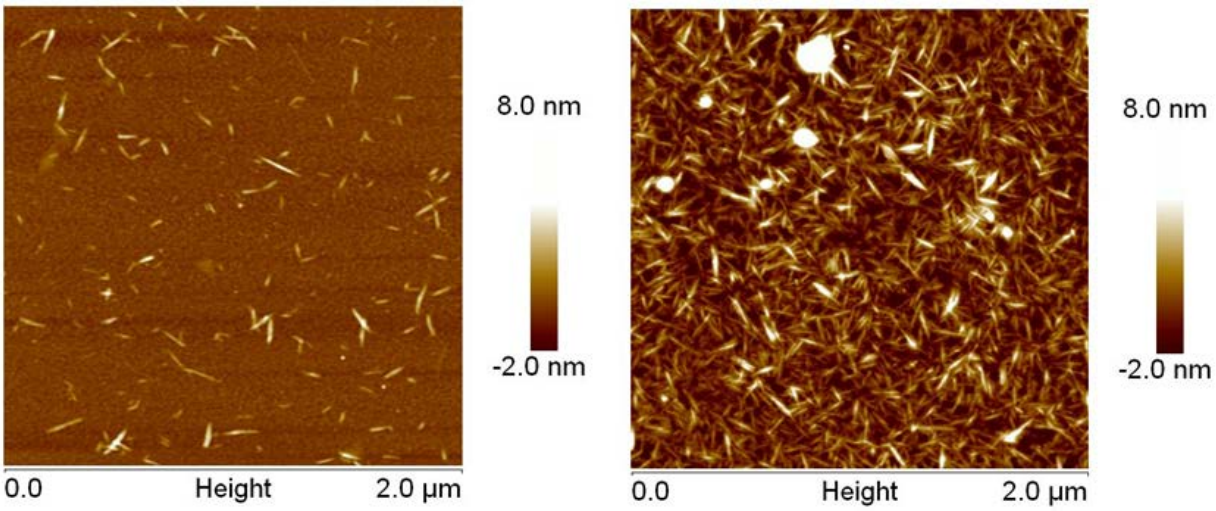

Figure 4.1 AFM images for the morphology of (a) ENCC (charge density 6 mmol/g) and (b) HENCC (charge density 1.2 mmol/g).

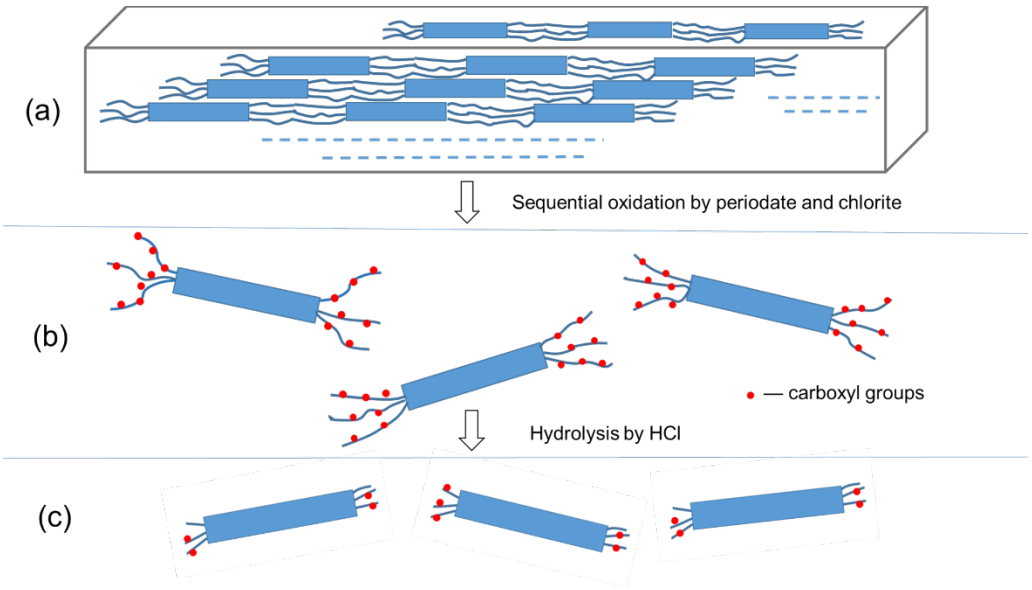

Figure 4.2 Schematic representation of (a) the alternative arrangement of crystalline and amorphous regions in cellulose fibers, (b) the releasing of ENCC particles by sequential oxidation and chlorite oxidation, and (c) protruding DCC chains on ENCC were cut (shortened) by HCl hydrolysis. The dots on the chains represent carboxyl groups.

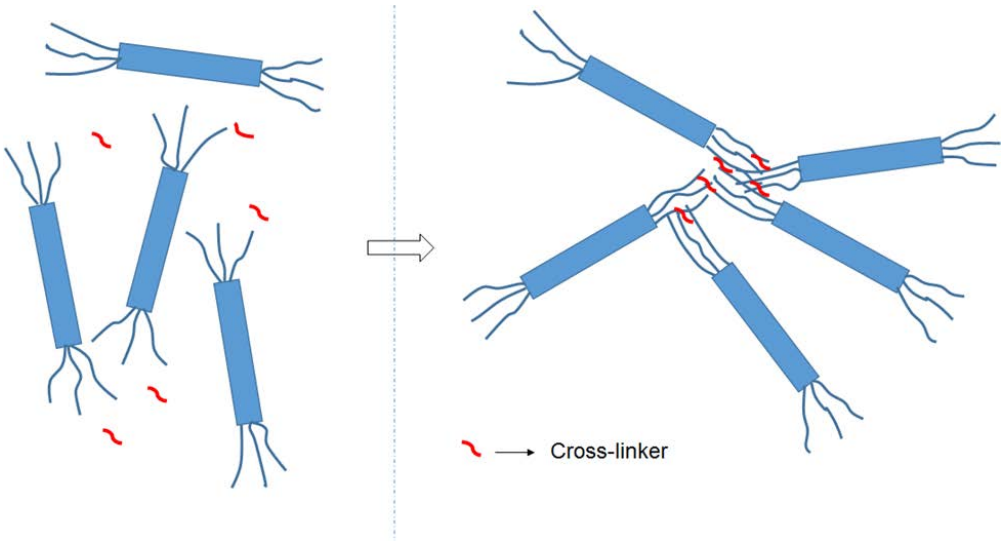

Figure 4.3 Schematic representation of the formation of ENCC aggregation from crosslinking with adipic acid dihydrazide (ADH) through a bio-conjugation reaction.

4.4.2 FTIR analysis

FTIR spectra are shown in Figure 4.4. The starting pulp showed the characteristic peaks for cellulose, including the broad peak at 3325 cm^{-1} which is due to the stretching of –OH groups, the peak at 1310 cm^{-1} is for the –OH bending vibration [25]; the peaks at 2900 cm^{-1}, 1410 cm^{-1} and 1020 cm^{-1} are assigned to the C-H stretching vibration, -CH_2 scissoring and CH_2-O-CH_2 stretching, respectively [26]. ENCC and HENCC showed similar feature peaks (Figure 4.4(b) and (c)), since the only difference between them is that part of the protruding DCC chains on ENCC was cut by HCl, but compared with the starting pulp, ENCC and HENCC both have a significant peak at 1605 cm^{-1}, which is for the carboxyl vibration in the sodium form [27]. ENCC has a much stronger peak at 1605 cm^{-1} than HENCC when compared with the intensity of the peak at 1020 cm^{-1}, which also confirmed a reduction of the number of carboxyl groups on HENCC through hydrolysis.

HENCC-AK and HENCC-AZ particles were obtained by conjugating of HENCC with an alkyne derivative (1-amino-3-butyne) and an azide derivative (3-azido-1-propanamine), respectively. The linkages were formed between the amine groups on derivatives and the carboxyl groups on HENCC. From the AFM images (Figure 4.5), HENCC-AK and HENCC-AZ both are rod-like nanoparticles, the dimension of these two types of modified HENCC did not show much change compared with HENCC.

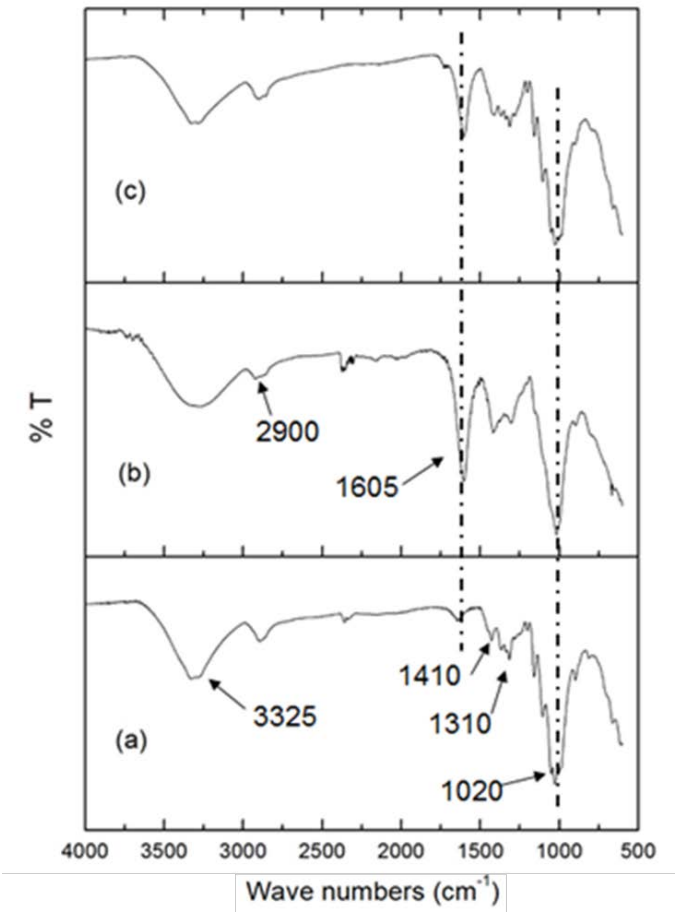

Figure 4.4 FITR spectra for (a) the starting pulp, (b) ENCC, and (c) HENCC.

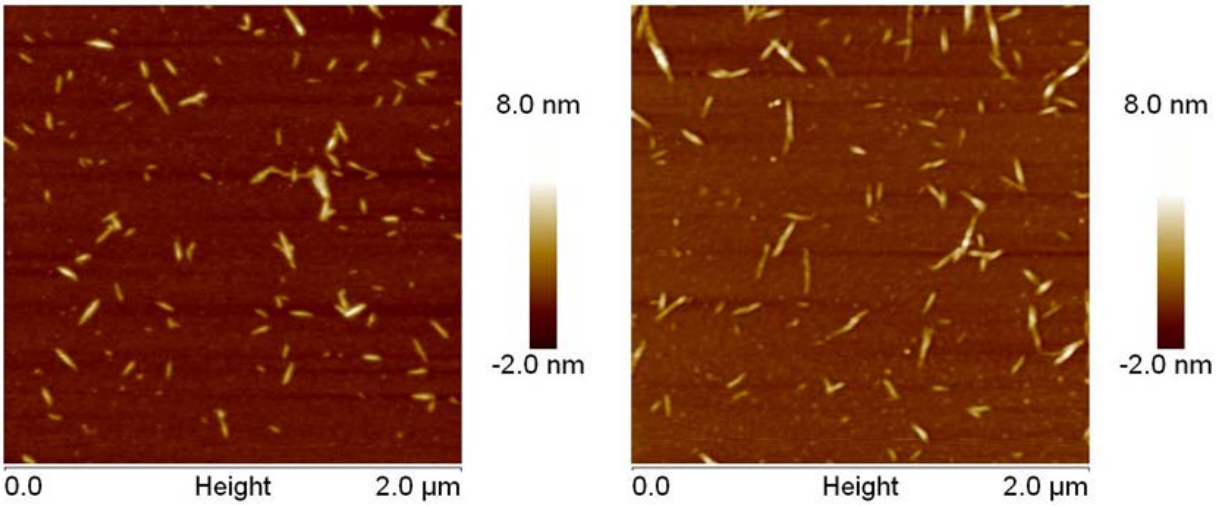

Figure 4.5 AFM images of (a) HENCC-AK and (b) HENCC-AZ.

4.4.3 Assembly of HENCC by a click reaction

After the click reaction between HENCC-AK and HENCC-AZ, the obtained FTIR spectra are shown in Figure 4.6. The HENCC-AZ has a characteristic peak at 2110 cm^{-1} as shown in Figure 4.6(a), which is for the stretching of -N3 groups [28]. The small peak at 1740 cm^{-1}, is for the carboxyl vibrations in acid conditions [19], which are from the remaining carboxyl groups which were not completely reacted with azide groups, since part of the carboxyl groups located inside of the bundle of the DCC chains are not easily accessible. Compared with the intensity of the peak at 1020 cm^{-1}, the number of carboxyl groups has been dramatically reduced after the hydrolysis of ENCC (Figure 4.4(c)). The cross-linking between HENCC and the azide derivative resulted in the generation of amide bonds as shown by the presence of C═O stretching via the 1650 cm^{-1} peak [29]. HENCC-AK shows a similar spectrum to HENCC-AZ except for the characteristic peak for azide groups. In Figure 4.6(c), the spectrum for nanofibers after the click reaction shows the disappearance of the peak at 2110 cm^{-1} for azide stretching, indicating the successful formation of 1,2,3-triazole linkages by the 1,3-dipolar cycloaddition reaction between HENCC-AZ and HENCC-AK.

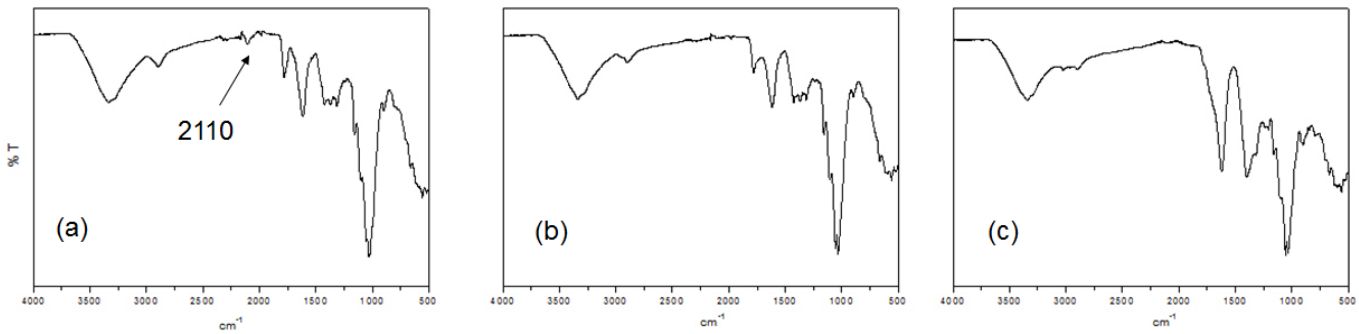

Figure 4.6 FITR spectra of (a) HENCC conjugated with 3-azido-1-propanamine (HENCC-AZ), (b) HENCC conjugated with1-amino-3-butyne (HENCC-AK), and (c) crosslinked HENCC-AZ and HENCC-AK by click reaction.

After the click reaction, the resulting nanoparticles were investigated by AFM. As shown in Figure 4.7, a long nanofiber formed, with a length of 1.2 μm, corresponding to about ten HENCC nanoparticles. The assembled long nanofiber has a width about 6 nm, which is as the same as HENCC. A cartoon representing the assembly process is shown in Figure 4.8 (a)-(b). The HENCC-AK and HENCC-AZ nanorods were alternatively assembled into a long nanofiber chain with high

aspect ratio in one dimension through an end-to-end crosslinking route. From the AFM image (Figure 4.7), it has the chance to grow "Y" shapes or branches when assembling into nanofiber, which may be due to some of the DCC chains not being sufficiently short. Thus the steric hindrance was not sufficiently high to allow only one HENCC to attach to another; and thus more than one HENCC were attached to the same site, forming a branch, as shown schematically in Figure 4.8 (c). Although lots of work still need to be done before we can finely control the assembly process to yield nanofibers with desired length or the number of individual nanocellullose, the promising assembling results enables us to obtain nanofibers with various aspect ratio by chemical assembly, rather than getting nanocellulose with certain dimensions, depending on the preparation methods. The assembly into larger rods also supports the hypothesis that most of the DCC chains on ENCC were protruding from the two ends.

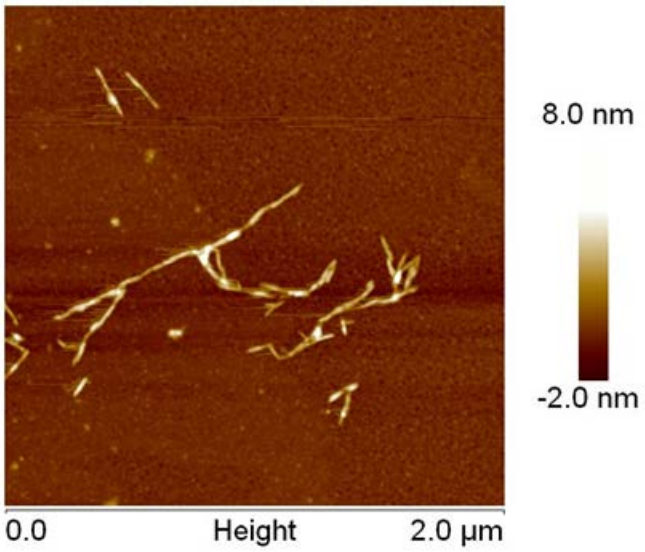

Figure 4.7 Assembled cellulose nanofiber from HENCC-AK and HENCC-AZ through click reaction.

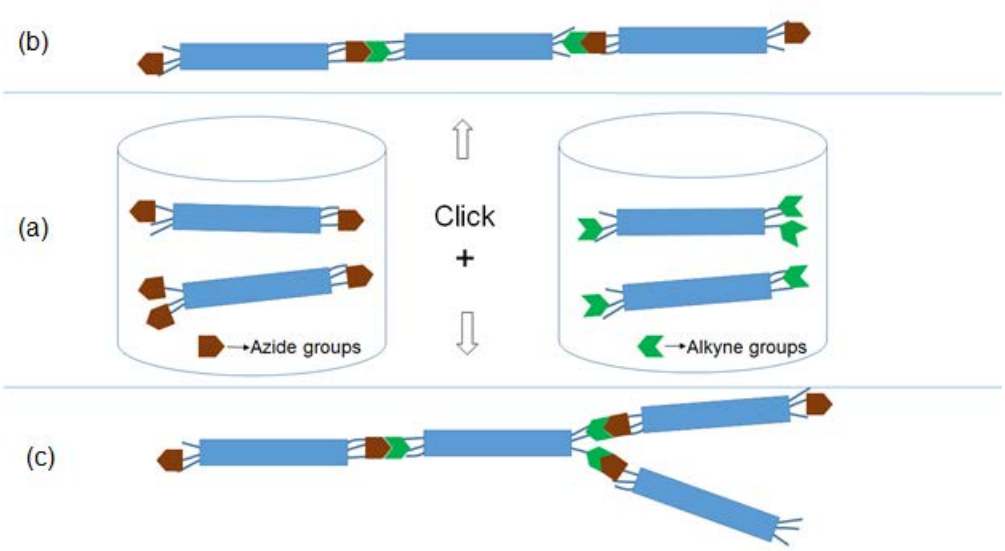

Figure 4.8 Schematic representation of (a) two sets of HENCC derivatives: HENCC-AK and HENCC-AZ, (b) HENCC-AK and HENCC-AZ alternatively assembled into one dimensional nanochains through end-to-end assembly, and (c) the possibility for forming side chains along the assembled cellulose nanofiber chains.

In order to reduce the possibility of forming side chains along the assembled cellulose nanofiber chains, HENCC with a low charge content was used in the click reaction. HENCC with a charge content of 0.35 mmol/g was obtained by the same hydrolysis process as mentioned in the experimental section, but with a hydrolysis time of fifteen hours. HENCC-AK and HENCC-AZ were also prepared according to the same method with the HENCC yield form prolonged hydrolysis. The AFM image of assembled cellulose nanofiber is shown in Figure 4.9. No side chains were formed for most of the assembled cellulose nanofiber. This may be due to prolonged hydrolysis yielding HENCC with shorter protruding DCC chains and hence a lower possibility for forming branches.

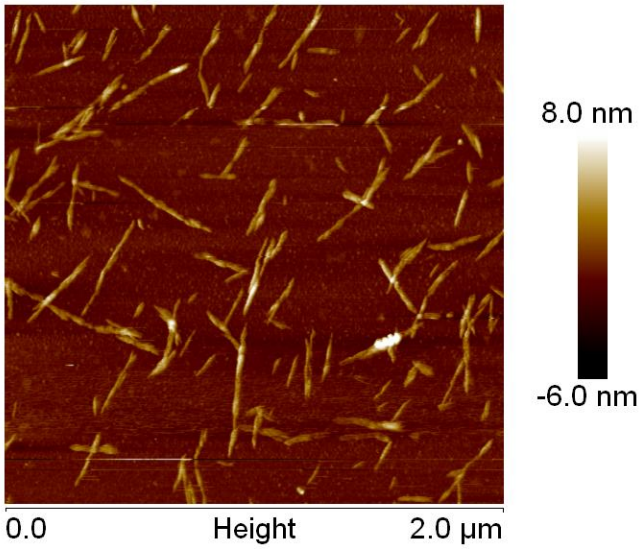

Figure 4.9 Assembled cellulose nanofibers from HENCC-AK and HENCC-AZ through click reaction with HENCC from prolonged hydrolysis. The nanofibers are much longer than those of HENCC, as can be concluded by comparison with Figure 4.1(b).

4.4.4 Assembly of HENCC by a bioconjugation reaction

HENCC-NH_2 was firstly prepared by the conjugation of ADH molecules onto HENCC though a bioconjugation reaction between the –NH_2 groups on ADH and –COOH groups on HNECC [30]. Then HENCC-NH_2 and HENCC were crosslinked via the same reaction as the first step. The crosslinked nanoparticles were investigated by AFM. As shown in Figure 4.10, long nanofibers were assembled by the bioconjugation reaction, the width of these nanofibers is about 6 nm, and the length is around 1 to 1.3 µm. Compared with the click reaction, the crosslinking process by bioconjugation does not require additional azide and alkyne reactants and metal catalyst; however, this bioconjugation reaction has the possibility to occur on the same HENCC nanoparticle even when adding excess ADH, due to the many available carboxyl groups on the same nanorod. Both methods provide the possibility to end-to-end assembly of short cellulose nanorods to long nanofibers.

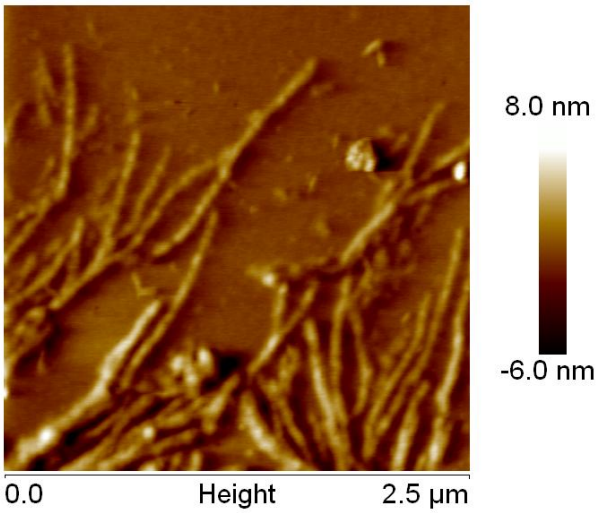

Figure 4.10 Assembled cellulose nanofiber from HENCC-NH_2 and HENCC through a bioconjugation reaction.

4.5 Conclusions

HENCC with shorter DCC chains have been prepared from a hydrolysis of ENCC which has long protruding DCC chains. The carboxyl groups on the protruding DCC chains on HENCC were successfully conjugated with an alkyne and an azide derivative, respectively. Cellulose nanofibers with a length of more than one µm and a width of 6 nm were obtained by crosslinking these two types of HENCC derivatives through a click reaction. End-to-end assembled HENCC nanofibers with a length of more than one µm were also obtained by a bioconjugation reaction. To the best of our knowledge, it is the first chemical assembly of rod-shaped nanocellulose by an end-to-end route in one dimension. It also provides evidence that most of the protruding DCC chains were located on the two ends of ENCC nanorods. This research may bring new opportunities for preparing cellulose nanofibers with designed length and aspect ratio, and extent their potential applications in the fabrication of various nanocellulose devices or composites.

4.6 Acknowledgements

The authors would like to thank the Natural Science and Engineering Research Council of Canada (NSERC) Discovery Grants, funding of the NSERC Strategic Research Network on Green Wood Fiber Products and the Centre for Self-Assembled Chemical Structures (CSACS).

4.7 References

[1] Klemm D, Kramer F, Moritz S, Lindstrom T, Ankerfors M, Gray D, et al. Nanocelluloses: A new family of nature-based materials. Angew Chem Int Edit 2011;50:5438-66.

[2] Habibi Y. Key advances in the chemical modification of nanocelluloses. Chemical Society Reviews 2014;43:1519-42.

[3] Klemm D, Heublein B, Fink HP, Bohn A. Cellulose: Fascinating biopolymer and sustainable raw material. Angew Chem Int Edit 2005;44:3358-93.

[4] Siegel RW, Hu E, C. RM. Nanostructure science and technology. Worldwide study on status and trends. Kluwer Academic Publishers 1999.

[5] Dong XM, Kimura T, Revol J-F, Gray DG. Effects of ionic strength on the isotropic−chiral nematic phase transition of suspensions of cellulose crystallites. Langmuir 1996;12:2076-82.

[6] Leung ACW, Hrapovic S, Lam E, Liu Y, Male KB, Mahmoud KA, et al. Characteristics and properties of carboxylated cellulose nanocrystals prepared from a novel one-step procedure. Small 2011;7:302-5.

[7] Yang H, Alam MN, van de Ven TGM. Highly charged nanocrystalline cellulose and dicarboxylated cellulose from periodate and chlorite oxidized cellulose fibers. Cellulose 2013;20:1865-75.

[8] Yang H, Chen DZ, van de Ven TGM. Preparation and characterization of sterically stabilized nanocrystalline cellulose obtained by periodate oxidation of cellulose fibers. Cellulose 2015;22:1743-52.

[9] Pääkkö M, Ankerfors M, Kosonen H, Nykänen A, Ahola S, Österberg M, et al. Enzymatic hydrolysis combined with mechanical shearing and high-pressure homogenization for nanoscale cellulose fibrils and strong gels. Biomacromolecules 2007;8:1934-41.

[10] Saito T, Kimura S, Nishiyama Y, Isogai A. Cellulose nanofibers prepared by TEMPO-mediated oxidation of native cellulose. Biomacromolecules 2007;8:2485-91.

[11] Liimatainen H, Visanko M, Sirviö JA, Hormi OEO, Niinimaki J. Enhancement of the nanofibrillation of wood cellulose through sequential periodate–chlorite oxidation. Biomacromolecules 2012;13:1592-7.

[12] Tejado A, Alam MN, Antal M, Yang H, van de Ven TGM. Energy requirements for the disintegration of cellulose fibers into cellulose nanofibers. Cellulose 2012;19:831-42.

[13] Rostovtsev VV, Green LG, Fokin VV, Sharpless KB. A stepwise Huisgen cycloaddition process: Copper(I)-catalyzed regioselective "ligation" of azides and terminal alkynes. Angewandte Chemie International Edition 2002;41:2596-9.

[14] Bock VD, Hiemstra H, van Maarseveen JH. CuI-catalyzed alkyne–azide "click" cycloadditions from a mechanistic and synthetic perspective. European Journal of Organic Chemistry 2006;2006:51-68.

[15] Pahimanolis N, Hippi U, Johansson L-S, Saarinen T, Houbenov N, Ruokolainen J, et al. Surface functionalization of nanofibrillated cellulose using click-chemistry approach in aqueous media. Cellulose 2011;18:1201-12.

[16] Karaaslan MA, Gao G, Kadla JF. Nanocrystalline cellulose/β-casein conjugated nanoparticles prepared by click chemistry. Cellulose 2013;20:2655-65.

[17] Chen J, Lin N, Huang J, Dufresne A. Highly alkynyl-functionalization of cellulose nanocrystals and advanced nanocomposites thereof via click chemistry. Polymer Chemistry 2015;6:4385-95.

[18] Filpponen I, Argyropoulos DS. Regular linking of cellulose nanocrystals via click chemistry: Synthesis and formation of cellulose nanoplatelet gels. Biomacromolecules 2010;11:1060-6.

[19] Yang H, Tejado A, Alam N, Antal M, van de Ven TGM. Films prepared from electrosterically stabilized nanocrystalline cellulose. Langmuir 2012;28:7834-42.

[20] Hou QX, Liu W, Liu ZH, Bai LL. Characteristics of wood cellulose fibers treated with periodate and bisulfite. Industrial & Engineering Chemistry Research 2007;46:7830-7.

[21] Hofreiter BT, Wolff IA, Mehltretter CL. Chlorous acid oxidation of periodate oxidized cornstarch. Journal of the American Chemical Society 1957;79:6457-60.

[22] Abitbol T, Kloser E, Gray D. Estimation of the surface sulfur content of cellulose nanocrystals prepared by sulfuric acid hydrolysis. Cellulose 2013;20:785-94.

[23] Sheikhi A, Safari S, Yang H, van de Ven TGM. Copper removal using electrosterically stabilized nanocrystalline cellulose. ACS Applied Materials & Interfaces 2015;7:11301-8.

[24] Hosseinidoust Z, Alam MN, Sim G, Tufenkji N, van de Ven TGM. Cellulose nanocrystals with tunable surface charge for nanomedicine. Nanoscale 2015;7:16647-57.

[25] Yuen S-N, Choi S-M, Phillips DL, Ma C-Y. Raman and FTIR spectroscopic study of carboxymethylated non-starch polysaccharides. Food Chemistry 2009;114:1091-8.

[26] Keshk SMAS. Homogenous reactions of cellulose from different natural sources. Carbohydrate Polymers 2008;74:942-5.
[27] Barbucci R, Magnani A, Consumi M. Swelling behavior of carboxymethylcellulose hydrogels in relation to cross-linking, pH, and charge density. Macromolecules 2000;33:7475-80.
[28] Yonekawa S, Goodpaster AM, Abel BA, Paulin RG, Sexton CW, Poole JS, et al. Synthesis, properties and X-ray structure of 5-azido-2-methoxy-1,3-xylyl-18-crown-5. Journal of Heterocyclic Chemistry 2006;43:689-94.
[29] Liu L, Liu D, Wang M, Du G, Chen J. Preparation and characterization of sponge-like composites by cross-linking hyaluronic acid and carboxymethylcellulose sodium with adipic dihydrazide. European Polymer Journal 2007;43:2672-81.
[30] Yang X, Cranston ED. Chemically cross-linked cellulose nanocrystal aerogels with shape recovery and superabsorbent properties. Chemistry of Materials 2014;26:6016-25.

Bridging Section between Chapters 4 and 5

In the previous chapters, various types of nanocellulose and assembled nanocellulose have been introduced. The properties of these nanocellulose have been characterized and discussed in detail, but without any application of these nanocellulose. In the next chapter, an application of one type of nanocellulose will be investigated. A novel biomaterial based aerogel was prepared from bi-functional nanocellulose (with aldehyde and carboxyl groups) and carboxylmethylated chitosan through a Schiff base reaction which is an environmental friendly crosslinking process. This negatively charged aerogel shows a good adsorption performance for methylene blue. The adsorption isotherms, kinetics and reusability of this aerogel were investigated in this chapter. The results of this research have been reported in the following paper:

Reusable green adsorbent aerogel from crosslinked cellulose nanofibers and modified chitosan for dye removal. Han Yang, Theo van de Ven. Submitted.

Chapter 5. Reusable green adsorbent aerogel from crosslinked cellulose nanofibers and modified chitosan for dye removal

5.1 Abstract

A novel biomaterial-based adsorbent aerogel was prepared by crosslinking bifunctional cellulose nanofibers and carboxymethylated chitosan through a Schiff base reaction. The adsorbent aerogel was characterized by solid carbon-13 NMR, atomic force microscopy, scanning electron microscopy. A cationic dye, methylene blue, is used as a model dye in this dye removal study. The equilibrium adsorption data were fitted well to the Langmuir isotherm, and the maximum adsorption capacity of this aerogel for methylene blue removal was found to be 785 mg/g at room temperature. To the best of our knowledge, this is the highest removal capacity as yet for any reusable adsorbents prepared from biomaterials. Although the adsorption process for this adsorbent was found to follow Langmuir kinetics, the rate determining step is the diffusion of the dye into the gel. The desorption/regeneration and pH effect were also investigated, which showed that this adsorbent has a good reusability, and can keep its adsorption capacity in dye solutions over a wide pH range.

5.2 Introduction

Synthetic dyes have complex structures and are difficult to decontaminate, and furthermore, they have harmful effects including teratogenetic, carcinogenic and mutagenic effects on human health [1]. Dyes are widely used in many industries, such as textile, leather, paper, plastics, printing and cosmetics [2]. The rapid development of global industrialization has further increased the dye pollution problems in water, which is the most important and necessary natural resource for human beings and other living creatures. Thus it is an important and challenging task to eliminate dyes in industrial effluents before they are discharged into our environment [3]. Various methods have been used for removing dyes from industrial wastewater, including photocatalytic oxidation, electrochemical destruction, membrane filtration, adsorption, etc. Among these methods, adsorption is recognized as an economic treatment method due to its easy operation and relatively low cost [4]. Adsorption is a physicochemical process in which molecules are attached to the surface of an adsorbent by physical forces (van der Waals forces or electrostatic attractions between the opposite charges of the adsorbate molecules and adsorbent surface) or chemical forces (e.g. covalent bonding). In order to obtain efficient adsorption, it is important to choose a suitable adsorbent according to the charges or functional groups carried by various dyes. Besides efficient adsorption, reducing the toxicity of an adsorbent itself is also important, to avoid secondary pollution. Thus an environmentally friendly and efficient adsorbent is always highly desired. Many biomaterials based adsorbents have been developed from agricultural waste and plants, such as rice husk [5], jute fiber carbon [6], wheat bran [7], sunflower seed shells [8], sugarcane bagasse [9], chitin [10], chitosan [11] and modified cellulose [12].

Among all natural available biomaterials, cellulose is the most abundant, environmentally friendly, renewable and biodegradable material on earth, and these advantages make cellulose one of the potential resources for producing green adsorbents. Nanomaterials, due to their higher specific surface area and more available active sites for interaction with dye molecules, are expected to have a high adsorption capacity, thus more and more researchers are applying nanomaterials in dye removal. Nanocrystalline cellulose (NCC) is a major type of bio-nanomaterial prepared from cellulose. NCC can be produced from wood pulp by sulfuric acid hydrolysis (introducing sulfate half-ester groups) [13], or by ammonium persulfate treatment (introducing carboxyl groups) [14]

or by periodate-chlorite oxidation (which yields electrosterically stabilized NCC (ENCC) with a high content of carboxyl groups) [15]. NCC has negatively charged functional groups which can interact with cationic dyes by electrostatic attraction [16]. The content of carboxyl groups on NCC can be increased through 2,2,6,6-tetramethylpiperidine-1-oxyl (TEMPO) radical mediated oxidation to improve the removal capacity of NCC [17]. NCC can also be modified with primary amines for adsorption of anionic dyes [18]. ENCC is a recent novel type of NCC, which has not yet been used in the study of dye removal, but it shows great capacity in the removal of heavy metals, such as copper ions, from water [19]. However, such NCC or ENCC adsorbents usually suffer from difficulties in separation from the waste water and regeneration.

Chitosan is also a biodegradable and renewable biomaterial, derived from deacetylation of the biopolymer chitin, which is the third most abundant polysaccharide in the world (after cellulose and hemicellulose) [20]. Traditionally, when chitosan is directly used in water purification, it is mostly effective in adsorbing negatively charged dyes [21] or heavy anions [22] in acidic conditions by its protonated amine groups. In this work, we will use chitosan as a green crosslinker, by taking advantage of its amine groups as functional moieties participating in the formation of covalent bonds.

We prepared nanocrystalline cellulose with bifunctional groups (carboxyl and aldehyde groups) by sequential periodate oxidation and partial chlorite oxidation followed by a hot water treatment. We refer to these NCC as bifunctional NCC or BNCC. Chitosan (CT) was modified in advance into carboxymethylated CT (CMCT) to increase its carboxyl group content. The amine groups on chitosan and aldehyde groups on NCC can form covalent imine bonds through a Schiff-base reaction to crosslink the BNCC particles and yield a hydrogel network. The adsorbent was readily obtained by freeze-drying the hydrogel to yield an all-natural aerogel (BNCC-CMCT). Characterization of BNCC-CMCT was done by solid carbon-13 NMR, atomic force microscopy (AFM) and scanning electron microscopy (SEM). Methylene blue (MB), a cationic dye (structure shown in Figure 5.1, molar mass 319.5 g/mol), is used as a model dye in this dye adsorption study. The adsorption isotherm and adsorption kinetics of MB removal by BNCC-CMCT were evaluated, and the pH effect and reusability were also investigated in this work.

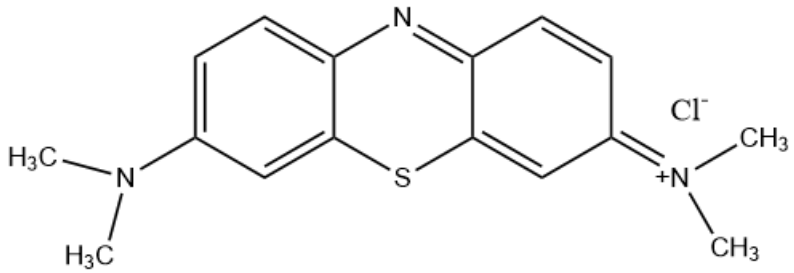

Figure 5.1 Molecular structure of MB.

5.3 Experimental section

5.3.1 Materials

Softwood kraft pulp sheets (provided by FPinnovations) were used as starting cellulose material. Chemicals for reactions: sodium (meta) periodate, ethylene glycol, hydroxylamine hydrochloride, sodium chlorite, chloroacetic acid, chitosan (from crab shell, viscosity 200-400 mPa·s, degree of deacetylation is 80%), methylene blue hydrate were purchased form Sigma-Aldrich, propanol from Fisher, hydrogen chloride (0.1 M and 1 M), sodium hydroxide (10 mM, 0.1 M and 1M) from Fluka, anhydrous ethyl alcohol from commercial Alcohols, sodium chloride from ACP chemicals Inc. All chemicals were used as received. Milli-Q water (18.2 MΩ cm, Millipore Milli-Q Purification System) was used in all experiments.

5.3.2 Preparation of bifunctional NCC (BNCC)

One gram of softwood kraft pulp was soaked in water and well dispersed by a disintegrator, and then filtered to remove extra water from the pulp. Next 0.98 g $NaIO_4$ and the wet pulp were added into 67 mL water, including the moisture from the wet pulp. The reaction beaker was wrapped with aluminum foil to prevent entry of light. The pulp was stirred at room temperature for 96 hours, then 1 mL ethylene glycol was added into this mixture to end the reaction by quenching the residual periodate. The dialdehyde modified cellulose (DAMC) was washed thoroughly with water by filtration. The aldehyde content of DAMC was determined by the hydroxylamine hydrochloride method previously reported [23].

BNCC was prepared by converting part of aldehyde groups on DAMC to carboxyl groups by chlorite oxidation and then followed by a hot water treatment [24, 25]. Briefly, one gram never

dried DAMC and 0.54 g $NaClO_2$, 2.9 g NaCl and 0.54 g H_2O_2 was dispersed in 50 mL 0.5 M acetic buffer solution (pH=5), and the slurry was stirred for 24 hours. Subsequently the oxidized pulp was washed with water, then washed four times with 70 % ethanol, and then dried in an oven at 50 °C. The bifunctionally modified cellulose fiber (0.2 g) and 20 mL water were added into a 50 mL flask, and the suspension was stirred at 80 °C in an oil bath for one hour and subsequently centrifuged at 8000 rpm for 10 minutes (Aventi J-E centrifuge from Beckman Coulter) to remove the unfibrilated fibers (a negligible amount). The supernatant (containing BNCC) was precipitated by adding propanol and collected, and then storied at 4 °C for further usage.

5.3.3 Preparation of carboxymethylated chitosan

For the carboxymethylation of chitosan we follow a previous method, with some modification [26]. Sodium hydroxide (1.35 g) was first dissolved in a propanol/water mixture with a volume ratio of 8:2. One gram chitosan was added to this alkaline solution which was stirred and allowed to swell at room temperature for one hour. Subsequently 1.5 g chloroacetic acid was dissolved in 2 mL propanol and added into the chitosan slurry in five equal portions in a period of 30 min. The mixture continued to react for another four hours at room temperature. The reaction was stopped by adding 50 mL 70% ethanol and filtered through a nylon cloth. The white solid was washed with 80% ethanol for four times and then with anhydrous ethanol. Finally the powder was dried in an oven at 50 °C to obtain carboxymethylated chitosan (CMCT).

5.3.4 Preparation of aerogel (BNCC-CMCT)

A BNCC suspension (1% wt) and a CMCT solution (1% wt) were prepared by stirring in an oil bath at 60 °C for one hour, respectively. Then these two sets of samples were mixed by a homogenizer (Polytron PT 2500E) at 8000 rpm for 1 minute to form a hydrogel. The hydrogel was frozen at -80 °C for 12 hours and then freeze-dried by a freeze dryer (Thermo ModulyoD).

5.3.5 Dye adsorption

The MB adsorption process was investigated in batch experiments. MB solutions with desired concentrations were prepared by successive dilution of a stock MB solution with water. To obtain the calibration curve of MB, the absorbance of MB solutions with predetermined concentrations at λ_{max}=664 nm was detected by a UV-vis spectrophotometer (Cary 5000 UV-Vis-NIR

Spectrophotometer). This calibration curve was used to determine the concentration of MB solution after absorption in the following adsorption experiments.

5.3.5.1 Equilibrium experiments

Batch adsorption measurements were performed to obtain the maximum adsorption of MB by the BNCC-CMCT aerogel. Five millilitres of MB solution of known various initial concentrations and 1 mg of the adsorbent were put into a 10 mL vial and agitated using a magnetic stirrer at 120 rpm for 24 h, to ensure the adsorption process has reached equilibrium. The equilibrium concentration (C_e) of MB was then determined using an UV-Vis spectrometer at 664 nm. Equation (1) was used to calculate the amount of adsorbed dye per gram of adsorbents (mg/g) at equilibrium.

$$\Gamma_e = \frac{(C_0 - C_e)V}{m} \quad (1)$$

where Γ_e (mg/g) is the amount of dye adsorbed for one gram of adsorbent, C_0 (mg/L) and C_e (mg/L) are the initial and equilibrium concentrations of MB, V (L) is the volume of MB solution, and m (g) is the weight of adsorbent. The volume of aerogel expands about ten times of its original size, but the amount of adsorbed dye Γ_e calculated from equation (1) does not include the dye inside of the pores of the aerogel.

5.3.5.2 Kinetic experiments

For kinetic adsorption studies, one milligram of BNCC-CMCT adsorbent was mixed with 5 mL of MB solution (240 mg/L) and stirred at 120 rpm. The experiments were repeated for various desired times. The MB concentration (C_t) at various times was measured by a UV-Vis spectrophotometer. The adsorbed dye amounts were calculated from equation (2).

$$\Gamma_t = \frac{(C_0 - C_t)V}{m} \quad (2)$$

where Γ_t (mg/g) is the amount of dye adsorbed for one gram of adsorbent at time t, C_0 (mg/L) and C_t (mg/L) are the initial concentration and concentration of MB at time t.

5.3.5.3 Effect of pH on adsorption

Various MB solutions with pHs initially varying from 2 -12 were investigated to determine the influence of pH on the efficiency of MB removal by BNCC-CT. The pH of a MB solution was

adjusted by adding 1 mol/L HCl or 1 mol/L NaOH solutions. The initial MB concentration was 100 mg/L and the experiments were performed for 4 hours with stirring at 120 rpm, then the concentration of MB was measured with a UV-Vis spectrophotometer. The removed amount of MB at each pH value was calculated by equation (1).

5.3.5.4 Reusability of adsorbent

The reusability of adsorbent was also investigated. One milligram of BNCC-CMCT was put into 5 mL MB (50 mg/L) solution and stirred at 120 rpm for one hour, then the concentration of MB was measured by UV-vis. The BNCC-CMCT was desorbed by soaking in 10 mL 0.1 M HCl and agitated at 80 rpm with a shaker for 10 minutes and then washed with 0.1 M NaOH and then with water, finally by rinsing with ethanol and air-dry. This procedure was repeated for six successive adsorption - desorption processes. The removal amount of MB at each step was calculated with equation (1).

5.3.6 Conductometric titration

The content of carboxyl groups on BNCC and CMCT were determined on a Metrohm 836 Titrando instrument according to a previously reported method [27]. A certain amount of sample (with a solid content of around 20 mg) and 2 mL NaCl solution (20 mmol/L) were added to 140 mL milli-Q water, and 0.1 M HCl was added to adjust the pH of this mixture to around 3.0. Then the suspension was titrated by a 10 mM NaOH solution at a rate of 0.1 mL/min till a pH of around 11 was reached. The part of the curve which represents weak acid on the titration graph gives the carboxyl content.

5.3.7 Solid carbon-13 NMR measurements

Solid carbon-13 NMR spectra were acquired on a Varian VNMRS400 NMR spectrometer operating at 100.5 MHz. Cross polarization spectra were obtained with a contact time of 1.5 ms and a recycle delay of 2 s. The sample was spun in a 7.5 mm rotor at 5000 Hz and spinning sidebands were suppressed by the TOSS sequence. Typically 8000 scans were acquired.

5.3.8 AFM measurement

The morphology of BNCC particles was investigated by AFM (Nanoscope IIIa MultiMode with Extender (Veeco Metrology Group, Santa Barbara, CA)). A drop of BNCC suspension was placed on a freshly cleaved mica surface for ten minutes and then rinsed off the excess liquid. The experiments were done in tapping mode using silicon cantilevers (ACTA model, AppNano) with a nominal spring constant of 37 N/m, nominal resonant frequency of 300 kHz and nominal tip radius of 6 nm. Nanoscope Analysis 1.4 was used to process the AFM images.

5.3.9 SEM measurement

The aerogel sample was first mounted on a specimen pin by double sided carbon tape, then was coated with a layer of Pt about 3 nm thick by a high vacuum coater (Leica EM ACE600). The microstructure of the aerogel was observed by scanning electron microscopes (FEI Inspect F-50 FE-SEM). The images were taken at an accelerating voltage of 10 kV.

5.3.10 Porosity measurement

The porosity of BNCC-CMCT aerogel was determined by the ethanol displacement method [28]. Ethanol can penetrates into pores easily and is not expected to change the geometrical volume of the aerogel. A piece of BNCC-CMCT (w_1) was immersed in 40 mL anhydrous ethanol (ρ=0.789 g/mL) and then placed in a desiccator under a reduced pressure for 8 min to remove air bubbles inside of the aerogel. Then the aerogel was taken out and the ethanol on its surface was gently removed by a piece of filter paper. The aerogel was re-weighed (w_2) immediately. The porosity ε was calculated by the following equation:

$$\varepsilon = \frac{(w_2 - w_1)/\rho}{V} \qquad (3)$$

V is volume of the aerogel calculated from its geometrical dimensions. An average value was taken from three replicates.

5.4 Results and discussion

5.4.1 Characterizations of BNCC and aerogel

The morphology of BNCC by AFM is shown in Figure 5.2. BNCC is a rod-like nanoparticle, obtained from a hot water treatment of periodate and partially chlorite oxidized cellulose fibers.

The major advantage of this process is that it does not require strong acid hydrolysis and/or extensive mechanical treatment (which usually involves a high energy consumption or specifically designed instruments), and no additional post-purification is required after the formation of the nanocellulose particles. Furthermore, in this way, one is able to easily obtain nanocellulose particles with desired charge content by adjusting the chlorite oxidation level on aldehyde groups prior to a hot water treatment. As shown in Figure 5.2, BNCC from this work has a length of about 110 -150 nm, and width of about 8 nm. BNCC particles have two types of functional groups, namely aldehyde and carboxyl groups besides the original hydroxyl groups. These two functional groups on one particle make BNCC potentially a more versatile nanocellulose than traditional NCC. The charge content of BNCC is around 3.0 mmol/g, and of CMCT is about 3.4 mmol/g measured by conductometric titration. By mixing a BNCC suspension with a CMCT solution, a transparent hydrogel is formed instantly, which remains stable even when the vial is upside down (Figure 5.3(a)). The content of carboxyl groups in the hydrogel is about 3.2 mmol/g. The hydrogel was freeze-dried to form an aerogel, which can easily stand on the tip of the fine awns of a green foxtail without bending the awns and the green foxtail (Figure 5.3(b)). This biomaterial based aerogel is highly porous and lightweight; the porosity of the aerogel determined by solvent exchange was 98.8 %. The microstructure of aerogel was investigated by SEM. The image shows that the aerogel has an open porous geometry with pore sizes in the range of 35 - 70 μm (Figure 5.3(c)), and these pores are separated by “walls” which are sheet-like and ultrathin structures revealed by the enlargement shown in the inset (Figure 5.3(c)). These large pores are beneficial for easy and quick mass penetration during adsorption.

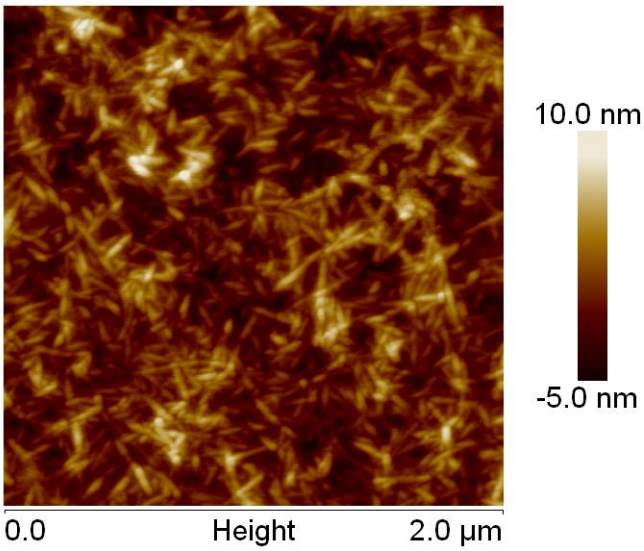

Figure 5.2 AFM image of BNCC nanoparticles.

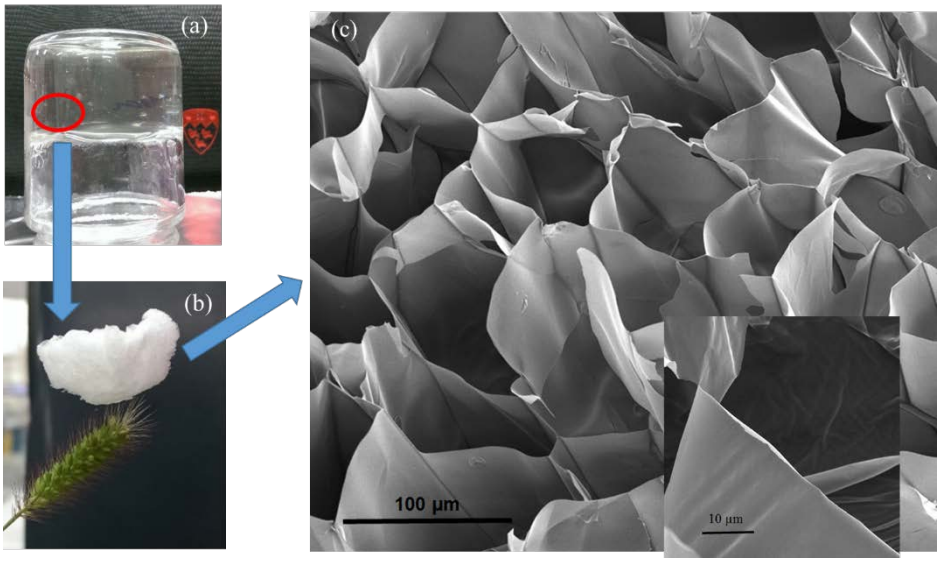

Figure 5.3 (a) Photograph of transparent hydrogel in an upside down vial, (b) photograph of a piece of aerogel standing on the tip of the fine awns of a green foxtail, and (c) SEM image of the aerogel, with the inset showing an enlargement of the "walls" formed in the aerogel.

5.4.2 Solid C-13 NMR

The chemical properties of all samples were investigated by solid carbon-13 NMR. The spectra of starting cellulose pulp and nanocellulose are shown in Figure 5.4(a). The peak at 105 ppm is for C1, 90 ppm for C4, 85 ppm for C40, 80-70 ppm region for C2, C3, C5, and 70-60 ppm for C6, respectively [24], after the periodate and partially chlorite oxidation treatment, the BNCC has a new peak at 180-170 ppm, which represents the carboxyl groups, and the broad double peak at the

110-55 ppm region is due to hemiacetal linkages formed by the aldehyde groups and hydroxyl groups on nanocelulose during drying [29]. As shown in Figure 5.4(b), for the starting chitosan, the peak at 106 ppm is for C1, 83 ppm is for C4, 75 ppm is for C3 and C5, 61 ppm is for C6, and 58 ppm is for C2, respectively [30]. This spectrum also shows that the starting chitosan is not fully deacetylated, since the small peak at 26-20 ppm and 180-170 ppm is for the methyl groups and carbonyl groups from the acetyl groups respectively which remain on chitosan [31]. After the carboxymethylation treatment on chitosan, the signal of the peak at 180-170 ppm has increased significantly, indicating the successful conjugation of carboxyl groups onto chitosan. The spectrum of the aerogel prepared from CMCT and BNCC is shown in Figure 5.4(c). Crosslinking has occurred between the amine groups on CMCT and the aldehyde groups on BNCC, by the formation of imine bonds, as shown in Figure 5.5(a). This crosslinking reaction occurs without adding any other chemicals, no hazardous by-products are formed in this reaction and there is no need of any post-purification treatment. All these advantages make this crosslinking process an environmentally friendly process. The cartoon in Figure 5.5(b) shows the formation of the hydrogel network. BNCC works as the supporting nanomaterial, the flexible CMCT polymer chains connect BNCC nano-rods, thus forming a porous network. Furthermore, BNCC and CMCT, not only function as a hydrogel construction material, but also both have negative charged carboxyl groups which can increase the available sites for binding with cationic dye molecules by electrostatic attraction, thus improving the ability of dye adsorption. The imine bond usually appears at the range of 175-160 ppm by solid C-13 NMR, but it is overlapped by its neighbouring strong peak for carboxyl groups (180-170 ppm). The broad peak at 180-160 ppm (Figure 5.4(c)) indicates the combination of the carboxyl groups and imine bonds.

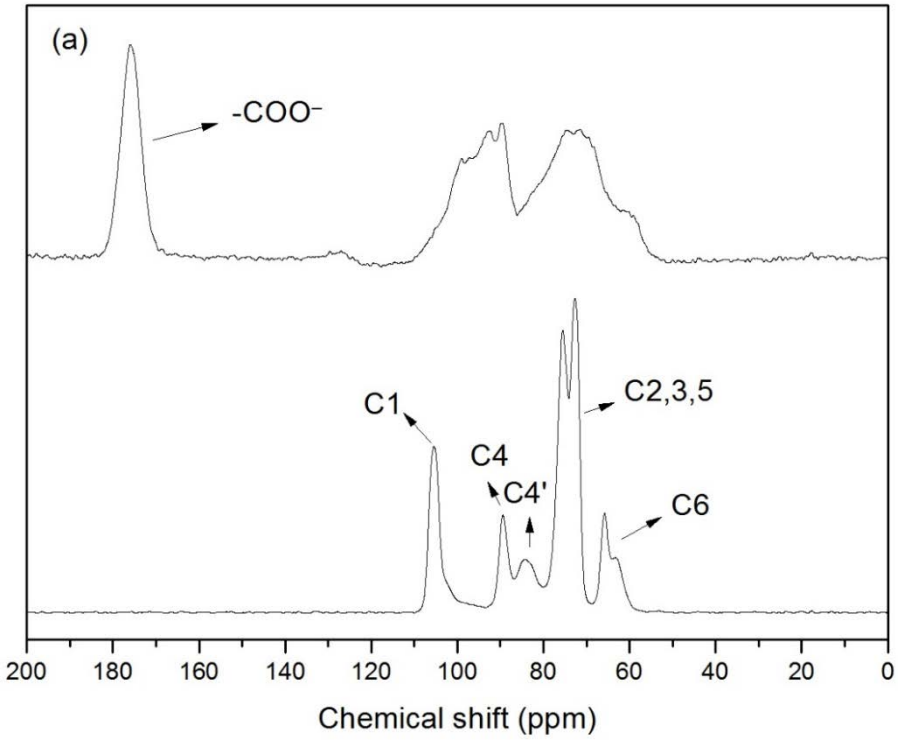
(a)
-COO⁻
C1
C4
C4'
C2,3,5
C6
200
180
160
140
120
100
80
60
40
20
0
Chemical shift (ppm)

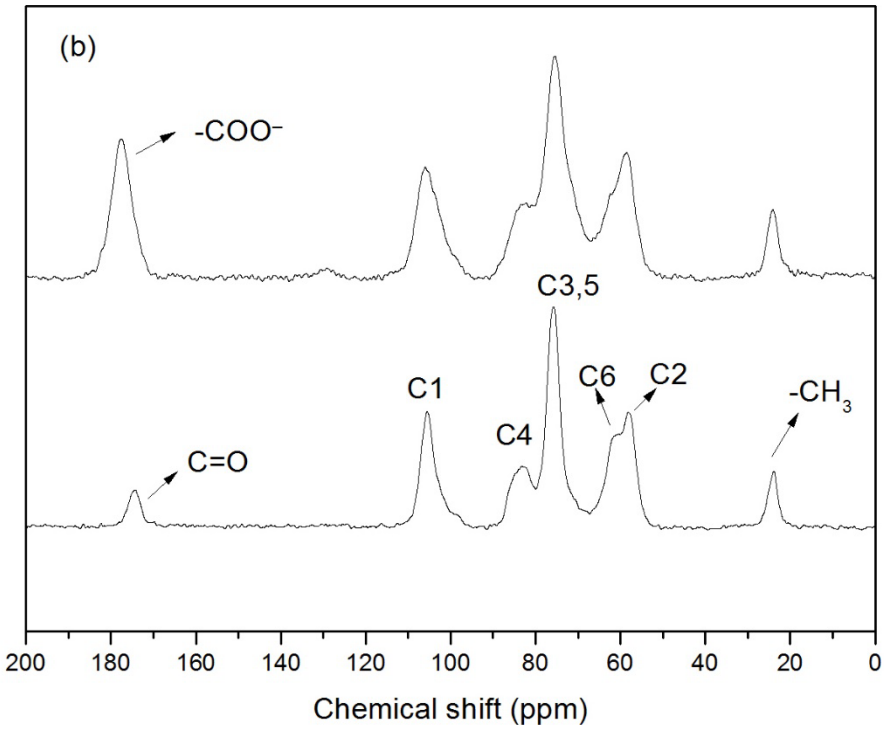
(b)
-COO⁻
C3,5
C1
C6
C2
-CH3
C4
C=O
200
180
160
140
120
100
80
60
40
20
0
Chemical shift (ppm)

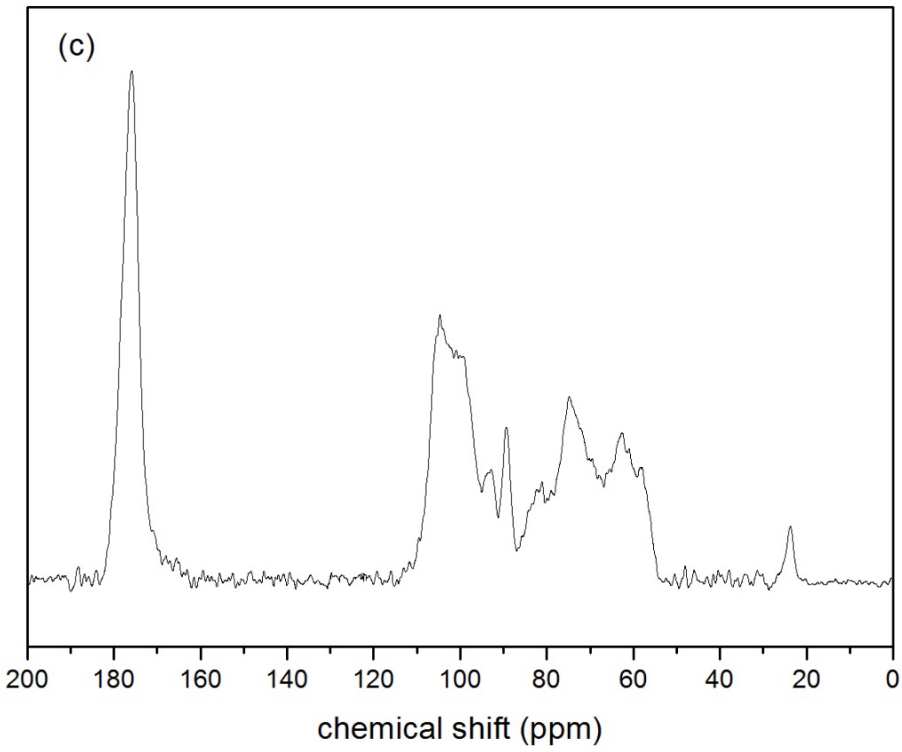

Figure 5.4 Solid carbon -13 NMR spectra for (a) cellulose pulp and BNCC, (b) chitosan and CMCT, and (c) aerogel prepared from BNCC and CMCT.

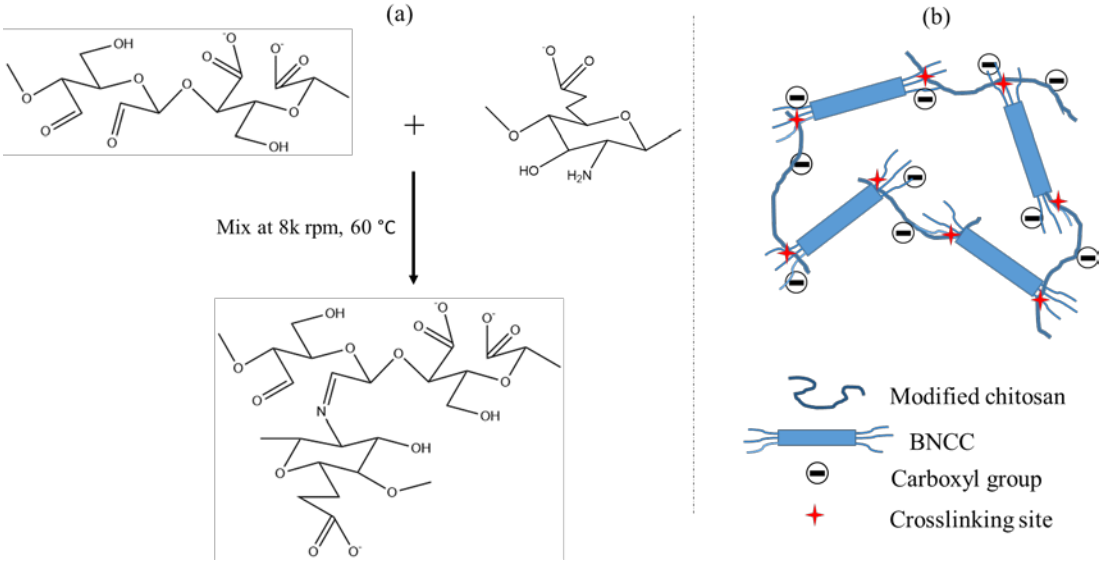

Figure 5.5 (a) Schematic crosslinking reaction between BNCC and CMCT, (b) cartoon for the formation of hydrogel.

5.4.3 Adsorption isotherm

An adsorption isotherm is an important tool for the description of how adsorbate molecules interact with an adsorbent surface. In order to investigate the relationship between the aerogel and the MB molecules at equilibrium and to obtain the maximum adsorption capacity of the aerogel, Langmuir and Freundlich isotherms were applied for data fitting of the adsorption experiment data. For Langmuir isotherms, one assumes that each adsorbate molecule adsorbing onto the adsorbent surface has the same adsorption activation energy, that the adsorption process results in a monolayer coverage over a homogeneous adsorbent surface (provided there is sufficient adsorbate), and it also assumes that no adsorbate migrates after adsorption. It does allow for desorption of the adsorbate. The Langmuir isotherm can be expressed by the following equation [32]:

$$\frac{1}{\Gamma_e} = \frac{K}{C_e} + \frac{1}{\Gamma_m} \qquad (4)$$

with the equilibrium constant K given by

$$K = \frac{\tau_{ads}}{\tau_{des}} \qquad (5)$$

and where Γ_e is the adsorption capacity at equilibrium, C_e the equilibrium concentration of MB in solution and Γ_m the maximum adsorption capacity. τ_{ads} and τ_{des} represent the characteristic times of adsorption and desorption, and equal the reciprocals of their corresponding rate constants. Langmuir plots for adsorption of MB in zero salt and 0.1 M NaCl are shown in Figure 5.6. Γ_m and K were calculated from the intercept and slope of the linear fitting. Addition of NaCl to the system screens the electrostatic attraction between the dye and the carboxyl groups, thus increasing τ_{ads} and thus decreasing the maximum adsorption capacity.

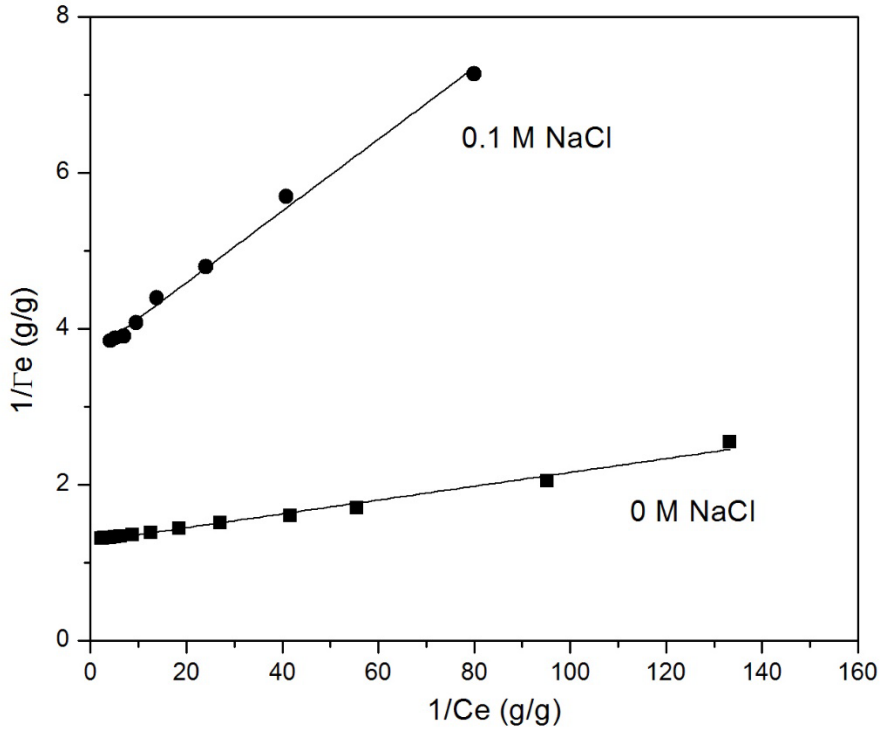

Figure 5.6 Langmuir plot for MB adsorption by BNCC-CMCT in zero salt and 0.1 M NaCl at pH 7.5 and 22 °C.

Table 5.1 Isotherm parameters for MB adsorption in 0 M and 0.1 M NaCl at 22 °C.

	Langmuir model			Freundlich model		
NaCl (M)	Γ_m (mg/g)	K	R^2	K_F	n	R^2
0	784.8	0.0089	0.986	493.7	9.1	0.796
0.1	272.2	0.046	0.990	130.9	5.2	0.917

A Freundlich isotherm, which can describe heterogeneous adsorption systems, and which is not restricted to the formation of monolayer coverage, can be represented as [33]:

$$\Gamma_e = K_F C_e^{1/n} \quad (6)$$

where Γ_e is the adsorption capacity at equilibrium, C_e is the equilibrium concentration of MB in solution, K_F and n are constants. A fit of a Freundlich adsorption isotherm in the absence and presence of NaCl is shown in Figure 5.7.

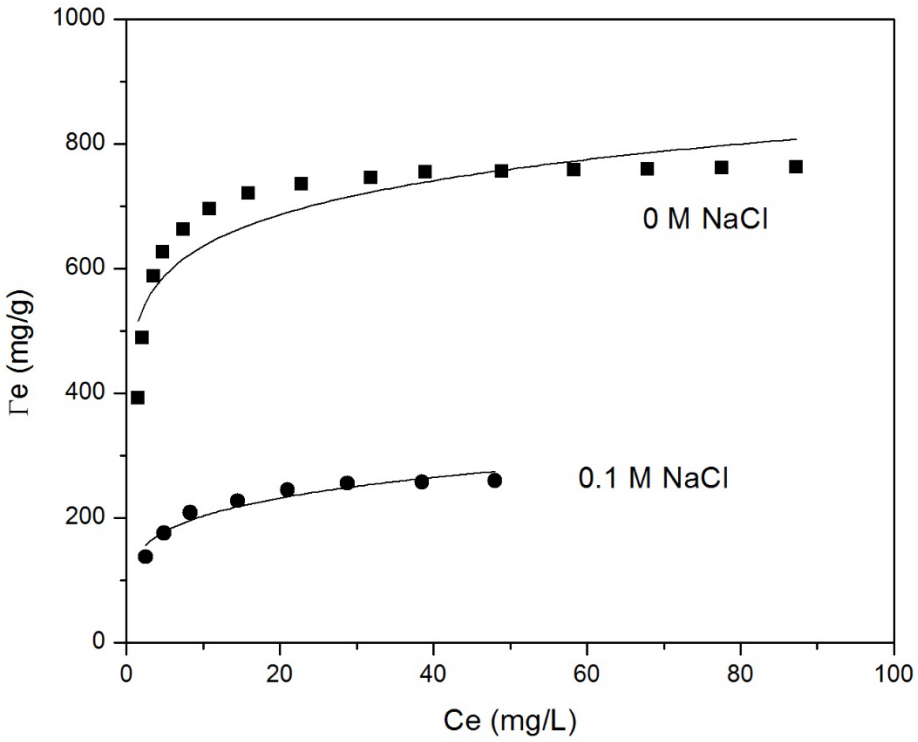

Figure 5.7 Experimental data and Freundlich isotherm fitting for MB adsorption by BNCC-CMCT in zero salt and 0.1 M NaCl at pH 7.5 and 22 °C.

Compared with the Freundlich adsorption isotherm, the Langmuir adsorption isotherm can describe this adsorption process much better, since the Langmuir isotherm fit has a much higher correlation coefficient (Table 5.1). The negatively charged carboxyl groups on the aerogel, are mainly responsible for binding MB onto the aerogel though electrostatic attraction. The maximum adsorption capacity of BNCC-CMCT was 785 mg/g, which is much higher than that of adsorbents made from other nature based materials (listed in Table 5.2). NCC modified by TEMPO-mediated oxidation reaction shows a capacity close to that of BNCC-CMCT [17], but this NCC adsorbent is difficult to recycle and regenerate. The adsorption of BNCC-CMCT is also comparable to commercial activated carbon (980.3 mg/g) [34], although its capacity is about 20% lower, but activated carbon is highly costly to prepare and regenerate. However, the maximum adsorption (in the absence of salt) is about 86% of the amount calculated from charge stoichiometry (the content of carboxyl groups is 3.2 mmo/g and the molar mass of a MB^+ ion is 284 g/mol), which is 909 mg/g. The reason that Γ_m is less than 909 mg/g may due to the unique hairy structure and charge distribution of BNCC. The charge groups on BNCC are dicarboxyl groups on C2 and C3 of a glucose ring, and the steric hindrance is unavoidable for a large molecule like MB, so the chance

for attraction of two MB molecules by each dicarboxyl group is low. Secondly, most of the charge groups are present in the hairy bundle on the two ends of BNCC, so some of the charge groups inside the bundles may not be easily accessible to dye molecules.

The relatively large MB adsorption in 0.1 M NaCl proves that MB^+ ions are adsorbed on COO^- groups, rather than involved in an ion exchange process between Na^+ ions (initially present as counterions) and MB^+ ions. If the process was an ion exchange process one would expect very little MB adsorption in the gel, since MB concentrations were less than 0.75 mM, much smaller than the concentration of Na^+ ions (0.1M).

Table 5.2 Comparison of the maximum MB adsorption by various adsorbents.

Adsorbent	pH	Γ_m (mg/g)	Ref.
Rice husk	7	312.0	[5]
Sugarcane bagasse	7	99.6	[9]
NCC	7.5	101.2	[16]
NCC modified by TEMPO reaction	6.5	769.0	[17]
Commercial activated carbon	7.4	980.3	[34]
Cellulose nanofibrils	9	122.2	[35]
Cellulose nanofibrils aerogel	--	3.70	[36]
Banana pith carbon	4	233.4	[37]
Chitosan/Bentonite Composite	5.1	142.9	[38]
BNCC-CMCT aerogel	7.5	785	This work

5.4.4 Adsorption kinetics

The MB adsorption as a function of time was investigated at an initial concentration of 240 mg/L. As shown in Figure 5.8, the MB adsorption increased very quickly in the first half an hour, and almost reached the adsorption equilibrium in one hour, then it slowly reached equilibrium. The MB adsorption kinetic was investigated using Langmuir kinetic. The classic Langmuir equation can be modified as [39]:

$$\frac{d\theta}{dt} = k_{ads}(n_0-\theta)(1-\theta) - k_{des}\theta \quad (7)$$

with

$$n_0=\frac{c_0}{\Gamma_m} \quad (8)$$

$$\theta=\Gamma/\Gamma_m \quad (9)$$

With the initial condition $\theta = 0$ at time $t = 0$, the analytical solution of the equation (7) is [39]:

$$\theta=\frac{2n_0(\lambda-1)}{A(\lambda-1)+B(\lambda+1)} \quad (10)$$

with

$$\lambda=e^{Bk_{ads}t} \quad (11)$$

$$A=K+n_0+1 \quad (12)$$

$$K=k_{des}/k_{ads} \quad (13)$$

$$B=[(n_0-1)^2+2K(n_0+1)+K^2]^{1/2} \quad (14)$$

From equation (9), the MB adsorption on BNCC-CMCT (Γ) can be expressed as fractional coverage (θ). By fitting the experimental date to equation (10), the adsorption rate constant k_{ads} can be obtained, which is the only adjustable parameter, since K is already known (cf. Table 5.1). Then by using equation (13) the desorption rate constant k_{des} can be obtained. The curve fitting is shown in Figure 5.8. The values of k_{ads} and k_{des} are 1.57 hr^{-1} and 0.0139 hr^{-1}. The size of the aerogel with which adsorption experiments are performed is about 4 mm. To reach the centre of the aerogel by diffusion takes about 2 hrs, as calculated from $\langle x^2 \rangle = 2Dt = 2kT/6\pi\eta a$ (x is mean square displacement take x to be the 2 mm, D the diffusion coefficient of a MB^+ ion, kT the thermal energy, η the viscosity of the medium and a the equivalent radius of MB, take a as 0.5 nm). This is the same order of magnitude as the adsorption process. One can conclude that the rate determining step is the diffusion of MB^+ ions into the gel. Inside the gel MB^+ adsorbs quickly on the COO^- groups. Hence the adsorption and desorption rate constants are only apparent values.

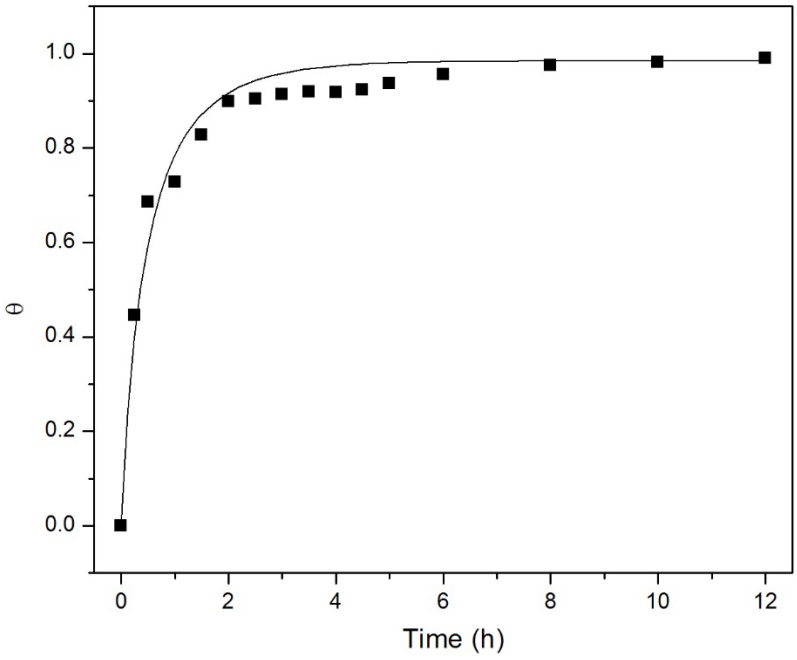

Figure 5.8 Adsorption MB onto BNCC-CMCT aerogel as function of time, and fitting curves to the Langmuir kinetic model, goodness of fit $R^2 = 0.970$. (The initial MB concentration is 240 mg/L, corresponding to $n_0 = 1.53$, pH 7.5 and T = 22 °C).

5.4.5 Effects of pH on adsorption process

The pH of the solution affects the charge density of the adsorbent, which in turn affects the adsorption behavior of the adsorbent. Figure 5.9 shows the results for the adsorption of MB by BNCC-CMCT aerogel for various pHs. One can see that the plateau value increases with increasing pH. When the pH of the solution is increased, more carboxyl groups are deprotonated, and the negative charge density of the aerogel increases, thus increasing the number of adsorption sites for MB^+ ions on carboxyl groups. Langmuir plots for MB adsorption for various pHs are shown in Figure 5.10 and the Langmuir isotherm parameters are listed in Table 5.3. At pH = 3, the maximum adsorption is about 192 mg/g, which is about 25% of the maximum adsorption at pH of 7.5. The adsorption capacity is decreased at low pH due to the protonation of carboxyl groups. It was noticed that at pH 2, almost no dye adsorbed onto the aerogel; this observation indicates that MB can be desorbed at low pH (<2) for regeneration and reused more than once. At pH 2 or less, besides the protonation of carboxyl groups, it is highly likely that some of the amine groups on CMCT were not crosslinked with aldehyde groups on BNCC, thus these free amine groups become

positively charged at low pH [18], which causes repulsion between the cationic dye molecules and the aerogel.

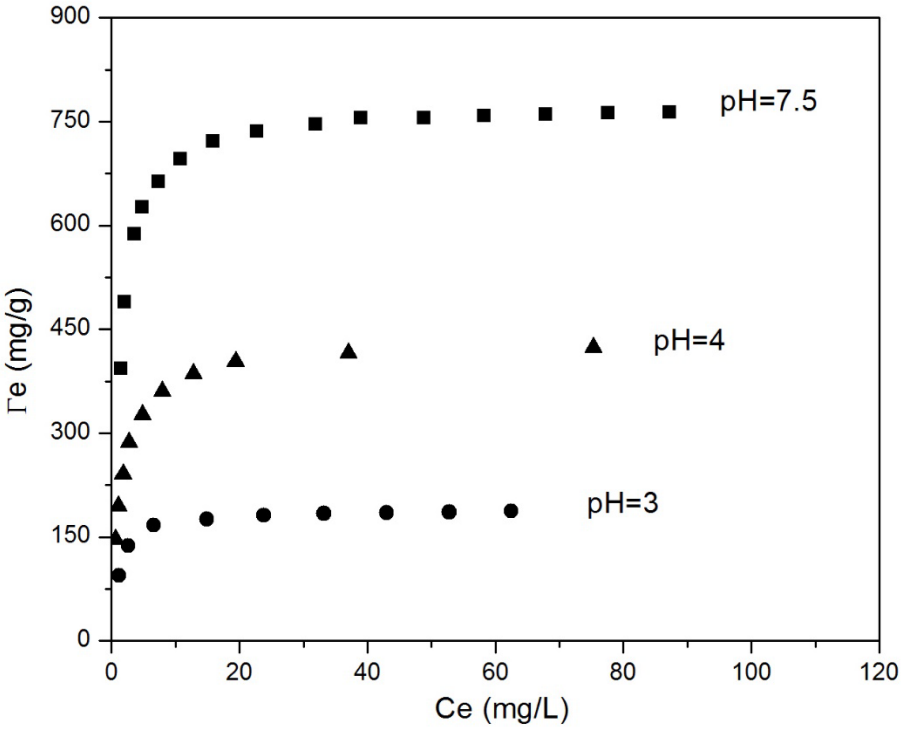

Figure 5.9 Adsorption isotherms of MB adsorption by BNCC-CMCT for various pHs at 22 °C.

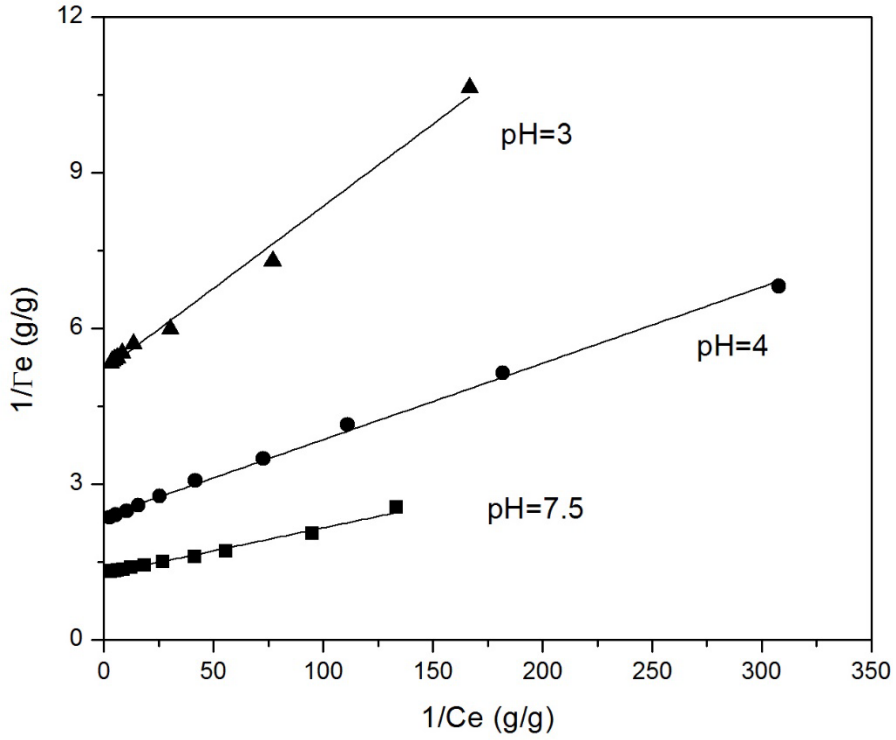

Figure 5.10 Langmuir plots for MB adsorption by BNCC-CMCT for various pHs at 22 °C.

Table 5.3 Langmuir isotherm parameters for MB adsorption for various pHs at 22 °C.

pH	Γ_m (mg/g)	K	R^2
3	192	0.0316	0.990
4	419	0.0147	0.995
7.5	785	0.0089	0.986

As discussed, the rate determining step is the diffusion of MB^+ ions into the gel. At high charge densities (high pH) more MB^+ ions need to diffuse into the gel. Hence one expects the apparent adsorption rate k_{ads} be the highest at high pH. This explains why the slope in Figure 5.10 increases with decreasing pH, since the slope equals the equilibrium constant K which is inversely proportional to k_{ads}. At pH ≤ pKa the adsorption is close to charge stoichiometry. Hence at pH 4, when only one of two neighboring carboxyl groups is dissociated, likely steric hindrance plays less of a role.

5.4.6 Desorption and regeneration

The easy regeneration and good reusability of adsorbent can reduce the costs of adsorbent materials and make the removal process more economically. The reusability of BNCC-CMCT aerogel was demonstrated with an initial MB concentration of 50 mg/L, with each adsorption process taking one hour. The results are shown in Figure 5.11. The adsorption capacity after the first cycle decreased from 225 mg/g to 194 mg/g, about 86.2 % of the initial capacity, and in the following test, it did not show a significantly decrease for the subsequent five cycles. The removed amount is still 188 mg/g, about 83.5 % of the initial adsorption capacity after six cycles, which shows the aerogel has a good reusability. The decrease in performance could be due to part of pre-adsorbed MB being trapped inside the aerogel, thus reducing the total available negative charged carboxyl groups for subsequent adsorption cycles. Decreasing the dye solution pH with HCl protonates the carboxyl groups on the aerogel surface, forming –COOH. During this process a MB^+ ion is removed. However MB^+ is still adsorbed onto dissociated –COO- groups, and stays on it for a long time, much longer than the time used for the desorption process (10 minutes). Even though we can improve the desorption by increasing the desorption time, this is not an economical process, since we already can reach at least 80% adsorption capacity even after six cycles.

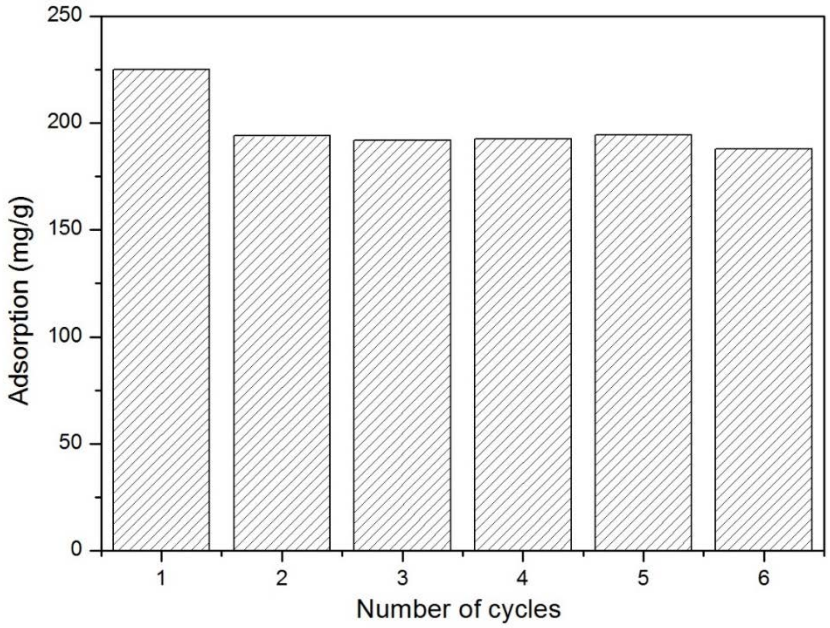

Figure 5.11 Adsorption of MB onto BNCC-CMCT aerogel over a few successive adsorption and desorption cycles. (The initial concentration of MB solution is 50 mg/L at 22 °C).

5.5 Conclusion

In this research, a novel biomaterial based BNCC-CMCT aerogel was prepared from bifunctional nanocellulose (BNCC) and carboxymethylated chitosan (CMCT) through a Schiff base reaction. BNCC can be obtained from sequential periodate and partially chlorite oxidation on cellulose followed by a hot water treatment. This highly porous and negatively charged aerogel showed a good adsorption performance. The maximum MB adsorption capacity of the aerogel was 785 mg/g obtained by fitting the data to a Langmuir plot, which is the highest one for any reported reusable adsorbent prepared from biomaterials. The adsorption capacity of this aerogel can be further improved or tuned by tailoring the functional groups on BNCC / CMCT or by modifying the mass ratio of BNCC / CMCT. The aerogel can keep its adsorption capacity in dye solutions over a wide pH range, and can regenerate and successively the reused for at least six cycles. The BNCC-CMCT aerogel is a promising "green" adsorbent since it is prepared from biodegradable starting materials and by an environmental friendly crosslinking process. This work might open new opportunities for the production of desirable bio-adsorbents.

5.6 Acknowledgements

The authors would like to thank the Natural Science and Engineering Research Council of Canada (NSERC), FPinnovations and Industrial Research Chairs Grants for funding support.

5.7 References

[1] Sharma P, Kaur H, Sharma M, Sahore V. A review on applicability of naturally available adsorbents for the removal of hazardous dyes from aqueous waste. Environ Monit Assess 2011;183:151-95.

[2] Tan KB, Vakili M, Horri BA, Poh PE, Abdullah AZ, Salamatinia B. Adsorption of dyes by nanomaterials: Recent developments and adsorption mechanisms. Separation and Purification Technology 2015;150:229-42.

[3] Hai FI, Yamamoto K, Fukushi K. Hybrid treatment systems for dye wastewater. Critical Reviews in Environmental Science and Technology 2007;37:315-77.

[4] Mittal A, Mittal J, Malviya A, Kaur D, Gupta VK. Adsorption of hazardous dye crystal violet from wastewater by waste materials. Journal of Colloid and Interface Science 2010;343:463-73.

[5] Shih M-C. Kinetics of the batch adsorption of methylene blue from aqueous solutions onto rice husk: effect of acid-modified process and dye concentration. Desalination and Water Treatment 2012;37:200-14.
[6] Porkodi K, Vasanth Kumar K. Equilibrium, kinetics and mechanism modeling and simulation of basic and acid dyes sorption onto jute fiber carbon: Eosin yellow, malachite green and crystal violet single component systems. Journal of Hazardous Materials 2007;143:311-27.
[7] Sulak MT, Yatmaz HC. Removal of textile dyes from aqueous solutions with eco-friendly biosorbent. Desalination and Water Treatment 2012;37:169-77.
[8] Osma JF, Saravia V, Toca-Herrera JL, Couto SR. Sunflower seed shells: A novel and effective low-cost adsorbent for the removal of the diazo dye Reactive Black 5 from aqueous solutions. Journal of Hazardous Materials 2007;147:900-5.
[9] Consolin Filho N, Venancio EC, Barriquello MF, Hechenleitner AAW, Pineda EAG. Methylene blue adsorption onto modified lignin from sugar cane bagasse. Eclética Química 2007;32:63-70.
[10] Akkaya G, Uzun İ, Güzel F. Kinetics of the adsorption of reactive dyes by chitin. Dyes and Pigments 2007;73:168-77.
[11] Wan Ngah WS, Teong LC, Hanafiah MAKM. Adsorption of dyes and heavy metal ions by chitosan composites: A review. Carbohydrate Polymers 2011;83:1446-56.
[12] Zhou Y, Zhang M, Wang X, Huang Q, Min Y, Ma T, et al. Removal of crystal violet by a novel cellulose-based adsorbent: Comparison with native cellulose. Industrial & Engineering Chemistry Research 2014;53:5498-506.
[13] Dong XM, Kimura T, Revol J-F, Gray DG. Effects of ionic strength on the isotropic−chiral nematic phase transition of suspensions of cellulose crystallites. Langmuir 1996;12:2076-82.
[14] Leung ACW, Hrapovic S, Lam E, Liu Y, Male KB, Mahmoud KA, et al. Characteristics and properties of carboxylated cellulose nanocrystals prepared from a novel one-step procedure. Small 2011;7:302-5.
[15] Yang H, Alam MN, van de Ven TGM. Highly charged nanocrystalline cellulose and dicarboxylated cellulose from periodate and chlorite oxidized cellulose fibers. Cellulose 2013;20:1865-75.

[16] He X, Male KB, Nesterenko PN, Brabazon D, Paull B, Luong JHT. Adsorption and desorption of methylene blue on porous carbon monoliths and nanocrystalline cellulose. ACS Applied Materials & Interfaces 2013;5:8796-804.
[17] Batmaz R, Mohammed N, Zaman M, Minhas G, Berry RM, Tam KC. Cellulose nanocrystals as promising adsorbents for the removal of cationic dyes. Cellulose 2014;21:1655-65.
[18] Jin LQ, Li WG, Xu QH, Sun QC. Amino-functionalized nanocrystalline cellulose as an adsorbent for anionic dyes. Cellulose 2015;22:2443-56.
[19] Sheikhi A, Safari S, Yang H, van de Ven TGM. Copper removal using electrosterically stabilized nanocrystalline cellulose. ACS Applied Materials & Interfaces 2015;7:11301-8.
[20] Mary SK, Sasidharan Pillai PK, Amma DB, Pothen LA, Thomas S. Aging and biodegradation of biocomposites. Handbook of biopolymer-based materials: Wiley-VCH Verlag GmbH & Co. KGaA; 2013. p. 777-99.
[21] Wong YC, Szeto YS, Cheung WH, McKay G. Equilibrium studies for acid dye adsorption onto chitosan. Langmuir 2003;19:7888-94.
[22] Gerente C, Lee VKC, Cloirec PL, McKay G. Application of chitosan for the removal of metals from wastewaters by adsorption—mechanisms and models review. Critical Reviews in Environmental Science and Technology 2007;37:41-127.
[23] Tejado A, Alam MN, Antal M, Yang H, van de Ven TGM. Energy requirements for the disintegration of cellulose fibers into cellulose nanofibers. Cellulose 2012;19:831-42.
[24] Yang H, Chen DZ, van de Ven TGM. Preparation and characterization of sterically stabilized nanocrystalline cellulose obtained by periodate oxidation of cellulose fibers. Cellulose 2015;22:1743-52.
[25] Yang H, van de Ven TGM. Preparation of hairy cationic nanocrystalline cellulose. Cellulose 2016;In press.
[26] Liu XF, Guan YL, Yang DZ, Li Z, De Yao K. Antibacterial action of chitosan and carboxymethylated chitosan. Journal of Applied Polymer Science 2001;79:1324-35.
[27] Yang H, Tejado A, Alam N, Antal M, van de Ven TGM. Films prepared from electrosterically stabilized nanocrystalline cellulose. Langmuir 2012;28:7834-42.
[28] Sang L, Luo D, Xu S, Wang X, Li X. Fabrication and evaluation of biomimetic scaffolds by using collagen–alginate fibrillar gels for potential tissue engineering applications. Materials Science and Engineering: C 2011;31:262-71.

[29] Kim U-J, Kuga S, Wada M, Okano T, Kondo T. Periodate oxidation of crystalline cellulose. Biomacromolecules 2000;1:488-92.
[30] Tachaboonyakiat W, Netswasdi N, Srakaew V, Opaprakasit M. Elimination of inter- and intramolecular crosslinks of phosphorylated chitosan by sodium salt formation. Polym J 2009;42:148-56.
[31] Heux L, Brugnerotto J, Desbrières J, Versali MF, Rinaudo M. Solid state NMR for determination of degree of acetylation of chitin and chitosan. Biomacromolecules 2000;1:746-51.
[32] Saint-Cyr K, van de Ven TGM, Garnier G. Adsorption of yellowing inhibitors on mechanical pulp. Journal of pulp and paper science 2002;28:78-84.
[33] Seki Y, Yurdakoc K. Adsorption of promethazine hydrochloride with KSF montmorillonite. Adsorption 2006;12:89-100.
[34] Kannan N, Sundaram MM. Kinetics and mechanism of removal of methylene blue by adsorption on various carbons—a comparative study. Dyes and Pigments 2001;51:25-40.
[35] Chan CH, Chia CH, Zakaria S, Sajab MS, Chin SX. Cellulose nanofibrils: a rapid adsorbent for the removal of methylene blue. RSC Advances 2015;5:18204-12.
[36] Chen W, Li Q, Wang Y, Yi X, Zeng J, Yu H, et al. Comparative study of aerogels obtained from differently prepared nanocellulose fibers. ChemSusChem 2014;7:154-61.
[37] Kadirvelu K, Kavipriya M, Karthika C, Radhika M, Vennilamani N, Pattabhi S. Utilization of various agricultural wastes for activated carbon preparation and application for the removal of dyes and metal ions from aqueous solutions. Bioresource Technology 2003;87:129-32.
[38] Bulut Y, Karaer H. Adsorption of methylene blue from aqueous solution by crosslinked chitosan/bentonite composite. Journal of Dispersion Science and Technology 2015;36:61-7.
[39] Kamiti M, van de Ven TGM. Kinetics of deposition of calcium-carbonate particles onto pulp fibers. Journal of Pulp and Paper Science 1994;20:199-205.

Chapter 6. Conclusions and suggestions for future work

6.1 Conclusions

Various novel types of nanocellulose have been introduced in this thesis, including sterically stabilized nanocrystalline cellulose (SNCC), hairy cationic nanocrystalline cellulose (CNCC), end-to-end assembled hydrolyzed electrosterically stabilized nanocrystalline cellulose (HENCC), bifunctional nanocrystalline cellulose (BNCC) and its application in aerogel preparation. The preparation methods of these nanocellulose are summarized in Scheme 6.1. These novel types of nanocellulose have unique properties comparing to the conventional nanocrystalline cellulose (NCC) from acid hydrolysis. The properties of these nanocellulose are summarized in Table 6.1. All these novel nanocellulose not only extend the family of nanocellulose, but also are promising to bring more opportunities to nanocellulose fundamental research and applications.

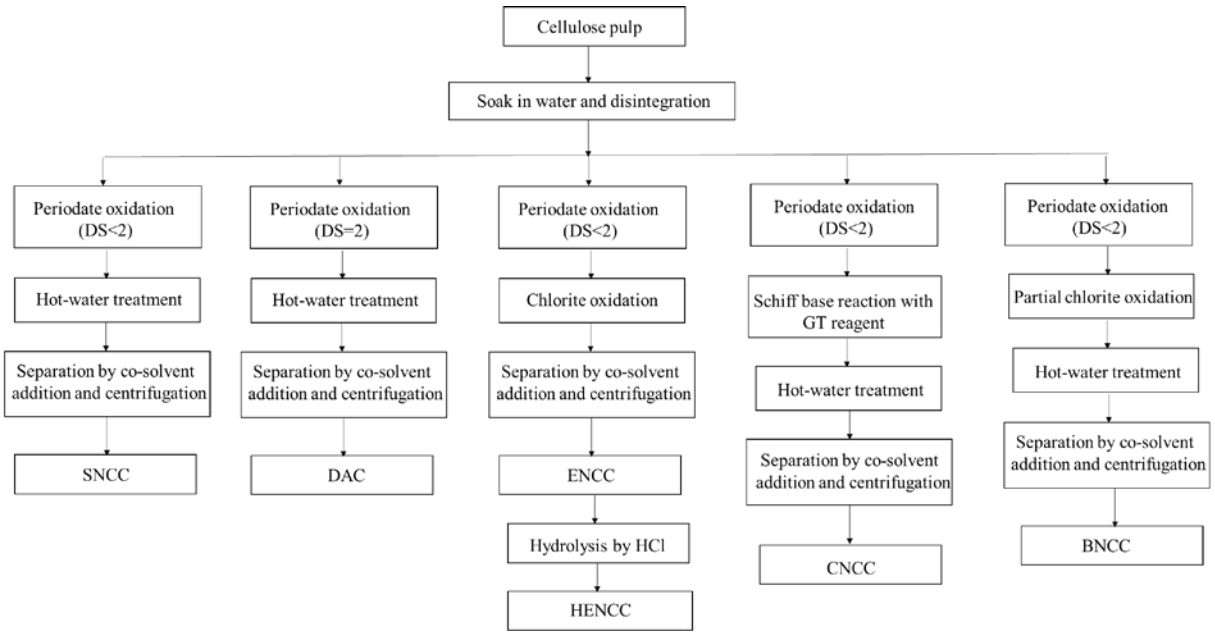

Scheme 6.1. Preparation of various nanocellulose material, including SNCC, DAC, ENCC, HENCC, CNCC and BNCC.

Table 6.1 Summarization of physical properties of various nanocellulose material.

	Length (nm)	Width (nm)	Functional groups	Charge density* (mmol/g)
SNCC	100-200	8	Aldehyde groups	- 8.2
CNCC	120	5	Quaternary ammonium	+1.7
ENCC	130	7	Carboxyl groups	- 6
HENCC	120	6	Carboxyl groups	-1.2 or -0.35
BNCC	110-150	8	Carboxyl groups	- 3
			Aldehyde groups	3

*The content of functional groups is adjustable.

SNCC was prepared and separated from hot water treatment of periodate oxidized cellulose fibers by addition of cosolvent followed by centrifugation. SNCC is sterically stabilized by protruding dialdehyde modified cellulose (DAMC) chains. SNCC has similar dimensions as conventional NCC produced by sulfuric acid treatment, but a better heat resistance due to the hemiacetal linkages. SNCC also has a lower intrinsic viscosity than NCC. The plenty of aldehyde groups on SNCC can serve as an intermediate for further functionization.

CNCC was produced by cationization of periodate oxidized cellulose fibers, followed by a hot water treatment. This is an easy and environmentally friendly method. Introducing positively charged groups onto DAMC fibers, greatly improves the efficiency of fibrillation of DAMC fibers into nanosize structures under aqueous thermo-treatment. CNCC typically has a width of 5 nm and a length about 120 nm, 67% crystalline index and a positive charge content of 1.68 mmol/g. CNCC has the potential application in anionic dye or heave metal removal, or colloid particle flocculation in water treatment, or used as coagulation aids for anionic fillers.

HENCC with shorter DCC chains have been prepared from a hydrolysis of ENCC. The carboxyl groups on the protruding DCC chains on HENCC were successfully conjugated with an alkyne and an azide derivative, respectively. Cellulose nanofibers with a length of more than one μm and a width of 6 nm were obtained by crosslinking these two types of HENCC derivatives through a click reaction. End-to-end assembled HENCC nanofibers with a length of more than one μm were also obtained by a bioconjugation reaction. To the best of our knowledge, it is the first chemical assembly of rod-shaped nanocellulose by an end-to-end route in one dimension. It also provides

evidence that most of the protruding DCC chains were located on the two ends of ENCC nanorods. This research may bring new opportunities for preparing cellulose nanofibers with designed length and aspect ratio, and extent their potential applications in the fabrication of various nanocellulose devices or composites.

Finally, a novel biomaterial based BNCC-CMCT aerogel was prepared from bifunctional nanocellulose and carboxymethylated chitosan through a Schiff base reaction. This highly porous and negatively charged aerogel showed a good adsorption performance and reusability. The maximum adsorption capacity for methylene blue was 785 mg/g, which is the highest one for any reported reusable adsorbents prepared from biomaterials. The adsorption capacity of this aerogel can be further improved or tuned by tailoring the functional groups on BNCC / CMCT or by modifying the mass ratio of BNCC / CMCT. The BNCC-CMCT aerogel is a promising "green" adsorbent and might open new opportunities for the production of desirable bio-adsorbents.

6.2 Suggestions for future work

For SNCC, it is worthwhile to investigate the properties of films made from SNCC particles. Due to its many aldehyde groups, which can form hemiacetal linkages with hydroxyl groups, thus it is expected to produce films with strong tensile strength, and the protruding dialdehyde cellulose chains on SNCC will contribute to the flexibility of the films. SNCC can also be used to replace glutaraldehyde (a common but toxic crosslinker), in the application as a green crosslinker for preparation of composite films, hydrogels or aerogels with PVA (polyvinyl alcohol). By adding and crosslinking with SNCC, which would improve the mechanical properties of PVA composites when applied in packaging as films, or in tissue engineering as hydrogels, or in adsorbents as aerogels. Due to the reducing property of aldehyde groups, the SNCC is also a promising candidate as a green reducing agent in preparation various metal nanoparticles, and the SNCC is easy to separate from the obtained nanoparticles by passing through a filter membrane with a pore size large than metal nanoparticles but smaller than the SNCC.

For end-to-end assembly of cellulose nanofiber, it would be interesting to compare the various films prepared from ENCC, HENCC, end-to-end assembled HENCC and nanocellulose fibers

from TEMPO-mediated oxidation. Some useful information might be obtained from this investigation, such as the relation between the morphology individual nanorod and the mechanical and optical properties of the assembled films.

The hairy CNCC obtained from our method, has unreacted aldehyde groups, which are able to be continually crosslinked with a diamine or chitosan, to form stable aerogels or films. It would be interesting to investigate the performance of these positively charged aerogels or films used as antimicrobial materials or as adsorbents for removal of negatively charged heavy metals or dyes in waste water treatment.

Appendix 1.

Highly stable, functional hairy nanoparticles and biopolymers from wood fibers: towards sustainable nanotechnology

Amir Sheikhi, Han Yang, Nur Alam, Theo G.M. van de Ven

Short abstract:

Synthesis schemes to prepare highly stable wood fiber-based hairy nanoparticles and functional cellulose-based biopolymers have been detailed.

Long abstract:

Nanoparticles, as one of the key materials in nanotechnology and nanomedicine, have gained significant importance during the past decade. While metal-based nanoparticles are associated with synthetic and environmental hassles, cellulose introduces a green, sustainable alternative for nanoparticle synthesis. Here, we present the chemical synthesis and separation procedures to produce new classes of hairy nanoparticles (bearing both amorphous and crystalline regions) and biopolymers based on wood fibers. Through periodate oxidation of soft wood pulp, the glucose ring of cellulose is opened at the C2-C3 bond to form 2,3-dialdehyde groups. Further heating of the partially oxidized fibers (e.g., T = 80 °C) results in three products, namely fibrous oxidized cellulose, sterically stabilized nanocrystalline cellulose (SNCC), and dissolved dialdehyde modified cellulose (DAMC), which are well separated by intermittent centrifugation and co-solvent addition. The partially oxidized fibers (without heating) were used as a highly reactive intermediate to react with chlorite for converting almost all aldehyde to carboxyl groups. Co-solvent precipitation and centrifugation resulted in electrosterically stabilized nanocrystalline cellulose (ENCC) and dicarboxylated cellulose (DCC). The aldehyde content of SNCC and consequently surface charge of ENCC (carboxyl content) were precisely controlled by controlling the periodate oxidation reaction time, resulting in highly stable nanoparticles bearing more than 7 mmol functional groups per gram of nanoparticles (e.g., as compared to conventional NCC bearing << 1 mmol functional group/g). Atomic force microscopy (AFM), transmission electron microscopy (TEM), and scanning electron microscopy (SEM) attested the rod-like morphology. Conductometric titration, Fourier transform infrared spectroscopy (FTIR), nuclear magnetic

resonance (NMR), dynamic light scattering (DLS), electrokinetic-sonic-amplitude (ESA) and acoustic attenuation spectroscopy shed light on the superior properties of these nanomaterials.

Introduction

Cellulose, as the most abundant biopolymer in the world, has been served recently as a key raw material to yield crystalline nanoparticles named nanocrystalline cellulose (NCC, also known as cellulose nanocrystals CNC) [1]. To understand the mechanism of NCC synthesis, the structure of cellulose fibers needs to be explored. Cellulose is a linear and polydispersed polymer comprising poly-beta(1,4)-D-glucose residues [2]. The sugar rings in each monomer are connected through glycosidic oxygen to form chains of (1-1.5) x 10^4 glucopyranose units [2,3], introducing alternating crystalline parts and disordered, amorphous regions, first reported by Nageli and Schwendener [2,4]. Depending on the source, crystalline parts of cellulose can adopt various polymorphs [5].

If a cellulose fiber is treated with a strong acid, such as sulfuric acid, the amorphous phase can be completely hydrolyzed away to disrupt the polymer and produce crystalline particles of various aspect ratio depending on the source (e.g., wood and cotton yield more than 90% crystalline nanorods of width ~ 5-10 nm and length ~ 100-300 nm, whereas tunicin, bacteria, and algae produce 5-60 nm wide and 100 nm to several micrometer long NCCs) [6]. Readers are referred to the vast amount of literature available on the scientific and engineering aspects of these nanomaterials [2, 5, 7-16]. Despite numerous interesting properties of these nanoparticles, their colloidal stability has always been an issue at high salt concentrations and high/low pH due to their relatively low surface charge content (less than 1 mmol/g) [17].

Instead of strong acid hydrolysis, cellulose fibers can be treated with an oxidizing agent (periodate), cleaving C2-C3 linkage in the anhydro D-glucopyranose residues to form 2,3-dialdehyde units with no significant side reactions [18, 19]. These partially oxidized fibers can be used as a valuable intermediate material to produce nanoparticles bearing both amorphous and crystalline regions (hairy nanocrystalline celluloses) using solely chemical reactions without any mechanical shear or ultrasonication [20]. When the partial oxidation degree DS < 2, heating oxidized fibers results in three batches of products, namely fibrous cellulose, water dispersible dialdehyde cellulose

nanowhiskers called sterically stabilized nanocrystalline cellulose (SNCC), and dissolved dialdehyde modified cellulose (DAMC), which can be isolated by precise control over the co-solvent addition and intermittent centrifugation[21].

Performing controlled chlorite oxidation on the partially oxidized fibers converts almost all the aldehyde groups to carboxyl units, which can introduce as high as 7 mmol COOH groups per gram of nanocrystalline cellulose depending on the aldehyde content [18], acting as stabilizers. These nanoparticles are called electrosterically stabilized nanocrystalline cellulose (ENCC). Furthermore, it has been confirmed that soft layers of charged hair-like protruding chains exist on ENCC [17]. This material has been used as a highly efficient adsorbent to scavenge heavy metal ions [22]. The charge of these nanoparticles can be precisely controlled by controlling the periodate reaction time [23].

Despite known oxidation reactions of cellulose, the production of SNCC and ENCC has never been reported by any other research groups most probably due to the separation challenges. We have been able to successfully synthesize and isolate various fractions of nanoproducts by precisely designing the reaction and separation steps. This visual article demonstrates with complete detail how to reproducibly prepare and characterize the aforementioned novel nanowhiskers bearing both amorphous and crystalline parts from wood fibers. This tutorial may be an asset for active researchers in the fields of soft material, biological, and medicinal sciences, nanotechnology and nanophotonics, environmental science and engineering, and physics.

Protocol

Caution: Read the material safety data sheets (MSDS) of all the chemicals before touching them. Many of the chemicals used in this work may cause severe health damages. Using personal protection such as lab coat, gloves, and goggles is a must. Do not forget that safety comes first. The water used throughout the synthesis is distilled water.

1. Preparation of partially oxidized fibers as an intermediate

1.1) Tear 4 g Q-90 softwood pulp sheets into small pieces of approximately 2 x 2 cm^2.

1.2) Soak the torn pulp sheets in water for at least one day.

1.3) Disintegrate the wet pulp using a mechanical disintegrator to achieve an almost-uniform dispersion.

1.4) To assemble the vacuum filter, secure a nylon filter in a Buchner funnel and place the funnel in a filter flask. Then, connect the filter flask to a vacuum pump using proper tubing. Turn on the pump and pour the disintegrated pulp solution in the funnel to separate the pulp from the liquid.

1.5) Measure the weight of wet pulp (m_1), and calculate the amount of adsorbed water by pulp: $m_{w,1} = m_1 - 4$.

1.6) Preparation of periodate oxidizing solution

1.6.1) For SNCC/DAMC synthesis: separately, dissolve 2.64 g sodium periodate ($NaIO_4$) and 15.48 g sodium chloride (NaCl) in 200-$m_{w,1}$ mL water.

1.6.2) For ENCC/DCC synthesis: separately, dissolve 5.33 g sodium periodate ($NaIO_4$) and 15.6 g sodium chloride (NaCl) in 266-$m_{w,1}$ mL water.

1.7) Add the wet pulp separately to the solutions prepared in 1.6. Make sure that the total amount of water (adsorbed by pulp plus added water) is equal to 200 mL for SNCC and 266 mL for ENCC syntheses.

1.8) Cover the beaker thoroughly with aluminum foil to prevent periodate deactivation while stirring at speed ~ 105 rpm in room temperature for a desired amount of time according to Table 1 to achieve a favored aldehyde content. As an example, to obtain ~ 6.5 mmol/g aldehyde, react for 96 h.

1.9) When the reaction time is elapsed, open the aluminum foil and add 1 mL (in case of SNCC/DAMC synthesis) or 3 mL (in case of ENCC/DCC synthesis) ethylene glycol to the mixture and stir for 10 min to stop the oxidation reaction by quenching periodate.

1.10) Collect the oxidized pulp by vacuum filtration (according to 1.4), redisperse it in 500 mL water, and stir it for 30 min. Repeat this step at least 5 times to clean the pulp from periodate thoroughly.

1.11) After the 5^{th} water wash on the oxidized pulp, separate the pulp from solution by vacuum filtration and store it in a cold (4˚C) place.

2. Synthesis of SNCC and DAMC

2.1) Divide the partially oxidized wet pulp (m_1), obtained in 1.11, by four: $m_2 = m_1/4$, and measure the weight of adsorbed water: $m_{w,2} = m_2 - 1$.

2.2) Disperse the pulp in (100 - $m_{w,2}$) g water in a round bottom flask (total water content = 100 g).
2.3) Place the round bottom flask in an oil bath and heat the partially oxidized pulp at 80˚C for 6 h while gently stirring.

Note: If pulp is completely oxidized with periodate (DS = 2), e.g., by reacting 1 g pulp with 1.85 g $NaIO_4$ (8.65 mmol) in a solution comprising 3.87 g NaCl (8.64 mmol) and 65 mL water while stirring for 6 days, depending on the heating condition and residence time in water, the property of the dialdehyde cellulose (DAC) is changed (Table 2).

2.4) Cool down the solution to room temperature.
2.5) Centrifuge the solution at 18500 x g for 10 min. The precipitate is unfibrillated cellulose (fraction 1).
2.6) Separate the supernatant carefully and weigh it (A).
2.7) Add 1.7(A) gram propanol to the supernatant obtained in 2.6 while stirring to precipitate SNCC. Details about the separated SNCC and added propanol is available in Figure 1.
2.8) Centrifuge the biphasic solution at 3000 x g for 10 min, and separate the resulted gel-like precipitate (second fraction, SNCC) by decantation, which is ready to be redispersed and dialyzed for further purification (section 4) and characterization (section 5).
2.9) To the supernatant obtained in 2.8, add 3.5(A) gram propanol to yield a white precipitate (third fraction, DAMC).
2.10) Centrifuge the solution of 2.9 at 3000 x g for 10 min, and collect the transparent gel-like DAMC precipitate (by pouring the supernatant in a separate beaker) ready to be redispersed in water, purified by dialysis (details available in section 4), and characterized (section 5).

3. Synthesis of ENCC and DCC
3.1) Prepare a solution of 0.5 M sodium hydroxide (NaOH) by dissolving ~ 2 g NaOH in 100 mL water and keep it aside. This will be used in step 3.7.
3.2) Divide the wet oxidized pulp, obtained in 1.11, by four: $m_3 = m_1/4$, and measure the weight of adsorbed water: $m_{w,3} = m_3 - 1$.
3.3) Separately, add 2.93 g sodium chloride (NaCl) and 1.41 sodium chlorite ($NaClO_2$) to (50 - $m_{w,3}$) mL water and stir to dissolve.

3.4) Suspend m_3 gram of wet oxidized pulp (containing ~ 1 g dry oxidized pulp) in the solution obtained in 3.3. Note that the final pulp concentration is 1 g in 50 mL total available water (free and adsorbed water).
3.5) Place a pH meter in the solution of 3.4.
3.6) Add 1.41 g hydrogen peroxide (H_2O_2) to the mixture of step 3.4 dropwise.
3.7) Stir the suspension of 3.6 for 24 h in room temperature at 105 rpm while maintaining the pH ~ 5 by gradually adding 0.5 M sodium hydroxide (NaOH) prepared in step 3.1.

Note: The pH starts decreasing rapidly after ~ 15 min from the beginning of reaction, and it should be kept constant for at least the first 4 hours of the reaction. For convenience, it is suggested that the reaction is started at 1 PM and the pH is controlled until 5 PM, then the reaction is left overnight and early in the morning the pH is increased to 5 again. After such a long time pH drop will not be significant indicating that most of the conversion is achieved. Now, almost no solid can be observed in the solution (large fibers are broken down into nanoparticles). Note that if the reaction is left for a longer time, the crystalline part may be disrupted.

3.8) Divide the suspension obtained from 3.7 into equally-weighted centrifuge tubes and centrifuge at 27000 x g for 10 min, and separate the supernatant (ENCC + DCC) from the micro-fibrous precipitate.
3.9) Weigh the supernatant obtained from 3.8 and call the solution mass (B).
3.10) Slowly add 0.16(B) g ethanol to the solution of 3.9 while stirring to form a white precipitate (second fraction, ENCC).
3.11) Centrifuge the solution of 3.10 at 3000 x g for 10 min, and separate the resulted transparent gel-like ENCC precipitate by decantation. ENCC is ready to be redispersed in water, purified by dialysis (details available in section 4), and characterized (section 5).
3.12) To the supernatant obtained in 3.11, add equal mass of ethanol as the solution mass to yield a white precipitate (third fraction, DCC).
3.13) Centrifuge the solution of 3.12 at 3000 x g for 10 min, and separate the transparent gel-like DCC precipitate ready to be redispersed in water, purified by dialysis (details available in section 4), and characterized.

4. Dialysis procedure to purify SNCC, DAMC, ENCC or DCC

4.1) Redisperse the gel-like precipitate obtained in any steps of 2.8 (SNCC), 2.10 (DAMC), 3.11 (ENCC), or 3.13 (DCC) in 10 mL water by vigorous stirring for 1 h.

4.2) Place the dispersion in a dialysis tubing (MW Cutoff = 12-14 kDa, Length ~ 30 cm, width ~ 4.5 cm) and secure the top and bottom by clipping.

4.3) Place the filled dialysis bag in ~ 4 L of distilled water and stir for 24 h to eject the salts.

4.4) Collect the dialyzed solution in a container and store in a cold (4 ˚C) place.

5. Post-purification characterization: solid phase and charge concentrations measurement

5.1) Concentration measurement

5.1.1) Weigh 3 mL of a desired dispersion in a weighting dish (Aluminum cup, 57 mm).

5.1.2) Place the weighing dish containing the dispersion in an oven (50 ˚C) overnight.

5.1.3) Weigh the dry film and calculate the concentration of nanoparticles or polymers in the dispersion: Concentration (w/v%) = 100 x mass of dry film / 3, or

Concentration (w/w%) = 100 x mass of dry film / mass of dispersion

5.2) Conductometric titration

5.2.1) Conductometric titration of SNCC or DAMC to determine aldehyde content

5.2.1.1) Prepare 0.1 M hydrochloric acid (HCl) by adding 0.82 mL HCl to 25 mL water followed by adjusting the final volume to 100 mL.

5.2.1.2) Separately, prepare NaOH 0.1 M by adding 0.4 g sodium hydroxide to distilled water to achieve 100 mL final solution.

5.2.1.3) Following the hydroxylamine hydrochloride method[24], add a known amount of a desired dispersion to a desired amount of water (e.g., 0.02 g in 50 mL H_2O).

5.2.1.4) Adjust the pH to 3.5 using dilute HCl (0.1 M).

5.2.1.5) Add 10 mL hydroxylamine hydrochloride solution (5% w/w) to the dispersion.

5.2.1.6) Monitor the pH and keep it at 3.5 by adding 0.1 M NaOH until pH becomes stable at 3.5.

5.2.1.7) Using the consumed volume of NaOH to neutralize the H^+ released from the reaction of aldehyde groups and $NH_2OH.HCl$, measure the aldehyde concentration (mole of consumed NaOH = mole of produced HCl during the reaction = mole of aldehyde groups on SNCC).

5.2.2) Conductometric titration of ENCC or DCC to determine carboxyl content

5.2.2.1) Following literature[25], add enough amount of a desired dispersion to have 0.02 g of solid in 140 mL distilled water.
5.2.2.2) Separately, prepare 20 mM NaCl by dissolving 0.117 g NaCl in distilled water to achieve 100 mL final solution. Add 2 mL of 20 mM NaCl to 5.2.2.1.
5.2.2.3) Reduce the pH to about 3 using dilute HCl (0.1 M).
5.2.2.4) Perform the conductometric titration by adding standard sodium hydroxide (NaOH, 10 mM) in 0.1 mL/min increments up to pH ~ 11.
5.2.2.5) Using the consumed volume of NaOH to neutralize charged groups (details in Figure 2), measure the surface charge concentration (1 mole of consumed base equals to one mole COOH on the particle surface).

Representative results

The mass portion and charge content of each fraction during the periodate and chlorite oxidation of pulp depends on the reaction time (Table 1). Moreover, DAC molecular weight depends on heating condition and residence time (Table 2). Once SNCC and DAMC are made, they precipitate out by adding propanol (Figure 1). To measure the charge content of ENCC, conductometric titration is performed (Figure 2). NCC and ENCC colloidal behavior is affected by the ionic strength and pH. The size and zeta-potential of NCC and ENCC versus KCl salt concentration and pH are presented in Figure 3. SNCC is a neutral particle and its size is affected by the added propanol (Figure 3). Transmission electron microscopy (TEM) and atomic force microscopy (AFM) images of NCC, ENCC, and SNCC (Figure 4) attest that these particles benefit from a similar crystalline body. Bearing a high carboxyl group content, ENCC is able to separate a high amount of copper ions from aqueous systems (Figure 5). FTIR spectra and ^{13}CNMR of ENCC/DCC and SNCC reveal the chemical structure differences with conventional NCC and cellulose pulp (Figure 6). Finally, X-ray diffraction (XRD) of various fractions of oxidized cellulose (Figure 7) shed light on the crystallinity of these materials.

Discussion

Following the chemistry discussed in this visual paper, a spectrum of highly stable cellulose based nanoparticles with tunable charge bearing both crystalline and amorphous phases (hairy

nanocrystalline celluloses) are produced. Depending on the periodate oxidation time, as shown in Table 1, various products are yielded: oxidized fibers (fraction 1), SNCC (fraction 2), and DAMC (fraction 3) each of which providing unique properties, such as defined size, morphology, crystallinity, and aldehyde content. Further oxidation of these intermediate materials by chlorite results in various negatively charged species, namely fraction 1 (carboxylated pulp fibers), fraction 2 (ENCC), and fraction 3 (DCC) as stated in Table 1. If the periodate completely-oxidized pulp (DS = 2) is cooked, depending on the heating condition (temperature and incubation time), a series of dialdehyde cellulose (DAC) with various molecular weights and degrees of polymerization can be produced. Table 2 presents the molecular weight of DAC versus heating condition. Heating provides a facile way of converting partially periodate oxidized pulp into neutral, aldehyde functionalized nanoparticles (SNCC) and polymers (DAMC), which can be used as highly active intermediates. SNCC and DAMC are carefully isolated by adding a co-solvent such as propanol. In Figure 1, separated SNCC and DAMC versus added propanol is presented.

Table 1: Mass portion and charge content of each fraction during periodate and chlorite oxidation of pulp [23].

Periodate oxidation time (h)	Aldehyde content (mmol/g)	Fraction	Mass ratio (%)	Charge content (mmol/g)
10	1.5	1	90	1.20
		2	3.5	3.60
		3	7.5	3.95
16	2.5	1	82	2.15
		2	5	4.25
		3	12	4.60
24	3.5	1	69	2.90
		2	10	4.80
		3	21	5.25
96	6.5	1	9	4.05
		2	52	6.60
		3	40	6.95

Table 2: DAC molecular weight dependency on heating condition and residence time [21].

Temperature (˚C)	Heating time (h)	Residence time in water at room temperature (days)	Average molar mass (kDa)	Degree of polymerization
80	6	1	85.1	532
80	6	15	41.3	258
80	6	61	4.1	26
80	10	61	3.4	21
90	6	61	3.3	21
90	17	61	1.6	10

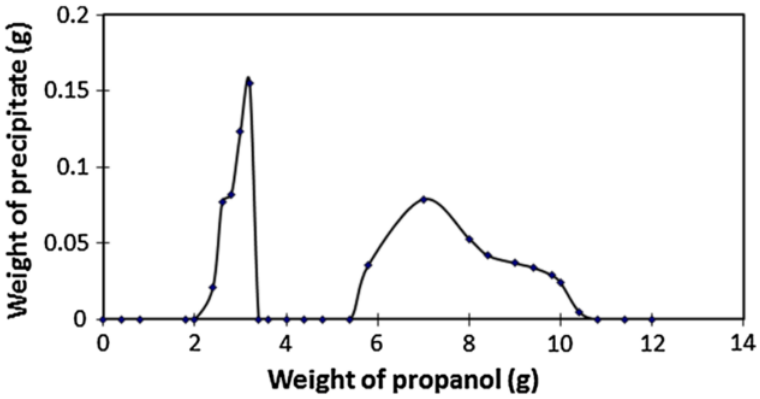

Figure 1: Precipitated SNCC and DAMC versus added propanol [21].

Once ENCC or DCC is made, simple conductometric titration is used to measure the surface charge (carboxyl) content as described in Figure 2. An equivalent amount of NaOH to neutralize the surface charge yields the charge density (e.g., ~ 6 mmol/g in Figure 2). The high charge density of ENCC stabilizes them electrostatically, which along with the excluded volume of the protruding dicarboxylated cellulose (DCC) chains, provide an electrosterically stabilization. In Figure 3a, it is shown that at ionic strength ~ 50 mM, NCC forms a gel, whereas ENCC remains as a stable dispersion up to at least 500 mM KCl. Such behavior is confirmed by studying the size of NCC and ENCC using acoustic attenuation spectroscopy: NCC size increases from ~ 50 nm to ~ 150 nm by increasing the ionic strength from 0 to 50 mM, while ENCC size decreases from ~ 220 nm to ~ 80 nm by increasing KCl concentration from 0 to 200 mM due to the retraction of protruding DCC chains (Figure 3c). The stable zeta-potential of ENCC at ~ -100 mV as compared to the decreasing trend of NCC zeta-potential from ~ -75 mV to ~ -40 mV attests a high, stable charge on ENCC (Figure 3d). Furthermore, ENCC surface acts as a weak acid as compared to the strong

acid surface groups on NCC (Figures 3 e&f), resulting in pH-dependent (pH-independent) zeta-potential (and size) for ENCC (NCC) at 3 < pH < 12. Interestingly, SNCC size is affected by the co-solvent concentration as depicted in Figure 3b.

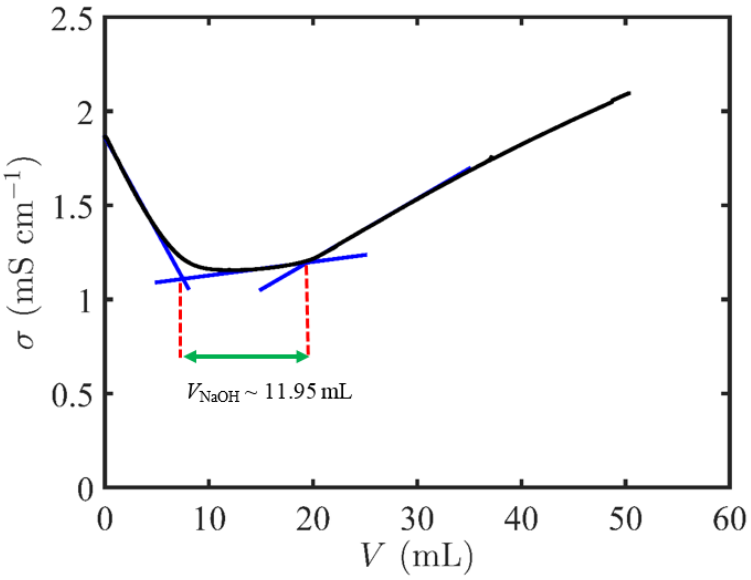

Figure 2: Conductometric titration graph for ENCC. COOH concentration = 0.01195 (V_{NaOH}) * 10 mM (NaOH concentration) / 0.02 g (initial ENCC) ~ 5.98 mmol/g.

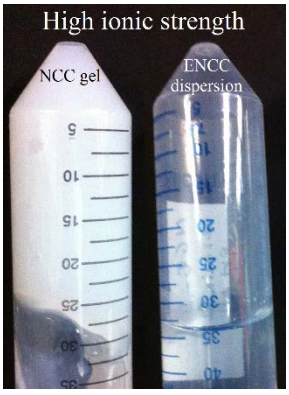

(a) NCC (left) and ENCC (right) behavior at high ionic strength (e.g., I = 50-500 mM).

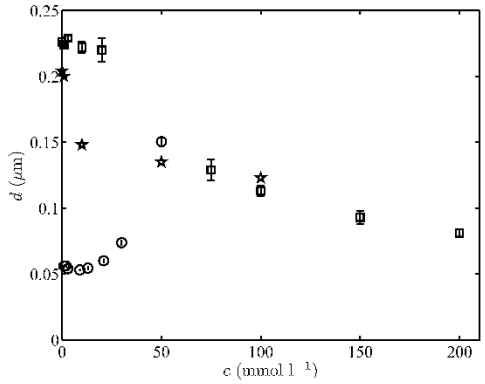

(b) ENCC and NCC size versus KCl concentration.

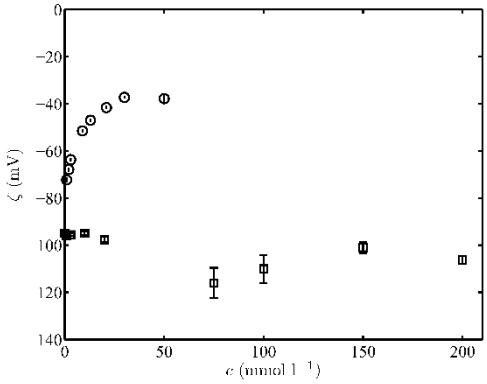

(c) ENCC and NCC zeta-potential versus KCl concentration.

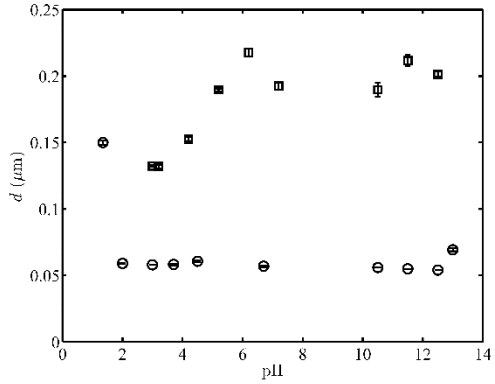

(d) ENCC and NCC size versus pH.

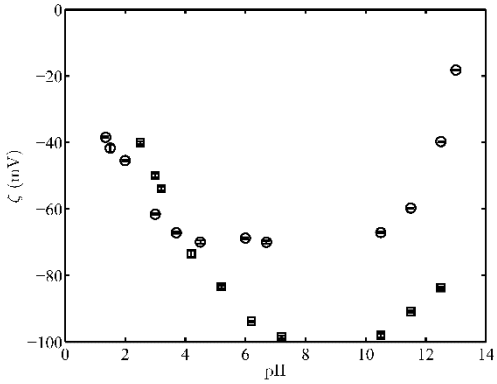

(e) ENCC and NCC zeta-potential versus pH.

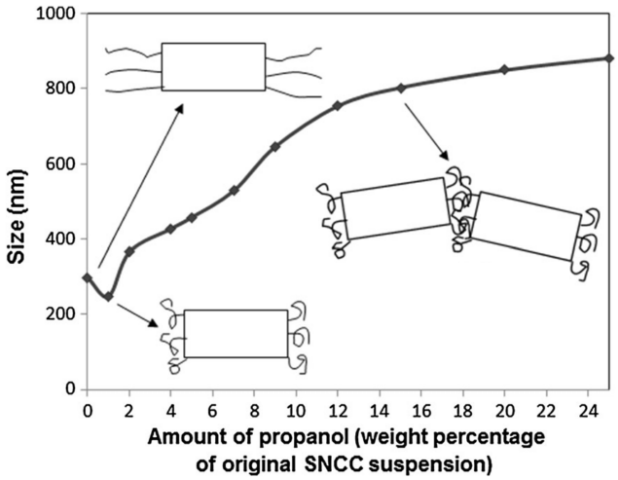

(f) SNCC size versus added propanol.

Figure 3 (a) NCC and ENCC behavior at high ionic strength [17]. (b) Size evolution of SNCC versus added propanol [21]. (c-f) NCC (circles) ENCC (squares) size and zeta potential versus KCl salt concentration and pH obtained from electrokinetic-sonic-amplitude (ESA) and acoustic attenuation spectroscopy [17]. Note that stars in panel (c) represent dynamic light scattering (DLS) size.

TEM and AFM images (Figure 4) of NCC, ENCC, and SNCC attest similar crystalline part. Also, in the presence of a divalent heavy metal ion, such as copper, ENCCs form highly stable star-like

aggregates at low Cu(II) concentration (e.g., 100 ppm, Figure 4c), whereas at high copper concentrations (e.g., 300 ppm, Figure 4d), large raft-like, unstable aggregates are formed. This is attributed to the partial and complete charge neutralization of ENCC at low and high copper concentrations, respectively [22]. Such tendency to adsorb heavy metal ions encouraged us to use ENCC to separate copper ions from aqueous systems. Figure 5 presents the copper removal capacity versus the equilibrium copper concentration [22]. Accordingly, 1 g ENCC is able to remove ~ 180 mg copper(II), which is equivalent to ENCC surface charge content. Such a high heavy metal ion removal capacity places this nanomaterial among highly efficient adsorbents [22].

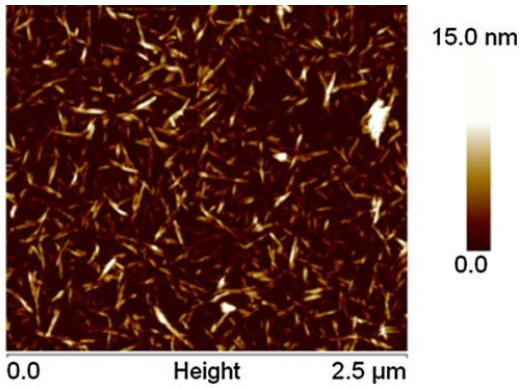

(a) AFM image of NCC.

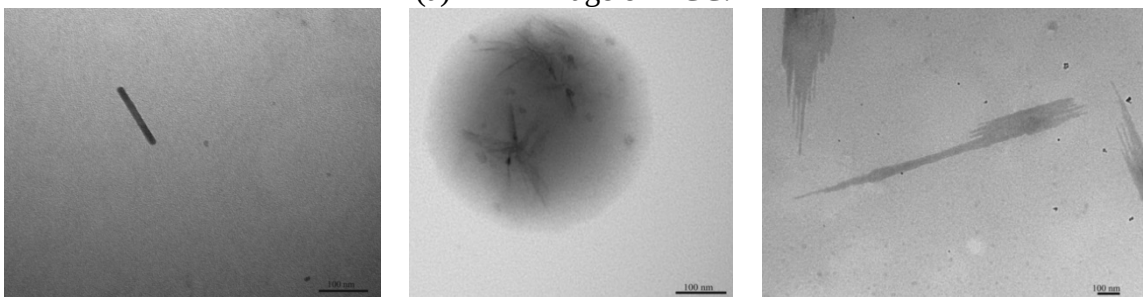

(b) TEM image of ENCC. (c) ENCC at Cu(II) = 100 ppm. (d) ENCC at Cu(II) = 300 ppm.

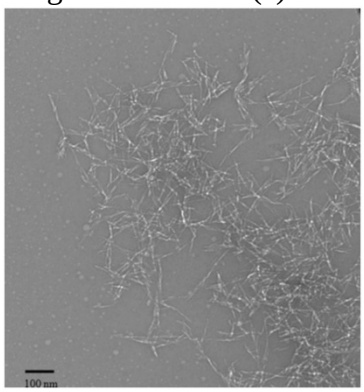

(e) TEM image of SNCC.

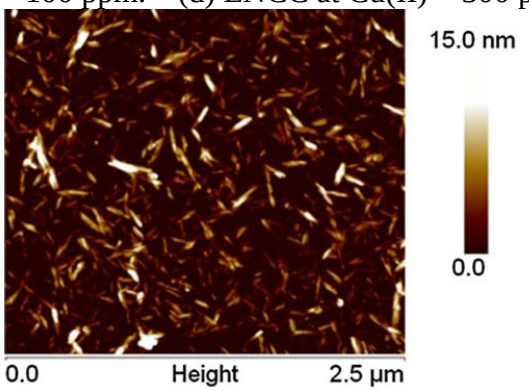

(f) AFM image of SNCC.

Figure 4 Transmission electron microscopy (TEM) and atomic force microscopy (AFM) images of NCC [21], ENCC [22], and SNCC [21] at various conditions.

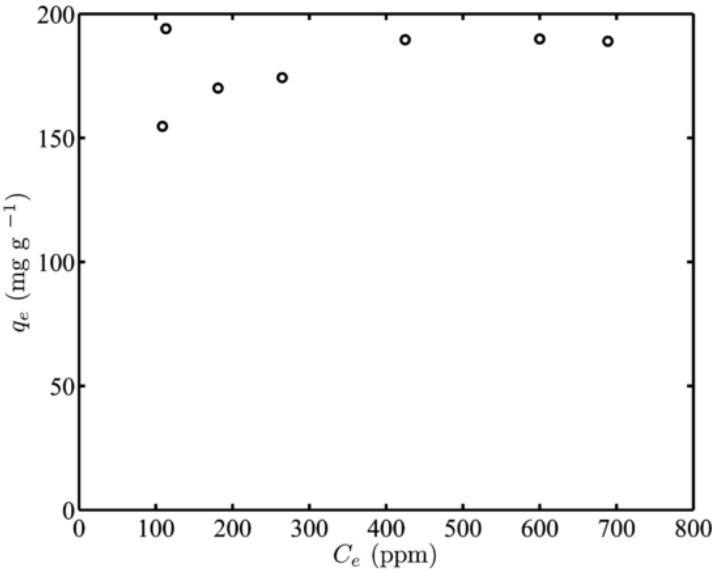

Figure 5 Copper removal capacity of ENCC q_e versus equilibrium copper concentration C_e [22].

Comparing the FTIR spectra of the different fractions of oxidized pulp (Figure 6a) suggests that by increasing the fraction number, the peak intensity at 1605 cm-1 corresponding to COONa increases as compared to the peak at 1015 cm-1 (CH2-O-CH2) [23]. This attests to the gradual increase in the carboxyl content of the fractions [23]. Interestingly, in Figure 6c, the characteristic peaks of SNCC at 1730 and 880 cm-1, as compared to cellulose pulp and NCC, reflect the stretching of carbonyl groups and the hemiacetal linkage, respectively [21]. The liquid phase 13CNMR of DCC (Figure 6b) shows peaks at 59 ppm (C6), and multiple peaks at 75-80 ppm (C4 and C5), 102 ppm (C1), and 175 ppm (carboxyl groups on C2 and C3) [23]. Figure 6d presents the solid state 13CNMR, which indicates the C4' shoulder peak corresponding to the amorphous phase of cellulose. The ratio of this peak to the sharp C4 peak (corresponding to crystalline cellulose) at 90 ppm is higher for NCC indicating higher crystallinity than cellulose pulp [21]. The broad peaks at 60-80 ppm and 85-105 ppm and the lack of carbonyl peaks at 175-180 ppm suggests hemiacetal linkage of aldehyde groups in SNCC [21]. X-ray diffraction (Figure 7) of cellulose and various oxidized fractions (1, 2, and 3) yields ~ 79%, 61%, 91%, and 23% crystallinity indices, respectively [23].

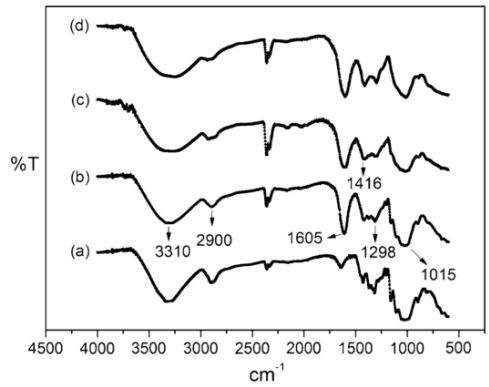

(a) FTIR spectra of cellulose pulp (a, 0.06 mmol/g), first fraction (b), second fraction (c, ENCC), and third fraction (d, DCC, charge content = 3.5 mmol/g).

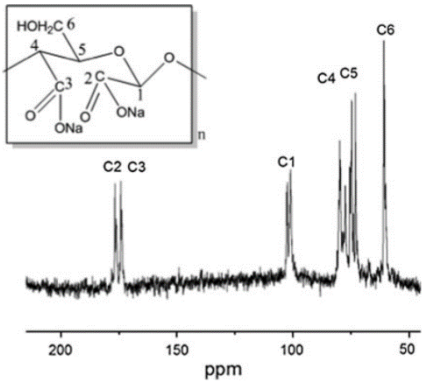

(b) Liquid phase ^{13}CNMR of DCC (charge content = 3.5 mmol/g).

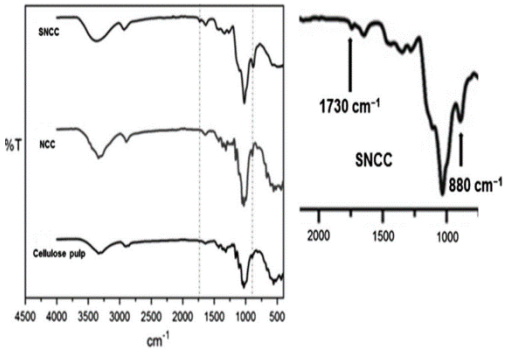

(c) FTIR sepectra of cellulose pulp, NCC, and SNCC.

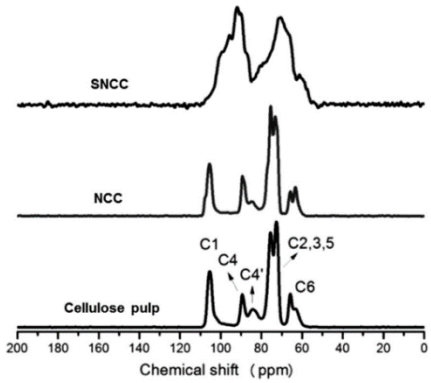

(d) Solid state ^{13}CNMR of cellulose pulp, NCC, and SNCC.

Figure 6 FTIR spectra and ^{13}CNMR of ENCC/DCC [23] and SNCC [21] as compared to NCC and cellulose pulp.

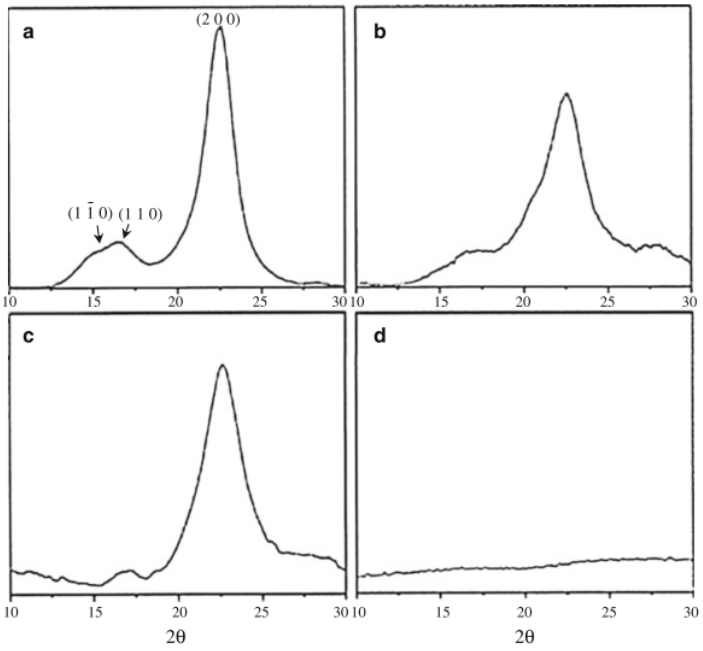

Figure 7 X-ray diffraction (XRD) of various fractions of oxidized cellulose: (a) initial cellulose, (b) first fraction of oxidized cellulose, (c) second fraction from oxidized cellulose, and (d) third fraction from oxidized cellulose (charge content = 3.5 mmol/g) [23].

In this article, it has been demonstrated how to prepare new classes of neutral or highly charged biopolymers and hairy nanoparticles from wood fibers. These novel green materials have exceptional colloidal and surface properties as compared to conventional nanocrystalline cellulose (NCC). They can be facilitated in a wide spectrum of applications such as environmental remediation, nanomedicine, nanocomposites and materials science, and micro- and nanoelectromechanical systems (MEMS/NEMS). This research and discovery opens a new horizon in the cellulose based nanotechnology.

Acknowledgments

Financial support from an Industrial Research Chair funded by FPInnovations and NSERC for a NSERC Discovery grant and from the NSERC Innovative Green Wood Fiber Products Network are acknowledged.

References

[1] Habibi, Y., Lucia, L. A. & Rojas, O. J. Cellulose nanocrystals: Chemistry, self-Assembly, and applications. Chem. Rev. 2010, 110 (6), 3479–3500.

[2] Samir, M. A. S. A., Alloin, F. & Dufresne, A. Review of recent research into cellulosic whisker, their Properties and their application in nanocomposites field. Biomacromolecules. 2005, 6 (2), 612–626.

[3] Sjöström, E. Wood chemistry: Fundamentals and applications. Academic Press: New York, 1993.

[4] Nageli, C. & Schwendener, S. Das Mikroskop, Theorie und Anwendung desselben. 2. Verbesserte auflage. Leipsig :W. Engelmann: Leipzig, 1877.

[5] Moon, R. J., Martini, A., Nairn, J., Simonsen, J. & Youngblood, J. Cellulose nanomaterials review: structure, properties and nanocomposites. Chem. Soc. Rev. 2011, 40 (7), 3941–3994.

[6] Klemm, D., Kramer, F., et al. Nanocelluloses: A new family of nature-based materials. Angew. Chem. Int. Ed. 2011, 50 (24), 5438–5466.

[7] Wang, N., Ding, E. & Cheng, R. Surface modification of cellulose nanocrystals. Front. Chem. Eng. China. 2007, 1 (3), 228–232.

[8] Siqueira, G., Bras, J. & Dufresne, A. Cellulosic bionanocomposites: A review of preparation, properties and applications. Polymers. 2010, 2 (4), 728–765.

[9] Siaueira, G., Bras, J. & Dufresne, A. Cellulose whiskers versus microfibrils: Influence of the nature of the nanoparticle and its surface functionalization on the thermal and mechanical properties of nanocomposites. Biomacromolecules. 2009, 10 (2), 425–432.

[10] Peng, B. L., Dhar, N., Liu, H. L. & Tam, K. C. Chemistry and applications of nanocrystalline cellulose and its derivatives: A nanotechnology perspective. Can. J. Chem. Eng. 2011, 89 (5), 1191–1206.

[11] Lu, P. & Hsieh, Y. Lo Preparation and properties of cellulose nanocrystals: Rods, spheres, and network. Carbohydr. Polym. 2010, 82 (2), 329–336.

[12] Liu, D., Chen, X., Yue, Y., Chen, M. & Wu, Q. Structure and rheology of nanocrystalline cellulose. Carbohydr. Polym. 2011, 84 (1), 316–322.

[13] Lam, E., Male, K. B., Chong, J. H., Leung, A. C. W. & Luong, J. H. T. Applications of functionalized and nanoparticle-modified nanocrystalline cellulose. Trends Biotechnol. 2012, 30 (5), 283–290.

[14] Kalia, S., Dufresne, A., et al. Cellulose-based bio- and nanocomposites: A review. Int. J. Polym. Sci. 2011, 1–35.

[15] Bai, W., Holbery, J. & Li, K. A technique for production of nanocrystalline cellulose with a narrow size distribution. Cellulose. 2009, 16 (3), 455–465.

[16] Eichhorn, S. J., Dufresne, A., et al. Review: Current international research into cellulose nanofibres and nanocomposites. J. Mater. Sci. 2010, 45 (1), 1–33.

[17] Safari, S., Sheikhi, A. & van de Ven, T. G. M. Electroacoustic characterization of conventional and electrosterically stabilized nanocrystalline celluloses. J. Colloid Interface Sci. 2014, 432, 151–157.

[18] Yang, H., Tejado, A., Alam, N., Antal, M. & Van De Ven, T. G. M. Films prepared from electrosterically stabilized nanocrystalline cellulose. Langmuir. 2012, 28 (20), 7834–7842.

[19] Guthrie, R. D. The “dialdehydes” from the periodate oxidation of carbohydrates. Adv Carbohydr Chem. 1961, 16, 105–158.

[20] van de Ven, T. G. M.; Tejado, A.; Alam, M. N.; Antal, M. Novel highly charged non-water soluble cellulose products, includes all types of cellulose nanostructures especially cellulose nanofibers, and method of making them. U.S. Provisional Patent Application 3776923-v3, WO 2012119229 A1. (2011).

[21] Yang, H., Chen, D. & van de Ven, T. G. M. Preparation and characterization of sterically stabilized nanocrystalline cellulose obtained by periodate oxidation of cellulose fibers. Cellulose. 2015, 22 (3), 1743–1752.

[22] Sheikhi, A., Safari, S., Yang, H. & van de Ven, T. G. M. Copper removal using electrosterically stabilized nanocrystalline cellulose. ACS Appl. Mater. Interfaces. 2015, 7 (21), 11301–11308.

[23] Yang, H., Alam, M. N. & van de Ven, T. G. M. Highly charged nanocrystalline cellulose and dicarboxylated cellulose from periodate and chlorite oxidized cellulose fibers. Cellulose.2013, 20 (4), 1865–1875.

[24] Kim, U. J., Kuga, S., Wada, M., Okano, T. & Kondo, T. Periodate oxidation of crystalline cellulose. Biomacromolecules. 2000, 1 (3), 488–492.

[25] Araki, J., Wada, M. & Kuga, S. Steric stabilization of a cellulose microcrystal suspension by poly (ethylene glycol) grafting. Cellulose. 2001, 17 (1), 21–27.

Appendix 2. Copper removal using electrosterically stabilized nanocrystalline cellulose

Amir Sheikhi, Salman Safari, Han Yang, and Theo G. M. van de Ven

Abstract

Removal of heavy metal ions such as copper using an efficient and low-cost method with low ecological footprint is a critical process in wastewater treatment, which can be achieved in a liquid phase using nanoadsorbents such as inorganic nanoparticles. Recently, attention has turned toward developing sustainable and environmentally friendly nanoadsorbents to remove heavy metal ions from aqueous media. Electrosterically stabilized nanocrystalline cellulose (ENCC), which can be prepared from wood fibers through periodate/chlorite oxidation, has been shown to have a high charge content and colloidal stability. Here, we show that ENCC scavenges copper ions by different mechanisms depending on the ion concentration. When the Cu(II) concentration is low ($C_0 \lesssim 200$ ppm), agglomerates of starlike ENCC particles appear, which are broken into individual starlike entities by shear and Brownian motion, as evidenced by photometric dispersion analysis, dynamic light scattering, and transmission electron microscopy. On the other hand, at higher copper concentrations, the aggregate morphology changes from starlike to raftlike, which is probably due to the collapse of protruding dicarboxylic cellulose (DCC) chains and ENCC charge neutralization by copper adsorption. Such raftlike structures result from head-to-head and lateral aggregation of neutralized ENCCs as confirmed by transmission electron microscopy. As opposed to starlike aggregates, the raftlike structures grow gradually and are prone to sedimentation at copper concentrations $C_0 \gtrsim 500$ ppm, which eliminates a costly separation step in wastewater treatment processes. Moreover, a copper removal capacity of ∼185 mg g–1 was achieved thanks to the highly charged DCC polyanions protruding from ENCC. These properties along with the biorenewability make ENCC a promising candidate for wastewater treatment, in which fast, facile, and low-cost removal of heavy metal ions is desired most.

Introduction

The presence of heavy metal ions such as copper in water can contaminate the food chain and have lethal effects on vital organs of not only humans but also all forms of life. Efficient removal of these pollutants is a prerequisite for wastewater recycling. Conventionally, heavy metal ion removal has been achieved using activated carbon in a liquid-phase adsorption process [1]. Due to

the high cost of activated carbon, the search for other low-cost adsorbents has been at the center of many research studies on wastewater treatment. Typical examples are fly ash [2], nanosized metal oxides [3], silica gel [4], zeolite [5], lignin [6], seaweed [7], wool [8], agricultural wastes such as coconut shell and rice husk [9, 10], chitin, and chitosan [11].

Nanoadsorbents are of particular interest for large-scale water remediation, due to their high surface area, which, on the one hand, can increase the contact area between the adsorbent and the heavy metal ions [12, 13] and, on the other, can be a substrate for the deposition of polyelectrolytes with high heavy metal ion removal capacity, thus assisting in their removal [14-18]. Moreover, upon adsorption of these polymers the colloidal stability of the hosting nanoparticles is increased, mainly due to the electrosteric effect of the adsorbed polymers [19].

Recently, it has been shown that derivatives of cellulose, a ubiquitous and abundant product of nature, can be exploited for the purpose of heavy metal ion removal [20-22]. The most desirable cellulose derivatives for wastewater treatment are cellulose nanofibers including bacterial cellulose [23], nanocrystalline cellulose [24, 25], and micro/nanofibrillar cellulose [26, 27], mainly because of their high surface area and feasibility of introducing functional groups with high affinity for heavy metal ions. Also, biodegradability and low cyto/genotoxicity of cellulose nanoparticles distinguish them from their inorganic counterparts [28, 29]. Electrosterically stabilized nanocrystalline cellulose (ENCC) has been introduced recently by Yang et al. as a new derivative of cellulose [30], in which dicarboxylated cellulose (DCC) chains are hypothesized to be protruding from the crystalline part. These polyelectrolytes are highly charged, which impart ENCC with a charge content about 20 times higher than that of conventional NCC and result in a high stability even at salt concentrations as high as 200 mmol L^{-1} [31]. A schematic diagram of an ENCC particle is presented in Figure 1. Note that the size of ENCC crystalline part is similar to that of conventional NCC (ENCC length and width are 100–200 nm and ~5–10 nm, respectively).

In this work, we investigate the mechanism of copper ion adsorption on ENCC at various Cu^{2+}concentrations using photometric dispersion analysis (PDA), dynamic light scattering (DLS), and transmission electron microscopy (TEM). Then the effect of Cu^{2+} initial concentration on ENCC copper removal capacity is studied.

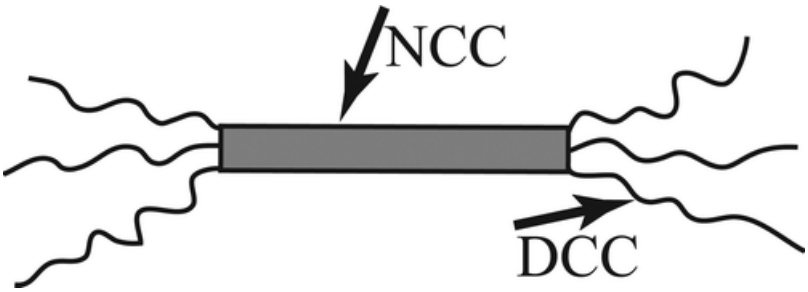

Figure 1. Schematic representation (not to scale) of an ENCC particle with its protruding dicarboxylated cellulose (DCC) chains.

Materials and Methods

Materials

Q-90 bleached softwood pulp sheets (Domtar, Canada) were used as starting cellulose material. Copper(II) sulfate (anhydrous powder, ≥99.99%), NaCl (ACS reagent, ≥99%), NaOH (ACS reagent, ≥97%), sodium chlorite (80%), and sodium (meta)periodate (≥99.99%) were purchased from Sigma-Aldrich, Canada, and used without further purification. Nitric acid (ACS reagent, 68–70%) was purchased from ACP Chemicals Inc., Canada. Anhydrous ethanol (95.27%) was supplied by Fisher Scientific, Canada.

Methods

ENCC was produced according to the procedure outlined by Yang et al [32]. Briefly, softwood pulp was first oxidized by periodate for 96 h (1 g of pulp and 1.33 g of $NaIO_4$ were mixed with 66 mL of water in a beaker, which was wrapped with aluminum foil to prevent entry of any light), followed by overnight oxidation using sodium chlorite at pH = 5 (1.41 g of $NaClO_2$, 1.41 g of H_2O_2, 2.93 g of NaCl, and 50 mL of water were used for 1 g of periodate oxidized pulp). ENCC was separated from the two-step oxidized pulp suspension by the addition of ethanol followed by centrifugation.

Conductometric titration was performed to obtain the ENCC charge density using a Metrohm 836 Titrando titrator (Ontario, Canada). A sample with 0.02 g of solids and 2 mL of 20 mmol L^{-1}NaCl was added to 140 mL of Milli-Q water [30]. Starting from pH = 2.7, 10 mmol L^{-1} NaOH solution

was added at 0.1 mL min^{-1} to the suspension up to pH = 11. This furnished the equivalent base volume required to neutralize the surface active groups from which the carboxyl content was calculated to be 5.5 ± 0.25 mmol g^{-1}.

Aggregation of ENCC in copper solutions was studied using a photometric dispersion analyzer (PDA2000, Rank Brothers Ltd., U.K.), in which flocculation causes an increase in the root mean square (RMS) value of the alternating current (ac) signal (proportional to the transmitted light intensity fluctuations), while the direct current (dc) component of the signal (proportional to the average transmitted light intensity) remains constant as long as the suspension turbidity does not change significantly. PDA is a powerful technique to monitor aggregate stability at various shear rates in real time [33]. An adequate amount of ENCC was added to a 8 mL copper solution at a desired concentration, which was being constantly pumped using a peristaltic pump at a constant flow rate corresponding to an average shear rate $\dot{\gamma} \approx 390\ s^{-1}$. The ENCC concentration after addition was 1000 ppm.

Transmission electron microscopy (TEM) specimens were prepared by leaving 10 μL of the Cu(II)/ENCC supernatant on a carbon-coated square mesh copper grid (mesh size 400, Electron Microscopy Sciences, USA) for 30 s. The liquid was absorbed from the side with a laboratory tissue, followed by air drying at room temperature for 5 min and imaging using Tecnai 12, 120 kV, Field Emission Inc.

The particle size distribution was obtained using dynamic light scattering at a 90° scattering angle and room temperature (Brookhaven light scattering instrument coupled with a BI9000 AT digital correlator).

A stock aqueous solution of 1000 ppm of copper was prepared by dissolving copper sulfate in distilled water, which was diluted to the desired copper solutions by adding distilled water. To perform adsorption experiments, 200 μL of a 20000 ppm ENCC suspension was added to 4 mL of a copper solution with an initial concentration, C_0, ranging from 300 to 900 ppm. For each treated sample, a control copper solution was prepared against which ENCC removal and capacity were compared. All Cu(II)–ENCC dispersions adjusted themselves to pH = 4 ± 0.2, which is well below

the copper hydroxide precipitation pH [34]. The Cu(II)–ENCC dispersions were filtered with 100 nm nylon syringe filters (Membrane-Solutions, China), and the filtrate was examined with DLS to evaluate the particle separation efficiency, followed by nitric acid digestion of the supernatant (final acid concentration 1 mol L^{-1}). The copper concentrations of treated and control samples were obtained using inductively coupled plasma emission spectroscopy (ICP-ES, Thermo Scientific 6000 series), which was calibrated using standard copper solutions (reference standard copper solution (1000 ppm ± 1%), Fisher Scientific, Canada).

Results and Discussion

Despite the high colloidal stability of ENCC in the presence of monovalent ions [31], addition of multivalent cations, such as Cu(II), to ENCC suspension may result in an instantaneous increase in particle size and aggregation. Figure 2 shows the ratio of the RMS (flocculation index, FI) [35] to dc signal, obtained by PDA, as an indication of aggregate size and number density versus time. Changes in the dc signal are mainly caused by the turbidity variation of the sample and approximately 2 orders of magnitude smaller than the ac fluctuations. The flocculation index of the initial copper solution C_0 is zero, because the solution is completely transparent. When the ENCC is added to the copper solution of concentration $C_0 \approx 100$ or 200 ppm, no change in the ratio is observed, probably due to the formation of aggregates smaller than the PDA detection limit or no aggregation occuring and light scattering by ENCC is low. On the other hand, for a copper solution with $C_0 \approx 300$ ppm, the FI starts growing with time and reaches a plateau after ∼12 min (Figure 2a), which suggests that aggregation has reached a steady state (i.e., a dynamic equilibrium between formation and breakup). The applied shear rate was $\dot{\gamma} \approx 390\ s^{-1}$ in a tube with inner diameter ≈ 3.2 mm. Increasing the average shear rate above 390 s^{-1} results in bubble formation in the circulating dispersion, which complicates the interpretation of aggregate stability. At higher copper concentrations, i.e., 400 and 500 ppm, the flocculation index reaches the instrument detection limit (ratio = 10) in ∼15 and 10 min after copper addition, respectively. These results show that in the case of a uniform initial copper concentration, at high enough final ENCC concentration (1000 ppm), stable copper-mediated ENCC aggregates are formed in a time scale of a few minutes.

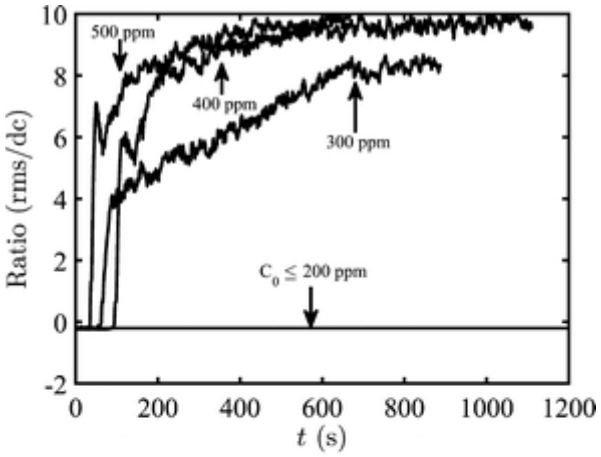

(a) ENCC is added to the copper solution.

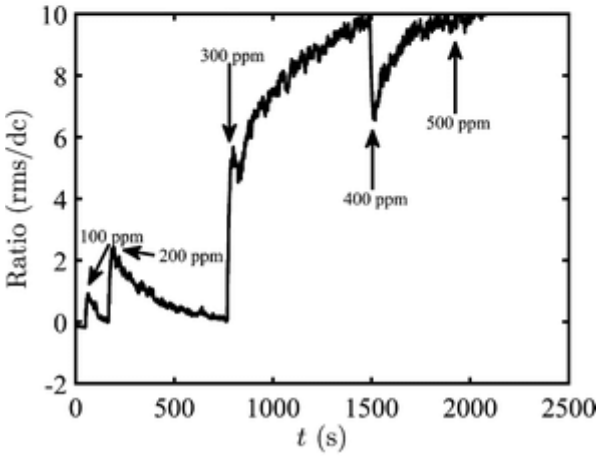

(b) Copper solution is added to the ENCC dispersion.

Figure 2. (a) Flocculation dynamics of ENCC (concentration C_{ENCC} = 1000 ppm) upon addition to copper solutions with $C_0 \lesssim 200$ ppm, $C_0 \approx 300$, 400, and 500 ppm, determined by photometric dispersion analysis (PDA), expressed in terms of ratio (rms/dc) versus time (t). (b) Flocculation dynamics of ENCC dispersion (1000 ppm) upon addition of 20 000 ppm copper solution to achieve the desired copper concentration (shown with arrows) using PDA. At $C_0 \lesssim 200$ ppm, high local copper concentration results in detectable ENCC aggregates, which are unstable against the shear; however, at $C_0 \approx 300$ ppm, the increase of ratio suggests a shear-induced aggregation. At $C_0 \gtrsim 300$ ppm, the aggregates remain stable. Stable aggregate formation is of great importance in particle separation processes after ion adsorption.

To shed light on how the local copper concentration affects the aggregate formation and to better understand the effect of copper and ENCC interactions, PDA experiments were also conducted on the aggregation of ENCC dispersions (1000 ppm) with stepwise addition of a concentrated copper solution (~20 000 ppm) at the same average shear rate of 390 s^{-1} to achieve C_0 spanning from 100 to 500 ppm (Figure 2b). Similar to a copper solution, an ENCC suspension yields FI = 0; however, upon copper addition, a sudden increase in the ratio occurs. When $C_0 \approx$ 100 or 200 ppm, the FI

relaxes back to zero after a few minutes, indicating that the final ENCC aggregates have become smaller than the detection limit of the instrument. Note that at $C_0 \lesssim 200$ ppm and ENCC concentration of 1000 ppm, when ENCC is added to Cu(II) solution, the initial copper concentration remains uniform and the FI adopts a zero value. Increasing the copper concentration to 300 ppm increases the FI in a fashion similar to the one seen in Figure 2a. Raising copper concentration more increases the ratio further, reaching the instrument detection limit at $C_0 \gtrsim 400$ ppm.

TEM images of ENCC aggregates reveal different morphologies at different copper concentrations. While individual ENCC particles are rodlike (Figure 3a), aggregates of ENCC particles at copper concentration $C_0 \approx 100$ ppm are starlike consisting of a few ENCCs aggregated from one end (Figure 3b). On the other hand, at copper concentration $C_0 \approx 300$ ppm lateral and head-to-head aggregation of ENCCs are observed, which results in raftlike features (Figure 3c).

Our hypothesis is that at copper concentrations $C_0 <300$ ppm, while some ENCC particles are (nearly) completely neutralized by copper ions, others are partially saturated. When these particles come into contact, they form aggregates, which results in ion redistribution in the overlapping protruding chains. This ion distribution weakens the bonds, leading to a transient agglomeration of ENCC particles. The breakup of these transient aggregates leads to the starlike entities at the final steady state condition (Figure 4a). The initial agglomeration of ENCCs is transient and only occurs when concentrated copper is added to ENCC suspension, perhaps due to the high local Cu/ENCC ratio resulting in agglomerates, which are broken into individual starlike features in a few minutes by the shear. In the absence of shear, we observed that these agglomerates sediment and do not break within the course of several days. Note that since the starlike entities are still charged and stable, similar to individual ENCC particles, the drying effect is probably minimal. The shaded area around the features may indicate that the initial droplet was broken into several small droplets upon drying (drying artifact).

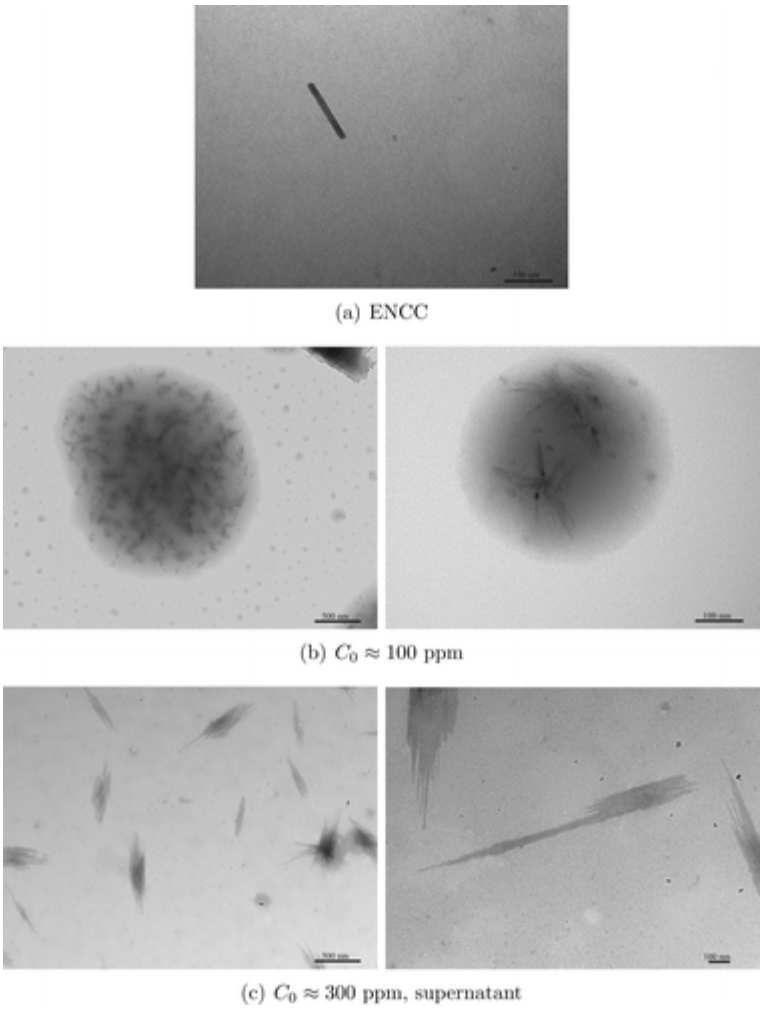

Figure 3. Transmission electron microscopy (TEM) images of an individual ENCC (a), starlike ENCC aggregates in the presence of 100 ppm of copper (b), and raftlike ENCC aggregates in a 300 ppm of copper solution (c).

At higher copper concentrations, 300 or 400 ppm, ENCC aggregates grow gradually with time regardless of the way ENCC and copper are mixed, since the copper concentration is sufficiently high to neutralize ENCC particles. Noteworthy is that lowering the pH facilitates the breakup of raftlike aggregates by replacing some of the adsorbed copper ions with protons. Previously, we showed that protonated ENCC particles do not aggregate even at pH = 1.5 [31], attesting to the importance of steric effects in stabilizing ENCC particles.

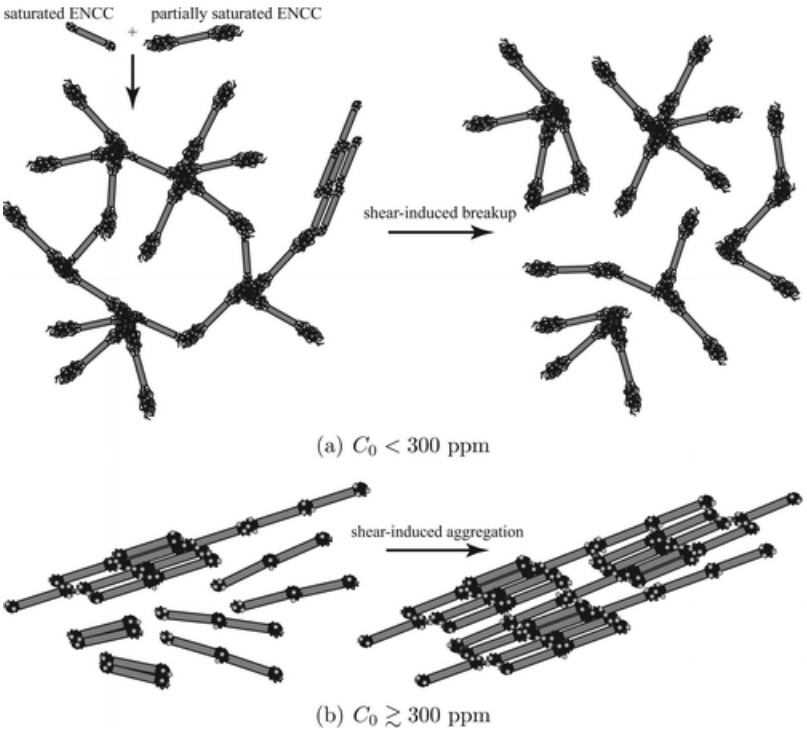

Figure 4. (a) Hypothesized mechanism of aggregation and breakup of ENCCs at copper concentration $C_0 < 300$ ppm. (b) Hypothesized mechanism of ENCC aggregation at copper concentration $C_0 \gtrsim 300$ ppm.

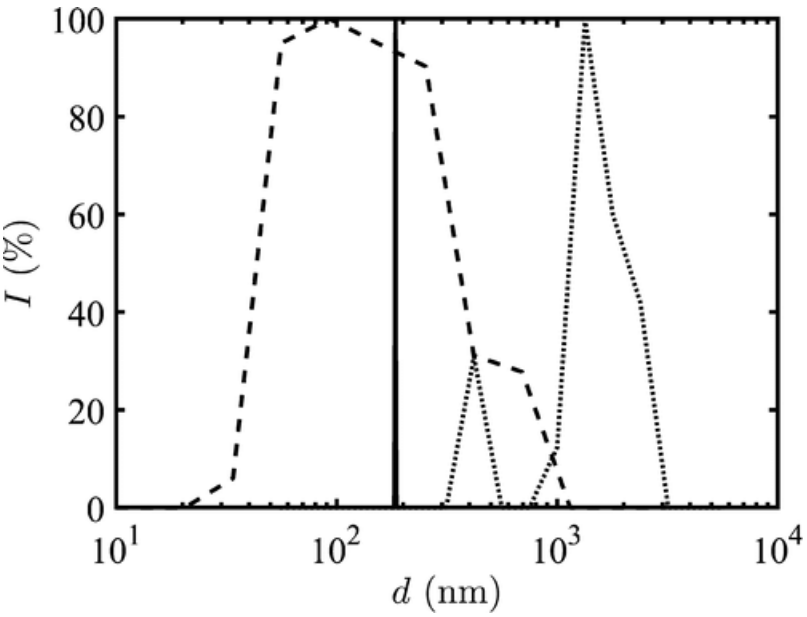

Figure 5. ENCC (1000 ppm) size distribution after 17 h unperturbed residence in copper solutions $C_0 = 0$ (solid line, which has a narrow size distribution), 100 (dashed line), and 400 ppm (dotted line), obtained by dynamic light scattering (DLS). Note that all samples are collected from the PDA experiments. At $C_0 \gtrsim 500$ ppm, DLS was not able to detect any particle in the supernatant.

This explanation is corroborated further by the DLS size distribution of ENCC aggregates. At neutral condition, ENCC particles are monodisperse with effective diameter $d \approx 185$ nm (Figure 5). Increasing the copper concentration (e.g., 100 ppm, shown with circles) has a dual effect: while the size of some particles decreases due to the contraction of protruding polymer chains because of the decrease in pH [31], likely because of formation of $Cu(OH)^+$, others experience a size increase due to the formation of stable polydisperse aggregates. On the other hand, a higher copper concentration, $C_0 \gtrsim 300$ ppm, results in almost complete neutralization of ENCC by copper ions. Neutralized particles tend to aggregate head-to-head and laterally (Figure 3c). These raftlike features grow further over a time period of a few minutes mainly due to shear-induced collisions (Figure 4b). DLS results are in good agreement with the PDA and TEM observations. Increasing the Cu(II) concentrations $C_0 \gtrsim 300$ ppm increases the aggregates size, which are sufficiently large at $C_0 \geq 500$ ppm that no particle is detected in the supernatant, implying that all ENCC aggregates sediment. This is mainly due to the large raftlike ENCC flocs that have been completely neutralized by copper ions (Figure 3c), which can settle even in the absence of a centrifugal force. When $300 \lesssim C_0 \lesssim 500$ ppm, DLS results indicate that raftlike aggregates collide and grow slowly over the course of 2 days, due to the Brownian motion. Moreover, at copper concentrations $300 \lesssim C_0 \lesssim 500$ ppm, filtration with 100 nm syringe filters removed all particles from the Cu(II) solution, whereas at $C_0 \lesssim 300$ ppm, filtration removed only some of the aggregates. Perhaps, in the latter case, the applied shear force in the syringe filter nanopores is strong enough to break the aggregates into individual ENCCs, which can pass through the filter.

Explaining the aggregation mechanisms of ENCCs quantitatively is more complicated. The difficulty arises when one wants to calculate aggregation and breakup rate coefficients. Both of these coefficients depend on the number of particles, their diameters, and the collision rate [33, 36]. As seen in Figure 5, ENCC aggregates are highly polydisperse, which can be attributed to the broad size distribution of freely suspending raftlike ENCC aggregates. Moreover, dicarboxylated cellulose (DCC) chains are protruding from the rodlike crystalline part of ENCC, which complicates calculation of the collision rate coefficient.

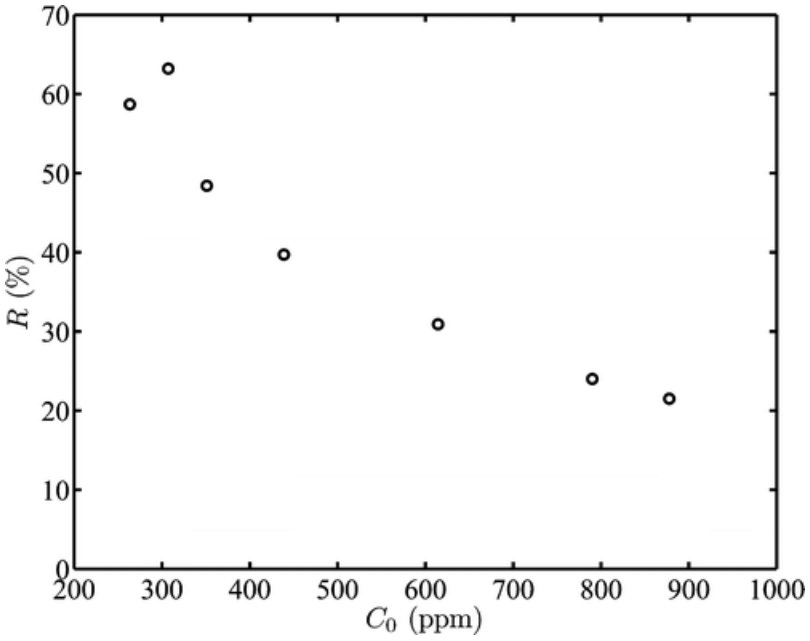

Figure 6. Copper removal $R = (C_0 - C_e)/C_0$ versus initial copper concentration C_0. The equilibrium copper concentration C_e is obtained from ICP experiments with less than 2% error. Note that R at $C_0 \lesssim 250$ ppm is an underestimation of the ENCC performance, because of failed tries to separate small ($d < 100$ nm) ENCCs.

As suggested by the flocculation dynamics, efficient Cu(II) ion separation condition is at C_{ENCC} = 1000 ppm and $C_0 \gtrsim 300$ ppm. Accordingly, we performed adsorption experiments by varying C_0between 200 and 900 ppm. The copper removal versus initial copper concentration is presented in Figure 6. The maximum removal $R_{max} \approx 63\%$ at pH ≈ 4 is achieved at $C_0 \approx 300$ ppm, because at lower Cu(II) concentrations, a complete adsorbent separation cannot be achieved either by filtration or by centrifugation, due to the weak particle bridging. Note that using filters with diameter less than 100 nm is not feasible due to the extremely high pressure drop across the membrane. The decreasing trend of removal versus initial copper concentration suggests that the maximum Cu(II) removal capacity of ENCC has been achieved. To evaluate this, the equilibrium copper removal capacity, q_e (mg g^{-1}), in the samples with final volume V (m^{-3}), $q_e = (C_0 - C_e)V/m_{ENCC}$, is plotted versus the ratio of equilibrium copper concentration over the amount of ENCC in Figure 7, in which C_0 (ppm) is the initial copper concentration, C_e (ppm) is the equilibrium copper concentration in the solution, and m_{ENCC} (g) is the ENCC dosage. The possible complexations of copper with carboxyl groups can be summarized in the following reactions [37].

$$COO^- + Cu^{2+} \rightleftharpoons [Cu(COO)]^+$$
$$COO^- + [Cu(COO)]^+ \rightleftharpoons Cu(COO)_2$$
$$COO^- + [Cu(OH)]^+ \rightleftharpoons Cu(COO)(OH)$$
$$COO^- + H^+ \rightleftharpoons COOH$$

Quantitative analysis of these complexes is cumbersome since their formation constants on ENCC's protruding polymers cannot be merely borrowed from the ones measured in the literature for carboxylic acid by conductometry; however, since all of ENCC aggregates precipitate, $Cu(COO)_2$ or Cu(COO)(OH) can be considered as the dominant species. Interestingly, the experimentally determined equilibrium removal capacity, 185 ± 4 mg g^{-1}, is close to the stoichiometric capacity of ENCC, i.e., 2.75 ± 0.125 mmol or 175 ± 8 mg Cu(II) per 1 g of ENCC, the difference not being significant. Note that the excess copper concentration may be the reason for achieving the maximum Cu(II) removal capacity of ENCC at pH 4, for which in the absence of excess copper about one-half of the carboxyl groups are protonated. Adding excess Cu(II) shifts the first three equilibria shown above to the right and the last one to the left. The removal capacity of ENCC is compared to some other adsorbents available in the literature (Table 1).

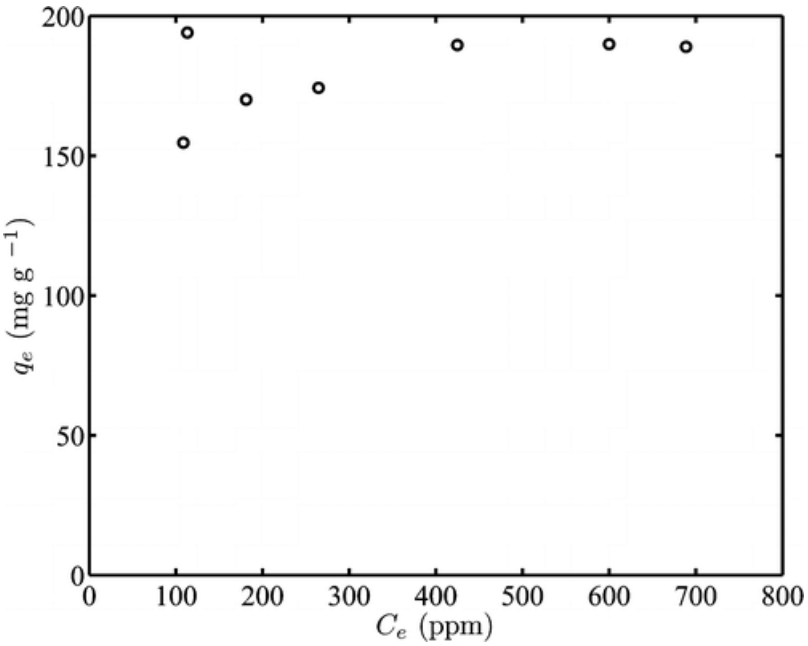

Figure 7. Copper removal capacity of ENCC $q_e = (C_0 - C_e)V/m_{ENCC}$ versus equilibrium copper concentration C_e. Sample volume $V \approx 4$ mL.

Table 1. Cu(II) Removal Performance of ENCC as Compared to Some Available Adsorbents

Adsorbent	q_e (mg g^{-1})	pH	Ref.
ENCC	185	4 ±0.2	this work
amino-modified nanostructured microfibrillated cellulose	174	5	[26]
carboxymethylated-bacterial cellulose	9.7	4.5	[23]
polymer-modified magnetic nanoparticles	129	5.5	[17]
anisotropic layered double hydroxide nanocrystal @ carbon nanosphere	20	5.7	[15]
carboxylated alginic acid	159	4	[38]
oxidized cellulose powder (sodiumm metaperiodate)	236	4.6	[39]
chitosan (various forms[a])	20-325	4.5-6	[40]
chitosan-coated perlite beads	196.08	5	[41]
chitosan coated perlite beads	104	4.5	[40]
tea waste	48	5.5±0.5	[41]
tobacco dust	36	6.5-7.2	[42]
tartaric acid-modified rice husk	31.85	4	[44]
newspaper pulp	30	5.5	[45]
sugar beet pulp	28.5	4	[46]
chitosan-cellulose blend	26.7	5.8	[47]
banana pitch	13.46	4.5	[48]
wheat shell	10.84	5	[49]
NaOH-treated poplar sawdust	6.92	4	[50]
chitosan-cellulose hydrogel beads	5 or 14.5[b]	5	[51]
activated carbon (coal)	4.4	5	[52]
chitosan-coated cotton fibers	1.0	4	[53]

a The chitosan extracted from shrimp has a high removal capacity q_e = 300 mg g^{-1}.
b Non-cross-linked hydrogels provide greater q_e.

Concluding Remarks

In this work, we explored the possibility of using electrosterically stabilized nanocrystalline cellulose (ENCC) as a biorenewable nanoadsorbent for copper removal from water. Photometric dispersion analysis was used to study the flocculation dynamics of ENCC aggregates in the presence of copper ions at a constant shear rate. It was found that at up to a copper/ENCC ratio of ~200 mg g^{-1} the aggregates were sufficiently small and stable which caused no change in the PDA flocculation index; however, at higher ratios, the aggregates started to grow gradually until they leveled off at a high flocculation index or reached the instrument detection limit. TEM images of

suspended aggregates at a copper/ENCC ratio ≈ 100 mg g^{-1} revealed the presence of starlike features consisting of a few ENCC particles aggregated from one end, whereas at a copper/ENCC ratio ≈ 300 mg g^{-1}, lateral and head-to-head aggregation of ENCCs led to raftlike aggregates, perhaps because of charge neutralization, which sediment shortly after formation, eliminating a costly separation step in wastewater treatment. Furthermore, the copper removal efficiency as high as ~63%, corresponding to removal capacity ≈ 185 mg g^{-1}, was obtained at pH ≈ 4. This removal capacity corresponds to a complete neutralization of the ENCC carboxyl groups by Cu^{2+} ions. Such a high copper uptake at this pH places ENCC among adsorbents with high copper removal capacity.

Acknowledgements

Financial support from an Industrial Research Chair founded by FPinnovations and NSERC and from the NSERC innovative Green Wood Fiber Products Network are gratefully acknowledged.

References

[1] Babel, S.; Kurniawan, T. A. Low-cost adsorbents for heavy metals uptake from contaminated water: a review. J. Hazard. Mater. 2003, 97, 219– 243.
[2] Panday, K. K.; Prasad, G.; Singh, V. N. Copper(II) removal from aqueous solutions by fly ash. Water Res.1985, 19, 869– 873.
[3] Hua, M.; Zhang, S.; Pan, B.; Zhang, W.; Lv, L.; Zhang, Q. Heavy metal removal from water/wastewater by nanosized metal oxides: a review. J. Hazard. Mater. 2012, 211–212, 317– 331.
[4] Mohan, D.; Pittman, C. U. Arsenic removal from water/wastewater using adsorbents-a critical review. J. Hazard. Mater. 2007, 142, 1– 53.
[5] Nguyen, T. A. H.; Ngo, H. H.; Guo, W. S.; Zhang, J.; Liang, S.; Yue, Q. Y.; Li, Q.; Nguyen, T. V. Applicability of agricultural waste and by-products for adsorptive removal of heavy metals from wastewater. Bioresour. Technol. 2013, 148, 574– 585.
[6] Demirbas, A. Heavy metal adsorption onto agro-based waste materials: a Review. J. Hazard. Mater. 2008,157, 220– 229.
[7] Suzuki, Y.; Kametani, T.; Maruyama, T. Removal of heavy metals from aqueous solution by nonliving ulva seaweed as biosorbent. Water Res. 2005, 39, 1803– 1808.

[8] Monier, M.; Nawar, N.; Abdel-Latif, D. A. Preparation and characterization of chelating fibers based on natural wool for removal of Hg(II), Cu(II) and Co(II) metal ions from aqueous solutions. J. Hazard. Mater.2010, 184, 118– 125.
[9] Sud, D.; Mahajan, G.; Kaur, M. P. Agricultural waste material as potential adsorbent for sequestering heavy metal ions from aqueous solutions - a review. Bioresour. Technol. 2008, 99, 6017–6027.
[10] Farooq, U.; Kozinski, J. A.; Khan, M. A.; Athar, M. Biosorption of heavy metal ions using wheat based biosorbents - a review of the recent literature. Bioresour. Technol. 2010, 101, 5043– 5053.
[11] Wu, F.; Tseng, R.; Juang, R. A review and experimental verification of using chitosan and its derivatives as adsorbents for selected heavy metals. J. Environ. Manage. 2010, 91, 798– 806.
[12] Li, J.; Zhang, S.; Chen, C.; Zhao, G.; Yang, X.; Li, J.; Wang, X. Removal of Cu(II) and fulvic acid by graphene oxide nanosheets decorated with Fe_3O_4 nanoparticles. ACS Appl. Mater. Interfaces 2012, 4,4991– 5000.
[13] Cao, C.; Qu, J.; Wei, F.; Liu, H.; Song, W. Superb adsorption capacity and mechanism of flowerlike magnesium oxide nanostructures for lead and cadmium ions. ACS Appl. Mater. Interfaces 2012, 4,4283– 4287.
[14] Chang, Y.; Chen, D. Preparation and adsorption properties of monodisperse chitosan-bound Fe_3O_4 magnetic nanoparticles for removal of Cu(II) ions. J. Colloid Interface Sci. 2005, 283, 446–451.
[15] Gong, J.; Liu, T.; Wang, X.; Hu, X.; Zhang, L. Efficient removal of heavy metal ions from aqueous systems with the assembly of anisotropic layered double hydroxide nanocrystals@carbon nanosphere. Environ. Sci. Technol. 2011, 45, 6181– 6187.
[16] Song, J.; Kong, H.; Jang, J. Adsorption of heavy metal ions from aqueous solution by polyrhodanine-encapsulated magnetic nanoparticles. J. Colloid Interface Sci. 2011, 359, 505– 511.
[17] Ge, F.; Li, M.; Ye, H.; Zhao, B. Effective removal of heavy metal ions Cd^{2+}, Zn^{2+}, Pb^{2+}, Cu^{2+} from aqueous solution by polymer-modified magnetic nanoparticles. J. Hazard. Mater. 2012, 211–212, 366–372.
[18] Farrukh, A.; Akram, A.; Ghaffar, A.; Hanif, S.; Hamid, A.; Duran, H. Design of polymer-brush-grafted magnetic nanoparticles for highly efficient water remediation. ACS Appl. Mater. Interfaces 2013, 5, 3784– 3793.
[19] Paria, S.; Khilar, K. C. A review on experimental studies of surfactant adsorption at the hydrophilic solid water Interface. Adv. Colloid Interface Sci. 2004, 110, 75– 95.
[20] Tan, L.; Zhu, D.; Zhou, W.; Mi, W.; Ma, L.; He, H. Preferring cellulose of Eichhornia Crassipes to prepare xanthogenate to other plant materials and its adsorption properties on copper. Bioresour. Technol. 2008, 99, 4460– 4466.
[21] O'Connell, D. W.; Birkinshaw, C.; O'Dwyer, T. F. Heavy metal adsorbents prepared from the modification of cellulose: a review. Bioresour. Technol. 2008, 99, 6709– 6724.

[22] Belhalfaoui, B.; Aziz, A.; Elandaloussi, E. H.; Ouali, M. S.; Menroval, L. C. D. Succinate-bonded cellulose: a regenerable and powerful sorbent for cadmium-removal from spiked high-hardness groundwater. J. Hazard. Mater. 2009, 169, 831– 837.
[23]Chen, S.; Zou, Y.; Yan, Z.; Shen, W.; Shi, S.; Zhang, X.; Wang, H. Carboxymethylated-bacterial cellulose for copper and lead ion removal. J. Hazard. Mater. 2009, 161, 1355– 1359.
[24] Yu, X.; Tong, S.; Ge, M.; Wu, L.; Zuo, J.; Cao, C.; Song, W. Adsorption of heavy metal ions from aqueous solution by carboxylated cellulose nanocrystals. J. Environ. Sci. 2013, 25, 933– 943.
[25]Suopajarvi, T.; Liimatainen, H.; Hormi, O.; Niinimaki, J.Coagulation-flocculation treatment of municipal wastewater based on anionized nanocelluloses. Chem. Eng. J. 2013, 231, 59– 67.
[26]Hokkanen, S.; Repo, E.; Suopajarvi, T.; Liimatainen, H.; Niinimaa, J.; Sillanpaa, M. Adsorption of Ni(II), Cu(II) and Cd(II) from aqueous solutions by amino modified nanostructured microfibrillated cellulose. Cellulose 2013, 21, 1471– 1487.
[27] Zheng, Q.; Cai, Z.; Gong, S. Green Synthesis of polyvinyl alcohol (PVA)-cellulose nanofibril (CNF) hybrid aerogels and their use as superabsorbents. J. Mater. Chem. A 2014, 2, 3110– 3118.
[28]Klemm, D.; Kramer, F.; Moritz, S.; Lindstrom, T.; Ankerfors, M.; Gray, D.; Dorris, A. Nanocelluloses: A new family of nature-based materials. Angew. Chem., Int. Ed. 2011, 50, 5438– 5466.
[29] Lin, N.; Dufresne, A. Nanocellulose in biomedicine: Current status and future prospect. Eur. Polym. J.2014, 50, 302– 325.
[30] Yang, H.; Tejado, A.; Alam, N.; Antal, M.; Van De Ven, T.G.M. Films prepared from electrosterically stabilized nanocrystalline cellulose. Langmuir 2012, 28, 7834– 7842.
[31] Safari, S.; Sheikhi, A.; van de Ven, T.G.M. Electroacoustic characterization of conventional and electrosterically stabilized nanocrystalline celluloses. J. Colloid Interface Sci. 2014, 432, 151– 157.
[32] Yang, H.; Alam, M.; van de Ven, T.G.M. Highly charged nanocrystalline cellulose and dicarboxylated cellulose from periodate and chlorite oxidized cellulose fibers. Cellulose 2013, 1– 11.
[33] Gregory, J. Monitoring particle aggregation processes. Adv. Colloid Interface Sci. 2009, 147–148, 109–123
[34] Cuppett, J. D.; Duncan, S. E.; Dietrich, A. Evaluation of copper speciation and water quality factors that affect aqueous copper tasting response. Chem. Senses 2006, 31, 689– 697.
[35] PDA Operating Manual. PDA2000 Photometric dispersion analyser operating manual; Rank Brothers Ltd.: 2013.
[36] Gaudreault, R.; Cesare, N. D.; Weitz, D.; van de Ven, T.G.M. Flocculation kinetics of precipitated calcium carbonate. Colloids Surf., A 2009, 340, 56– 65.
[37] Borges, F.; Guimaraes, C.; Lima, J. L. F. C.; Pinto, I.; Reis, S. Potentiometric studies on the complexation of copper(II) by phenolic acids as discrete ligand models of humic substances. Talanta 2005, 66, 670–673.

[38] Jeon, C.; Yoo, Y. J.; Hoell, W. H. Environmental effects and desorption characteristics on heavy metal removal using carboxylated alginic acid. Bioresour. Technol. 2005, 96, 15– 19.
[39] Maekawa, E.; Koshijima, T. Properties of 2,3-dicarboxy cellulose combined with various metallic ions. J. Appl. Polym. Sci. 1984, 29, 2289– 2297.
[40] Hasan, S.; Ghosh, T. K.; Viswanath, D. S.; Boddu, V. M. Dispersion of chitosan on perlite for enhancement of copper(II) adsorption capacity. J. Hazard. Mater. 2008, 152, 826– 837.
[41] Kalyani, S.; Priya, J.; Rao, P.; Krishnaiah, A. Removal of copper and nickel from aqueous solutions using chitosan coated on perlite as biosorbent. Sep. Sci. Technol. 2005, 40, 1483– 1495.
[42] Amarasinghe, B.; Williams, R. Tea waste as a low cost adsorbent for the removal of Cu and Pb from wastewater. Chem. Eng. J. 2007, 132, 299– 309.
[43] Qi, B.; Aldrich, C. Biosorption of heavy metals from aqueous solutions with tobacco dust. Bioresour. Technol. 2008, 99, 5595– 5601.
[44] Wong, K.; Lee, C.; Low, K.; Haron, M. Removal of Cu and Pb from electroplating wastewater using tartaric acid modified rice husk. Process Biochem. 2003, 39, 437– 445.
[45] Chakravarty, S.; Pimple, S.; Chaturvedi, H. T.; Singh, S.; Gupta, K. Removal of copper from aqueous solution using newspaper pulp as an adsorbent. J. Hazard. Mater. 2008, 159, 396– 403.
[46] Aksu, Z.; Isoglu, I. A. Removal of copper(II) ions from aqueous solution by biosorption onto agricultural waste sugar beet pulp. Process Biochem. 2005, 40, 3031– 3044.
[47] Sun, X.; Peng, B.; Ji, Y.; Chen, J.; Li, D. Chitosan(chitin)/cellulose composite biosorbents prepared using ionic liquid for heavy metal ions adsorption. AIChE J. 2009, 55, 2062– 2069.
[48] Low, K.; Lee, C.; Leo, A. Removal of metals from electroplating wastes using banana pith. Bioresour. Technol. 1995, 51, 227– 231.
[49] Basci, N.; Kocadagistan, E.; Kocadagistan, B. Biosorption of copper(II) from aqueous solutions by wheat shell. Desalination 2004, 164, 135– 140.
[50] Sciban, M.; Klasnja, M.; Skrbic, B. Modified hardwood sawdust as adsorbent of heavy metal ions from water. Wood Sci. Technol. 2006, 40, 217– 227.
[51] Li, N.; Bai, R. Copper adsorption on chitosan-cellulose hydrogel beads: behaviors and mechanisms. Sep. Purif. Technol. 2005, 42, 237– 247.
[52] Chu, K. H.; Hashim, M. A. Adsorption of copper(II) and EDTA-chelated copper(II) onto granular activated carbons. J. Chem. Technol. Biotechnol. 2000, 75, 1054– 1060.
[53] Zhang, G.; Qu, R.; Sun, C.; Ji, C.; Chen, H.; Wang, C.; Niu, Y.Adsorption for metal ions of chitosan coated cotton fiber. J. Appl. Polym. Sci. 2008, 110, 2321– 2327.

Appendix 3. Controlled crosslinking of nanocelluloses using ammonium zirconium carbonate

Amir Sheikhi, Han Yang, Pierre Carreau, Theo G.M. van de Ven

Abstract

Designing new platforms for controlled crosslinking of soft materials has attracted a broad range of scientific communities for developing advance materials. Precise adjustment of crosslinking density in a gel can help tune mesh size distribution and viscoelastic properties. Among the widely used crosslinkers, ammonium zirconium carbonate (AZC) has provided a cheap and reliable material for physical crosslinking of macromolecules through hydrogen bonding upon heating. Expectedly, functional groups with a large electronegativity gradient form strong hydrogen bonds; however, counterintuitively, we show that at the molecular (AZC)-colloidal (nanocellulose and/or biolatex) interaction level, the colloidal repulsion is able to prevail the hydrogen bonding and partially inhibit the bond formation. Hinging on the molecular-colloidal interactions, we have been able to design heat responsive AZC based soft bionanocomposites with controlled viscoelasticities ranging from $O(10^{-3})$-$O(10^{1})$ times that of an AZC mono-system. Such bionanocomposites will pave the way towards high quality, effective, and fast processing of AZC-mediated crosslinking.

*This paper will be submitted when patent implications are sorted out.